Neuronal circuits in the brainstem and spinal cord involved in forelimb behaviors and locomotion

Inauguraldissertation

zur

Erlangung der Würde eines Doktors der Philosophie

vorgelegt der

Philosophisch-Naturwissenschaftlichen Fakultät

der Universität Basel

von

Ludwig Ferdinand Christian Ruder

aus Frick, AG

2021

Genehmigt von der Philosophisch-Naturwissenschaftlichen Fakultät

Auf Antrag von

Prof. Dr. Silvia Arber

Prof. Dr. Pico Caroni

Basel, den 19.11.2019

_____

Prof. Dr. Martin Spiess

Dekan der Philosophisch-

Naturwissenschaftlichen Fakultät

Table of contents

1. Summary

Complexity, stability as well as flexibility of human and animal behavior is dependent on highly organized and intricate neuronal networks throughout the nervous system, many of which are poorly understood. The motor system in particular is composed of widely distributed neuronal circuits controlling the variable, often complicated patterns of muscle activity seen during behavior. The brainstem and spinal cord are both structures that are of critical importance for motor actions. However, mechanistic understanding on the construction and interaction of distinct motor actions at the neuronal level is largely missing.

This dissertation unravels organization and function of brainstem and spinal cord circuits important for locomotion and forelimb movements. Using intersectional genetic, viral, electrophysiological and behavioral tools allows the targeting, manipulation and read out of involved circuits at fine resolution. In the spinal cord, we employ molecular entry points to disentangle the identity and organization of long-distance projection neurons and show their role in the coordination of fore- and hindlimbs as well as speed during locomotion. In a second part, we investigate circuits in the lateral rostral medulla of the brainstem we demonstrate to be involved in forelimb movements. In particular, we reveal the existence of multiple intermingled, but cellularly segregated circuits implicated in different forelimb actions stretching from simple to complex paired with differential functional coding properties of single neurons into distinct cell ensembles.

Together, we identify neuronal circuit elements important for dedicated aspects of whole body and fine skilled motor behavior and provide evidence for how selected actions are controlled and constructed by specific neurons embedded into highly organized circuits.

2. Introduction

Movement is the language our body uses to interact with the environment. It can range from simple, autonomous acts such as eye blinking all the way to the very sophisticated and highly coordinated patterns of muscle contractions seen during speech or the usage of a music instrument, resulting in an almost infinite amount of potential motor actions. The control over when and how to activate these muscles is exerted by the nervous system. Specific motor neurons in the brainstem and spinal cord control the contraction of distinct body muscles through the selective innervation of the muscle fibers forming the neuromuscular junction. Upstream of motor neurons there is a complex network of interconnected neurons in the brain and spinal cord that harbors the vast neuronal modules needed to produce, develop and adapt motor behaviors. This dissertation investigates the organization and function of neuronal circuits for body movements in the spinal cord and brainstem. More specifically, the first experimental part focuses on the role of long spinal projection neurons in interlimb coordination during locomotion (chapter 3), whereas a second experimental part focuses on brainstem circuits involved in forelimb movements (chapter 4). Later, broader implications of these and other related findings are discussed in the context of the supraspinal control of locomotion (chapter 5) and the organization of brainstem circuits for action diversification (chapter 6).

2.1. The spinal cord

Neuronal circuits executing body movements are located in the spinal cord. Upon receiving input from supraspinal or sensory sources, sophisticated networks of spinal interneurons are taking part in forming signals that lead to the precise and correct activation of motor neurons controlling muscle contractions. These networks, often referred to as central pattern generators, show highly specific development, genetic identity and distinct wiring and have been studied extensively for a long time using a wide array of methods (Jessell 2000, Kiehn 2006, Goulding 2009, Arber 2012). Alternatively, motor neurons can also be activated directly from sensory or supraspinal inputs as shown anatomically, and also functionally for the monosynaptic reflex (Chen et al. 2003, Lemon et al. 2004). Motor neurons positioned all along

the rostro-caudal extent in the ventral spinal cord control the contraction of specific muscle and their organization is determined by complex transcription profiles in combination with distinct axon guidance mechanisms. Roughly, motor neurons controlling body muscles can be distinguished into 3 major categories in limbed animals depending on the muscles they innervate and their position in the spinal cord. First, the lateral motor column (LMC) encompasses motor neurons controlling limb muscles and are only present in the cervical and lumbar enlargement, second the medial motor column (MMC) that controls the activity of axial body musculature and is present throughout the rostro-caudal axis of the spinal cord and finally motor neurons of the hypaxial motor column (HMC) are located in the thoracic spinal cord and control muscles of the body wall (Guthrie 2004, Dasen and Jessell 2009). The complex network organization enabling the interplay between specific spinal interneurons and select motor neurons resulting in distinct movement pattern served as a model system to study the development and function of circuits in the nervous system.

Subpopulations of spinal cord neurons defined by developmental origin as a stepping stone for modern systems neuroscience

Early lesion experiments established not only the critical role the spinal cord has in motor execution and especially locomotion, but also revealed interesting network properties of spinal circuits for locomotion. Namely, it was shown that even in the absence of any supraspinal inputs, by virtue of spinal transection experiments, neuronal circuits below the lesion remain in a quiescent, but functional state that can be engaged by sensory feedback or chemical mimicking of supraspinal input. Cats with chronic thoracic spinal transections show coordinated hindlimb stepping movements on a weight-supported treadmill or upon artificial sensory stimulation of the spinal cord through the dorsal roots (Shik and Orlovsky 1976, Forssberg et al. 1980, Forssberg et al. 1980). Even animals with acute high cervical transections of the spinal cord show bouts of quadrupedal stepping on a weight-supported treadmill in the presence of neuromodulatory drugs promoting locomotion (Miller and van der Meché 1976). All these experiment lead to the conclusions that networks of neurons within the

spinal cord have the autonomous ability to translate sensory or supraspinal inputs into the sophisticated, temporally precise patterns of distinct muscle activation seen during locomotion. Together with modern genetic tools developed in the chick and mouse this provides a unique opportunity to bring together functional and developmental work leading to a deeper understanding of general programs for circuit assembly in the nervous system. In the spinal cord, early work started addressing the genetic and developmental origins of motor neurons and how their axons find their appropriate muscle target through a complex interplay of transcription factors, most notably Hox-genes, and distinct expression patterns of axon guidance molecule interactions (Guthrie 2004, Dasen and Jessell 2009, Bonanomi and Pfaff 2010). Further work on sensory feedback, and especially the direct, monosynaptic proprioceptive neuron – motor neuron interaction brought together the power of development and functional readout in one of the simplest neuronal circuits in mammals and enabled the subsequent investigation of spinal networks important for locomotion on a molecular basis (Chen et al. 2003, Lemon et al. 2004). A multitude of genetic experiments have established different classes of spinal cord neurons based on their genetic, developmental and axonal wiring characteristics. One can identify 11 cardinal classes of developmental spinal progenitor domains compromised of 10 interneuron subpopulations and motor neurons. They map along the dorso-ventral axis of the neural tube during development and their unique transcription profile is established by a dorsal, ectoderm-derived TGF-β signal and a ventral, notochord-derived sonic hedgehog signal. Depending on gradient concentrations of the two molecules unique profiles of transcription factors are induced giving rise to neurons with distinct morphological properties such as positioning in the spinal cord, midline-crossing of their axons or length of their projections. Besides the ventrally located motor neuron progenitors, there are 6, early-born, dorsally-derived (dI1 – dI6) and 4 late-born, ventrally-derived (V0 – V3) spinal progenitor classes (Jessell 2000, Kiehn 2006, Goulding 2009, Alaynick et al. 2011, Arber 2012). This genetic "toolbox" finally allowed to target and identify genetic spinal circuit elements and relate them to very specific functional motor attributes by virtue of genetic knockouts, transient silencing or killing of the involved spinal subpopulation *in vivo*.

Studies involving the dorsally-derived dI1 – dI6 interneurons demonstrated a strong role in sensory processing of pain, touch or sensorimotor adaptations (Lai et al. 2016, Koch et al. 2018). As one example, excitatory dI3 interneurons can be targeted through the LIM homeodomain transcription factor Isl1. Selective knock-out of excitatory neurotransmission from dI3 neurons leads to specific defects in the strength and performance of grasping reflexes that could be traced back to a disynaptic pathway relaying cutaneous sensory inputs to motor neurons via dI3 interneurons through a series of electrophysiological and genetic experiments (Bui et al. 2013). Ventrally-derived V0-V3 interneurons are more engaged with direct motor functions during locomotion or fine, skilled behaviors. The V0 progenitor domain can be targeted via the expression factor Dbx1 and is involved in interlimb coordination via commissural neurons interconnecting the two sides of the spinal cord, with genetic knock-out animals showing a distinct hopping phenotype (Lanuza et al. 2004, Talpalar et al. 2013). Interneurons derived from the V1 population and targetable through the transcription factor En1 have an established role in setting the speed of locomotion, while Sim1-positive, V3 derived neurons are important for the locomotor rhythm (Gosgnach et al. 2006, Zhang et al. 2008). One of the functionally most diverse population of neurons is the V2 population. While the V2a population also has a role in interlimb coordination, likely interacting with the V0 population, the V2b derived population is more involved with the intralimb coordination between antagonistic flexors and extensors of one limb (Crone et al. 2008, Crone et al. 2009, Britz et al. 2015, Callahan et al. 2019). Additionally, a population of V2a neurons with ascending projections to the precerebellar brainstem nucleus lateral reticular nucleus (LRN) has been shown to be important for accurate, skilled reaching movements (Azim et al. 2014). Beyond these 11 cardinal progenitor domains, more subpopulations are beginning to emerge. For example, modern sequencing methods have already established a much finer readout and approach to identifying these subpopulations and future experiments will show how these relate to function and overall circuit assembly (Bikoff et al. 2016, Gabitto et al. 2016, Hayashi et al. 2018, Sweeney et al. 2018).

Together these experiments establish developmentally defined, molecular spinal subpopulations and networks involved in specific aspects of motor behavior or sensory processing and allow for the potential identification of translational entry points to develop efficient therapies for spinal cord injury or chronic pain. Further spinal cord and whole nervous system circuits for locomotion will be discussed in more detail in chapter 5.

Interlimb coordination during locomotion – connecting distributed neuronal networks

In quadrupedal animals, locomotion can be subdivided into three main muscle coordination categories working together to achieve a reliable locomotor pattern. First, there is the intralimb coordination of muscles within one extremity to establish a firm stance and swing phase executed by antagonistic flexor and extensor muscle pairs. Second coordination in between two limbs at the forelimbs or the hindlimbs is needed for an accurate alternation or synchronization depending on your gait. Finally, coordination in between forelimbs and hindlimbs is required for accurate locomotion. While neuronal circuits involved in the first two categories, intralimb and interlimb coordination at the same axis (e.g. hindlimbs), have been studied quite extensively (Gosgnach et al. 2006, Crone et al. 2008, Zhang et al. 2008, Crone et al. 2009, Talpalar et al. 2013, Britz et al. 2015, Callahan et al. 2019), not much is known about the neuronal substrates involved in the long-distance coordination of fore- and hindlimbs. Circuits required for long-distance interlimb coordination are located within the spinal cord as demonstrated by high cervical spinal cord transections in cats who still show coordinated quadrupedal locomotion on a weight supported treadmill under the influence of locomotion-promoting drugs (Miller and van der Meché 1976). This is further exemplified in experiments using an in vitro bath preparation of extracted neonatal spinal cords with neuromodulatory drugs inducing fictive locomotion (Kiehn and Butt 2003). Here, quadrupedal coordination of bilateral cervical and ventral roots during fictive locomotion is critically dependent on the activity of neurons projecting across multiple spinal segments (Juvin et al. 2005, Juvin et al. 2012). This demonstrates the existence of long projecting neuronal circuits interconnecting the

cervical and lumbar spinal, but essentially nothing is known about their identity, wiring pattern and if and how they contribute to interlimb coordination.

In chapter 3, we identified long projection neurons connecting the cervical and lumbar enlargement of the spinal cord and show opposing projection patterns depending on neurotransmitter identity. Further subdivisions can be made into distinct long projection neurons derived from selected progenitor domains. Functional studies to ablate long projection neurons *in vivo* resulted in reduced coordination between forelimb and hindlimbs as well as decreased speed during locomotion. Together we demonstrated the existence and importance of a long projecting, molecularly defined spinal network important for interlimb coordination.

2.2. The brainstem

Upon transitioning rostrally from the spinal cord to the brain, the brainstem represents the first brain structure to encounter. Originally, the brainstem has been involved in many autonomous homeostatic functions such as stress-related adaptations of blood pressure or breathing (Ulrich-Lai and Herman 2009, Feldman et al. 2013, Ghali 2017, Del Negro et al. 2018), relaying sensory information from the periphery (Appler and Goodrich 2011, Kitazawa and Rijli 2018, Palmiter 2018) or sleep (Weber and Dan 2016). There is also a lot of evidence that the brainstem has a critical role in active control of motor output signaling most notably coming from lesion experiments and electrical stimulations. Early work in cats and later in rodents demonstrated that many motor functions, such as locomotion, mating and feeding are preserved and unaffected upon removal of the cortex pointing to subcortical circuits involved in motor behaviors (Bjursten et al. 1976, Kawai et al. 2015, Otchy et al. 2015). Other lesion studies in different species in subcortical areas pointed to the brainstem as an important structure harboring circuits essential to motor behavior (Lawrence and Kuypers 1968, Shik and Orlovsky 1976, Roh et al. 2011). Additionally, multiple higher-order motor centers have strong projections to the brainstem including cortical structures and basal ganglia output nuclei (Li et al. 2015, Capelli et al. 2017, Caggiano et al. 2018, Mercer Lindsay et al. 2019). Electrical stimulation experiments showed that there are several sites within the mammalian brainstem

from which different motor behaviors can be elicited, most notably locomotion within the mesencephalic locomotor region (MLR) as the prominent and best studied site. Here, unilateral electrical stimulation of the MLR elicits coordinated, quadrupedal locomotion whose speed correlates with stimulation strength (Shik et al. 1966, Shik and Orlovsky 1976, Skinner and Garcia-Rill 1984, Garcia-Rill et al. 1987, Mori et al. 1989, Takakusaki et al. 2016). However, besides the MLR there are many other regions and structures within the brainstem whose electrical stimulation elicits motor behavior, albeit not as natural and coordinated as locomotion through the MLR. Different stimulation protocols and sites within the midbrain, pons and medulla elicit movements of all four, two or a single limb, adjustments to posture or movements involving the head, but few of them really resembling any kind of naturalistic behaviors (Ross and Sinnamon 1984, Drew and Rossignol 1990). Additionally, in several sites within the brainstem, motor related neural activity has been observed (Drew et al. 1986, Buford and Davidson 2004, Schepens and Drew 2004, Soteropoulos et al. 2012). Nevertheless, even within the MLR, there is controversy as to which is the exact site and neuronal population that elicits locomotion. On top different kind of locomotor behaviors from slow, exploratory to high-speed and targeted have been observed at slightly different MLR positions (Jordan 1998, Takakusaki et al. 2016). All of these experiments point towards a crucial role of the brainstem in motor behavior beyond only spatial location of neurons, but instead hinting at circuits composed of intermingled and interacting subpopulations involved in distinct actions. In recent years, combinatorial approaches bringing together mouse genetics, viral and optogenetic tools, modern electrophysiology and sophisticated behavioral readouts have allowed to begin the dissection of the complex brainstem networks involved in motor control.

The brainstem as an orchestrator of diverse body actions from breathing to locomotion
To address the ambiguity surrounding the MLR and the involved subpopulations and locations for locomotion, optogenetic tools to selectively target a distinct subpopulation and control its activity with high temporal specificity were used (Niell and Stryker 2010, Lee et al. 2014, Roseberry et al. 2016, Caggiano et al. 2018, Josset et al. 2018). These experiments revealed

that within an intermingled mix of glutamatergic, cholinergic and inhibitory neurons in the MLR, the glutamatergic population is the only one able to elicit locomotion, whereas the inhibitory population stops ongoing motor actions, while cholinergic stimulation leads to variable results in terms of locomotor output, potentially relatable to neuromodulation (Caggiano et al. 2018, Josset et al. 2018). Further usage of similar tools lead to the discovery of distinct functional subpopulations within the MLR differently impacting on locomotion. While the excitatory neurons in the pendunculopontine nucleus (PPN), as one anatomical part of the MLR, only elicited slow, longer latency locomotion, the adjacent excitatory neurons in the cuneiform nucleus (CnF) were able to trigger short latency, high-speed locomotion depending on the strength of stimulation (Caggiano et al. 2018, Josset et al. 2018). The revelation of different MLR subpopulations and their differential involvement in locomotion represents a solid stepping stone to further investigate the implementation of these locomotor signals in downstream circuitry within the brainstem and the spinal cord.

Early experiments have suggested that downstream implementation of MLR output signals is dependent on a relay station in the caudal brainstem. Most notably cooling experiments in the caudal brainstem weakened MLR elicited locomotion (Orlovsky et al. 1999, Ryczko and Dubuc 2013, Brownstone and Chopek 2018). However, the exact circuitry and neuronal populations involved in this remained elusive. Using similar approaches as in the MLR to combine the power of mouse genetics with viral and optogenetic tools, distinct subpopulations in medial regions of the medulla were identified that are important for halting or during high-speed locomotion (Bouvier et al. 2015, Capelli et al. 2017). Even more strikingly compared to the MLR, subpopulation identity of targeted circuit elements proved to be of crucial importance. While optogenetic stimulation of all neurons together did not have any effect, the distinguished targeting of excitatory or inhibitory neurons revealed their opposing roles in controlling the speed of locomotion (Capelli et al. 2017). Importantly these medial medullary regions show direct projections to the spinal cord and are therefore in a prime position to serve as a link between instructive and executive locomotor signals in the brain and spinal cord respectively (Bouvier et al. 2015, Capelli et al. 2017). While there are certainly still a lot of unknowns as to

how locomotion is controlled, e.g. with multiple other sites inducing being involved in locomotion as well the role of behavioral state (Shik and Orlovsky 1976, Han et al. 2017, Evans et al. 2018), these studies are a clear example of how studying distinct circuit components is advancing the understanding of brainstem circuits for action.

Besides locomotion, quadrupedal animals can engage in two other behavioral categories that are strongly dependent on brainstem circuitry. First there are orofacial movements such as eating, licking or breathing that are mostly performed by muscles of the face, head and neck. Second there are motor actions involving the forelimbs ranging from simple reaching movements all the way to complex acts such as grasping or manipulating objects. This behavioral categorization is discussed in more detail in chapter 6. Orofacial behaviors represent a very appealing case to study the interplay between different, but related motor actions, imagining just the simple act of eating in which movements of the jaw, the tongue, as well as the breathing rhythm need to be coordinated with each other to be performed correctly. Most of these behaviors are rhythmic in nature, and the identification and interplay between these rhythms has been studied extensively behaviorally as well as by revealing involved brainstem circuitry (Welzl and Bures 1977, Travers et al. 2000, Naganuma et al. 2001, Moore et al. 2013, Kleinfeld et al. 2014, Moore et al. 2014, Morquette and Kolta 2014, Deschenes et al. 2016, Kurnikova et al. 2017, Del Negro et al. 2018, McElvain et al. 2018). A majority of structures involved are located in the medulla but in more lateral positions than neuronal populations important for locomotion and conversely to body movements these circuits are in close proximity to their motor neurons, which are organized into distinct motor nuclei within the brainstem (Guthrie 2007). In one study, careful behavioral tracking of whisking and breathing movements in rodents showed a tight temporal coupling in the oscillatory nature of these behaviors that can be traced back to two distinct brainstem oscillators in the intermediate reticular nucleus (IRt) and the preBötzinger complex (preBötz) for whisking and breathing respectively. Inactivation and recording experiments further demonstrated the special nature of the breathing oscillator in the preBötz as a master regulator of other orofacial behaviors (Moore et al. 2013).

All together a brainstem picture emerges of a structure that integrates distinct motor plans or choices and acts as a commanding and coordinating center to engage the specific circuits crucial for the precise execution of a desired motor action. This emergent brainstem properties and the integration into higher motor circuits will be discussed in more detail in chapter 5 and 6.

Brainstem circuits in the context of forelimb behaviors

Forelimb behaviors represent the third large group of motor behaviors besides whole-body movements such as locomotion and orofacial behaviors and are also strongly dependent on brainstem circuits. Recording experiments in rodents, cats and monkeys showed forelimb related neuronal activity in neurons in different parts of the midbrain, pons and medulla (Buford and Davidson 2004, Schepens and Drew 2004, Soteropoulos et al. 2012). Additionally, upon systematic screening of the cat medulla with electrical stimulations, distinct sites in the medulla and pons were discovered to reliably evoke unilateral and bilateral forelimb dominated movements (Ross and Sinnamon 1984, Drew et al. 1986). Also, lesioning or silencing experiments of different parts of brainstem regions or projections demonstrated a clear role in forelimb-dominated behaviors. In one classical study, monkeys recovered essentially all motor functions except fine finger dexterity upon lesions of the corticospinal tract, subsequent lesions in the same animal of specifically the lateral medulla however abolishes essentially all forelimb-specific movements permanently, but importantly does not impact much on whole body behaviors such as locomotion (Lawrence and Kuypers 1968, Lemon et al. 2012). Further, lesions in rodents of the dorsolateral tract in the spinal cord, in which most descending lateral brainstem neurons project, leads to specific defects in a reaching behavior (Morris et al. 2011). Another study in mice, showed the importance of the medullary reticular formation, ventral part (MdV) in the most caudal medulla for grasping movements specifically (Esposito et al. 2014). Together these experiments point at yet again intermingled, distinct circuit elements within the brainstem important for forelimb behaviors. However, almost nothing is known about the

identity of subpopulations, circuit organization or how distinct forelimb movements from simple to complex are constructed with brainstem circuitry.

Here in chapter 4, we show the existence of reaching and handling related neural activity differentially encoded in distinct ensembles along the dorsoventral axis in the lateral rostral medulla (latRM) in freely moving mice. This physiological organization coincides with distinct, largely non-overlapping anatomical subpopulations of excitatory neurons within the latRM that can be identified based on their projection patterns within the medulla and the spinal cord. Optogenetic activation of these subpopulations elicits different forelimb movements with varying degrees of complexity ranging from simple reaching movements to complicated movement sequences as seen during handling and eating food. We further demonstrate the necessity of these neurons for precise directional targeting during a reaching movement and relate this to the presence of reaching directionality-encoding latRM neurons. Together, we unravel neuronal circuitry in the lateral rostral medulla that is implicated in the coordination and diversification of distinct forelimb movements through specific connectivity within and between the brainstem and the spinal cord.

3. Long-Distance Descending Spinal Neurons Ensure Quadrupedal Locomotor Stability

Ludwig Ruder, Aya Takeoka and Silvia Arber

3.1. Abstract

Locomotion is an essential animal behavior used for translocation. The spinal cord acts as key executing center but how it coordinates many body parts located across distance remains poorly understood. Here we employed mouse genetic and viral approaches to reveal organizational principles of long-projecting spinal circuits and their role in quadrupedal locomotion. Using neurotransmitter identity, developmental origin and projection patterns as criteria, we uncover that spinal segments controlling fore- and hindlimbs are bidirectionally connected by symmetrically organized direct synaptic pathways that encompass multiple genetically tractable neuronal subpopulations. We demonstrate that selective ablation of descending spinal neurons linking cervical to lumbar segments impairs coherent locomotion, by reducing postural stability and speed during exploratory locomotion, as well as perturbing interlimb coordination during reinforced high-speed stepping. Together, our results implicate a highly organized long-distance projection system of spinal origin in the control of postural body stabilization and reliability during quadrupedal locomotion.

3.2. Introduction

Locomotion is a universal and robust animal behavior to efficiently translocate from one place to another. In quadrupedal animals, whole body stabilization in concert with the precise timing and sequence of limb movements is a prerequisite to ensure smooth locomotion at different speeds. Even in bipedal species like humans, efficient walking depends on the leg and arm coordination aligned with body stabilization and has been hypothesized to use evolutionarily conserved pathways (Wannier et al. 2001, Dietz 2002, Dominici et al. 2011). To understand how locomotor reliability is regulated in limbed animals, it is critical to identify and understand the function of neuronal circuit elements central to the coordination of the different aspects of locomotion.

Quadrupedal locomotion requires continuous postural adjustments involving the finely tuned coordination of trunk and limb muscle contraction patterns (Gramsbergen 1998, Ivanenko et al. 2004, Ceccato et al. 2009). Acting within this background of body stabilization, translocation to propel the body forward depends on coordinated limb movements that can roughly be divided into three behavioral subroutines. First, within a single limb, patterns of complex muscle synergies are activated sequentially contributing to stance and swing as two main locomotor phases (Brown 1911, Krouchev et al. 2006). Second, in most quadrupedal species including rodents, pairs of fore- or hindlimbs on opposite sides of one girdle exhibit left-right alternation and at high speed, shift to gaits with more synchronous movement patterns (English and Lennard 1982, Grillner 2006, Kiehn 2011, Bellardita and Kiehn 2015, Lemieux et al. 2016). Third, fore- and hindlimbs are diagonally coupled during locomotion dominated by left-right alternation and these patterns are adjusted with different gaits (Miller et al. 1975, English and Lennard 1982, Bellardita and Kiehn 2015, Lemieux et al. 2016).

Spinal cord transection experiments were helpful to begin to dissect which parts of the nervous system support locomotion by coordinating movement of distributed body parts. Cats with thoracic spinal cord transection still produce hindlimb stepping with patterned extensor-flexor

muscle contractions and left-right limb alternation on a weight-supported treadmill (Forssberg et al. 1980, Forssberg et al. 1980), but the coordination between fore- and hindlimbs is disrupted (Eidelberg et al. 1980). In contrast, cats with high cervical transection carry out episodes of coordinated quadrupedal locomotion upon systemic application of locomotion-promoting drugs to mimic activity of severed supraspinal centers (Miller and van der Meche 1976). Together, these experiments have put forward the idea that spinal neurons linking cervical and lumbar segments might play a role in regulating quadrupedal locomotion, but genetic identity, diversification and function of involved neurons in intact animals are currently unknown.

Many studies demonstrate that neuronal subpopulations contributing to local spinal circuits exhibit distinct roles in locomotion based on progenitor domain origin marked by differential transcription factor expression during development (Goulding 2009, Alaynick et al. 2011, Kiehn 2011, Arber 2012). For example, whereas V1 and V2b interneurons are important for the regulation of extension-flexion (Zhang et al. 2014, Britz et al. 2015), V0 and V2a interneurons are needed for coordination of left-right limb movements (Lanuza et al. 2004, Crone et al. 2008, Crone et al. 2009, Talpalar et al. 2013). In contrast, genetic identity and possible neuronal diversity of long-distance spinal projection neurons communicating between local circuits at cervical and lumbar spinal levels remain obscure. Nevertheless, anatomical tracing studies show that bidirectional axonal projections between cervical and lumbar spinal segments exist in several species including humans (Matsushita et al. 1979, Skinner et al. 1979, Menetrey et al. 1985, Nathan et al. 1996, Dutton et al. 2006). Furthermore, electrophysiological recordings identified a diversity of response properties and supraspinal input pathways in these neurons (Skinner et al. 1980, Alstermark et al. 1987), suggesting that the overall population encompasses functional subtypes.

Here we studied long-distance projection neurons coupling cervical and lumbar segments of the mouse spinal cord to reveal their genetic identity and behavioral function in locomotion.

We found that descending projection neurons diversify into excitatory and inhibitory subsets with mirrored synaptic terminations to contra- and ipsilateral lumbar spinal segments. Within the excitatory cohort, developmental stratification by progenitor domain origin distinguishes contra- and ipsilaterally projecting populations, providing evidence for the existence of genetically tractable subgroups of long-distance spinal projection neurons. Using intersectional viral approaches to assess the function of cervico-lumbar projection neurons, we define their importance in regulating reliability of quadrupedal locomotion, including postural stability, speed control and interlimb coordination.

3.3. Results

Cervico-lumbar projection neurons diversify by neurotransmitter identity

To visualize long-distance axonal projection patterns and synaptic arborizations of spinal neurons, we first carried out unilateral injections into cervical mouse spinal cords (Figure 1A). Since neurons expressing excitatory or inhibitory neurotransmitters (NT) are functionally opposing, we studied these populations separately, using different *NT::Cre* mice. We injected double-inverted-orientation-LoxP-flanked AAVs (AAV-flex-Tag) conditionally expressing a cytosolic marker protein (AAV-flex-Tomato) and/or synaptically-tagged proteins (AAV-flex-SynTag) into spinal cords of *vGlut2^Cre* (excitatory) or *vGAT^Cre* (inhibitory) mice (Vong et al. 2011), leading to high-level marker protein expression within two weeks.

We first focused on axonal trajectories of descending cervical projection neurons (Figure 3.1.A-E; injection center at segmental levels C4-C7). Axons across multiple spinal segments project in white matter tracts surrounding the spinal grey matter (Figure 3.1. D, E). We found that both vGlut2^ON and vGAT^ON cervical neurons extend axons to lumbar levels, but they differ with respect to two important properties. Firstly, descending axons of excitatory vGlut2^ON cervical neurons persist to lumbar levels to a higher degree than axons of inhibitory vGAT^ON neurons (Figure 3.1.B), ultimately resulting in significantly more lumbar descending axons for excitatory vGlut2^ON than inhibitory vGAT^ON cervical neurons (Figure 3.1.C). And secondly, while significantly more axons derived from excitatory vGlut2^ON cervical neurons cross the midline to descend contralaterally, inhibitory vGAT^ON neurons display the opposite bias with a dominance of ipsilaterally descending axons (Figure 3.1.D).

To determine the spatial distribution of excitatory and inhibitory synaptic contacts of cervico-lumbar projection neurons in the lumbar spinal cord, we reconstructed AAV-derived SynTag protein accumulations in lumbar synaptic terminals (Figure 3.1.F-I). Synapses of both neuronal populations were strongly biased to ventral over dorsal spinal territory, and occupied mostly laminae in which motor-related interneurons and motor neurons reside (Figure 3.1.H, I). When

we quantified synapse position with respect to injection laterality, we found that the relative contributions of the two populations to ipsi- and contralateral spinal cord were mirrored. Whereas excitatory vGlut2^{ON} cervical projection neurons terminated preferentially contralaterally, inhibitory vGAT^{ON} counterparts exhibited a bias towards the ipsilateral lumbar spinal cord (Figure 3.1.H, I).

Together, these findings show that the cervical spinal cord contains both excitatory and inhibitory neurons with projections to lumbar spinal neurons located in motor-related laminae. However, there was a preference for excitatory over inhibitory cervical neurons to establish these long-range connections, and excitatory neurons preferentially contacted contralateral lumbar targets, whereas inhibitory counterparts had the opposite bias.
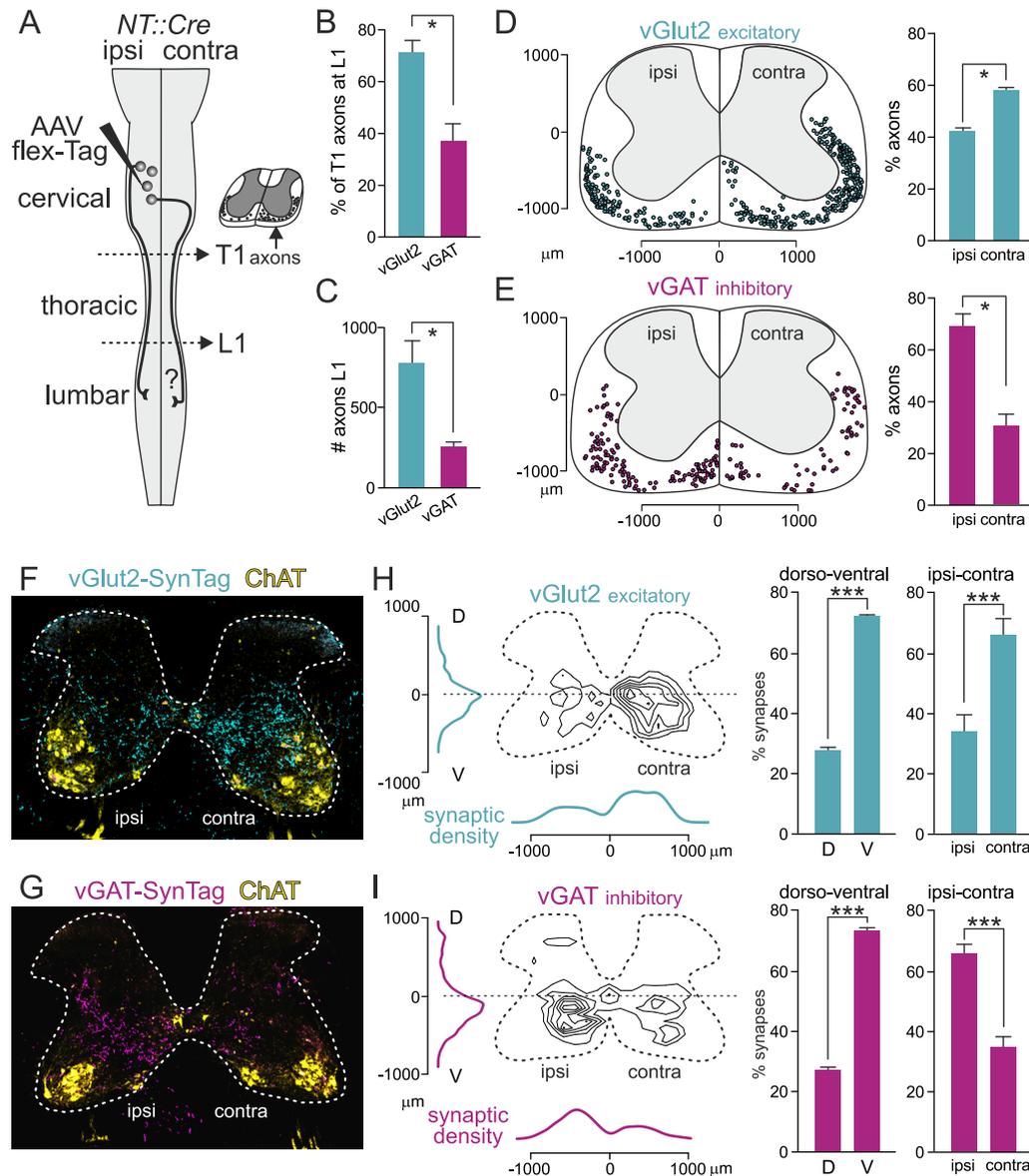
Figure 3.1. Neurotransmitter identity subdivides cervico-lumbar projection neurons

(A) Experimental strategy to visualize axonal and synaptic patterns of cervical spinal neurons projecting to lumbar spinal segments. Unilateral intraspinal cervical injection of AAV-flex-Tag viruses into mice expressing Cre recombinase from excitatory (vGlut2) or inhibitory (vGAT) neurotransmitter locus (*NT::Cre*) to assess axon number in white matter at T1 and L1 on transverse sections.

(B) Percentage of T1 axons reaching L1 spinal levels (vGlut2: n=4 mice; vGAT: n=3 mice), of experiments shown in (A).

(C) Axon counts at L1 upon cervical injections into *vGlut2^{Cre}* and *vGAT^{Cre}* mice (vGlut2: n=4 mice; vGAT: n=3 mice).

(D, E) Representative reconstruction of axon tract distribution at L3 (left) in *vGlut2^{Cre}* (D; n=4 mice) and *vGAT^{Cre}* (E; n=3 mice) mice with quantitative assessment of ipsi- and contralateral ratios (right).

(F-I) Representative images (F, G), distribution of synaptic density (left; including dorso-ventral and medio-lateral densities) as well as dorso-ventral and ipsi-contralateral ratios (right) (H, I) of SynTag terminals at L3 upon cervical spinal cord injection into *vGlut2^{Cre}* (F, H; n=8 mice) and *vGAT^{Cre}* (G, I; n=6 mice) mice.

See also Figure 3.2.

Excitatory ascending communication from lumbar to cervical spinal cord

Since communication between cervical and lumbar spinal cord is expected to be bidirectional, we next assessed whether and how lumbar spinal neurons interact synaptically with cervical neurons. We carried out unilateral injections of AAV-flex viruses expressing axonal and synaptic marker proteins into lumbar spinal segments (L2-L5) of *vGlut2^{Cre}* and *vGAT^{Cre}* mice (Figure 3.2.A). We found that excitatory vGlut2^{ON} lumbar neurons project to cervical segments. These neurons exhibited similar persistence of long-distance projections and contralateral distribution bias of synaptic terminals to the ventral spinal cord as descending cervico-lumbar counterparts (Figure 3.2.B, C). In contrast, lumbar inhibitory vGAT^{ON} neurons only very sparsely projected to the cervical spinal cord, and synaptic terminals derived from these neurons were confined mostly to ventral motor neurons at C7/8, innervating the cutaneous maximus muscle (Figure 3.2.E) (Vrieseling and Arber 2006).

Together, our findings reveal that cervical and lumbar spinal segments are bidirectionally coupled by distinct neuronal subpopulations identified by neurotransmitter identity and projection laterality. We focused our subsequent analyses mostly on the elucidation of identity and function of cervico-lumbar projection neurons, due to their predicted involvement in

transmitting supraspinal commands to lumbar circuits (Alstermark et al. 1987, Mitchell et al. 2016).
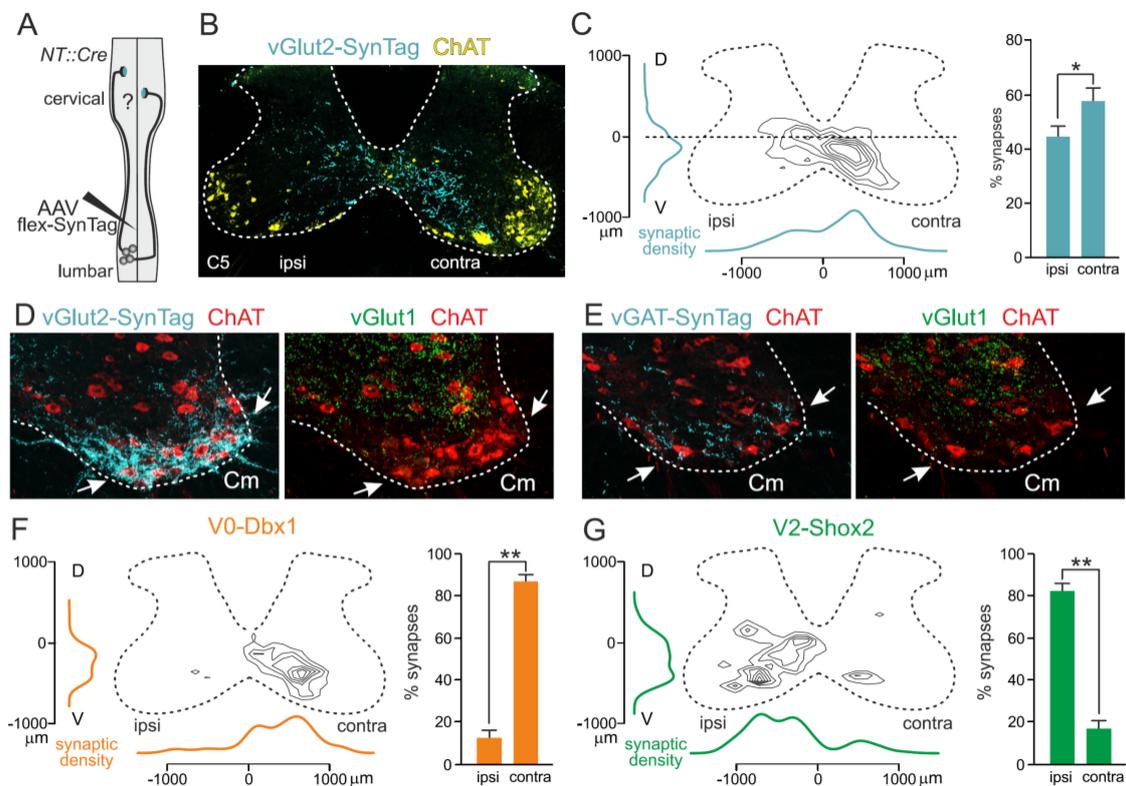
Figure 3.2. Projection neurons from lumbar to cervical spinal cord stratify into subpopulations, Related to Figure 3.1.

(A) Experimental strategy to visualize synaptic patterns of lumbar spinal neurons projecting to cervical spinal segments. Unilateral intraspinal lumbar injection of AAV-flex-SynTag viruses into mice expressing Cre recombinase from excitatory (vGlut2) or inhibitory (vGAT) neurotransmitter locus ($NT::Cre$) allows for analysis of terminal distribution of marked neurons at cervical segments. (B, C) Representative image (B) and distribution of SynTag-marked synaptic terminals depicted as synaptic density (left; including dorso-ventral and medio-lateral densities) and ipsi-contralateral ratios (right) (C) at C7 upon lumbar spinal cord injection into $vGlut2^{Cre}$ mice (n=3). Note the similarity in the organization of the projection pattern to the excitatory, descending population.

(D, E) Ascending synaptic input of lumbar vGlut2^{ON} (D) and vGAT^{ON} (E) neurons to Cm motor neurons at cervical level C7, identified by ChAT expression and lack of vGlut1 synaptic input

(arrows). Note that no other major synaptic input was detected from lumbar vGAT[ON] neurons to cervical spinal levels (data not shown).

(F, G) Distribution of SynTag-marked synaptic terminals depicted as synaptic density (left; including dorso-ventral and medio-lateral densities) and ipsi-contralateral ratios (right) at C7 upon lumbar spinal cord injection into *V0-Dbx1* (F; n=3) and *V2-Shox2* (G; n=4) mice. Note similarity in the organization of the projection pattern to the V0-Dbx1 and V2-Shox2 descending populations.

Confined residence of cervico-lumbar spinal projection neurons to ventral spinal cord

To map the precise location of cervico-lumbar projection neurons and their cellular identity, we carried out retrograde tracing experiments from the lumbar spinal cord. We labeled cervico-lumbar projection neurons by bilateral injection of Rabies viruses expressing fluorescent proteins (Rab-FP) into the lumbar spinal cord (Figure 3.3.A), an established method for efficient retrograde neuronal targeting (Wickersham et al. 2007). The majority of Rab-FP-marked cervico-lumbar projection neurons resided lateral and slightly ventral to the central canal in Rexed's laminae VII/VIII, with a second smaller cluster in the dorsal spinal cord (Figure 3.3.B-D). Comparable distribution patterns were also observed by injection of retrograde CAV-Cre into lumbar spinal segments of mice with Cre-dependent expression of tdTomato reporter protein (Figure 3.4.A), or when combined with cervical injections of AAV-flex-Tomato into wild-type mice (Figure 3.3.F). These patterns are reminiscent of the ones described before in other species using conventional tracers (Matsushita et al. 1979, Skinner et al. 1979, Menetrey et al. 1985, Nathan et al. 1996, Dutton et al. 2006).

To assess relative abundance and positioning of cervico-lumbar projection neurons with different neurotransmitters, we injected AAV-flex-TVA in the cervical spinal cord of *vGlut2[Cre]* and *vGAT[Cre]* mice, followed by lumbar axonal infection with EnvA-coated Rab-FP to specifically target neurons with lumbar projections (Figure 3.3.G). In agreement with our anterograde tracing experiments, we found that excitatory cervico-lumbar projection neurons

were targeted more efficiently than the inhibitory population. In addition, there was a bias for differential cell body distribution between these two populations with inhibitory neurons located closer to the central canal (Figure 3.3.G). Since this strategy results in much lower tracing efficiency than straight Rab-FP injections and cannot be used for quantitative purposes, we carried out Rab-FP injections into lumbar spinal cords of *GlyT2^{GFP}* mice (Zeilhofer et al. 2005). We found that only ~20% of Rab-FP marked cervico-lumbar projection neurons are glycinergic and that many of these resided in spinal territory around the central canal, compared to the broader distribution pattern of the remaining non-glycinergic cervico-lumbar projection neurons (Figure 3.3.I-J).
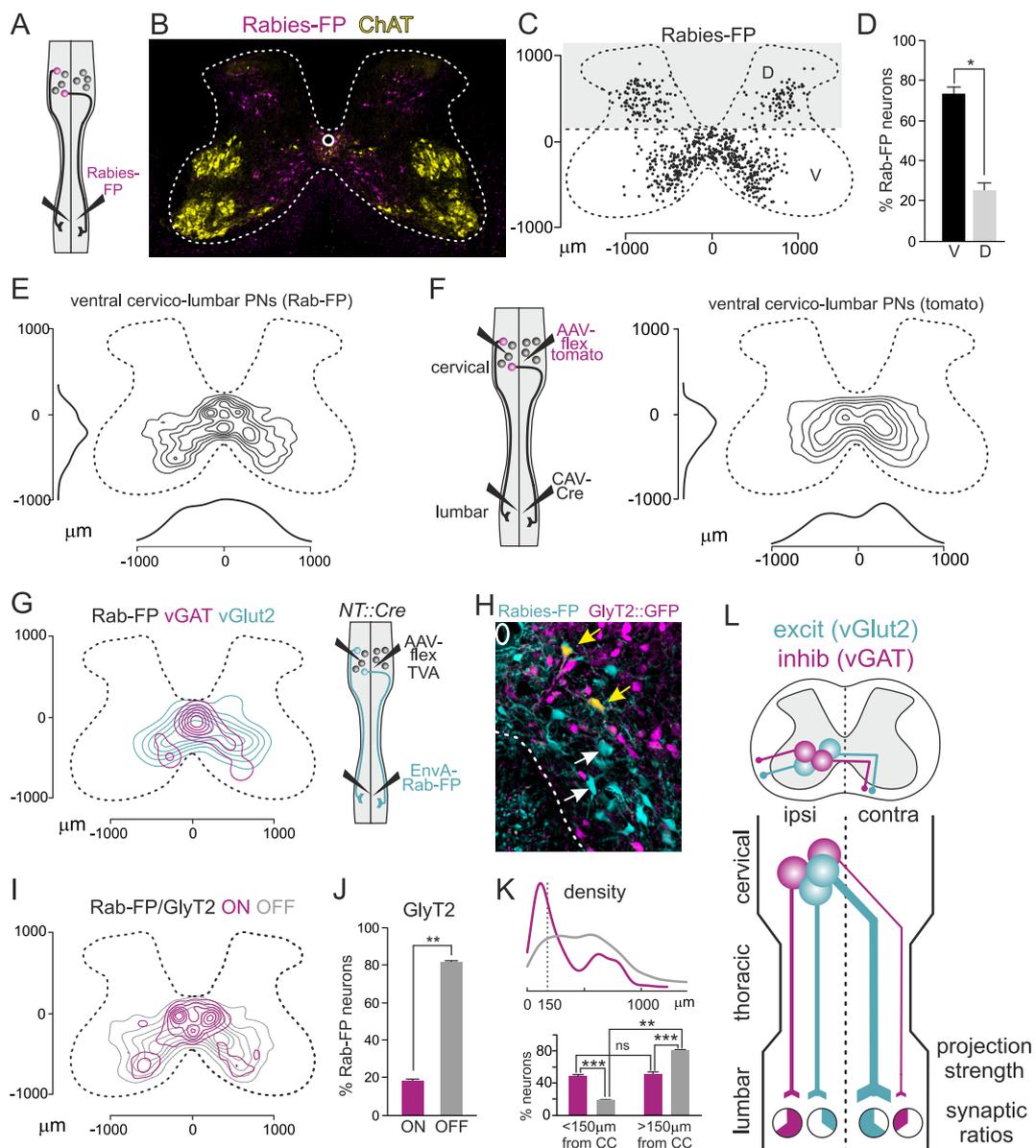
Figure 3.3. Restricted spinal distribution of cervico-lumbar projection neurons

(A) Experimental strategy to visualize cell body distribution of cervical-lumbar projection neurons by Rab-FP injection into the lumbar spinal cord.

(B) Representative image of cervical section showing Rab-FP marked cervico-lumbar projection neurons (purple) and ChAT (yellow).

(C, D) Reconstruction of Rab-FP marked cervico-lumbar projection neurons (C) and quantification of dorsal and ventral populations (D; n=3 mice), using a boundary of 150 μm dorsal to the central canal position (dotted horizontal line) as a cut-off for analysis (corresponding approximately to the ventral boundary of the dorsal funiculus). All subsequent contour plot reconstructions shown in this Figure (E-G, I) use this cut-off for analysis and focus on the ventral population since neurons in these locations are genetically accessible through progenitor domain origin and have demonstrated locomotor functions.

(E) Contour plot for distribution of ventral cervico-lumbar projection neurons marked by Rab-FP, including dorso-ventral and medio-lateral density distributions (n=3 mice).

(F) Experimental strategy (left) and contour plot of reconstructions (right) for ventral cell bodies of AAV-flex-Tomato marked cervico-lumbar projection neurons (n=6 mice).

(G) Contour plots of reconstructions for ventral vGlut2^{ON} and vGAT^{ON} cervico-lumbar projection neurons, infected by EnvA-coated Rab-FP from the lumbar spinal cord through conditionally expressed TVA in cervical neurons (right: experimental scheme).

(H-K) Representative image of Rab-FP infected cervico-lumbar projection neurons in *GlyT2::GFP* mice (H), contour plot (I), quantification (J), density from central canal (CC) and position analysis in bins <150μm and >150μm from CC (K) for reconstructions of ventral reconstructed population of GlyT2^{ON} and GlyT2^{OFF} cervico-lumbar projection neurons (n=3 mice).

(L) Summary diagram depicting division of cervico-lumbar projection neurons into four classes based on neurotransmitter status (vGlut2/vGAT) and projection/connectivity patterns.

See also Figure 3.4.

As a complementary approach and to determine whether cervico-lumbar projection neurons connect to both excitatory and inhibitory neurons at lumbar levels, we used retrograde viral transfer initiated from lumbar segments with monosynaptic restriction (Figure 3.4.B). Reconstructions of cervical spinal cords showed that cervico-lumbar neurons connect to neuronal subtypes of both neurotransmitter phenotypes in the lumbar spinal cord.

Together, these experiments establish the preferential excitatory nature of cervico-lumbar projection neurons. The position of the larger number of cervico-lumbar projection neurons makes it likely that the developmental origin of this overall population includes progenitor cells of ventral origin or neurons migrating ventrally after generation. We therefore used genetic strategies to try to target these neurons based on developmental origin by probing relevant candidate transgenic mouse lines intersectionally with viral injections.
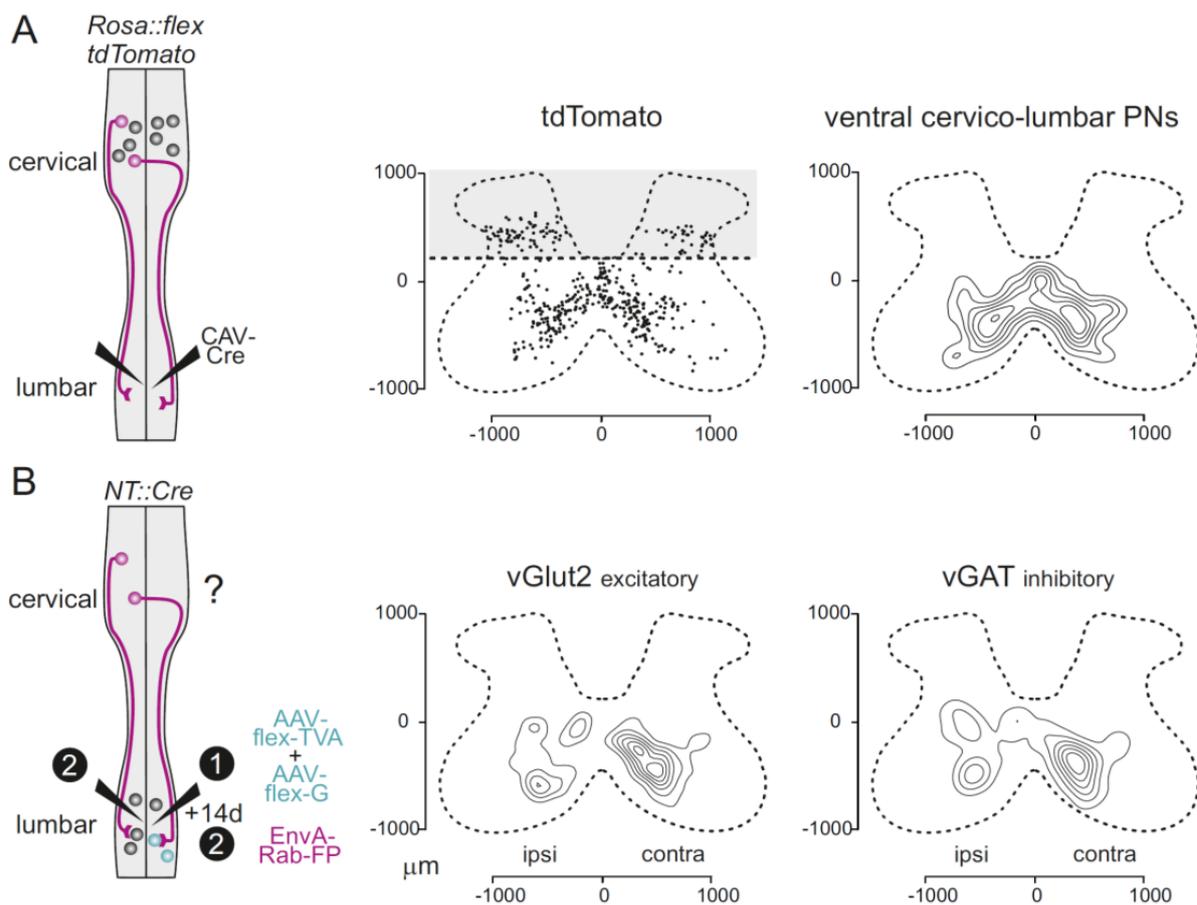
Figure 3.4. Spinal distribution of cervico-lumbar projection neurons. Related to Figure 3.3.

(A) Injection of CAV-Cre into the lumbar spinal cord of mice with Cre-dependent expression of tdTomato reporter protein (left) results in labeling of cervico-lumbar projection neurons (middle; scatter plot). These marked neurons distribute in a similar pattern as when we use two other experimental strategies depicted in Figure 2 (right; only density distribution of ventral neurons is shown, using cut-off depicted in the middle panel).

(B) Outline of experimental strategy used for displayed results. Specifically, AAV-flex-TVA and AAV-flex-G were co-injected unilaterally into lumbar spinal cord segments in $vGlut2^{Cre}$ or $vGAT^{Cre}$ mice and EnvA-coated Rab-FP was injected into the same segments bilaterally 14 days later to initiate monosynaptic transsynaptic spreading from local excitatory and inhibitory lumbar circuits (left). Note that Rab-FP marked neurons at cervical levels were found for injections into both mouse strains, indicating that both excitatory vGlut2^{ON} and inhibitory vGAT^{ON} lumbar neurons receive input from ventral cervico-lumbar projection neurons (right). For both populations, long projection neurons were detected preferentially contralaterally, indicating a predominantly contralateral bias of spinal long projection circuits.

Restricted progenitor domain origin of excitatory cervico-lumbar projection neurons

To gain genetic access to spinal neurons derived from individual transcriptionally-defined progenitor domains, we surveyed transgenic mouse lines expressing Cre-recombinase under the control of progenitor-domain specific transcription factors (Figure 3.5.A, B; *PD::Cre*). Since most developmentally expressed spinal transcription factors are no longer expressed by postnatal stages, we crossed *PD::Cre* mouse strains to mice conditionally expressing FLP-recombinase and a nuclear LacZ marker gene upon Cre recombination (*Tau^{lox-STOP-lox-FLPo-INLA}*) (Pivetta et al. 2014). We injected FLP-dependent AAVs into cervical spinal cords of mice derived from these intersectional crosses to probe connectivity of marked progenitor domain-tagged cervical neurons to the lumbar spinal cord (Figure 3.5.B).

We probed five *PD::Cre* mouse strains for their capability to mark cervico-lumbar projection neurons in this assay. While all five experimental configurations resulted in efficient marking of cervical spinal neurons at the segments of injection (data not shown), only a constellation with V0-Dbx1 (*Dbx1::CreERT2*) or V2-Shox2 (*Shox2a::Cre*), but not with V1 (*En1::Cre*), V3 (*Sim1::Cre*) or dI3 (*Isl1::Cre*) alleles resulted in labeling of cervical neurons with axonal projections to the lumbar spinal cord (Figure 3.5.C, Figure 3.6.).

V0-Dbx1 and V2-Shox2 populations were entirely distinct with respect to their projection- and arborization patterns. Axon reconstructions in the white matter showed that lumbar spinal cord-reaching axons of V0-Dbx1 cervico-lumbar projection neurons project almost exclusively contralaterally, whereas V2-Shox2-derived counterparts are restricted to the ipsilateral side (Figure 3.5.D). Moreover, also synaptic reconstructions at lumbar levels revealed an almost exclusive unilaterally restricted pattern on sides opposite to injection for V0-Dbx1 and V2-Shox2 populations, respectively (Figure 3.5.E-H). The laminar distribution of synapses of both populations was very similar, with a peak of synaptic density in the ventral spinal cord to areas with motor-related interneurons and motor neurons (Figure 3.5.G, H). When we assayed the identity of lumbar projection neurons with axons targeting cervical spinal levels, we found that the same two progenitor domains contributed to this group of neurons (Figure 3.6.F, G). Synaptic distribution patterns were also reminiscent of the cervico-lumbar projection neuron counterparts, with V0-Dbx1-derived neurons targeting contra- and V2-Shox2-derived neurons targeting ipsilateral spinal territory (Figure 3.6.F, G).

Since neurons originating from a single spinal progenitor domain can give rise to distinct neuronal subpopulations (Alaynick et al. 2011, Kiehn 2011, Arber 2012), we assessed the fraction of synaptic terminals derived from marked cervical V0-Dbx1 and V2-Shox2 neurons in the lumbar spinal cord with accumulation of the vesicular glutamate transporter vGlut2. We found that for both populations, the vast majority of terminals is derived from excitatory cervical

neurons (Figure 3.5.I, J), suggesting that V0-Dbx1 cervico-lumbar projection neurons are likely of V0v and not V0d identity (Talpalar et al. 2013).

In summary, we identified two excitatory subpopulations of cervico-lumbar projection neurons stratified by the expression of distinct transcription factors during development as well as by connectivity to divergent synaptic targets in the lumbar spinal cord. These findings indicate that cervico-lumbar projection neurons include many distinct subpopulations, making functional analysis a challenging task. For this reason, we next set up an experimental approach to specifically target and analyze the function of the overall population of cervico-lumbar projection neurons.
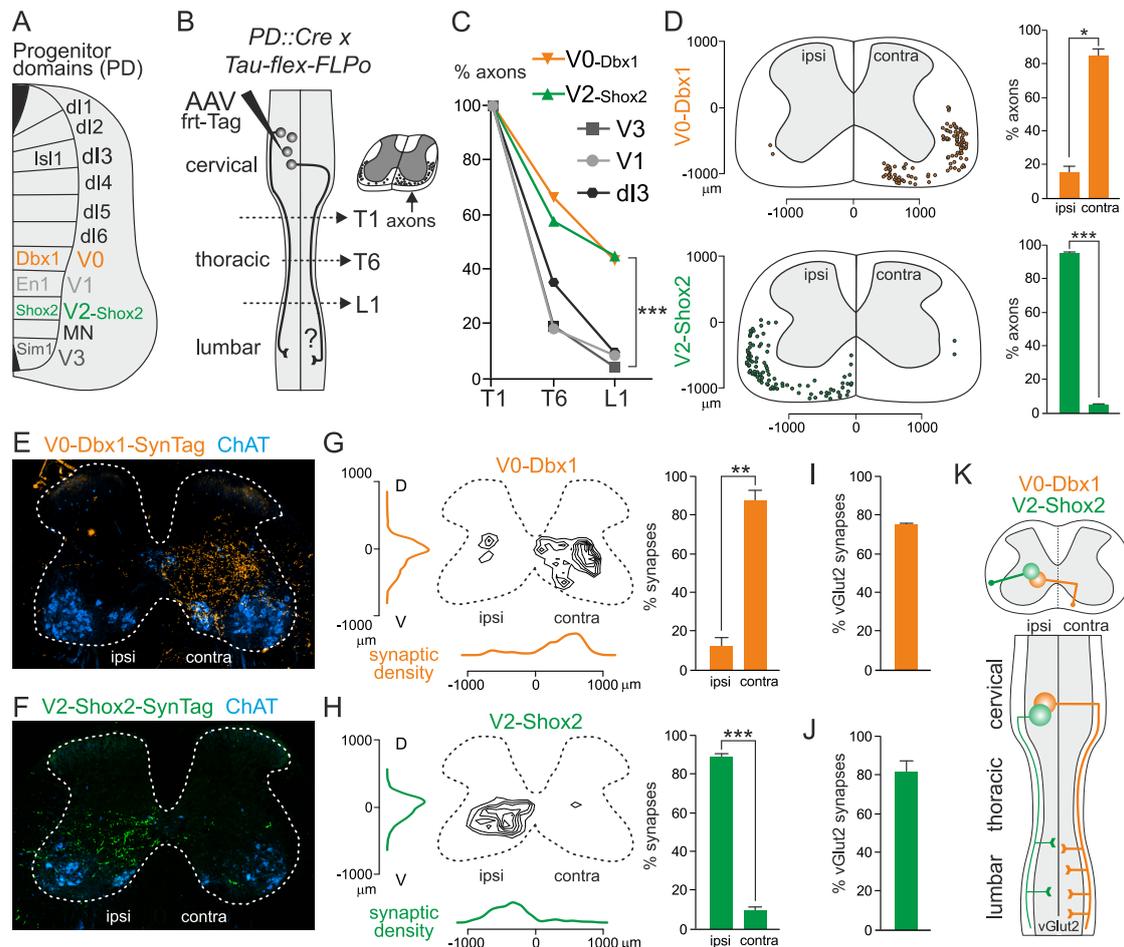
Figure 3.5. Progenitor domain origin subdivides cervico-lumbar projection neurons

(A) Scheme of spinal cord progenitor domains (dl1-dl6, V0-V3, MN) and transcription factor code of analyzed domains (dl3-Isl1; V0-Dbx1; V1-En1; V2-Shox2; V3-Sim1).

(B) Cre recombinase expression from progenitor domain transcription factor loci (*PD::Cre*) and individual mouse lines are crossed to *Tau-flex-FLPo* mice to achieve permanent expression of FLPo recombinase in neuronal descendants of different progenitor domains. Unilateral cervical spinal injection of AAV-FRT-Tag allows analysis of lumbar projections and synaptic terminals in the lumbar spinal cord.

(C) Percentage of axons at T1 segmental levels upon cervical AAV-injections as outlined in (B), reaching T6 and L1 spinal levels for different progenitor domain neuron descendants. Note that of five analyzed lines, only axons of V0 and V2-Shox2 neurons reach lumbar levels (L1) at high numbers (Dbx1: n=3; Shox2: n=4; En1: n=5; Isl1: n=4; Sim1: n=1 mice).

(D) Representative reconstruction of axon tract distribution at L3 (left) and quantification of ipsi- and contralateral ratios (right) in *V0-Dbx1* (n=3) and *V2-Shox2* (n=4) mice.

(E-J) Representative images (E, F), distribution of synaptic density (left; including dorso-ventral and medio-lateral densities), ipsi-contralateral ratios (right) (G, H; Dbx1: n=3; Shox2: n=4 mice), and percentage of vGlut2^{ON} terminals (I, J) of SynTag terminals at L3 upon cervical spinal cord injection into *V0-Dbx1* (E, G, I) and *V2-Shox2* (F, H, J) mice.

(K) Summary diagram of V0-Dbx1 and V2-Shox2 cervical projection neuron arborizations to the lumbar spinal cord.

See also Figure 3.6.
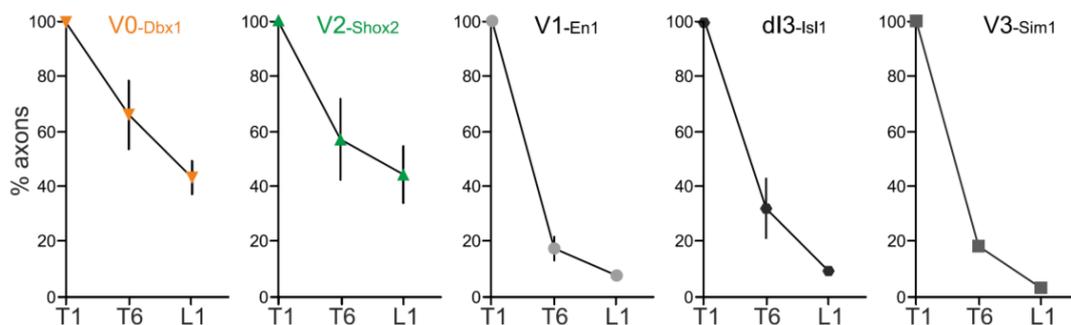
Figure 3.6. Subset of progenitor domains gives rise to cervico-lumbar projection neurons. Related to Figure 3.5.

Separate plots with error bars (SEM) for five analyzed mouse lines (Dbx1: n=3; Shox2: n=4; En1: n=5; Isl1: n=4; Sim1: n=1 mice) displaying percentage of axons at T1 segmental levels upon cervical AAV-injections of axonal tracers reaching T6 and L1 spinal levels for different progenitor domain neuron descendants (combined data without error bars are shown in Figure 3C). For these experiments, PD::Cre mouse lines were crossed to Tau-flex-FLPo mice to achieve permanent expression of FLPo recombinase in neuronal descendants of different progenitor domains.

Ablation of cervico-lumbar projection neurons impairs exploratory locomotion

To study the function of cervico-lumbar projection neurons, we used combinatorial virus targeting approaches similar to the ones validated anatomically before (Figure 3.3.F). We performed lumbar spinal injections of CAV2-Cre to retrogradely infect neurons with lumbar projections (Figure 3.8.A). To target expression of human Diphtheria toxin receptor (DTR) to cervico-lumbar projection neurons, we injected an AAV with Cre-dependent expression of DTR (AAV-flex-DTR) jointly with AAV-flex-Tomato into the cervical spinal cord (PN-DTR; Figure 3.8.A), and compared these to a control group with no or only AAV-flex-Tomato injections (PN-CON). Using this approach, ablation of cervico-lumbar projection neurons was induced by intraperitoneal application of Diphtheria Toxin (DTX) to PN-DTR mice, leading to efficient elimination of AAV-flex-Tomato-marked neurons in PN-DTR but not PN-CON mice (Figure 3.7.). This strategy allowed us to determine behavioral baseline values for individual mice of both groups in different behavioral assays (pre-DTX), and to compare performance of these mice after DTX application in the same behaviors (post-DTX; Figure 3.8.A).
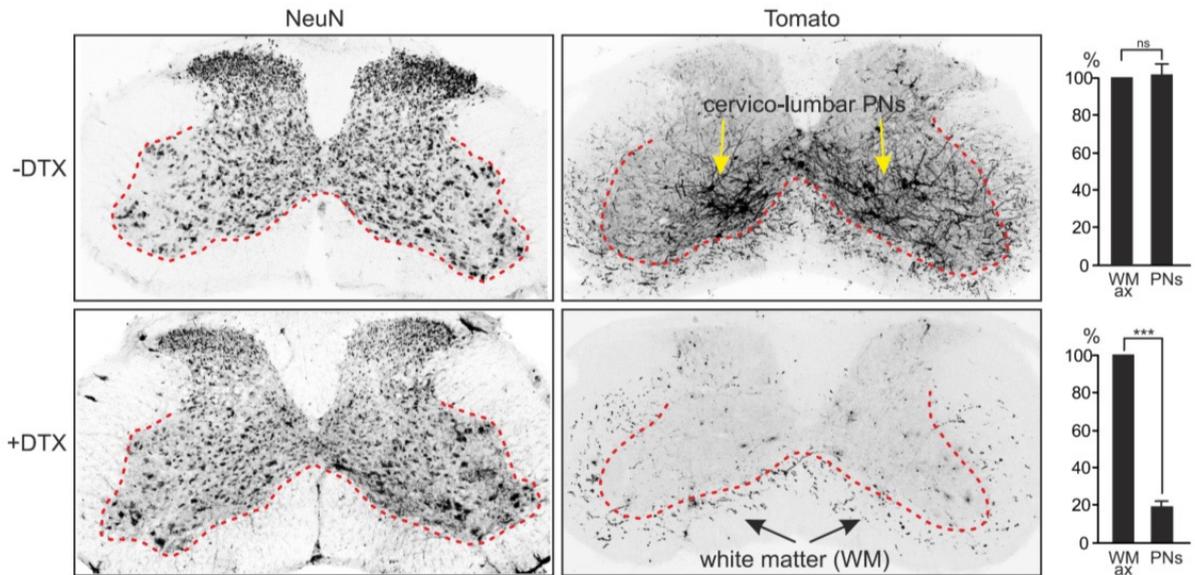
Figure 3.7. Selective ablation of cervico-lumbar projection neurons. Related to Figure 3.8.

NeuN staining (left) of representative cervical spinal cord sections before (top left) and 14 days after (bottom left) DTX injection in mice with DTR and Tomato expression in cervico-lumbar projection neurons demonstrates overall integrity of spinal cord and absence of broad excitotoxic lesion. Serial sections of the same mice stained for Tomato are shown in middle panels to illustrate elimination of DTR/Tomato expressing neurons 14 days after DTX injections. Graphs to the right show quantification of neuronal ablation efficiency by performing a normalization of the number of marked cervico-lumbar projection neurons (PNs) at segmental levels of AAV injection (C4-7) to the number of white matter axon fragments (WM ax) on transverse sections below injection (T1). Data shown include mice before (top; n=6 mice) and 14 days after (bottom; n=10 mice) DTX injection. Note that before DTX injection, WM axon number and PN neuron number is not significantly different, but there is a highly significant reduction 14 days after DTX injection.

We first analyzed spontaneous exploratory behavior in an open field area. Mice navigate through the open field territory in locomotor bouts typically interrupted by stationary episodes including grooming or rearing. To restrict quantitative analysis to locomotor behavior, we tracked the center of body mass of mice and extracted locomotor bouts with a defined

threshold for locomotor onset (>200ms at >5cm/s) and termination (<5cm/s). Disassembly of the exploratory behavior into chunks allowed locomotor bout extraction as separate behavioral episodes to evaluate and analyze their structure (Figure 3.8.B; Experimental Procedures).

We found that before cervico-lumbar projection neuron ablation, tracks of locomotor bouts were generally smooth until the end of an episode for both PN-CON and PN-DTR mice (Figure 3.8.C, D). When we analyzed the same mice 14 days after DTX injection, we observed no changes for PN-CON mice (Figure 3.8.C, D). In contrast, locomotor trajectories of PN-DTR mice after neuronal ablation were uneven reflecting postural instability. This property was captured quantitatively in tracked bouts by significantly higher turning angles compared to time points before ablation in these mice, or to PN-CON mice analyzed at the same time after DTX application (Figure 3.8.C). Together, these data indicate that cervico-lumbar projection neuron ablation leads to impairment in postural stability during the execution of locomotor bouts in exploratory behavior.

To determine whether PN-DTR mice exhibit additional defects, we next analyzed other parameters extracted from isolated locomotor bouts (Figure 3.8.E-G). To visualize the distance of many locomotor bouts, we aligned starting points of individual events to a central point (Figure 3.8.E). Whereas in PN-CON mice, average distance of locomotor bouts before and after DTX application was not significantly different, in PN-DTR mice, we found a significant decrease after cervico-lumbar projection neuron ablation compared to baseline (Figure 3.8.E, G). Despite this decrease, there was no difference in the average duration of locomotor bouts between experimental and control groups (Figure 3.8.G). This observation indicates that once initiated, the readiness to complete explorative locomotion is not affected in PN-DTR mice. The most likely reason for shorter-distance locomotor bouts after cervico-lumbar projection neuron ablation therefore is the appearance of significantly decreased maximum speed parameters (Figure 3.8.G), as also depicted in representative individual trial speed traces along locomotor bout duration (Figure 3.8.F). To get a precise assessment of this phenotype

at the level of individual locomotor events, we plotted the fractions of measured locomotor episodes in relation to their associated maximal speed values (Figure 3.8.H). Whereas the fractional distribution of maximal speed-stratified events remained the same for PN-CON mice before and after DTX application, we found a decrease of locomotor events at high speeds and an increase in lower speed events in PN-DTR mice after DTX application (Figure 3.8.H).

Together, these findings demonstrate that the ablation of cervico-lumbar projection neurons impairs proficiency of exploratory locomotion, notably leading to postural instability accompanied by decreases in speed but not duration of locomotor bouts.
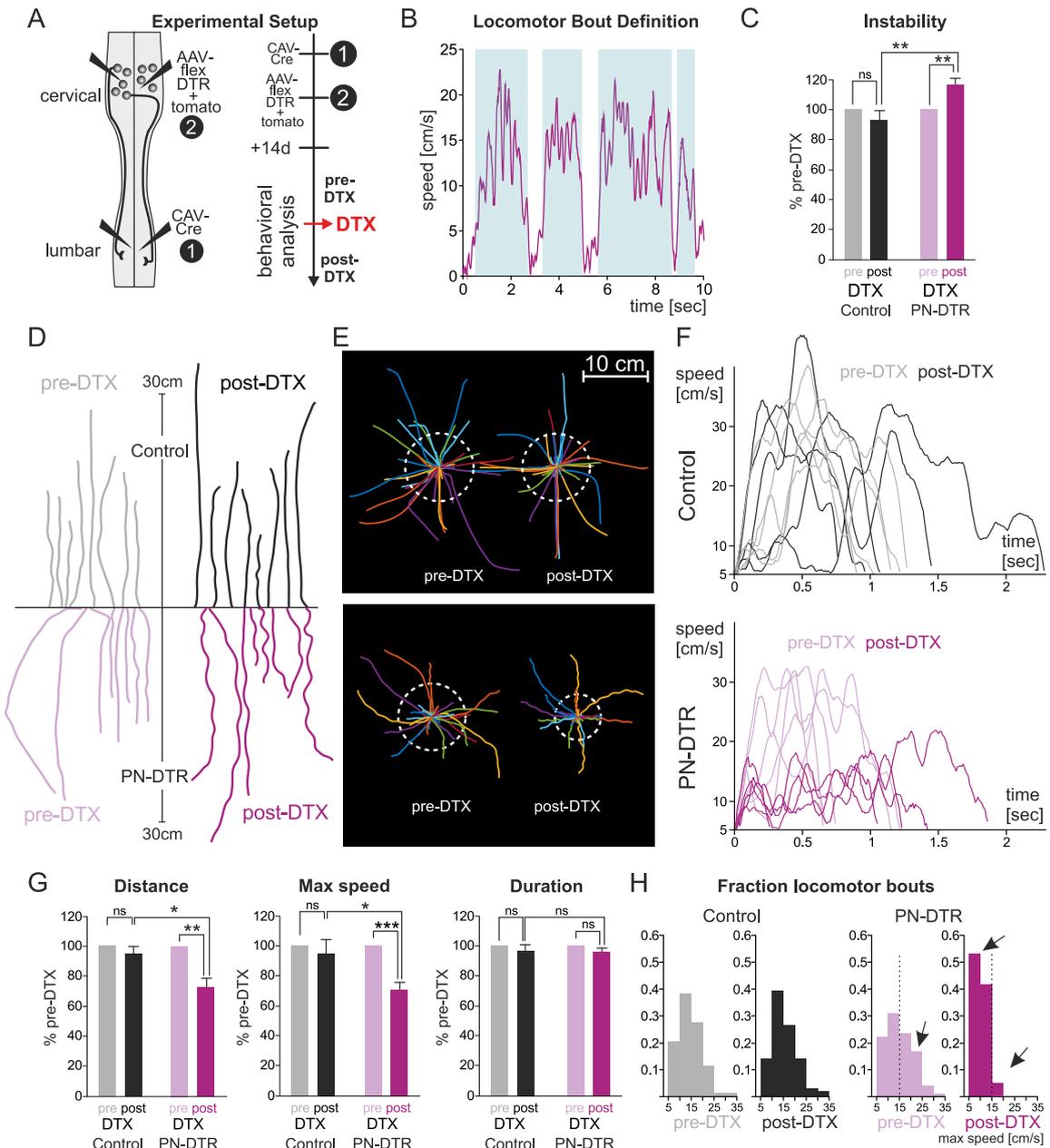
Figure 3.8. Ablation of cervico-lumbar projection neurons impairs exploratory locomotion

(A) Scheme of cervico-lumbar projection neuron targeting strategy and time line for behavioral analyses.

(B) Representative plot illustrating the definition of a locomotor bout (light blue window) during open field exploration with a threshold for locomotor onset (>200ms at >5cm/s) and termination (<5cm/s).

(C, D) Quantification of postural instability (C) and representative example traces (D) of locomotor bouts for control (n=7) and PN-DTR (n=10) mice before (left) and 14 days after (right) DTX injection.

(E) Representative locomotor bout traces for control and PN-DTR mice before and 14 days after DTX injection, displayed in different colors and centered according to initiation time point (white dashed line indicates average distance of locomotor bouts).

(F) The five highest speed trials for one representative mouse of each control and PN-DTR group before and 14 days after DTX injection are displayed in a speed versus time plot.

(G) Quantification of distance, maximal speed and duration for control and PN-DTR group before and 14 days after DTX injection.

(H) Fractional analysis of locomotor bouts with respect to maximal speed achieved during each of the analyzed bouts for one representative mouse of each control and PN-DTR group before and 14 days after DTX injection (0/6 PN-CON and 8/10 PN-DTR mice with $p<0.05$ changes in speed histogram distribution before and 14 days after DTX injection).

See also Figure 3.7.

Cervico-lumbar neuron ablation impairs limb coordination in high-speed locomotion

Since our previous unsupervised exploratory locomotor analysis showed a decrease in high-speed locomotor bouts in mice with ablated cervico-lumbar projection neurons, we next studied locomotor kinematics on a speed-controlled treadmill (Takeoka et al. 2014). We chose 20cm/s corresponding to an average exploratory speed and 40cm/s as a speed above the highest maximum speed of most locomotor bouts in the open field that can be accommodated by all mice.

To quantify interlimb coordination, we measured phase relationships of all four limbs, using the left hindlimb as a reference limb. At 20cm/s treadmill speed, PN-DTR mice before or after DTX injection exhibited antiphasic relationships between left and right hindlimbs, as well as between left hind- and forelimbs, analyzed using stance-swing timings as criteria to determine

phase values (Figure 3.10.A). At 40cm/s treadmill speed, PN-CON mice showed no difference in phase relationship before and after DTX injection (Figure 3.10.B), consistent with previous findings that wild-type mice alternate homologous limbs and show the same phase relationship for diagonal fore- and hindlimbs at this speed (Bellardita and Kiehn 2015). In contrast, while the same reliable phase relationship was present in all PN-DTR mice before DTX injection, the majority of PN-DTR mice (n=5/6) exhibited interlimb coordination defects 14 days after DTX application (Figure 3.9.A, B, 3.10.C). Notably, at 40cm/s, there was a significant defect in the phase relationship between the left and right hindlimb, with clusters of steps during which PN-DTR mice used synchronous hindlimb gait, but alternating stepping for forelimbs (Figure 3.9.B). Even though we observed interlimb coordination defects in PN-DTR mice at 40cm/s, we did not detect obvious abnormalities in intralimb coordination during regular stepping episodes upon cervico-lumbar projection neuron ablation (Figure 3.9.C, D). Interestingly, at maximal speeds (50-60cm/s) achieved by mice with interlimb coordination defects, we also frequently detected forelimb- in addition to the hindlimb coordination defects (Figure 3.10.E). Together, these data provide evidence that ablation of cervico-lumbar projection neurons leads to speed-dependent interlimb coordination defects in the majority of mice.
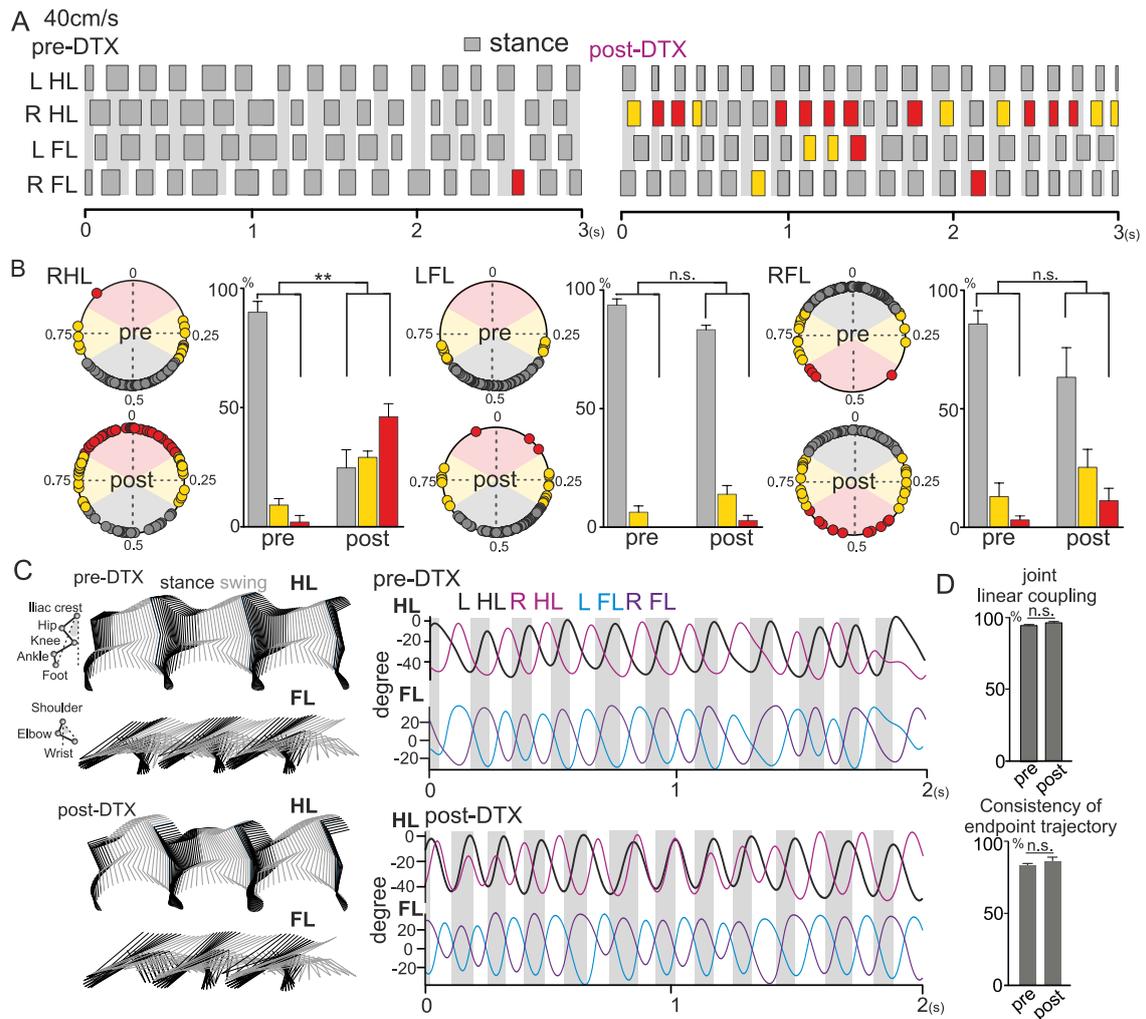
Figure 3.9. Cervico-lumbar projection neuron ablation impairs gait at high speeds

(A, B) Representative example and quantification of interlimb coordination for PN-DTR mice (n=6) at 40cm/s treadmill speed before (pre) and after (post) cervico-lumbar projection neuron ablation. Each analyzed step is categorized as gray, yellow and red depending on the calculated phase value (Satoh et al. 2016) and as defined in the Experimental Procedures. Phase values of right hindlimb (RHL), left and right forelimb (LFL, RFL) are in reference to the left hindlimb (LHL). Compiled circular phase value plots and bar plots of corresponding experiments displaying the percentage of corresponding categories are shown in (B).

(C) Reconstructed fore- and hindlimb trajectories and a representative example of calculated fore- and hindlimb oscillation at 40cm/s before and after cervico-lumbar projection neurons ablation are shown.

(D) Intralimb coordination parameters including the degree of linear coupling of joint oscillation and the consistency of endpoint trajectory are not affected by cervico-lumbar projection neuron ablation.

See also Figure 3.10.
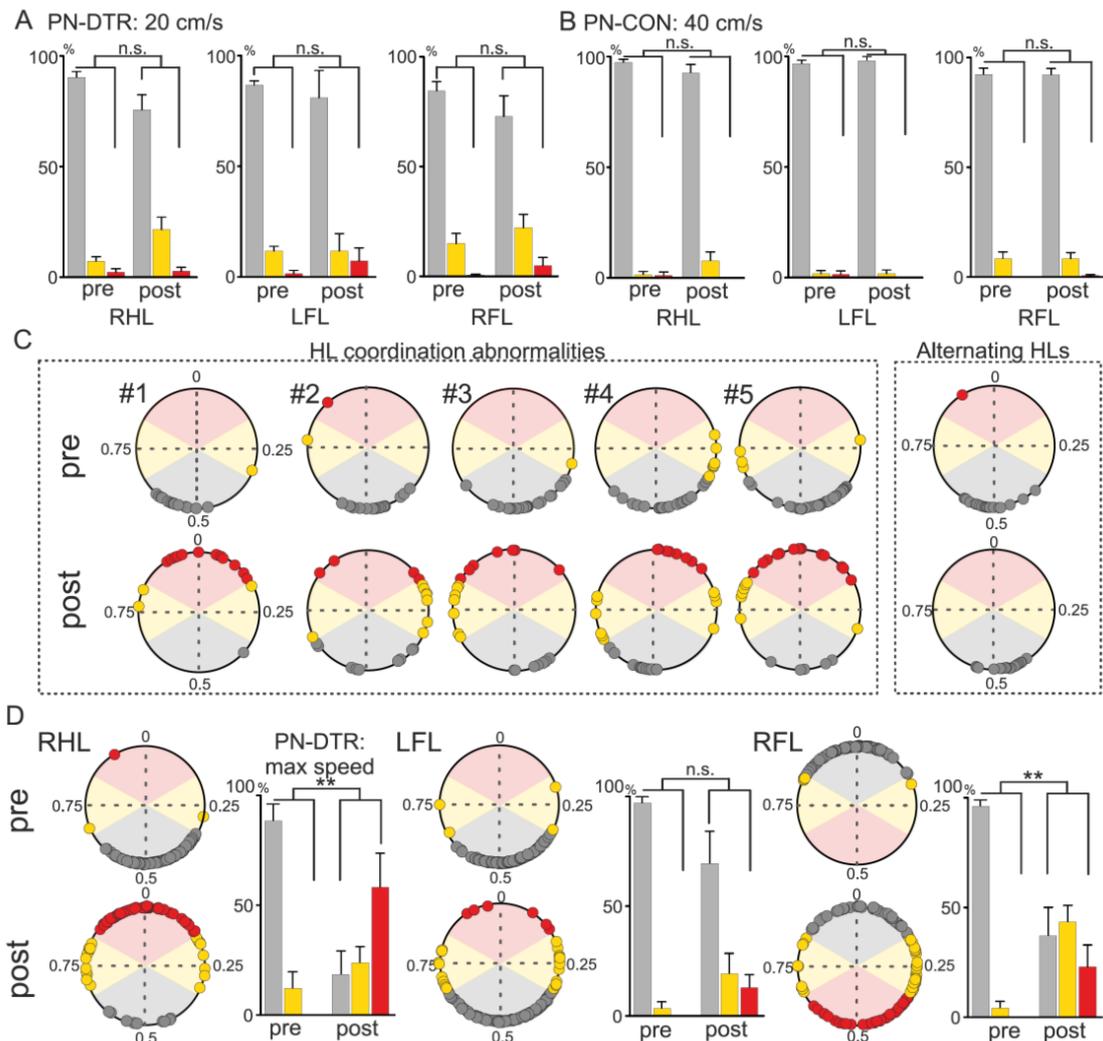
Figure 3.10. Cervico-lumbar projection neuron ablation causes speed-dependent interlimb coordination defects. Related to Figure 3.9.

(A) Categorization of phase values (see Figure 5 legend) in bar plots indicating that ablation of cervico-lumbar projection neurons does not affect interlimb coordination at a treadmill speed of 20cm/s. Data shown for individual limbs in reference to the left hindlimb.

(B) PN-CON mice do not show interlimb coordination defects at 40cm/s, the speed at which

PN-DTR cohorts upon DTX injection show left-right hindlimb coordination abnormalities. (C) Phase plots of individual mice at 40 cm/s are shown (combined data shown in Figure 5B), indicating that 5/6 mice show defects in left-right hindlimb stepping after DTX induced ablation of cervico-lumbar projection neurons. (D) Phase plots and bar plots demonstrating that at maximal treadmill speed achievable by mice with synchronous hindlimb phenotypes (50-60 cm/s; n=5 mice), also forelimb coordination is affected in PN-DTR mice 14 days upon DTX injection. Data shown for individual limbs in reference to the left hindlimb.

Cervico-lumbar projection neurons broadcast to widely distributed synaptic targets

The uncovered behavioral role of cervico-lumbar projection neurons in several aspects of locomotion raises the question of whether these neurons have other synaptic targets in addition to their projections to the lumbar spinal cord. To visualize the overall synaptic output of cervico-lumbar projection neurons, we combined retrograde neuronal targeting by CAV2-Cre viruses from the lumbar spinal cord with infection of cervical neurons by AAV-flex-Tomato/Syn-Tag viruses (Figure 3.11.A). We found that targeted cervico-lumbar projection neurons also establish synapses at segments of cell body residence in the cervical spinal cord, as well as along the entire thoracic spinal cord (Figure 3.11.B). In addition, we detected Syn-Tag marked synapses at cervical levels above AAV injection sites (C1-C3; Figure 3.11.B). To determine the fraction of neurons with both descending and ascending branches, we quantified the number of Tomato-marked axons in the white matter at C2 and T1, and found that 40.9±0.53% (n=4 mice) of cervical neurons with axons descending to lumbar levels also establish an ascending branch to levels above cell body location.

This observation prompted us to determine whether ascending axonal branches also collateralize to supraspinal centers. We found two prominent sites in the brainstem with axonal arborizations derived from these neurons. First, the lateral reticular nucleus (LRN) in the caudal brainstem, a precerebellar source of mossy fibers, was a prominent arborization center (Figure

3.11.C), suggesting that a fraction of previously characterized cervical spinal neurons with ascending projections (Pivetta et al. 2014) also projects to lumbar levels. Second, the parabrachial nucleus also received input from cervico-lumbar projection neurons (Figure 3.11.C), a termination area likely attributable to fraction of these neurons localized in the dorsal spinal cord (Yamada and Kitamura 1992, Bernard et al. 1995, Cameron et al. 2015). Together, these findings demonstrate that cervico-lumbar projection neurons not only target neurons in the lumbar spinal cord but also broadcast synaptic output information much more widely.
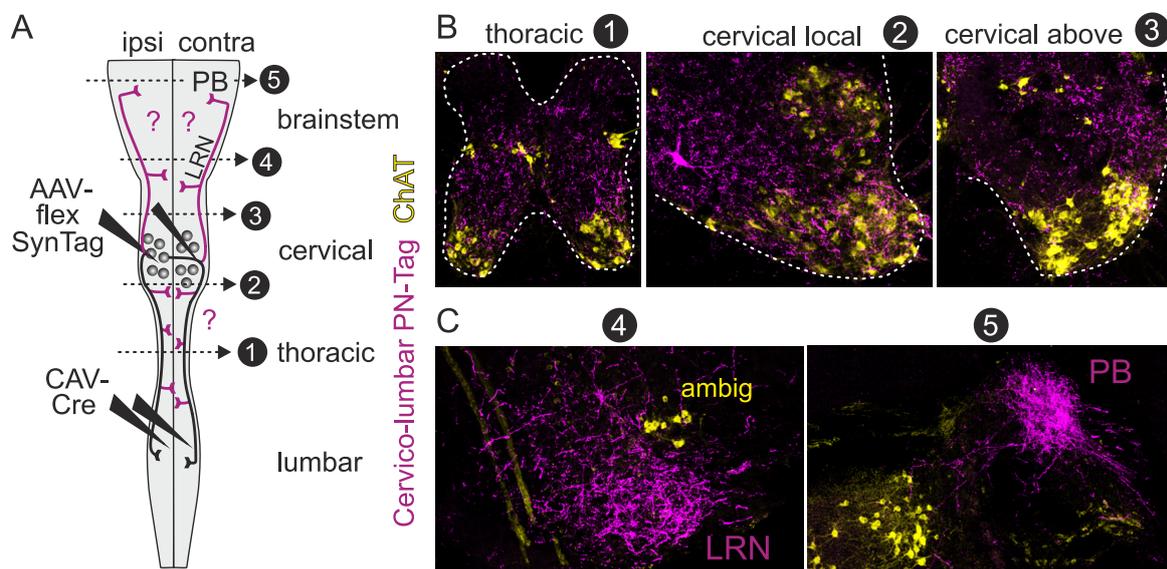
Figure 3.11. Cervico-lumbar projection neurons broadcast information to other targets

(A) Scheme of experimental strategy to mark synapses of cervico-lumbar projection neurons, and assess collateralization throughout the spinal cord and to supraspinal structures.

(B, C) Synaptic terminals of cervico-lumbar projection neurons are observed throughout the spinal cord (B; n=6 mice), including at thoracic levels (1), at cervical levels where cell bodies reside (2), at cervical levels rostral to cell body residence (3), as well as within the brainstem, where these neurons mainly terminate within the lateral reticular nucleus (LRN; 4) and parabrachial nucleus (PB; 5).

Cervico-lumbar projection neurons integrate a wide range of supraspinal inputs

The broad diversity of synaptic output structures targeted by cervico-lumbar projection neurons raises the question of their sources of synaptic input. To separately score for inputs to excitatory and inhibitory cervico-lumbar projection neurons, we targeted AAV-flex-TVA and AAV-flex-G injections to the cervical spinal cord of *vGlut2^Cre* or *vGAT^Cre* mice respectively (Figure 3.12.A). Two weeks later, we infected corresponding cervico-lumbar projection neurons from the lumbar spinal cord by EnvA-coated Rab-FP injections (Figure 3.12.A). This strategy allows mapping the origin of synaptic inputs to vGlut2^{ON} or vGAT^{ON} cervico-lumbar projection neurons or their presynaptic local but same neurotransmitter network.

We found that both excitatory and inhibitory cervico-lumbar projection neurons receive input from a broad range of supraspinal centers. The most abundant supraspinal input to cervico-lumbar projection neurons originates from the medullary reticular formation (MRF), and exhibits a bias towards vGlut2^{ON} over vGAT^{ON} neurons. Moreover, also other subcortical motor centers including pontine reticular formation (PRF), vestibular nucleus (VN), red nucleus (RN) and medullary reticular formation ventral part (MdV) are major input contributors, but these do not show any obvious bias in input distribution between the two genotypes (Figure 3.12.B-D). The most striking difference we observed was a much more pronounced input representation from primary motor and somatosensory cortices to excitatory compared to inhibitory cervico-lumbar projection neurons (Figure 3.12.C, D). We confirmed this bias through anterograde synaptic tracking of cortical input to Rab-FP cervical neurons retrogradely infected from the lumbar spinal cord in *GlyT2^GFP* mice (Figure 3.12.E). In addition, we found that cervico-lumbar projection neurons also receive synaptic input from ascending vGlut2^{ON} neurons (Figure 3.13.), providing evidence for bidirectional monosynaptic communication between these two types of projection neurons. Together, these findings demonstrate that cervico-lumbar projection neurons integrate input from many supraspinal centers and spinal neurons, and are thus in an ideal position to monitor and mediate aspects of whole body movement.
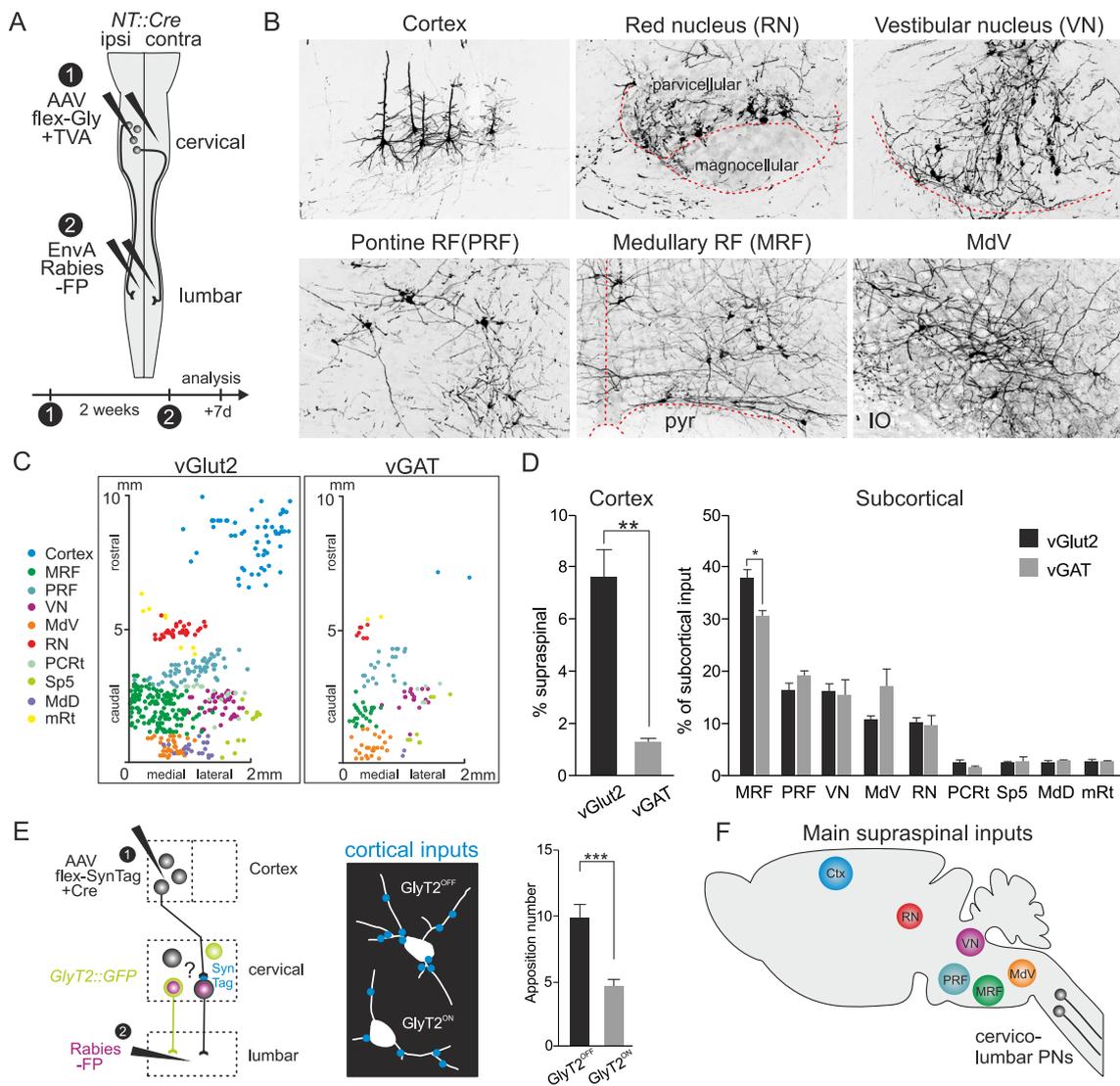
Figure 3.12. Broad supraspinal input to cervico-lumbar projection neurons

(A) Two-step viral experimental strategy to map supraspinal synaptic input to cervico-lumbar projection neurons of different neurotransmitter identity in *NT::Cre* mice (*vGAT^Cre* and *vGlut2^Cre*). Possible input from dorsal root ganglia sensory neurons was not assessed.

(B) Example images of supraspinal regions providing input to excitatory vGlut2^ON cervico-lumbar projection neurons. Rab-FP^ON neurons are shown in cortex, red nucleus (RN; parvicellular division), vestibular nucleus (Ve), pontine reticular formation (PRF), medullary reticular formation (MRF) and medullary reticular formation, ventral part (MdV).

(C) Top-down projection of three-dimensional reconstructions of supraspinal neurons connected to vGlut2^ON or vGAT^ON cervico-lumbar projection neurons by using rabies transfer

with monosynaptic restriction. Color code for different supraspinal populations is indicated (left) and regional definitions are specified in the Experimental Procedures.

(D) Quantification of cortical neuron contribution to all supraspinal neurons (left) and the contribution of subcortical neurons to different structures (right; nomenclature as in C).

(E) Anterograde mapping of cortical input to GlyT2^{ON} and GlyT2^{OFF} cervico-lumbar projection neurons by cortical AAV-SynTag injections and retrograde Rab-FP labeling from the lumbar spinal cord in GlyT2^{GFP} mice. Experimental scheme (left), example neurons for Neurolucida reconstructions (middle) and quantification (right; n=2 mice, bilateral injections, 4-5 neurons per mouse and side of each GlyT2^{ON} and GlyT2^{OFF} population) of cortical input to cervico-lumbar projection neurons.

(F) Summary diagram of main supraspinal structures providing input to descending cervico-lumbar projection neurons (color code as in C).

See also Figure 3.13.
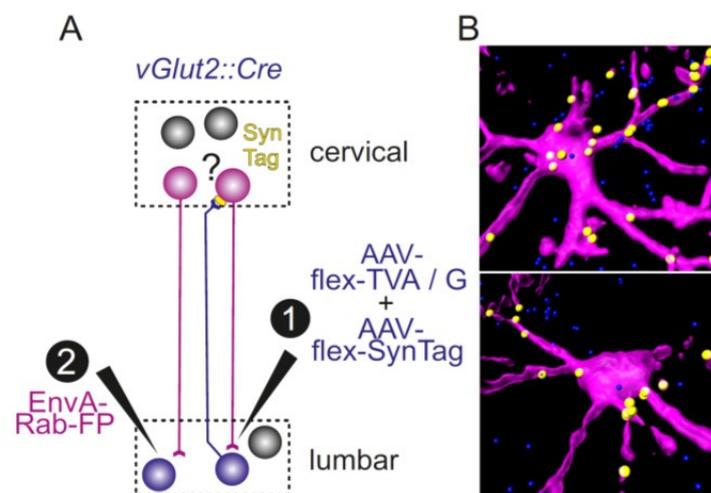
Figure 3.13. Recurrent connectivity of long-distance spinal projection neurons. Related to Figure 3.12.

(A) Experimental strategy to assay whether there is recurrent connectivity between excitatory neurons coupling cervical and lumbar spinal segments. AAV-flex-TVA, AAV-flex-G and AAV-flex-SynTag were co-injected into lumbar spinal cord segments in *vGlut2^{Cre}* mice and EnvA-coated Rab-FP was injected into the same segments 14 days later to initiate monosynaptic transsynaptic spreading. This strategy therefore labels cervico-lumbar projection neurons

connected to lumbar vGlut2^{ON} neurons and assays whether such neurons receive SynTag input from excitatory lumbar neurons projecting to cervical segments.

(B) Two examples of reconstructions for synaptic input (SynTag) derived from lumbar vGlut2^{ON} neurons to cervico-lumbar projection neurons connected to vGlut2^{ON} lumbar neurons (B).

3.4. Discussion

A defining feature of locomotion is the need to coordinate movement of many body parts while ensuring stabilization of the entire body. This is in contrast to other forms of movement in which smaller parts of the entire body are involved such as digit movements, whisking or swallowing. Here we characterized genetic diversity and patterns of connectivity of long descending spinal projection neurons, and assessed their behavioral contributions in quadrupedal locomotion. We will discuss how our work using intersectional circuit dissection and behavioral approaches helps to shed light on principles of long-range circuit organization and function to enable the coordination of smooth whole body locomotion.

Symmetries in spatial organization of genetically diverse long spinal projection neurons

The dissection of long spinal projection neurons into defined subpopulations based on neurotransmitter identity, developmental origin and projection pattern allowed us to uncover several striking symmetries and specificities in the organization of this long-range communication network. One intriguing organizational principle in the system coupling cervical and lumbar spinal circuits is the existence of reciprocally symmetrical excitatory pathways, supplemented by purely descending inhibitory pathways. These findings raise the question of what might be the functional significance of such an organization and the functional contributions of individual components. Cervico-lumbar projection neuron ablation affects interlimb coordination at high speeds, but not during exploratory behavior or low-speed treadmill locomotion, suggesting that perhaps the functionally intact ascending excitatory component of this recurrent network suffices for interlimb coordination under less challenging conditions.

Interestingly, quantitative analysis of synaptic terminal contributions of cervico-lumbar projection neurons to the lumbar spinal cord reveal a striking imbalance in excitation-inhibition with a strong excitatory dominance to the contralateral spinal cord. Such a pattern matches the known diagonal coupling of fore- and hindlimbs at most locomotor speeds (Miller et al.

1975, English and Lennard 1982), during which long-range commissural excitation might carry a locomotor signal across the midline to local lumbar circuits. In contrast, we found no such major imbalance in excitatory-inhibitory inputs to ipsilateral lumbar circuits. Unfortunately, *in vivo* recordings from cervico-lumbar projection neurons are currently not available to determine whether the firing patterns of different excitatory or inhibitory subpopulations are compatible with such an idea.

It is also unclear why long-range inhibitory spinal pathways are mainly restricted to the descending direction, although one possible explanation may be a function in inhibiting local lumbar circuits during forelimb-restricted motor tasks. Alternatively, inhibitory pathways may be used to synchronize local rhythmic activities across many spinal segments. Such a mode of operation would be conceptually similar to long-range GABAergic signaling in the brain including in the hippocampal formation (Melzer et al. 2012).

Behavioral attributes influenced by long descending spinal projection neurons

Smooth performance during quadrupedal locomotion depends on limb coordination aligned with postural adjustments. Our work demonstrates that selective ablation of cervico-lumbar projection neurons causes several behavioral defects, raising the question of how these behavioral attributes relate to each other. Two reliable phenotypes we observed jointly upon cervico-lumbar projection neuron ablation were defects in postural stability and speed during exploratory locomotion. Regulation of postural stability by cervico-lumbar projection neurons is compatible with our observation that these neurons not only connect to lumbar circuits, but also establish synapses all along the thoracic spinal cord. An important role for cervico-lumbar projection neurons beyond direct communication between cervical to lumbar spinal segments may therefore be the distribution of information to circuitry along the spinal axis to coordinate postural adjustments. It is difficult to determine whether other defective measured parameters in these PN-ablated mice, in particular reduced speed, may be secondary consequences of

postural instability. Since these two phenotypes are linked, it is impossible to disentangle cause and consequence.

Past analysis of mouse mutants targeting identified spinal interneuron populations has drawn conclusions on neuronal function primarily with a view on how local lumbar spinal circuits regulate limb coordination. However, since manipulations in most studies involved extended spinal segments along the rostro-caudal axis, it is possible that long spinal projection neurons also contribute to aspects of the described phenotypes. Notably, V0v and V2a, but not V0d neurons were implicated in securing left-right limb alternation at high speeds (Crone et al. 2009, Talpalar et al. 2013, Bellardita and Kiehn 2015). In our study, we found that specifically V0v, but not V0d contribute to excitatory commissural long projection neurons, whereas V2-Shox2 neurons, overlapping with V2a neurons (Dougherty et al. 2013), contribute to ipsilateral cervico-lumbar projection neurons. Our behavioral analysis demonstrates that interlimb coordination defects are only detected at higher speeds. Such defects may be caused by cervico-lumbar projection neuron ablation of V0v and/or V2-Shox2 identity. Regardless of the precise neuronal identity, a striking finding of our study is that cervico-lumbar projection neurons largely do not affect intralimb parameters, and predominantly influence left-right hindlimb but not forelimb interlimb coordination at 40cm/s speed, demonstrating that not only local circuitry but also long projection neurons can influence limb coordination at one girdle. Beyond ensuring reliable interlimb coordination at high speed, cervico-lumbar projection neurons may therefore also be involved in regulating gait transitions or changes in limb coordination when animals have to adjust quadrupedal stepping. Indeed it has been shown that such transitions can occur very rapidly (Miller et al. 1975, Bellardita and Kiehn 2015), compatible with the idea of an involvement of long spinal projection neurons.

Broadcasting and integration role of long spinal projection neurons in the motor system

To better understand the behavioral role of cervico-lumbar projection neurons, it is useful to consider their integration into the broader circuitry of the motor system. A previous

transsynaptic virus tracing study found that descending neurons with direct connections to lumbar motor neurons predominantly reside at thoracic and only sparsely at cervical levels (Ni et al. 2014), but interestingly, neurons of V2 genetic identity were encompassed within these populations. Our work demonstrates that cervico-lumbar projection neurons mostly terminate in spinal laminae not containing motor neurons. These combined results suggest that transmission of cervical signals may reach lumbar motor neurons through both thoracic descending neurons and local lumbar neurons as intermediaries, a model compatible with our observation of postural stability defects in mice with cervico-lumbar neuron ablations.

Finally, we found that cervico-lumbar projection neurons receive synaptic inputs from a broad range of supraspinal centers. Some of these inputs also appear to be evolutionarily conserved, as electrophysiological input mapping to individual but not genetically identified neurons in cat demonstrates (Alstermark et al. 1987, Alstermark et al. 1987). However, the number of different supraspinal centers providing input to an individual neuron or to a genetically identified population is currently unknown both from our own and past work. Nevertheless, while we found that input from subcortical centers was more numerous than from the cortex for both excitatory and inhibitory descending projection neurons, one clear distinction was the more dominant cortical input to excitatory compared to inhibitory subpopulations. In addition, three cervico-lumbar projection neuron subtypes were observed based on differential input from cortex and vestibular neurons (Alstermark et al. 1987). Together with our work, these findings suggest that not all cervico-lumbar projection neurons are controlled by the same supraspinal input sources, but how these input properties align with genetic identity and different functional subtypes remains to be determined.

It is intriguing that upon incomplete spinal cord injury, cervico-lumbar projection neurons but not locally projecting cervical neurons attract permanent cortical input normally directly targeting lumbar segments (Bareyre et al. 2004), suggesting that long spinal projection neurons may indeed be special in terms of synaptic input processing. Since we found that the

output of cervico-lumbar projection neurons is broadcasted widely within the nervous system including to many segments within the spinal cord and to some defined supraspinal centers including the LRN, our work proposes a key role for these neurons in the integration and distribution of motor information implicated in the regulation and coordination of smooth and coherent whole body movement.

3.5. Experimental Procedures

Mouse genetics

Wild-type (C57Bl6), *Tau*$^{lox-STOP-lox-Flp-INLA}$ (Pivetta et al. 2014), *vGlut2*^{Cre} (RRID: IMSR_JAX:028863, (Vong et al. 2011), *vGAT*^{Cre} (RRID: IMSR_JAX:028862, (Vong et al. 2011), *GlyT2*^{GFP} (RRID: IMSR_RBRC04708, (Zeilhofer et al. 2005), *Dbx1*^{CreER} (RRID: IMSR_JAX:028131, (Hirata et al. 2009), *Shox2*^{Cre} (Dougherty et al. 2013), *Isl1*^{Cre} (RRID: IMSR_HAR:3350, (Srinivas et al. 2001), *En1*^{Cre} (RRID: IMSR_JAX:007917, (Sapir et al. 2004), *Sim1*^{Cre} (Zhang et al. 2008), tdTomato reporter Ai14 JAX 007908 (RRID: IMSR_JAX:007908, (Madisen et al. 2010) mouse strains were maintained on a mixed genetic background (129/C57Bl6). To induce transient CreER expression, tamoxifen injections were carried out in intersectional crosses between *Tau*$^{lox-STOP-lox-Flp-INLA}$ and *Dbx1*^{CreER} mice at e10.5. Housing, surgery, behavioral experiments and euthanasia were performed in compliance with the Swiss Veterinary Law guidelines.

Virus production and injections

Rabies viruses (Rabies-mCherry and Rabies-GFP: Rab-FP, as well as EnvA coated versions) used were amplified and purified from local viral stocks following established protocols (Wickersham et al. 2007, Stepien et al. 2010, Osakada and Callaway 2013). All AAVs used in this study were described previously (Esposito et al. 2014, Pivetta et al. 2014, Takeoka et al. 2014) and of genomic titers >1x10e13. CAV2-Cre amplification and purification were carried out following established protocols (Kremer et al. 2000).

Anterograde AAV and retrograde rabies tracing experiments

Intraspinal injections: Intraspinal injections were performed as previously described (Pivetta et al. 2014, Takeoka et al. 2014) and as detailed in the Supplemental Material.

Targeting cervico-lumbar spinal projection neurons for behavioral analyses: The first injection using Canine adeno-virus encoding Cre recombinase (CAV-Cre) targeting lumbar projecting neurons was carried out into the lumbar spinal cord of p0-2 wild-type mice using ultrasound

guidance (Visualsonics, Canada). Five weeks later, a second injection with AAV-flex-DTR (Esposito et al. 2014) and/or AAV-flex-Tomato in the cervical spinal cord was carried out. Details on injections and inclusion criteria for behavioral experiments are described in the Supplemental Material.

Immunohistochemistry, imaging and analysis

Immunohistochemistry: All mice were perfused with 4% paraformaldehyde. All tissue was cryoprotected in 30% sucrose/PBS and cut on a cryostat (brain: 80μm coronal slices; spinal cord: 20-80μm transverse sections). Antibodies used in this study were: chicken anti-GFP (RRID: AB_2534023 Invitrogen), goat anti-ChAT (RRID: AB_2079751 Millipore), guinea pig anti-vGlut2 (AB_11213019 Millipore), mouse anti-Myc (RRID: AB_2148607 ATCC), mouse anti-NeuN (AB_2298772 Millipore), and rabbit anti-RFP (RRID: AB_2209751 Rockland). Fluorophore-coupled secondary antibodies were from Jackson or Invitrogen. Floating tissue sections were incubated with antibodies in individual wells and mounted for imaging in sequential order.

Spinal cord and brainstem reconstructions: Spinal cord images were acquired using a confocal (Olympus, 10x objective) or a custom-made dual spinning disk (Life Imaging Services GmbH, Basel Switzerland, 10x objective) microscope. Brain images were acquired using an Axioscan light microscope (Zeiss, 5x objective) or a confocal microscope (Olympus, 10x objective). Pictures were aligned using ImageJ as previously described (Takeoka et al. 2014). Labeled neurons were assigned manually using custom written MATLAB scripts for spinal cord reconstruction and color-coded with Imaris spot detection (Bitplane) according to location based on Paxino's mouse brain atlas for brain reconstructions with the exception of MRF and PRF, for which combined definitions were used (MRF combines GiA, GiV, Gi, LPGi, Raphe; PRF combines PnO and PnC).

Synaptic analysis: Images for synaptic density analysis were acquired using an Olympus confocal microscope (FV1000, 20x objective) using a step size of 1.22μm for sections of 40μm thickness. Density and distribution of synaptic terminals were reconstructed as previously

described (Takeoka et al. 2014). High-resolution input analysis of synaptic input to retrogradely marked cervico-lumbar projection neurons were acquired with a custom-made dual spinning disk (Life Imaging Services GmbH, Basel Switzerland, 60x objective, 0.2μm step size) and quantified using Neurolucida (v10.0, Microbrightfield) as described previously (Basaldella et al. 2015).

Behavioral analyses

Open field and kinematic analyses were performed as previously described (Esposito et al. 2014, Takeoka et al. 2014) and as detailed in the Supplemental Material.

Statistics

All statistical analysis and plots were made using GraphPad PRISM (v6.0), R or MATLAB. One-dimensional kernel densities were obtained using the Matlab function 'ksdensity'. Two-dimensional kernel density estimation used to compute the distribution contours was obtained using the Matlab function 'kde2d' with the contour lines connecting points of equal densities and drawn for density values between 20% and 100% of the estimated density range, in 6 steps. Graphs represent the average value ± SEM. The means of different data distributions were compared using an unpaired Student's t test (Figures 3.1.B, 3.1.C, 3.5.C, 3.8.C, 3.8.G, 3.9.D, 3.12.D, 3.12.E), paired Student's t test (Figures 3.1.B, 3.1.C, 3.1.H, 3.1.I, 3.3.D, 3.3.J, 3.3.K, 3.3.D, 3.3.G, 3.3.H, 3.8.C, 3.8.G, 3.2.C, 3.2.F, 3.2.G, 3.7.) or Kolmogorov-Smirnov test (Figures 3.9.B, 3.10.A, 3.10.B, 3.10.D). Significance level is defined as follows for all analyses performed: *$p < 0.05$; **$p < 0.01$; ***$p < 0.001$.

Supplementary Experimental Procedures

Anterograde AAV and retrograde rabies tracing experiments

Intraspinal injections: For both retrograde and anterograde viral delivery into the spinal cord, a pulled borosilicate glass pipette (World Precision Instruments, Inc.) was used for local

application of ~300nl virus by multiple short pulses (3msec, 0.5Hz) using a picospritzer (Parker). For direct retrograde labeling using Rab-FP (Wickersham et al. 2007), mice were sacrificed 3 days after injection. For anterograde tracing, all mice were co-injected with AAV-nuclear tags to verify injection precision and efficiency of infection. No significant difference in the number of infected neurons at the injection site was detected between $vGlut2^{Cre}$ or $vGAT^{Cre}$ mice for both cervical (vGlut2: 346±84, n=6; vGAT: 322±65, n=5; p=0.77) and lumbar (vGlut2: 272±34, n=3; vGAT: 252±26, n=3; p=0.66, values per hemi-spinal cord) spinal injections. Two weeks post-virus transduction, mice were sacrificed and unilaterality of injections was confirmed by immunohistochemistry. To map supraspinal synaptic connectivity to cervico-lumbar projection neurons, we first performed co-injections of AAVs conditionally expressing G-protein and TVA into $vGlut2^{Cre}$ or $vGAT^{Cre}$ mice and injected EnvA-coated Rab-FP two weeks later as previously described (Takeoka et al. 2014). Experiments were terminated for analysis 7 days after EnvA-coated Rab-FP injections. For cortical anterograde synaptic mapping to cervico-lumbar projection neurons in $GlyT2::GFP$ mice, AAV-SynTag was injected bilaterally into the cortex two weeks prior to analysis (+0.25 mm antero-posterior from bregma, ± 1.5 mm lateral and 0.8 mm ventral). For anterograde mapping of lumbar vGlut2^{ON} synaptic input to cervico-lumbar projection neurons, AAV-flex- SynTag was injected at lumbar levels in $vGlut2^{Cre}$ mice.

Targeting cervico-lumbar spinal projection neurons for behavioral analyses: For CAV-Cre injections in p0-2 mice, a pulled calibrated glass pipette (Origio Inc, USA) was used for local application of ~ 200nl virus by multiple short pulses (3msec, 0.5Hz) using an infusion pump (Visualsonics, Canada). Cervico-lumbar projection neurons targeted retrogradely by CAV- Cre at p0-2 still project to lumbar levels in the adult (t-test for % T1 axons projecting to L1 segments in adult: p=0.4898; 87.55 % ±15.86 SEM; n=4), indicating that no long-distance developmental pruning occurs for this population. The following criteria were applied for mice excluded from behavioral analysis: Mice with <25 locomotor bouts during any of the analyzed sessions (n=2 mice), mice displaying obvious movement abnormalities after cervical injection surgery (n=3

mice), and mice in which postmortem analysis revealed low viral labeling efficiency by quantification of white matter axon number at T1 (n=1 mouse; <100 axons).

Behavioral analyses

Open field task: To assess basic locomotor activity, videos were acquired from above (Allied Vision, Inc.) for 4 minutes in a square arena (35 x 35 cm) placed inside a noise-isolated chamber. Whole body tracking was performed using tracking software (Plexon Inc.) and speed values were calculated from extracted coordinates. Whole body and speed traces were clustered into defined locomotor bouts (>5cm/s for >200msec) and maximum speed (highest 5 speed values per mouse from all extracted locomotor bouts), duration and distance parameters were calculated using custom-written MATLAB scripts. Postural stability was defined as the angular deviation from a straight line on a frame-by-frame (for 30 fps acquisition) or on a 3 frames-by-3 frames (for 100 fps) basis and includes only locomotor bouts of >1s. PN-CON mice include mice with CAV-Cre and AAV-flex-tomato but no DTR injections (n=3) and mice with no injections (n=4), both of which received DTX application in parallel with PN-DTR mice. These two control groups were not significantly different from one another and were therefore combined in this study. We also assessed open field behavior of PN-DTR mice 7 days post-DTX compared to the pre-DTX time point and found behavioral abnormalities similar to 14 days post-DTX (distance: 78.3±6.1%, p=0.005; maximal speed: 80.1±4.7%, p=0.017; duration: 94.0±6.7%, p=0.212; instability: 116.6±4.3%, p=0.001; n=10 mice; Figure 4C, G). We observed no significant difference in control mice comparing pre- DTX and +7 days post-DTX time points (distance: 103.9±6%, p=0.661; maximal speed: 109.1±7.6%, p=0.341; duration: 105.7±3.5%, p=0.123; instability: 101.9±4.8%, p=0.935; n=7 mice). These findings prompted us to use the +14 days post-DTX time point for all other analyses, when DTR-infected neurons are anatomically eliminated.

Kinematic recordings: Whole-body kinematics during treadmill (BIOSEB, France) locomotion were recorded using the high-speed motion capture system Vicon (Vicon Motion Systems, UK) and reflective markers were attached bilaterally overlying the iliac crest, the greater trochanter

(hip), the lateral condyle (knee), the malleolus (ankle), and the base of the metatarsal phalangeal joint (MTP) for the hindlimbs; and the proximal head of the humerus (shoulder), epicondyle of humerus (elbow) and on the medial head of metacarpal (forepaw) for the forelimbs. Limb trajectories from approximately 20-30 steps/mouse were then reconstructed offline. For interlimb analysis, the left hindlimb was used as a reference limb. Phase values for division of treadmill steps into three categories (gray, yellow and red) as displayed in Figure 5 and S5 were: for right hindlimb and left forelimb: 0.332-0.668; 0.166- 0.332 and 0.668-0.834; 0-0.116 and 0.834-1, respectively and for right forelimb: 0-0.116 and 0.834-1; 0.166-0.332 and 0.668-0.834; 0.332-0.668, respectively. Mice were defined to have irregular hindlimb gait after cervico-lumbar projection neuron ablation when > 50% of hindlimb steps consisted of phase values ranging from 0 to 0.332 or 0,668 to 1 (trotting or bound; n=5/6). Parameters describing gait timing, joint kinematics, and limb endpoint trajectory were computed for each gait cycle using custom written MATLAB or R (R Foundation for Statistical Computing, Vienna, Austria, 2005, http://www. r-project.org) scripts.

3.6. Author Contributions

L.R. designed and carried out most experiments, and analyzed all data except treadmill and cortical input mapping experiments. A.T. was involved in treadmill and cortical input mapping experiments, and analyzed corresponding datasets. S.A. initiated the project, designed experiments, analyzed data and wrote the manuscript. All authors were involved in commenting on the manuscript.

3.7. Acknowledgements

4. A functional map for diverse forelimb actions within brainstem circuitry

Ludwig Ruder, Riccardo Schina, Harsh Kanodia, Sara Valencia-Garcia,

Chiara Pivetta and Silvia Arber

4.1. Summary

The brainstem is a key centre in the control of body movements. Although the precise nature of brainstem cell types and circuits that are central to full-body locomotion are becoming known (Ferreira-Pinto et al., 2018, Rosberry et al., 2016, Caggiano et al., 2018, Capelli et al., 2017, Bouvier et al., 2015), efforts to understand the neuronal underpinnings of skilled forelimb movements have focused predominantly on supra-brainstem centres and the spinal cord (Lemon 2008, Alstermark and Isa, 2012, Klaus et al., 2019, Peters et al., 2017, Wang et al., 2017, Azim et al., 2014, Pivetta et al., 2014). Here we define the logic of a functional map for skilled forelimb movements within the lateral rostral medulla (latRM) of the brainstem. Using in vivo electrophysiology in freely moving mice, we reveal a neuronal code with tuning of latRM populations to distinct forelimb actions. These include reaching and food handling, both of which are impaired by perturbation of excitatory latRM neurons. Through the combinatorial use of genetics and viral tracing, we demonstrate that excitatory latRM neurons segregate into distinct populations by axonal target, and act through the differential recruitment of intra-brainstem and spinal circuits. Investigating the behavioural potential of projection-stratified latRM populations, we find that the optogenetic stimulation of these populations can elicit diverse forelimb movements, with each behaviour stably expressed by individual mice. In summary, projection-stratified brainstem populations encode action phases and together serve as putative building blocks for regulating key features of complex forelimb movements, identifying substrates of the brainstem for skilled forelimb behaviours.

4.2. Introduction

Understanding how diverse body movements are regulated necessitates the identification of neuronal circuit mechanisms that are central to this process. The brainstem represents a key integration and processing junction that establishes links between upper motor centres involved in planning actions and circuits in the spinal cord that are required for execution of body movements (Grillner et al. 1997, Grillner 2006, Lemon 2008, Kim et al. 2017, Arber and Costa 2018, Svoboda and Li 2018, Klaus et al. 2019, Ruder and Arber 2019). Specific neuronal circuits within the brainstem and their outputs to the spinal cord are dedicated to the regulation of locomotion (Bouvier et al. 2015, Roseberry et al. 2016, Capelli et al. 2017, Caggiano et al. 2018, Ferreira-Pinto et al. 2018), a behavior requiring full-body coordination. Whether neuronal circuit modules devoted to skilled forelimb movements exist within the brainstem, how they interact with spinal circuits and coordinate the construction of complex forelimb movements is poorly understood.

A major historical focus to understand how the nervous system regulates skilled forelimb movements has been on higher motor centers including motor cortex and basal ganglia (Georgopoulos et al. 1982, Lemon 2008, Alstermark and Isa 2012, Peters et al. 2017, Klaus et al. 2019, Wang et al. 2017). However, several lines of evidence suggest that the execution of skilled forelimb movements engages and is dependent on subcortical structures, especially the brainstem. Evolutionary analysis demonstrates that behavioural elements of skilled forelimb movements, including reaching and food handling, are already present in species without corticospinal tracts (including frogs) (Iwaniuk and Wishaw 2000). In mice, the ablation of specific excitatory neurons in the caudal medulla impairs food grasping (Esposito et al., 2014). The medulla and pons of the brainstem also contain neurons that are recruited during forelimb reaching in cats (Schepens and Drew 2006, Schepens et al. 2008) and digit movements in monkeys (Soteropoulos et al. 2012). Monkeys with lesions of the cortico-spinal tract compensate all aspects of skilled forelimb movements except the use of single digits (Lawrence and Kuypers 1968, Lemon et al. 2012). Notably, an additional specific lesion of the

lateral—but not the medial—lower brainstem entirely abrogates these behavioural compensations (Lawrence and Kuypers 1968, Lemon et al. 2012). Finally, systematic electrical microstimulation experiments in these regions, albeit focused on locomotion as read-out, have identified sites within the lateral medulla, the stimulation of which elicited specifically forelimb movements with no effects on hindlimbs (Ross and Sinnamon 1984). Together, these findings point to the existence of important, yet uncharacterized, neuronal substrates in the lateral medulla that are required for the execution of skilled forelimb movements.

4.3. Results

Lateral rostral medulla neurons are tuned to specific forelimb actions

To assess the activity of neurons in the latRM, we performed in vivo recordings using chronic silicon probe implants in the mouse brainstem. We centred the implant in the parvicellular reticular nucleus (Franklin and Paxinos 2007) at the rostrocaudal level of the facial nucleus (Fig. 4.2.a), a region of the brainstem in which we had observed neurons specifically premotor to motor neurons innervating forelimb muscles (Esposito et al. 2014). This allowed us to monitor the activity of single neurons while freely moving mice performed different behavioural tasks (Fig. 4.1.; Fig. 4.2.a). We trained mice on a food-pellet reaching and retrieval task (hereafter, pellet task) to specifically engage in unilateral forelimb reaching and subsequent food handling (Xu et al. 2009). As a distinct but behaviourally similar forelimb-engaging task, we trained mice to reach for and press a lever (hereafter, lever task), the successful execution of which allowed them to retrieve a reward (Jin and Costa 2010). we assessed latRM neuron activity during full-body locomotion, which represents a behaviour that also strongly engages forelimb muscles but does so in a very different context.
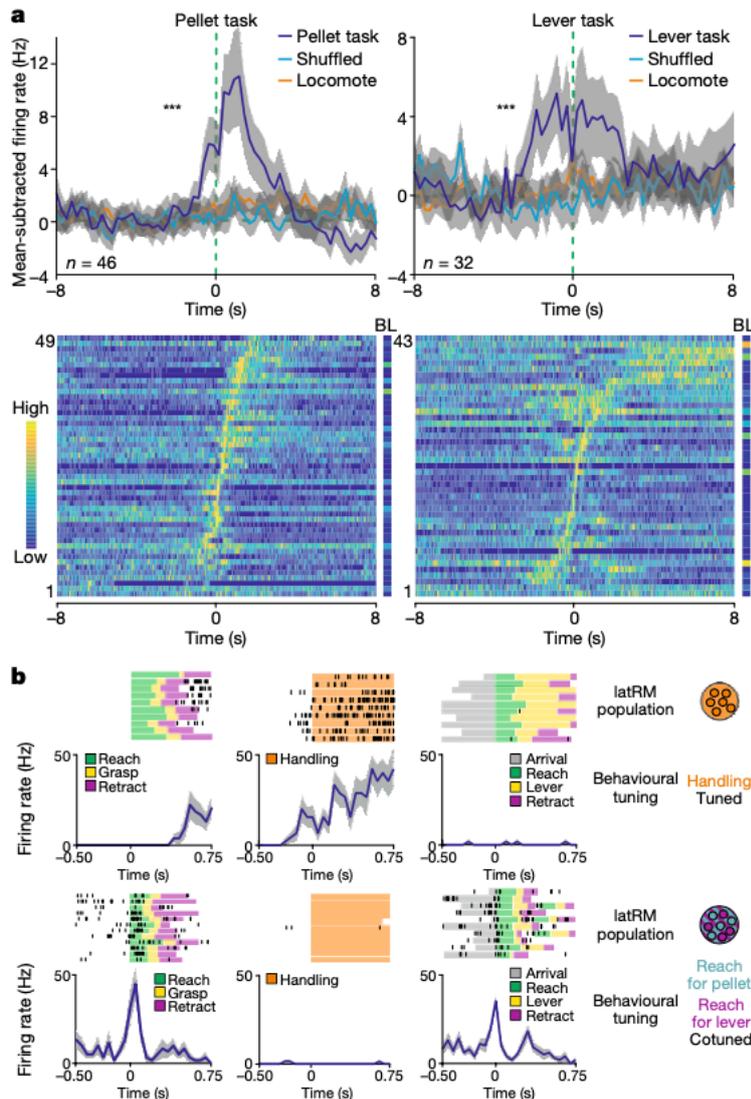
Figure 4.1. Brainstem neurons specifically tuned to forelimb behaviours.

(a) Mean subtracted firing rate of all task-tuned latRM neurons analysed for the pellet (left) and lever (right) tasks, depicting average over all neurons (top; recorded also in locomotion) or individual neurons sorted by time of maximal relative mean subtracted firing rate (bottom, recorded in shown task), with time 0 representing reaching onset. Bottom, colour scale shows low (0) to high (1) for relative mean-subtracted firing rate and low (0 Hz) to high (100 Hz) for baseline (BL) firing rate. Top, average of mean-subtracted firing rate of the task-tuned latRM neurons identified commonly in all tasks considered during onset of locomotion trials (locomote) or shuffled data. n = 5 mice; n = 46 neurons assessed during both pellet task and locomotion; n = 32 for neurons assessed during both lever task and locomotion (Methods)

(b) Examples for two latRM neurons during pellet task (left), food handling (middle) and lever task (right). Behavioural phases are marked in colour for all trials and summary schemes are shown on the right. Example unit on the top displays tuning preference for handling over other behavioural phases; the bottom unit displays tuning preference for reaching (for lever or pellet) over handling (average firing rate in Hz is shown below single trials; n = 1 example neuron each). Grey shade denotes ±s.e.m. ***P< 0.00033; Wilcoxon signed-rank test. Bonferroni correction was applied to account for multiple comparisons
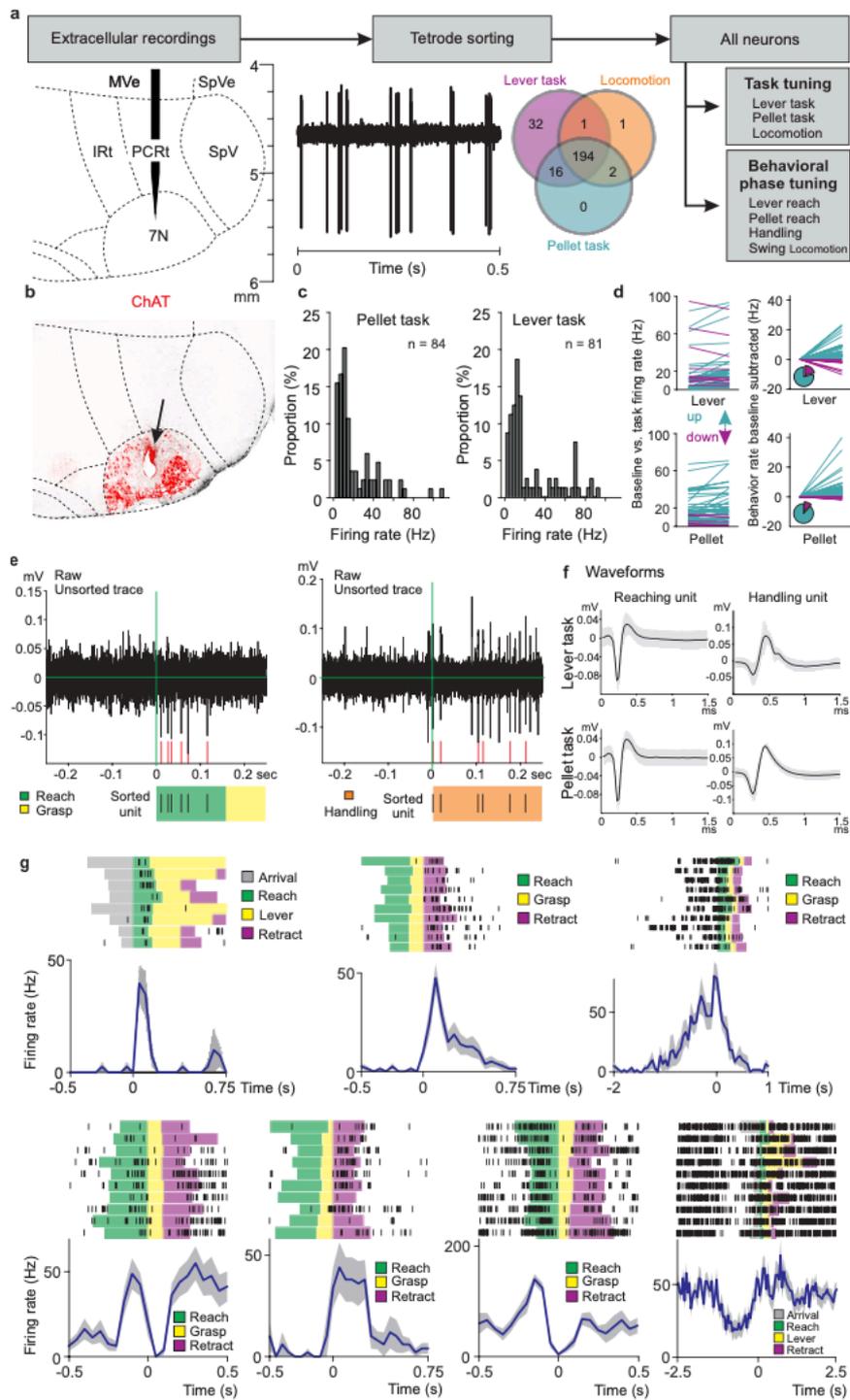
Figure 4.2. Methodological approaches and firing properties of latRM neurons

(a) Scheme outlining experimental setup and analysis pipeline for single unit recordings of latRM neurons. A total of 194 neurons were recorded in lever task, pellet task and open field assay

(b) Representative latRM section from mouse undergoing single-unit recordings, depicting end point of silicon probe trajectory, visualized through electrical lesion (arrow) performed at the end of all recording sessions, counterstained for ChAT to visualize 7N neurons

(c) Analysis of average firing rates of behaviourally relevant neurons for pellet (left, n = 84 neurons) and lever (right, n = 81 neurons) tasks, demonstrating that most neurons fire at relatively low rates

(d) Analysis of changes in firing rate of task-tuned neurons comparing baseline to behaviour. The large majority of neurons upregulate their firing rate, and only few downregulate it (n = 43 neurons for lever task, n = 49 neurons for pellet task)

(e, f) Two examples of raw unsorted traces (e), aligned to reaching (left) or handling (right) onset, depicting the spiking pattern of the subsequently sorted unit below with indication of behavioural time windows. Waveforms for these two units are shown for lever and pellet tasks, which were carried out sequentially

(g) Recordings from seven example LatRM neurons during lever or pellet task, displaying single trials aligned to behavioural phases (spikes shown as lines) as well as average firing rate (Hz) below single trials (n = 1 neuron each); grey shade, ±s.e.m.

To get an overview of activity changes of latRM neurons during a task, we analysed the mean-subtracted firing rate of all neurons tuned to one of the two forelimb tasks. We observed a notable overall increase in firing rate during each of the forelimb tasks (pellet and lever tasks), but not during locomotion or when analysing shuffled data from the same neurons (Fig. 4.1.a). For both forelimb tasks, individual neurons contributed to the overall curve by tiling the behavioural space from preparation to execution (Fig. 4.1.a), and a large majority of neurons upregulated their firing rate (Fig. 4.2.c, d). Analysis of the changes in firing profile revealed diversity, with selectivity to particular time windows (Fig. 4.1.a; Fig. 4.2.e–g).

We next addressed the question of whether populations of latRM neurons are tuned to specific behavioural phases. We analysed changes in neuronal activity during sharp, behaviourally defined time windows (Methods). We identified neurons tuned to the reaching phase of the

pellet or lever task (relatively similar forelimb actions), and compared these to neurons tuned to food handling, an action phase that is behaviourally distinct from reaching (Fig. 4.1.b). At the population level, action-ensemble cotuning for both reaching phases was significant, whereas we observed no significant cotuning or anticorrelation for either of these behaviours and food handling (Fig. 4.3.a–f). By contrast, we found that the handling-tuned latRM population is not recruited during the lever task or locomotion swing phases (Fig. 4.1.b, Fig. 4.3.a). However, it is recruited with delay during the pellet task, in which reaching is followed by food handling. Thus, the handling-tuned latRM population is engaged during skilled forelimb behaviours that involve food handling. In agreement with the interpretation of action-specific tuning, the latRM population tuned to lever reaching was also recruited during pellet reaching, but not during the handling or locomotion swing phases (Fig. 4.3.b). These findings demonstrate that latRM neurons fractionate into distinct ensembles, which display behaviour-specific tuning within the forelimb action space (Fig. 4.1.b, Fig. 4.3.f), and are unlikely to be recruited exclusively according to a muscular or receptive field map (Schepens et al. 2008)
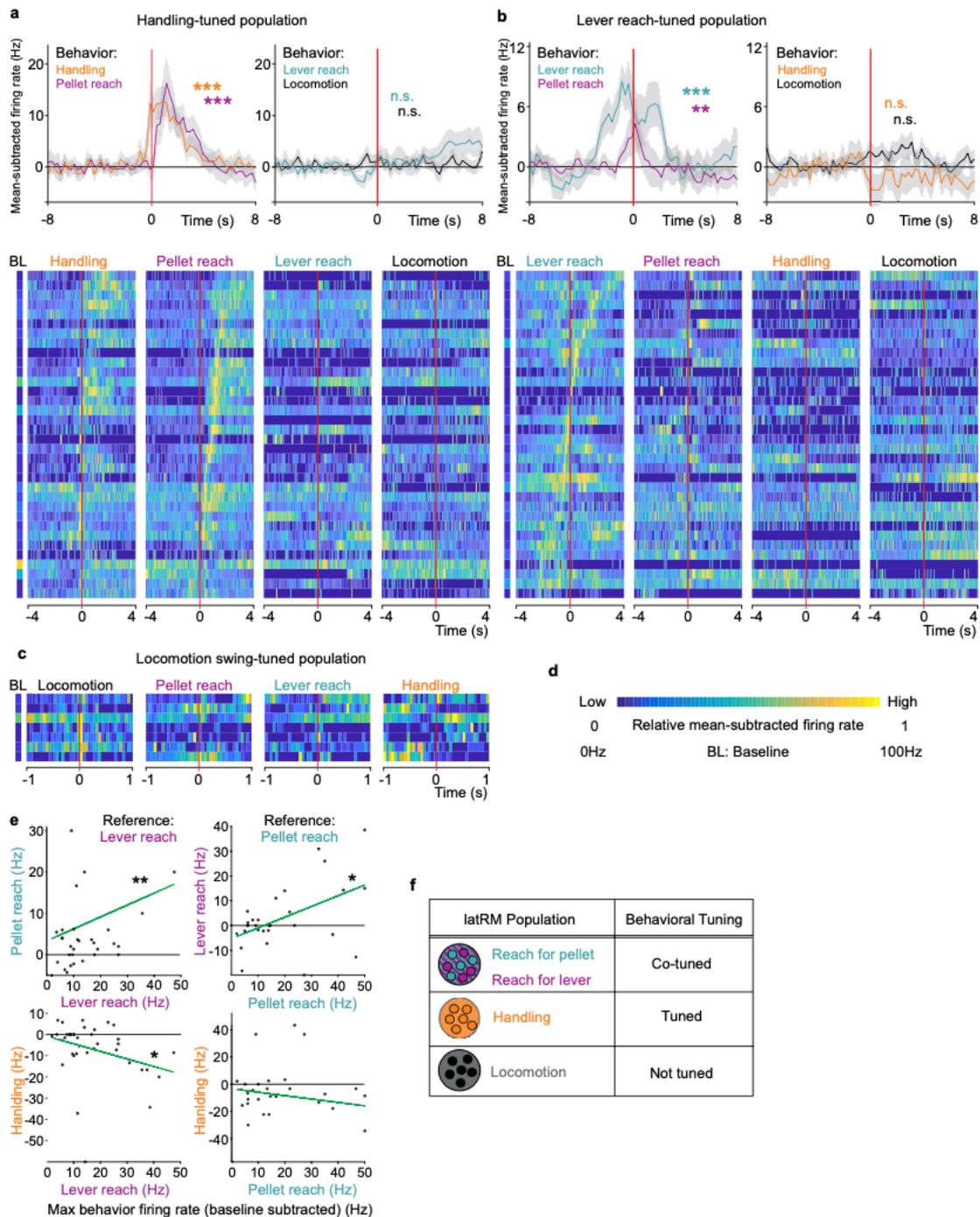
Figure 4.3. Behavioural tuning properties of latRM neurons.

(a-d) Analysis of handling-tuned (a) and lever-reach-tuned (b) latRM populations (n = 34 neurons each), depicting response properties of all respective neurons aligned to behavioural onset of handling, pellet reach, lever reach or locomotion swing phase (top: average of all neurons, bottom: raster plot for individual neurons ordered by peak time of pellet reach) (a) or lever reach (b). c, Data depicted in raster plots for the small number of latRM neurons making up a locomotion swing-phased tuned latRM population. Colour scale in d depicts low (0) to

high (1) for relative mean-subtracted firing rate and low (0 Hz) to high (100 Hz) for baseline firing rate

(e) Correlation analysis of behavioural tuning of all units analysed in lever, pellet and handling task (n = 5 mice; n = 38 neurons for lever-reach-tuned population, n = 30 neurons for pellet-reach-tuned population (Methods))

(f) Summary scheme displaying population cotuning for latRM neurons during lever reaching and pellet reaching. By contrast, the handling-tuned latRM population is not engaged in reaching. Analysed neurons are not tuned to locomotion (swing phase). Grey shades, ±s.e.m.; **$P < 0.0025$; ***$P < 0.00025$; Wilcoxon non-parametric signed-rank test. Bonferroni correction was applied to account for multiple comparisons. In a, b, **$P < 0.01$; ***$P < 0.001$. Spearman's rank correlation test (e)

Skilled forelimb behaviours require latRM

To determine whether and which aspects of forelimb behaviours require latRM neurons for execution, we used loss-of-function tools in mice trained in forelimb reaching or food handling, two behaviours that recruit distinct latRM populations. We expressed the inhibitory designer receptor exclusively activated by designer drugs (DREADD) hM4Di, the activity of which can be regulated by systemic injection of clozapine N-oxide (CNO) (Roth, 2016) or—as a second tool—diphtheria toxin receptor (DTR), the expression of which, upon systemic injection of diphtheria toxin (Esposito et al. 2014) leads to neuronal ablation in the latRM of vGlut2cre (vGlut2 is also known as Slc17a6) mice (Fig. 4.5.a).

We found no difference in open-field locomotor activity comparing conditions with or without CNO (Fig. 4.5.b). By contrast, forelimb reaching and food handling were severely affected in mice with chemogenetically silenced or ablated excitatory latRM neurons (Fig. 4.4). First, we evaluated mice for their performance in the pellet task. We found a highly significant and reversible decline in the success rate to retrieve food pellets and place them in the mouth over baseline after injections of CNO, in vGlut2cre mice that had been injected with adeno-associated virus (AAV) encoding hM4Di (hereafter, latRM-hM4Di-vGlut2 mice) (Fig. 4.4.b).

The drop in success rate reflected a significant increase in the miss rate of the pellet by the forepaw during the reaching phase in CNO-injected latRM-hM4Di-vGlut2 mice (Fig. 4.4.c). Reconstructions of the point of maximal extension of reaching trajectories showed that these mice consistently over-reached the pellet position and displayed significantly higher variability in endpoint position (Fig. 4.4.d, Fig. 4.5.c–e). Recording from latRM neurons during a two-choice reaching assay demonstrated that reaching-task-tuned latRM neurons line up along a spectrum of differential firing rate changes comparing medial to lateral reaches (Fig. 4.5.f, g). Our findings demonstrate that excitatory latRM neurons are essential during forelimb reaching for end point targeting. In addition, some neurons exhibit signatures of reaching directionality, a property that has previously been observed in the cortex of monkeys and mice (Georgopoulos et al. 1982, Galinanes et al. 2018).

We next assayed the performance of latRM-hM4Di-vGlut2 mice or of vGlut2cre mice injected in the latRM with an AAV encoding DTR (hereafter, latRM-DTR-vGlut2 mice; referred to collectively as latRM-hM4Di/ DTR-vGlut2 mice) in pasta handling, a well-established paradigm for determining and quantifying the ability of rodents to manipulate food with their forepaws (Tennant et al. 2016, Whishaw et al. 2017). Rodents rarely drop the pasta piece and use stereotypical handling patterns (Tennant et al. 2016, Whishaw et al. 2017), using a constant forepaw to guide the pasta into the mouth (guide paw) while the second paw grasps the pasta piece further away to stabilize it (grasp paw), together allowing for a relatively stable angle of the pasta (Fig. 4.4.e). The latRM-hM4Di/DTR-vGlut2 mice exhibited severe pasta-handling defects, dropping pasta pieces significantly more frequently than during control sessions (Fig. 4.4.f). We also found that latRM-hM4Di/ DTR-vGlut2 mice frequently switched hands during handling (Fig. 4.4.g) and that pasta-angle stability was severely affected, which led to an overall broadening of the pasta-angle tuning curve owing to handling instability and hand switching (Fig. 4.4.h, Fig. 4.6.a). However, despite these notable defects in pasta handling, latRM-hM4Di/ DTR-vGlut2 mice were not deficient in grip strength (Fig. 4.6.b), which suggests that the forelimb behavioural defects relate to the orchestrated use of forepaws in manipulation. Together, these experiments demonstrate that excitatory latRM neurons are

required for various aspects of skilled forelimb movements, as shown here for reaching and food handling.
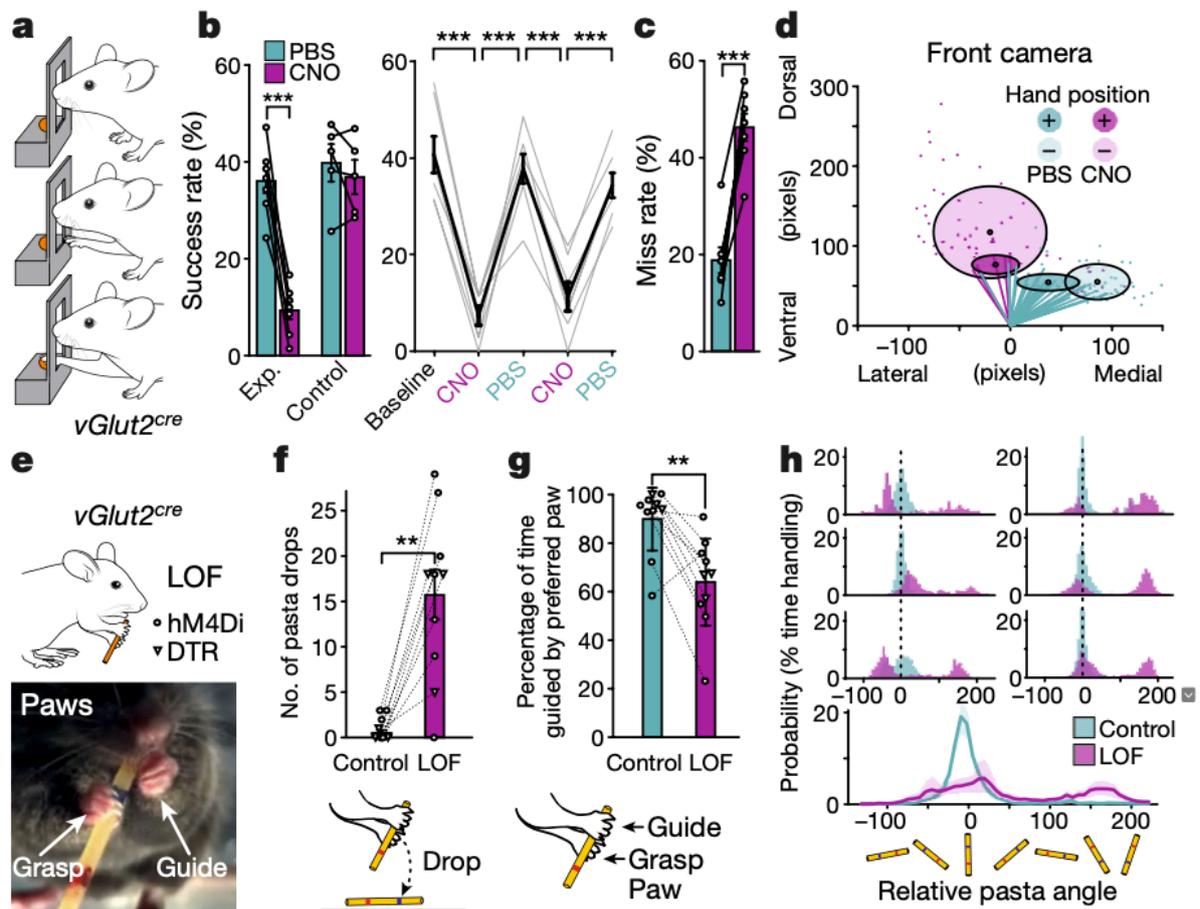
Figure 4.4. Excitatory latRM neurons are required for reaching and handling.

(a) Experimental design for food-pellet reaching assay, displaying mouse before reaching onset, during reaching and at target

(b) Success rate for the same group of experimental (exp.) mice trained on pellet task (exp., n = 7 mice; control, n = 5 mice), displaying overall success rate (left) and success rate separately displayed by baseline recording day as well as two days each with the injection of CNO or phosphate-buffered saline (PBS) (right)

(c) Increased miss rate of food-pellet targeting upon CNO injections in latRM-hM4Di-vGlut2 mice (n = 7 mice)

(d) Point of maximal extension for reaching trajectories. Solid circles, average position of trials not missing the target; transparent circles, same measure for missed trials (each on days with PBS or CNO injection, respectively)

(e) Illustration of pasta-handling assay, displaying guide and grasp forepaw used in the handling task and the markings on pasta used for tracking of pasta position

(f) Quantification of the number of pasta drops per behavioural session for latRM-hM4Di/DTR-vGlut2 mice without (control) or with (loss of function (LOF)) perturbation of excitatory latRM neurons. n = 7 mice for hM4Di; n = 3 mice for DTR

(g) Quantification of percentage of time during which the preferred paw (as defined for the control condition) is used as guide paw. n = 7 mice for hM4Di; n = 3 mice for DTR

(h) Fraction of time spent handling pasta at a given angle, relative to the preferred pasta angle for each mouse defined in the control session (set to 0 degrees) (Methods) shown for six representative mice (top) and average of all analysed (bottom) (n = 7 mice for hM4Di; n = 3 mice for DTR). Data are mean ± s.e.m. (b, c) and mean ± s.d. (f, g); Shades around mean denotes ±s.d. **P < 0.01 ***P < 0.001, two-sided paired t-test (b, c) or Wilcoxon signed-rank test (f, g)
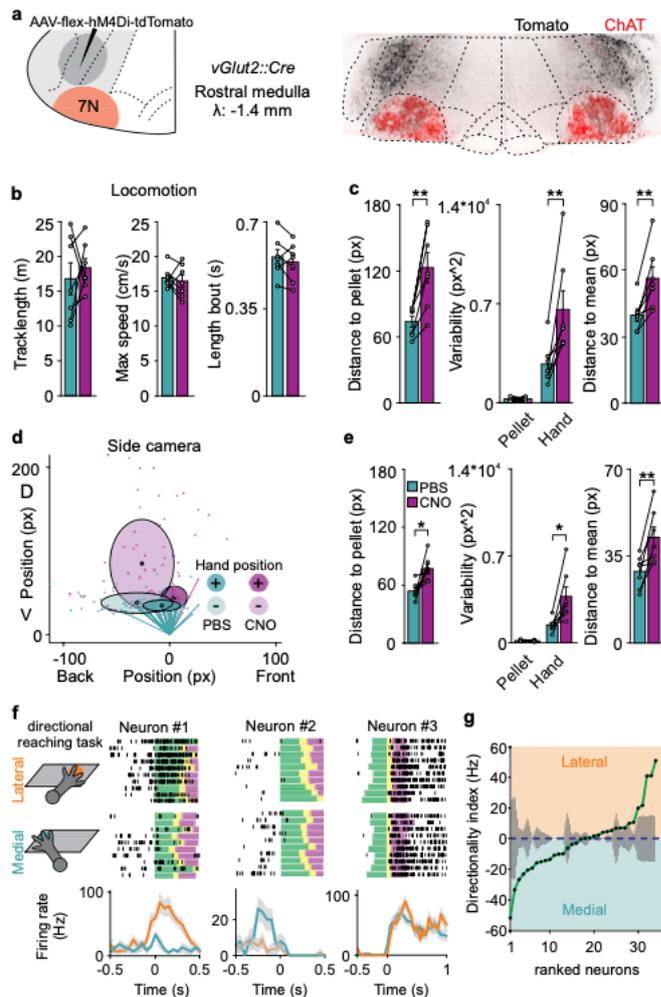
Figure 4.5. Excitatory latRM neurons are required for precise directional reaching.

(a) Experimental scheme for injection of AAV-flex-hM4Di to the latRM of vGlut2cre mice and representative picture of targeting specificity for behavioural experiments, counterstained for ChAT

(b) Attenuation of excitatory latRM neurons does not lead to defects in open field locomotion (track length, maximal speed and length of locomotor bouts), comparing PBS and CNO trials (n = 7 mice)

(c) Quantitative analysis of distance to food pellet, variability and distance to mean, separately shown for PBS and CNO trial days (front camera analysis, same mice as in Fig. 2; n = 7 mice).

(d) Analysis of point of maximal extension for reaching trajectories using a side camera for recordings (dark coloured circles: average position of trials not missing the target; light coloured circles: same measure for missed trials; each on days with PBS or CNO injection, respectively)

(e) Quantitative analysis of distance to food pellet, variability and distance to mean, separately shown for PBS and CNO trial days (side camera analysis; n = 7 mice)

(f) Experimental design for two-choice directional reaching task with lateral and medial reaching positions (left), three examples for recorded latRM neurons (right; n = 1 neuron each), each displaying single trials aligned to behavioural phases (green: reach; yellow: grasp; magenta: retract), spikes shown as lines (top), as well as average firing rates for lateral versus medial recorded trials (bottom)

(g) Quantification of directionality index (sorted from medial to lateral in ascending order, n = 34 neurons) for latRM neurons recorded during the two-choice directional reaching task. Data are mean ± s.e.m. (grey shades); *P < 0.05; **P < 0.01; two-sided paired t-test
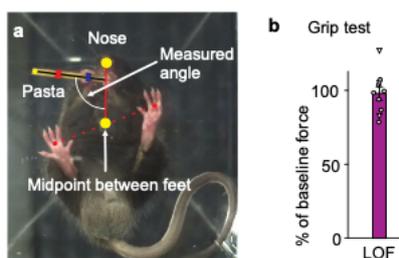
Figure 4.6. Excitatory latRM neurons are required for pasta handling but not grip strength.

(a) Scheme explaining the approach to quantify pasta angle during handling

(b) latRM-hM4Di/DTR-vGlut2 mice do not display defects in grip strength (n = 7 mice hM4Di and n = 3 mice DTR; data are mean ± s.e.m.)

Projection targets divide latRM neurons

The behavioural requirement and differential recruitment of excitatory latRM neurons in distinct phases of skilled forelimb movements raises the question of whether latRM neurons can be meaningfully stratified using anatomical and genetic approaches. We used anterograde tracing approaches with latRM-centred injections of AAV-flex-SynTag into vGlut2cre mice (Extended Data Fig. 4.8.) to select three major termination regions for further analysis. These were the cervical spinal cord, the caudal medulla at the level of 10N and 12N (vagus and hypoglossal)

motor neurons, and the contralateral latRM (Extended Data Fig. 4.8.). We injected AAVs with retrograde targeting potential (Tervo et al. 2016) that conditionally express nuclear tags (retAAV-flex-nTag) into these downstream regions of vGlut2cre mice and mapped distribution of neurons retrogradely marked in the rostral medulla (Fig. 4.7.a, Fig. 4.9.). We subdivided caudal medulla injections into medially (medullary reticular formation, ventral part (MdV)) and laterally (medullary reticular formation, dorsal part (MdD)) centred positions (Fig. 4.7.a).

We first compared neuronal distributions between the medial rostral medulla (medRM) and latRM. For spinally or MdV-projecting populations, about 80% of the neurons were located within the medRM and there was a high level of overlap between these populations (Fig. 4.9.). MdD-projecting neurons showed the opposite distribution profile, with around 80% residing in the latRM. Neurons projecting to the contralateral latRM were also dominant within the latRM (Fig. 4.9.). We next assessed the distribution patterns of the four retrogradely marked populations within the latRM. We observed a notable difference between spinally and MdD-projecting excitatory latRM neurons: the first population showed a dominant neuronal cluster immediately dorsal to the facial nucleus within the ventral parvicellular reticular nucleus. The latter exhibited a dorsally shifted cluster split between the parvicellular reticular nucleus and the adjacent spinal trigeminal nucleus (Fig. 4.7.b, Fig. 4.9.). MdV-projecting neurons were more evenly distributed within the latRM, but the highest neuronal density coincided with the spinally projecting population. Contralaterally projecting excitatory latRM neurons were also broadly distributed, but with a more medial location of the highest density (Fig. 4.7.b, Extended Data Fig. 4.9.). We determined the extent of overlap between spinally, MdV- and contralaterally projecting excitatory latRM neurons and found that the majority were anatomically separate (Fig. 4.9.). Much higher overlap was found within the medRM for spinally and MdV-projecting excitatory neurons, or when two retrograde viruses were co-injected into single target sites (Fig. 4.9.). Together, these findings demonstrate that— within the latRM—populations that are anatomically largely distinct and have different projection targets share a tight space, but exhibit spatial organization. Whereas spinally projecting latRM neurons reside most ventrally and MdD-projecting latRM neurons locate towards the dorsal pole, MdV- and contralaterally

projecting latRM neurons distribute more broadly throughout the territory (Fig. 4.7.b, Extended Fig. 4.9.).
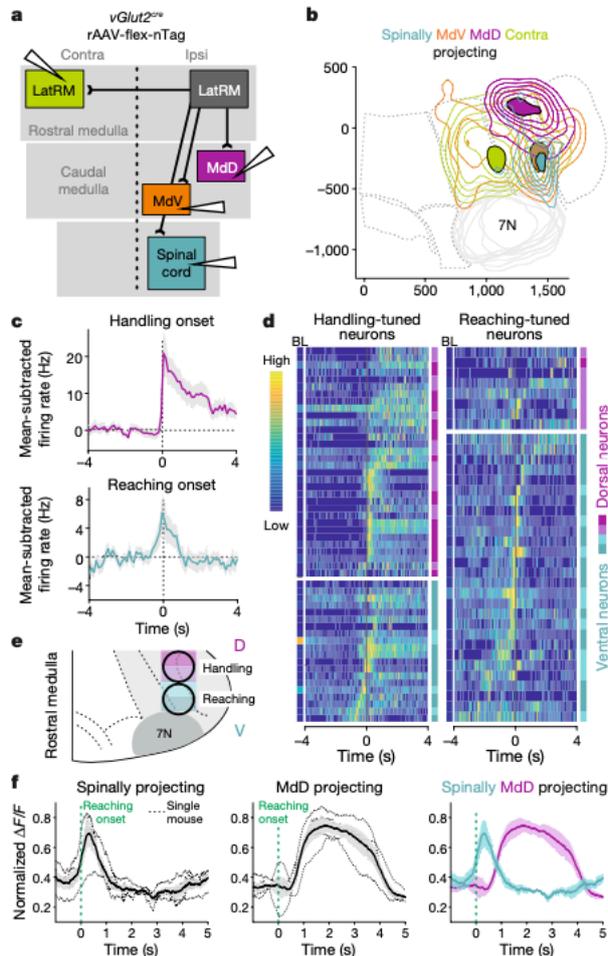
Figure 4.7. Differential tuning of latRM subpopulation to forelimb behaviours.

(a) Experimental design to analyse neuronal distribution of excitatory latRM neurons with projections to cervical spinal cord, the caudal medulla regions centred to MdV and MdD, and the contralateral (contra) latRM in vGlut2cre mice. Ipsi, ipsilateral.

(b) Density analysis of retrogradely marked neuronal cell bodies within the latRM upon injection in the four different downstream regions. Solid area marks the sites of highest sixth of density

(c, d) Mean-subtracted firing rate of behaviourally tuned latRM neurons divided by dorsal (two shades of magenta) and ventral (two shades of cyan) recording sites during pellet task. (c) Data depict average over all dorsal (top) (aligned to handling onset) or all ventral (bottom) (aligned to reaching onset) behaviourally tuned neurons. Neurons, n = 37 dorsal, n = 43

ventral. (d) Raster plot depicts individual neurons tuned to handling (left) (aligned to handling onset) (n = 52) or reaching (right) (aligned to reaching onset) (n = 36), sorted by time of maximal relative mean-subtracted firing rate. Colour scales on the left depict low (0) to high (1) for relative mean-subtracted firing rate, and low (0 Hz) to high (100 Hz) for baseline firing rate.

(e) Summary diagram to illustrate that dorsal (D) recording sites encompass preferentially latRM neurons active during handling, whereas ventral (V) sites encompass latRM neurons active already during or before forelimb reaching.

(f) Fibre photometry data analysing the dynamics of calcium activity in excitatory latRM neurons retrogradely targeted from the cervical spinal cord (left, n = 4 mice), from MdD-centred injections (middle, n = 4 mice) and overlay of the two. Shades around mean denote ±s.e.m.
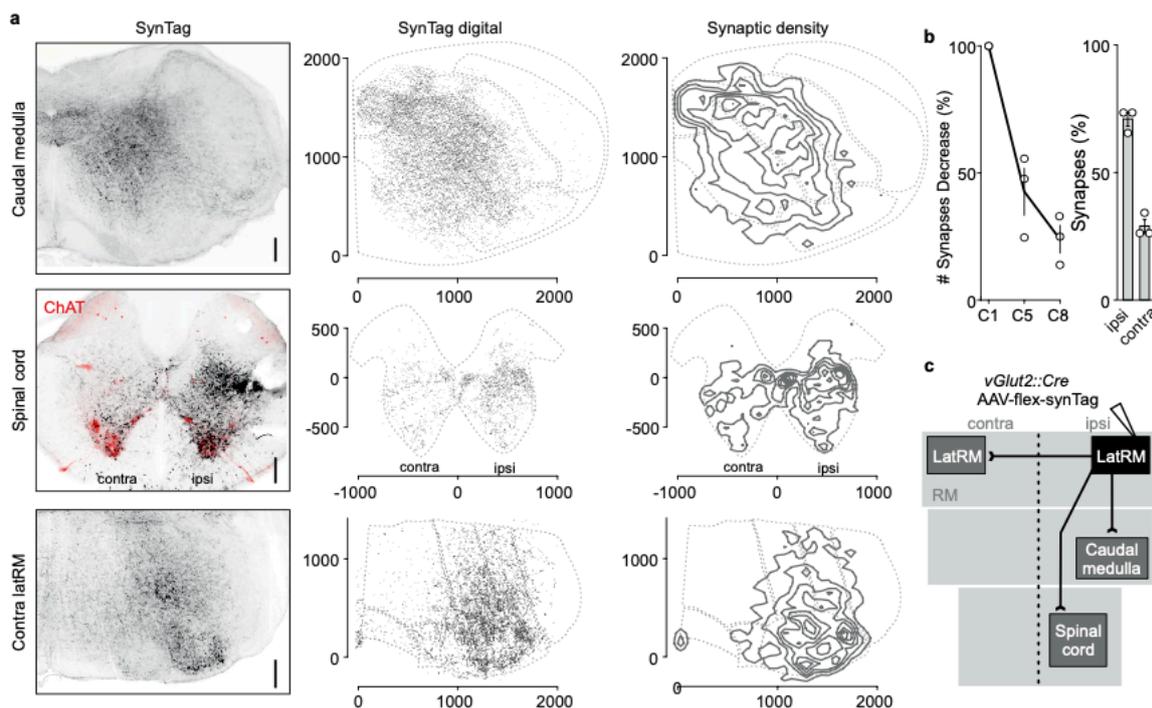
Figure 4.8. Major synaptic targeting regions of excitatory latRM neurons.

(a) Analysis of synaptic output derived from excitatory latRM neurons in vGlut2cre mice to the cervical spinal cord, caudal medulla and contralateral latRM. Representative pictures (left; from one of three mice used for quantification in b) and reconstructions (middle) of SynTag puncta and synaptic density (right) plots for these output structures are shown. Scale bar, 250 µm

(b) Quantification of synaptic numbers along the rostro-caudal axis of the cervical spinal cord (C1, C5 and C8). The decrease in synapses between rostral and caudal cervical spinal cord segments demonstrates that spinally projecting excitatory latRM neurons terminate more strongly in rostral cervical spinal cord segments compared to caudal counterparts (n = 3 mice, data are mean ± s.e.m.)

(c) Summary scheme of main synaptic output areas by excitatory latRM neurons
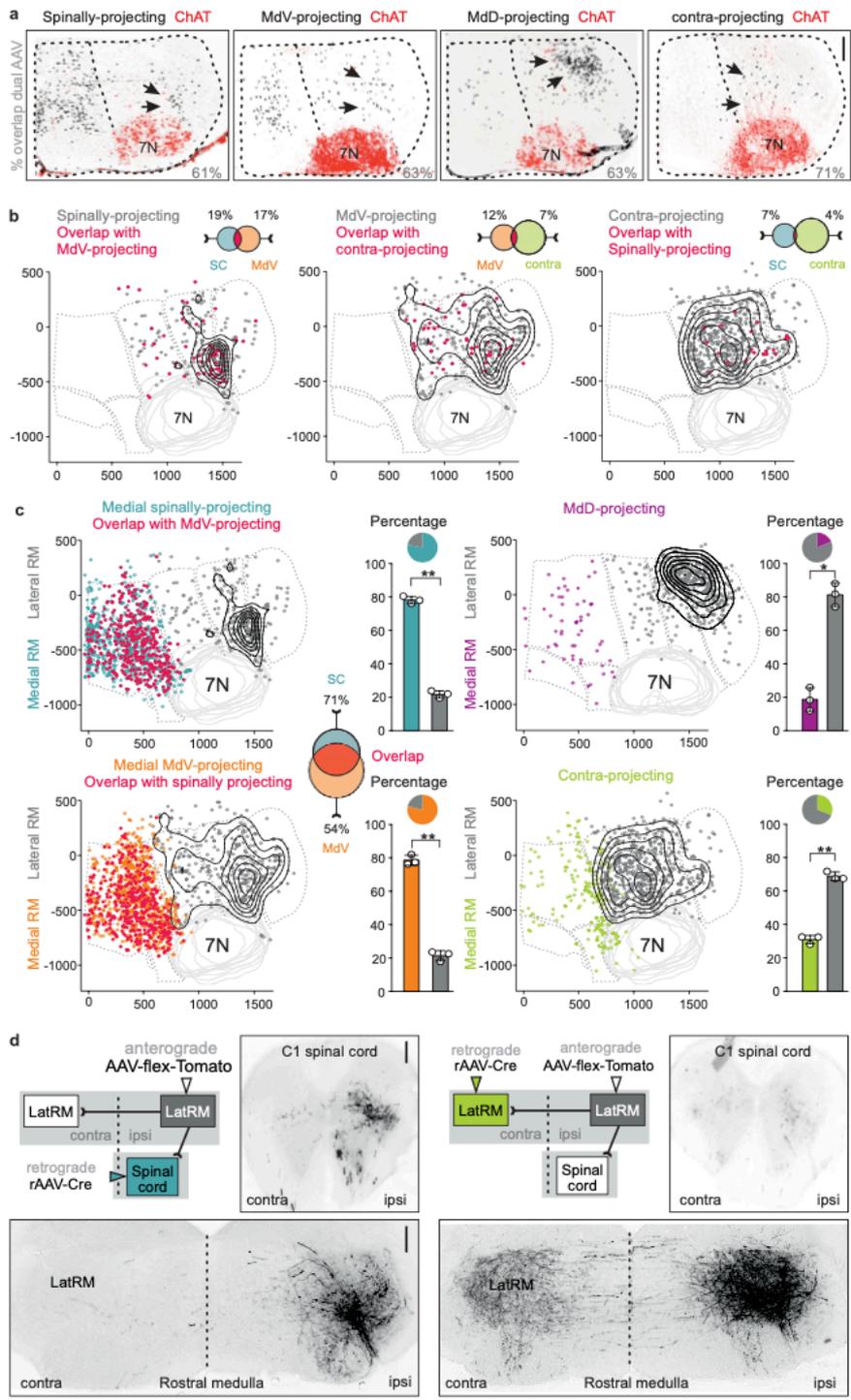
Figure 4.9. Anatomical investigation of rostral medulla neurons on the basis of projections.

(a) Example pictures of retrogradely targeted excitatory latRM neurons from cervical spinal cord (from n = 3), MdV- (from n = 2), MdD- (from n = 2) or contralateral (from n = 3) latRM-centric injections counterstained with ChAT (red). Arrows point to cluster of neurons within the latRM, dotted vertical line depicts division between medRM and latRM. Numbers in grey shown

in bottom right corner depict percentage overlap for co-injection of two retrograde AAVs into the corresponding output structure. Scale bar, 250 µm.

(b) Cellular overlap in excitatory latRM neurons retrogradely marked from triple injections in the cervical spinal cord, centred in MdV and in contralateral latRM; representative example shown. There is a minor overlap between the three populations, as indicated by the Venn diagrams (n = 3 mice; dots: position of individual neurons; red dots: overlap with other displayed population; contour lines: density for distribution).

(c) Analysis of fractions of excitatory rostral medulla neurons residing in medRM versus latRM for four analysed populations shown in different colours (colour code as in Fig. 3, n = 3 mice from triple injections in the spinal cord, MdV-centric and contra latRM, n = 3 mice from MdD-centric), as well as overlap between excitatory medRM neurons retrogradely labelled from the cervical spinal cord and MdV-centric injections (red).

(d) Experiment combining retrograde targeting of latRM neurons with rAAV-Cre from the spinal cord (left; from n = 3 independent replicates) or contralateral latRM (right; from n = 2 independent replicates) with anterograde injections of AAV-flex-Tomato into ipsilateral latRM. Pictures demonstrate sparse projections of spinally projecting latRM neurons to contralateral latRM (left), and sparse projections of contralaterally projecting latRM neurons to the spinal cord (right), visualizing Tomato immunofluorescence. Scale bar, 250 µm. Data are mean ± s.e.m.; *P < 0.05; **P < 0.01; two-sided paired t-test.

Functional tuning in latRM populations

To determine whether neurons in the dorsal and ventral latRM exhibit differential neuronal activities during forelimb tasks, we acquired single-unit data along different dorsoventral latRM positions (Fig. 4.7.c–e, Fig. 4.10.). Aligning behaviourally defined windows with neuronal activity, we found that reaching-tuned neurons were much more prevalent for ventral than dorsal latRM recording sessions.

Conversely, latRM neurons from dorsal recording positions exhibited a considerable bias towards handling tuning compared to reaching tuning (Fig. 4.7.c–e, Fig. 4.10.).

We next determined whether differential functional signatures in the dorsal and ventral latRM coincide with the activity of different populations stratified by axonal projection. We used retrograde viral injections to selectively target the expression of GCamp7s to excitatory latRM neurons projecting either to the spinal cord or the MdD, which reside mostly in ventral or dorsal latRM positions, respectively (Fig. 4.7.f, Fig. 4.11.). We found that, whereas the signal of spinally projecting latRM neurons started to be upregulated before reaching, MdD-projecting populations showed preferential upregulation during handling after reaching (Fig. 4.7.f, Fig. 4.11.). These findings demonstrate that, within the latRM, neurons tuned to the distinct fore-limb subfunctions of reaching and handling map onto a dorsoventral axis aligned with their axonal projections.
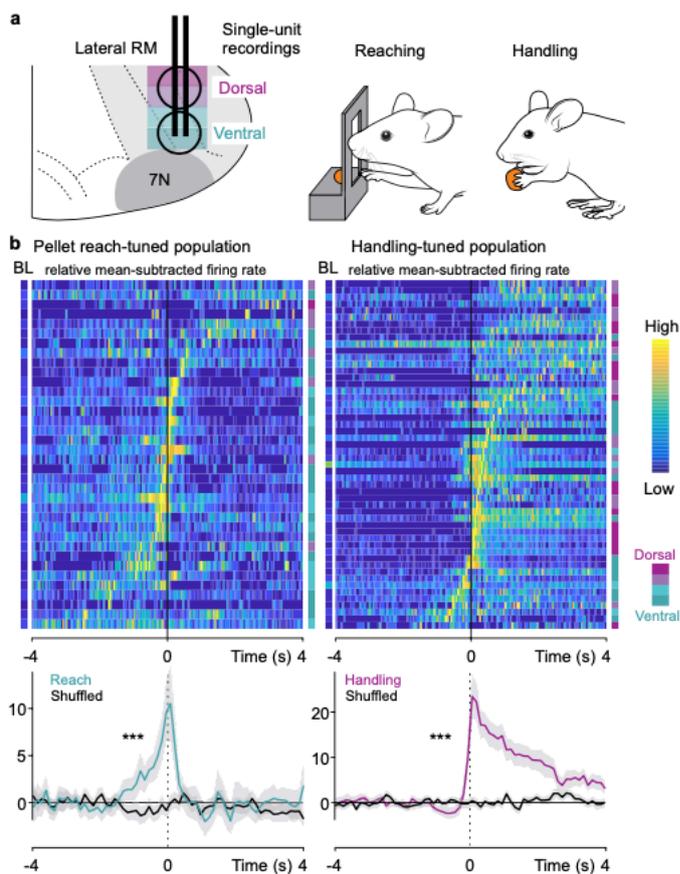
Figure 4.10. Analysis of activity along the dorsoventral axis in latRM

(a) Experimental scheme depicting recording in dorsal versus ventral latRM during pellet task, with the focus on reaching versus food handling as behaviours (magenta shades: dorsal recording sites; cyan shades: ventral recording sites)

(b) Pellet-reach-tuned (left; n = 36) and handling-tuned (right; n = 52) latRM population ordered by peak time of respective behaviour onset. Dorsoventral recording position (4 depth) are indicated to the right of plot by a colour code. Bottom plots show average responses of all neurons as well as corresponding shuffled data. Colour scale depicts low (0) to high (1) for relative mean-subtracted firing rate and low (0 Hz) to high (100 Hz) for baseline firing rate; grey shades, ±s.e.m.; ***P < 0.001; Wilcoxon non-parametric signed-rank test. Bonferroni correction was applied to account for multiple comparisons
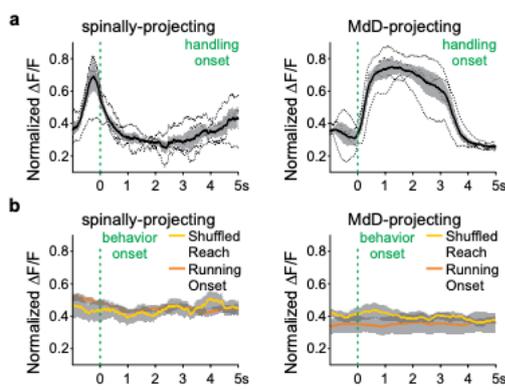
Figure 4.11. Monitoring calcium activity from spinally and MdD-projecting latRM neurons.

(a) Fibre photometry data analysing the dynamics of calcium activity in excitatory latRM neurons retrogradely targeted from the cervical spinal cord (n = 4 mice) and from MdD-centred injections (n = 4 mice). Traces are aligned relative to handling onset (dotted line). Shades around mean of individual mice are ±s.e.m.

(b) Average of mean dynamics of calcium activity for neurons shown in a during onset of locomotion trials (running, n = 4 mice MdD-centred projections, n = 3 mice spinal cord projections) or shuffled data (aligned to reaching onset, n = 4 mice MdD centred projections, n = 4 mice spinal cord projections). Shades around mean of individual mice are ±s.e.m.

LatRM neurons elicit forelimb behaviours

We next asked whether and what kind of behaviour can be induced by optogenetic stimulation of the excitatory latRM neuron populations identified by axonal targets. To contrast these

latRM-centred experiments, we also probed spinally projecting medRM neurons. We targeted rostral medulla neurons retrogradely using retAAV-(flex)-FLP-V5 injections in the different downstream targets of vGlut2cre mice and injected a dual-recombinase activated AAV (Fenno et al. 2014) expressing ReaChR into the rostral medulla with optic-fibre placement dorsal to the previously mapped highest neuronal density (Fig. 4.12.a, Fig. 4.13.a). To quantify the repertoire of behaviours elicited in these optogenetic stimulation experiments, we charted their nature and reliability for individual mice (Fig. 4.12.b–d). We found that individual mice express stable behavioural phenotypes at high reliabilities (Fig. 4.12.d). Moreover, the nature of the expressed phenotype was linked to the identity of the downstream target of the studied neuronal population, but we observed further behavioural diversity for experiments targeting MdV- or MdD-projecting latRM neurons.

Optogenetic stimulation of spinally projecting excitatory latRM neurons induced unilateral forelimb reaching, but not more-complex forelimb movements that involve digit flexure (Fig. 4.12.b–d, Fig. 4.13.). Electromyographic recordings from biceps and triceps forelimb muscles showed that the same muscle-activation sequence occurred during naturally executed and optogenetically induced forelimb reaching—albeit that the latter occurred at a faster time scale (Yakovenko et al. 2011) (Fig. 4.14.). Moreover, although this was challenging owing to the freely moving nature of our experiments, analysis of reaching-trajectory end points showed higher similarity between trials of one mouse than to the trials of other mice (Fig. 4.12.c, Fig. 4.13.b), which possibly indicates that the precise composition of the optogenetically targeted ensemble is instrumental for behavioural nuances between mice. Stimulation of MdV-projecting latRM neurons elicited ipsilateral reach-to-grasp movements in a fraction of mice, characterized by the supplementation of induced reaches by digit flexing and/or grasping, or ipsilateral forelimb tapping movements, in the remaining mice of this category (Fig. 4.12.b–d, Fig. 4.13.b). By contrast, the stimulation of MdD-projecting latRM neurons produced hand-to-mouth movements or grooming (Fig. 4.12.b–d, Fig. 4.13.). The stimulation of contralaterally projecting excitatory latRM neurons did not induce obvious movements (Fig. 4.12.d, Fig. 4.13.). Notably, whereas the behaviours elicited by stimulation of latRM subpopulations all involved

forelimb use, the stimulation of medially located spinally projecting medRM neurons induced head-turning that was ipsilateral to implantation (Fig. 4.12.d). These findings suggest a mediolateral segregation of neuronal substrates for head turning and forelimb movements within the rostral medulla in mice; this is perhaps distinct from cats, in which both elements seem to be located rather medially (Drew and Rossignol, 1990). Finally, optogenetic stimulations of excitatory latRM neurons targeted by direct injection into the latRM elicited only simple, ipsilateral forelimb movements that included reaching and tapping-like behaviours. Thus, the successful production of behavioural diversity by latRM neurons is critically dependent on the specific latRM ensemble that is targeted for optogenetic stimulation experiments through its distinct axonal projections. Whether these latRM populations also exhibit differential roles in the execution of natural forelimb behaviours awaits the generation of viral tools for more-complete retrograde targeting than is currently possible.
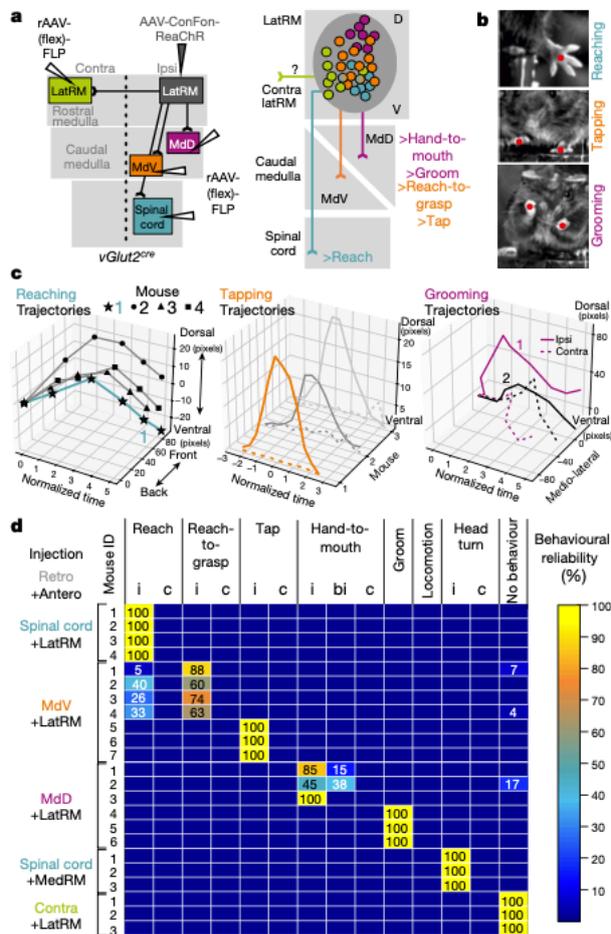
Figure 4.12. Stimulation of latRM populations elicits specific forelimb movements.

(a) Left, injection scheme for experimental design to optogenetically stimulate excitatory latRM neurons projecting to different downstream targets. Neurons were retrogradely targeted through spinal cord injections, MdV- or MdD-centred injections in the caudal medulla or contralateral latRM-centred injections of rAAV- (flex)FLP in vGlut2cre mice, combined with ipsilateral latRM-centred injections of AAV-ConFon-ReaChR to target latRM neurons co-expressing Cre and FLP. Right, summary diagram displays the alignment between identity of excitatory latRM neuron population by projection target and observed behaviours. The stimulation of latRM neurons that engage circuits in the caudal medulla elicits more-complex forelimb movements involving digits than those elicited by stimulation of excitatory latRM neurons that directly engage spinal circuits

(b) Spatiotemporal analysis of optogenetically induced movements using DeepLabCut. Data depict example pictures from movies of different behaviours as indicated, including DeepLabCut-tracked positions (red dots).

(c) Average trajectories of DeepLabCut-tracked, optogenetically induced reaching (left) (n = 4 mice), tapping (middle) (n = 3 mice) and grooming (right) (n = 2 mice). Solid and dotted lines indicate the trajectory of the ipsi- and contralateral forelimb during grooming respectively.

(d) Chart displaying behavioural repertoire of mice included in the optogenetic stimulation data set. Mouse identifier (ID) on the left is stratified by injection sites for retrograde (retro) (rAAV-(flex)FLP) and anterograde (AAV-ConFon-ReaChR) AAVs. Vertical columns depict observed behaviours, using a colour scale for behavioural reliability (0–100%) and summing up to 100% for all columns. antero, anterograde; bi, bilateral; c, contralateral; i, ipsilateral.
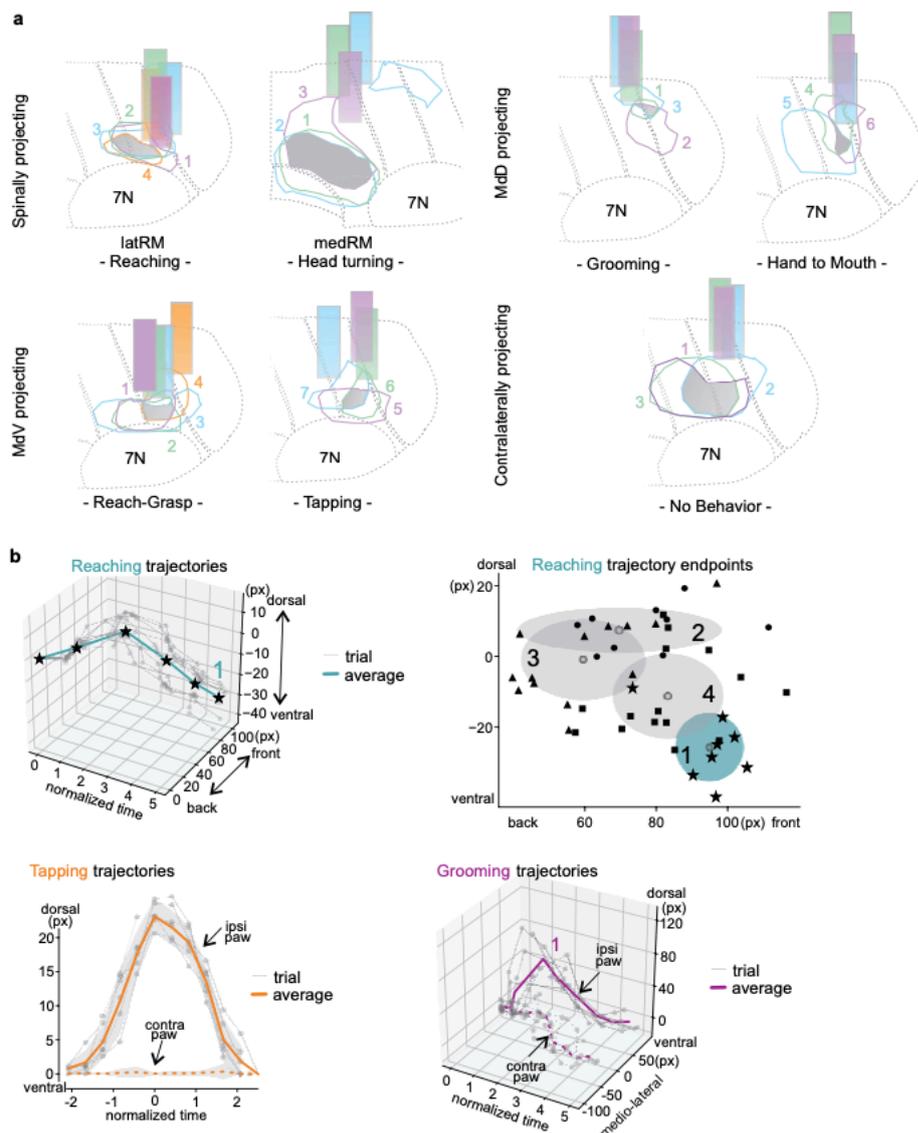
Figure 4.13. Optogenetic activation of rostral medulla subpopulations.

(a) Reconstruction of fibre placements and local virus expression sites at the rostral medulla level. Each colour corresponds to one mouse included in the analysis shown in Fig. 4.12. (code corresponds to mouse ID number shown in Fig. 4.12.d).

(b) Spatiotemporal analysis of optogenetically induced movements using DeepLabCut. Data depict reaching trajectories (top, left) of different stimulation trials (grey lines) in one mouse (average: cyan), and the lateral view of the trajectory endpoints of reaching mice shown in Fig. 4.12.c using a side-camera (top, right) (Methods). Trajectories of different stimulation trials reconstructed for forepaws ipsi- and contralateral to stimulation during optogenetically-induced tapping (bottom left; average: orange; grey shade, ±s.d.) or grooming (bottom right; average: purple) are also shown.
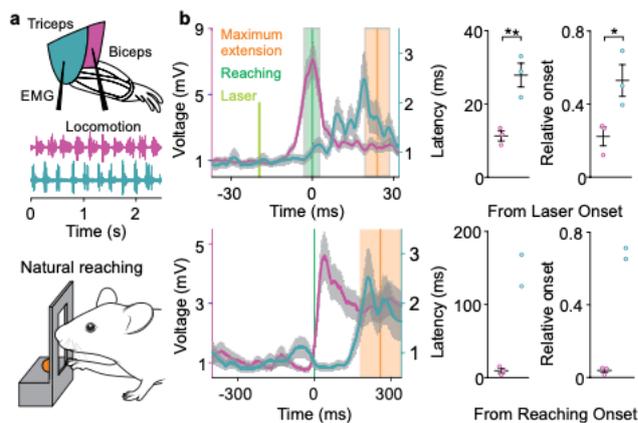
Figure 4.14. Stimulation of spinally projecting excitatory latRM neurons recruits forelimb muscles in a sequence resembling natural reaching.

(a) Scheme depicting implantation of EMGs into forelimb biceps and triceps muscles, and raw signal demonstrating that these muscles are active in alternation during natural locomotion (below), according to their flexor (biceps) and extensor (triceps) function.

(b) EMG recordings and quantification (latency and relative onset) for biceps and triceps recordings during optogenetically induced reaching by stimulation of spinally projecting excitatory latRM neurons (top; n = 3 mice for biceps and triceps) or natural reaching (bottom; 0 = reaching onset; n = 3 mice for biceps and n = 2 mice for triceps). Grey shades, ±s.e.m.; *P < 0.05; **P < 0.01; two-sided paired t-test.

4.4. Discussion

The use of forelimbs to access and manipulate objects in the environment is one of the most essential additions to the movement repertoire that arose in limbed animals, and it encompasses behavioural phases and attributes that are evolutionarily conserved from rodents to humans (Whishaw et al. 1992, Iwaniuk and Whishaw 2000, Alstermark and Isa 2012). Our work describes the latRM of the brainstem as a critical orchestrator in the execution of skilled forelimb movements. Here we discuss models of how complex, skilled forelimb movements may be regulated by the combinatorial use of specific brainstem-to-spinal cord and intra-brainstem circuits. We found that latRM neurons divide into at least four anatomically

distinct populations by axonal targets. The initiation of most skilled forelimb movements requires the transport of one or both hands to the site of action (commonly referred to as forelimb reaching). Optogenetic stimulation of the spinally projecting latRM subpopulation elicits unilateral reaching. In agreement with this, latRM neurons exhibit preferential projections to the ipsilateral rostral cervical spinal cord, which contains circuits for the control of proximal forelimb muscles. Notably, latRM neurons with direct spinal projections are not sufficient to elicit forelimb movements that are more complex than reaching. Excitatory latRM neurons projecting to the caudal medulla signal and can generate diverse and complex forelimb movements, which involve the use of digits during grasping and/or action bilateralization during grooming or hand-to-mouth movements. These diverse forelimb behaviours are stably expressed in individual mice in a 'winner-take-it-all' fashion, probably owing to the targeting of specific neuronal ensembles through retrograde axonal infection (which is instrumental for obtaining behavioural diversity through optogenetic probing). Caudal medullary neurons then establish functional links to the caudal cervical spinal cord essential for generating distal forelimb movements (Esposito et al. 2014), which probably involve propriospinal neurons with direct connections to motor neurons (Alstermark and Isa 2012, Pivetta et al. 2014).

Our work uncovers the existence and organization of brainstem circuits that encompass task- and action-phase-selective neuronal ensembles in the rostral medulla. Notably, shared latRM neuronal ensembles are engaged during related forelimb actions (that is, reaching in different forelimb behaviours), whereas distinct ensembles are used for dissimilar forelimb movements (that is, reaching versus food handling). No significant encoding in the latRM is observed for locomotion. The circuit elements described here are, therefore, non-overlapping with pathways that implement full-body movements including locomotion (Shik and Orlovsky 1976, Roseberry et al. 2016, Capelli et al. 2017, Caggiano et al. 2018), which engages the same muscles but in an entirely different task and context. These findings resonate with recent work in the striatum, in which closer actions are also encoded by overlapping neuronal ensembles whereas distant actions engage distinct ensembles (Barbera et al. 2016, Klaus et al. 2017, Parker et al. 2018). In the striatum, these ensembles are found in common overall space,

whereas our findings demonstrate that the anatomical demixing of signals for locomotion and skilled forelimb movements has occurred within brainstem circuits. The brainstem neuronal populations we identify here are in a prime position to integrate cortical and other brain-wide signals and transmit them for precise forelimb execution to the spinal cord. Even beyond its role in execution of forelimb movements, the lateral brainstem is a complex integration hub for higher motor centres that are also engaged in regulating orofacial behaviours (Ruder and Arber, 2019, Han et al. 2017, Svoboda and Li 2018, Mercer Lindsay et al. 2019, Petersen 2019), which suggests additional integration and coordination in this area. The discovery that neuronal segregation by task specificity in action space exists in the most caudal part of the brain, and that the identified brainstem neurons together are needed to implement different aspects of skilled forelimb movements, provides a deep understanding of how body actions that use limbs are regulated through the engagement of dedicated neuronal circuits.

4.5. Methods

Mice

We used *vGlut2^{Cre}* mice (RRID: IMSR_JAX:028863) (Vong et al. 2011) maintained on a mixed genetic background (129/C57Bl6). Experimental mice originating from different litters were used in individual experiments. No criteria were applied to allocate mice to experimental groups, and mice had marks for unique identification. For all behavioral experiments, we used 2-4-month-old heterozygous males, backcrossed to C57Bl6. Mice were maintained on a 12-h light–dark cycle in a temperature (22 ± 1 °C) and humidity controlled (45–65%) environment. Housing, surgery procedures, behavioural experiments and euthanasia were performed in compliance with the Swiss Veterinary Law guidelines.

Virus production and injections

We used the following, previously described adeno-associated viruses (AAV), all based on a backbone derived from Allen Brain (AAV-CAG-flex-tdTomato-WPRE-bGH): AAV-flex-SynGFP (Pivetta et al., 2014) and AAV-flex-SynMyc (referred to as AAV-flex-SynTag) (Takeoka et al.

2014), AAV-flex-Flp-H2B-V5 and AAV-H2B-10xMyc (Capelli et al. 2017). Viral constructs that have not previously been reported were designed by analogy with the above constructs: AAV-flex-H2B-GFP, AAV-flex-H2B-TdTomato, AAV-flex-H2B-V5 (last three AAVs commonly referred to as AAV-flex-nTag), AAV-flex-hM4Di-Tomato, AAV-flex-GCaMP7s (Dana et al. 2019) and AAV-Flp-H2B-V5. The AAV-ConFon-ReaChR-Citrine-YFP construct was created using a previously described strategy(Fenno et al. 2014). To infect neuronal cell bodies but not axons, a serotype plasmid 2.9 was used as in previous studies(Esposito et al. 2014, Pivetta et al. 2014, Takeoka et al. 2014, Basaldella et al. 2015). For retrograde labeling by means of axonal infection, a recently developed rAAV2-retro capsid plasmid(Tervo et al. 2016) was used for coating as previously(Capelli et al. 2017). AAVs used in this study were of genomic titers >1x10e13 and produced following standard protocols.

Viruses were injected into the brainstem with high precision stereotaxic instruments (Kopf Instruments, Model 1900) under isofluorane anesthesia as previously described (Esposito et al. 2014, Capelli et al. 2017). Viral injections in the spinal cord were targeted to the cervical spinal cord comprising spinal segments C1–C5 (approximate injection volume of 300–500 nl). The following coordinates were used to target the investigated brainstem regions referenced with lambda as the point of origin for anterior–posterior (AP), mediolateral (ML) and dorsoventral (DV) axes (approximate injection volumes of 50–100 nl): latRM (−1.4; ±1.55; −4.8 (AP; ML; DV; in mm)); MdV (−3.0; ±0.6; −5.5); MdD (−3.0; ±1.4; −5.3); latRM dorsal (−1.4; ±1.55; −4.3); and medRM (−1.4; ±0.5; −4.8). To map output projections of excitatory latRM neurons, we injected AAV-flex-SynTag and waited more than two weeks for expression. Retrograde tracings of latRM outputs using retro-flex-nTag viruses were carried out by injections in the spinal cord before brainstem injections. After the final injection, we waited for over ten days. Triple injections were performed for the combination of spinal cord, MdV and the contralateral latRM. MdD injections were performed in separate experiments. For co-injections into single target regions, viruses were mixed before injection. Injections to bilaterally target excitatory latRM neurons for loss-of-function experiments were carried out more than

two weeks before baseline reaching-success rates were assessed or handling proficiency was assayed, to allow for sufficient time for expression of hM4Di. CNO (Tocris, cat. no. 4936) was injected intraperitoneally at 10 mg per kg body weight in PBS to initiate attenuation of neuronal firing upon interaction with the hM4Di receptor (Caggiano et al. 2018, Armbruster et al. 2007). For mice expressing DTR in excitatory latRM neurons, diphtheria toxin (Sigma D0564) was administered intraperitoneally (100 ng per g body weight) after baseline behaviours were recorded. For optogenetic activation of selected neuronal subpopulations, injections involving the cervical spinal cord were conducted first, as described for anatomical experiments and using retro-(flex)-Flp-H2B-V5. Subsequently, the latRM was injected unilaterally with AAV-ConFon-ReaChR-Citrine-YFP and an optic fibre was implanted 200 µm above the injection site (diameter of 200 µm, MFC_200/230-0.48_6mm_ZF1.25_FLT Mono Fibreoptic Cannula; Doric lenses). For all other subpopulations stratified by projections involving targets in the brainstem (contralateral latRM, MdV and MdD), injections and implantations were targeted only to the brainstem. For fibre photometry experiments, the optic fibre was implanted 100 µm above the neuronal population of interest (diameter of 200 µm, MFC_200/230-0.48_6mm_ZF1.25_FLT Mono Fibreoptic Cannula; Doric lenses). For electrophysiological recordings, single-shank chronic 16-channel or dual-shank chronic 32-channel silicon probes were implanted (Cambridge NeuroTech, P-series, 6 mm length). These were mounted on a nanodrive (Cambridge NeuroTech) allowing for sequential recordings at different depths and implanted in the latRM (AP and ML coordinates as for virus injections) at a dorsal–ventral depth of around −3.0 mm using light curable cement (Relyx Unicem 2, 3M). Stimulation experiments were started over two weeks after injection and implantation. We assessed injection sites after termination of experiments by using ChAT immunohistochemistry (as described in 'Immunohistochemistry and microscopy') to visualize motor nuclei. For electrophysiological recordings, we also visualized the site of electrical lesion at the end of the recordings to confirm correct probe placement. The mouse brain atlas was used as reference for determining the spatial injection specificity of the viral labelling[29]. For optogenetic activation experiments with latRM and medRM subpopulations, we mapped fibre placement as well as

the extent of targeted neurons at injection sites. Only mice with confirmed anatomical precision were included in the subsequent analysis. The region here referred to as the latRM combines sites of the brainstem regions indicated as intermediate reticular nucleus, parvicellular reticular nucleus and spinal trigeminal nucleus (Franklin and Paxinos 2007) in the rostral part of the medulla spanning the rostro-caudal extent of the facial motor nucleus (7N). The rostro-caudally aligned region medial to latRM is referred to as medRM. For MdV and MdD nomenclature, we followed the boundaries delineated in the mouse brain atlas (Franklin and Paxinos 2007).

Electrophysiological recordings

Following surgery (as described in 'Virus production, injections and implantations'), the probe was lowered during subsequent days to the starting position in the latRM. After every recording session, the probe was lowered by 100–200 µm to record along the dorso-ventral axis of the latRM to finally reach the position in the facial nucleus (7N, DV: −5.0 mm from the brain surface) on the last experimental day. For recordings specifically focusing on DV position analysis, the electrode was lowered in steps of 200 µm, spanning the latRM DV axis in four steps (the first two grouped as dorsal indicated by shades of magenta and second two grouped as ventral indicated by shades of cyan in the corresponding figure panels). Electrical lesions (3 s at 200 µA) shortly before perfusions were performed to confirm recording locations (Fig. 4.2.) using an electrical stimulator (WPI, Stimulus isolator A360). The extracellular signal was amplified and acquired at 40 kHz using a commercially available soft- and hardware recording system (OmniPlex, Plexon). Filtered, continuous data from each recording session consisting of all behavioural tasks carried out within this session were grouped into adjacent, fictive tetrodes and sorted manually in tetrode mode, using commercially available software (Offline Sorter v.3.3.5, Plexon). Autocorrelation, high relative signal-to-noise ratios as well as waveform comparison were used to ensure high-quality data using commercially available software (NeuroExplorer v.5, Plexon) (Fig. 4.2.e). Further cross-correlation between channels ensured the elimination of units recorded at multiple recording sites. For recordings comparing multiple behaviours (as described in 'Behavioural experiments'), we recorded a total of 243 neurons in

the lever task, 212 neurons during pellet reaching and handling and 198 neurons during open field behaviour, totalling 246 neurons across all behaviours and 194 neurons that were stable and reliably present across all behaviours in 5 mice (Fig. 4.2.a). For recordings assessing differential encoding along the dorsoventral axis and distinct response properties depending on mediolateral reaching direction (as described in 'Behavioural experiments'), we recorded a total of 144 neurons in 2 mice. Sorted, single-unit data and spiking time points were used for further analysis on other freely moving behaviours (as described in 'Behavioural experiments' and 'Behavioural analysis, scripts and statistics').

Electromyographic recordings

For electromyographic (EMG) recordings during stimulation of spinally projecting latRM neurons, injections and fibre implantation were conducted as described in 'Virus production, injections and implantations'. Cable preparation and EMG implantation of the biceps and triceps muscle were conducted as previously reported[53]. Acquisition was carried out either in response to optogenetic stimulation (as described in 'Optogenetic activation experiments') or during pellet reaching (as described in 'Pellet reaching task'). The signal was amplified and bandpass-filtered (A-M systems 1700, gain 100, bandpass 100–1,000 Hz) and acquired using a Plexon recording system (Omniplex, Plexon) at 5,000 Hz. We subsequently applied a mean subtraction to correct for the DC offset.

Photometry recordings

Recordings of calcium activity started two weeks after surgery, using a multi-fibre photometry system (CineLyzer, Plexon). Implants were connected to the system through a customized patch cord (Doric Lenses) to simultaneously allow for delivery of excitation light (470 nm Plexon) and collection of GCaMP emission at 60 Hz. A continuous excitation intensity of 30–40 µW was used for all experiments, measured as described in 'Optogenetic activation experiments'. Experimental sessions were repeated to collect at least ten successful, first-reaching trials, as describing in 'Pellet task' in 'Behavioural experiments').

Immunohistochemistry and microscopy

Immunohistochemistry to visualize virally expressed transgenes was performed on all mice used in this study. This included mice from anatomical and behavioural experiments. Mice were anaesthetized using a ketamine–xzylazine solution before transcardial perfusion with cold PBS and subsequent fixation using a 4% paraformaldehyde (PFA) solution (Sigma). Brains and spinal cords were carefully dissected and post-fixated with PFA for over 8 h following perfusion. To cryopreserve the tissue, we incubated brains and spinal cord in a 30% sucrose w/v in PBS solution for at least one day. We cut 80-µm-thick slices on a cryostat, collected sections sequentially into individual wells (coronally for brain tissue and transversely for spinal cord). Following a one-hour incubation in blocking solution (1% BSA/0.2% TritonX100/PBS), we added primary antibodies diluted in blocking solution for 1–3 days of incubation at 4 °C. Secondary antibodies were used for one-day incubations at 4 °C, after extensive washing of tissue sections. After final washing, we mounted sections on glass slides with anti-bleach preservative medium in sequential order along the rostro-caudal axis. Primary antibodies used in this study were: chicken anti-GFP (Invitrogen, 1:2,000), chicken anti-MYC (Invitrogen, 1:5,000), goat anti-ChAT (Millipore, 1:500), mouse anti-MYC (ATCC, 1:100), mouse anti-V5 (Invitrogen, 1:1,000) and rabbit anti-RFP (Rockland, 1:5,000). Secondary antibodies used were: Alexa Fluor 488 donkey anti-chicken IgY (Jackson, 1:1,000), Cy3 donkey anti-mouse IgG (Jackson, 1:1,000), Cy3 donkey anti-rabbit IgG (Jackson, 1:1,000), Alexa Fluor 488 don- key anti-goat (Jackson, 1:1,000), Cy3 donkey anti-goat IgG (Jackson, 1:1,000) and Alexa Fluor 647 donkey anti-goat IgG (Jackson, 1:1,000). To acquire low-resolution overview images, we used an Axioscan light microscope (Zeiss, 5× objective) and for higher-resolution imaging, we used a FV1000 confocal microscope (Olympus) or a custom-made spinning disc microscope (Visitron).

Anatomical reconstructions

<u>Three-dimensional reconstructions of latRM neurons stratified by projection target:</u> To assess the spatial location, quantitative contributions and overlap between populations of latRM neurons projecting to the contralateral latRM, ipsilateral MdV, ipsilateral MdD and spinal cord, 80μm thick coronal brainstem sections were acquired with the 20x objective of a FV1000 confocal microscope tiling mosaics of multiple fields of view (tile number was variable depending on the size of the medulla at different rostro-caudal levels) in order to cover the full section (z-step= 4μm). Subsequent stitching and maximum intensity projection images were used as previously described (Esposito et al. 2014, Capelli et al. 2017). Manual alignment using Amira (Thermo Fisher Scientific) preceded automatic cell-body position assignment with customized image analysis workflows in Knime. Respective regions were assigned using the mouse brain atlas as previously described (Franklin and Paxinos 2007) , and as described in 'Virus production, injections and implantations'. Two-dimensional density plots were generated using 2D kernel density estimates, plotting 6 density lines covering the space of 20–100% of highest density equally using the MATLAB function kde2d (Botev et al. 2010).

<u>Reconstructions of synaptic output of excitatory latRM neurons:</u> To assess major output projections of excitatory latRM neurons, 80-μm-thick coronal brainstem sections or transverse spinal cord sections were acquired with a 40× objective of a confocal microscope (FV 1000, Olympus) or a custom-made spinning disc microscope (Visitron), tiling mosaics of multiple fields of view (z-steps of 2 μm). Subsequent stitching and maximum intensity projection images were generated using custom-made macros in Fiji. Automatic synaptic spot detection was carried out in Imaris (v.9.1.2. Oxford Instruments, Bitplane) and 2D density plots were generated using 2D kernel density estimates, plotting 6 density lines covering the space of 10–100% of highest density equally using the MATLAB function kde2d (Botev et al. 2010). To assess the decrease of synapses derived from excitatory latRM neurons along the rostro-caudal axis in the spinal cord, the total number of detected synapses at C1 was used as a reference to calculate the decrease in synaptic numbers at C5 and C8 levels.

Behavioral experiments

Open Field Assay: Mice were placed in a 35 × 35-cm square arena, which they were allowed to explore freely for at least 10 min. For single-unit recording experiments, mice were exposed to tasks in a sequential manner, including the open field assay at the end. For loss-of-function and photometry experiments, open field sessions were carried out after the experimental days during which the pellet task was completed.

Lever Task: Mice were kept under water restriction and body weight was monitored to not drop below 85% of the original weight. We used a custom-made behavioral chamber allowing for high-speed videography from the two sides of an ultra-sensitive (2g sensitivity) lever (MedAssociates Inc.) adapted from previous work (Jin and Costa 2010). Water rewards (50 µl) were delivered in the chamber at a spatially separate location from the lever in response to single lever presses using electrically controllable water pumps (MedAssociates). Training consisted of exposure to the behavioural box during 3 training days for a maximum of 60 min or 5 (day 1), 10 (day 2) or 20 (day 3) rewards. Experiments with mice that did not achieve at least 20 rewards on the 4th training day were not continued. Selected mice were then trained to reliably achieve at least 20 rewards by pressing the lever during at least 4 more training sessions. The entire training did not exceed two weeks. For analysis, only first-attempt forelimb lever presses (as described in 'Behavioural analysis, scripts and statistics') were used. During experimental sessions, mice were allowed to press the lever for as long as they were engaged in the task to achieve a maximum number of successful trials for analysis. The protocol was applied in closed-loop using an Arduino Uno board (Arduino) coupled with transistor–transistor logic (TTL) pulses recording lever-press time points and triggering water rewards via the Arduino MATLAB extension package (The Mathworks). A synchronizing start TTL pulse was sent from the Arduino Uno board to the OmniPlex recording system to allow for correct alignment of behavioural with electrophysiological data.

Pellet Task: Mice were kept under food restriction and body weight was monitored to not drop below 85% of the original weight. A custom-made chamber was designed as previously reported(Xu et al. 2009, Esposito et al. 2014), containing a slit through which mice were trained to reach for a food reward. Movies were taken using one camera from the front and one from

the side (Pike, Allied Vision, 200 frames per second (fps)) or only a side camera for photometry experiments (Plexon, 60 fps). On the first day, mice were allowed to also obtain food pellets with their tongue. On following days, food pellets were placed at a marked, consistent position outside the slit further away, to not allow for tongue retrievals to enforce forelimb reaching trials. The position of the pellet was slightly moved to the side relative to the slit, depending on whether mice were right- or left-handed. Mice were trained for at least 8 days, aiming for a success rate of over 30% and with a goal of retrieving more than 15 pellets or 35 reaches. For loss-of-function experiments, mice with a baseline success rate of less than 30% were excluded. Following the baseline session, mice were injected intraperitoneally first with CNO (10 mg per kg body weight in PBS) and then with PBS, spaced by at least 24 h from each other, followed by another analogous exposure paradigm. CNO or PBS injections occurred 40 min before initiation of the pellet task. For single-unit recordings, mice were exposed to other behavioural tasks consecutively and no success-rate exclusion rate was applied. For photometry experiments, mice were exposed to the pellet task and subsequent food handling. For analysis, only successful, first-attempt forelimb reaches (as described in 'Behavioural analysis, scripts and statistics') were used. For the two-choice pellet reaching task and recordings along the dorsoventral axis, mice were first trained the same way for three sessions with only one slightly shifted pellet position. From the fourth training session onward, a second pellet was placed exactly in the middle at the same distance, aligned with the slit. Mice were trained to reach for both positions to retrieve pellets for at least another 12 sessions before silicon probe implantation. During experimental sessions, mice were allowed to reach for as long as they were engaged in the task to achieve a maximum number of successful trials for analysis. For analysis along the dorsoventral axis, medial and lateral reaches were pooled into one reaching category (as described in 'Electrophysiology analysis').

Handling Task: Mice were kept under food restriction as described in 'Pellet task'. During habituation, they were provided with short spaghetti sticks in the home cage and exposed to the testing chamber (10 min, once a day for 2 days). For loss-of-function experiments, the testing chamber was a 8.2 by 7.1-cm custom-made plexiglass box with transparent floor,

mounted on a holder containing a 45°-inclined mirror, allowing for a bottom view of the paws during pasta handling. Movies were taken using one camera from the front and one directed at the mirror (Pike, Allied Vision, 200 fps). During behavioural testing (20-min session), spaghetti sticks (about 2 cm in length) were presented, upon which mice started bilateral handling as previously reported (Tennant et al. 2010). For data analysis of electrophysiological data, additionally, successful trials in the pellet task resulted in the retrieval of food pellets, thereafter handled with both hands, resulting in qualitatively similar movements as during spaghetti handling. These trials were pooled for analysis.

Grip strength analysis: Forelimb grip strength of mice was tested as previously described (Esposito et al. 2014).

Optogenetic activation experiments: Optogenetic activation of rostral medulla neurons was performed using a PlexBright Optogenetic Stimulation System (Plexon) in combination with laser stimulation (Cobolt 06-MLD; 473 nm; 100 mW). The laser was triggered manually when mice were at rest. Unless otherwise specified, we used continuous light exposure at intensities of 5 or 10 mW. We measured the laser intensity at the beginning of every experimental session at the tip of an optic fibre of the same length as the one implanted to ensure precise and reliable stimulation strength with an optical power meter (Thorlabs). Mouse behaviours and responses were monitored simultaneously with two cameras (Pike, Allied Vision) at 200 fps or a Sony alpha 7s camera (Sony) at 100 fps in an open field environment. For trajectory reconstructions with DeepLabCut (Mathis et al. 2018, Nath et al. 2019) (as described in 'Behavioural analysis, scripts and statistics') high-frame rate videos (uEyeCP, IDS, 450–668 fps) were acquired to allow for successful tracking.

Behavioral analysis, scripts and statistics

Open Field Assay: To quantify basic locomotor parameters in the open field, videos acquired from above (Pike, Allied Vision, 200 fps or an integrated camera for photometry, 60 fps, Plexon) were used. Mice were placed in a square arena (35 × 35 cm) within a noise-isolated chamber for 10 min. Centre-of-mass body tracking was performed using the CinePlexStudio tracking

function (CinePlexStudio v.3.7.1. Plexon) and speed values were calculated from extracted coordinates on a frame-by-frame basis. Whole-body and speed traces were clustered into defined locomotor bouts (>5 cm s−1 for >200 ms) and for analysis of loss-of-function experiments, maximum speed (highest single speed value during a locomotor bout), bout duration and bout distance parameters were calculated using custom-written MATLAB scripts. For electrophysiological recording and photometry experiments, locomotor bout start- and end-points were extracted and aligned with single-unit activity data, as detailed in 'Electrophysiology analysis'. To determine the timing of locomotion swing phase, we annotated ipsilateral forelimb footfalls during open field locomotion, and used the time window 0.1 s before footfall for analysis. Because forelimbs were often not discernable on the recorded top-camera videos, we also used coincidence of diagonal hindlimb footfall data for annotation of forelimb data, a behavioural feature confirmed by video analysis using top and bottom cameras in another dataset.

Lever Task: Lever reaching behaviour was recorded using high-speed videography from both sides of the lever (Pike, Allied Vision, 200 fps). Video capture was triggered synchronized with electrophysiology measurements using commercially available software (Omniplex, Plexon). Relevant behavioural time points were extracted manually using CinePlexEditor (v.3.6.0, Plexon). Definition of the behavioural time points was as follows. Time points when the mouse was present and attending in front of the lever were defined as arrival. The video frame in which the forepaw was first observed to lift off the ground or start to move towards the lever from an already slightly lifted position was defined as reaching start. For lever on and off, the first frame in which the paw touched the lever was defined as the onset of the lever phase and the last frame in which the paw was still observed on the lever was defined as the offset. After retrieving the paw from the lever, the last video frame in which the paw was observed in a retraction movement before being placed on the ground or slightly stopped above in the air was defined as the end of retraction. For electrophysiological analysis, only first-attempt lever-pressing sequences were analysed. Secondary lever-pressing sequences (that is, the immediate initiation of another lever-pressing sequence after the first attempt) were not used

for electrophysiological analysis to ensure minimal trial-to-trial variability. These extracted time points were then used for analysis and alignment with electrophysiology data as detailed in 'Electrophysiology analysis'.

Pellet Task: Movies taken from the front and side (Pike, Allied Vision, 200 fps) were used for manual assignment of behavioural time points and for coordinate extraction using CinePlexEditor (v.3.6.0, Plexon) or MATLAB (The Mathworks). Synchronization of movies with electrophysiological and fibre photometry data was achieved using commercially available software (Omniplex, Plexon). Movies for photometry experiments were acquired using a system-integrated camera from the side (Plexon) acquiring at 60 fps allowing for precise alignment with calcium transients. For loss-of-function experiments assessing reaching behaviour, success rate was defined as the fraction of successful trials of all reaching attempts when a pellet was presented. Single reaching attempts were defined as whenever the tip of the fingers exited and re-entered the slit opening of the pellet reaching box. Successful trials were defined as the complete successful behavioural sequence composed of reaching for, grasping and retrieving a pellet to the inside of the pellet reaching box. We defined 'miss trials' as trials during which the mouse missed touching the pellet during reaching. To assess directionality defects, the spatial location of the hand at the most extended time point was registered in camera pixel coordinates from both the side and front camera and used for plotting and quantification of the endpoint variability and distance from the pellet using MATLAB. Pixel coordinates were first normalized to a defined spatial constant at the behavioural box and then to the pellet position itself to correct for any potential trial-to-trial effects in pellet or camera positioning. Variability was defined as the area of the ellipse with x and y diameters defined as the average s.d. of all endpoint coordinates in the x and y direction in pixels, respectively. Distance was defined as the average pixel distance of all the endpoints from the pellet position. For single-unit electrophysiology, behavioural time points were defined as follows. The video frame in which the forepaw was first observed to lift off the ground or start to move towards the slit from an already slightly lifted position was defined as reaching start. Time points at which the fingers started to spread in anticipation of grasping for the pellet

were defined as the onset of the grasping movement. Time points during which the pellet was firmly grasped and the retraction sequence initiated were defined as the endpoints of grasping. This often, but not always, coincided with paw supination. After grasping the pellet, the hand is transported towards the mouth; time points at which the pellet arrived at the mouth were defined as retraction endpoints. For electrophysiological and fibre photometry analysis, only first-attempt successful reaching sequences were analysed. Unsuccessful or secondary successful reaching sequences (that is, the immediate initiation of another reaching sequence after an unsuccessful attempt) were not used for electrophysiological and fibre photometry analysis to ensure minimal trial-to-trial variability. Sessions during which mice achieved fewer than four successful reaching sequences were excluded. Further analysis was conducted as detailed in 'Electrophysiology analysis' and 'Photometry analysis'.

<u>Handling Task:</u> Handling episodes were recorded using high-speed videography (for electrophysiology, Pike, Allied Vision, 200 fps; for photometry, integrated camera, 60 fps, Plexon) and behavioural time points were defined using CinePlexEditor (v.3.6.0, Plexon) or MATLAB (The Mathworks) as follows. Handling start was defined as the time point at which both forelimbs arrived at the mouth before stereotypic, coordinated handling was initiated. The end of the handling was defined as the video frame in which both forelimbs were retrieved from the mouth and any subsequent food handling ceased. Synchronization with electrophysiological and photometry data was achieved through commercially available software (Omniplex, for electrophysiology, CineLyzer for photometry, Plexon) and analysed as detailed in 'Electrophysiology analysis'.

For loss-of-function experiments, handling sessions were recorded using high-speed videography (Pike, Allied Vision, 200 fps). On the basis of previously reported data (Tennant et al. 2010) , the following parameters were quantified: number of pasta drops, percentage of time during which the preferred paw is used as guide paw, as well as probability distribution of pasta handling angle. Pasta drop rates were quantified manually, whereas all other quantifications were based on pose estimation performed with DeepLabCut (Mathis et al. 2018, Nath et al. 2019) (as described in 'Optogenetic activation experiments'). The network

was trained using at least 200 frames annotated on the following body parts: nose, forepaws and feet, as well as on the extremities and marks on the pasta pellet. Pasta drops were defined as events in which a mouse inadvertently released the pasta pellet from its forepaws, causing it to fall on the floor of the test chamber. For quantification of preferred paw use as guide paw, the guide paw was defined as the one kept closer to the snout during handling (Fig. 4.4.e). For each mouse, the preferred paw was defined as the one preferentially used as a guide paw during the control handling session. After pose estimation, the distance between each paw and the nose was computed over all handling episodes and the time at which 'preferred-hand to nose' distance was shorter than 'non-preferred-hand to nose' distance was calculated as a percentage of the total handling time. For the probability of distribution of pasta handling angle, for each handling frame we quantified the angle comprised between the line fitting the tracked marks on the pasta pellet and the body midline. The body midline was calculated as the line connecting the nose and the midpoint between the feet (Fig. 4.6.a). Probability was calculated on the basis of the total number of handling frames, and relative handling angle values were offset from median angle value for each mouse during control sessions.

Optogenetic Activation Experiments: For analysis of optogenetically induced behaviours, quantification of the reliability to elicit the assessed behaviour upon stimulation was performed manually, using high-speed videography (Pike, Allied Vision, 200 fps, Sony alpha 7s, Sony, 100 fps or uEyeCP, IDS, 450–668 fps). For each mouse, a minimum of 30 optogenetic stimulation events were scored. Each stimulation event was analysed frame by frame and, whenever laser-induced movements were detected, assigned to the appropriate behavioural category. Reliability percentages for each behavioural category were calculated as the fraction of trials eliciting that specific behaviour from all scored stimulation trials. Behavioural categories referred to in Fig. 4.12. were defined according to the following observed phenotypes. Reaching was defined as single event, unilateral lifting and extension of the forelimb accompanied only by spreading of individual fingers. Grasping was defined as unilateral lifting and extension of the forelimb in combination with flexing finger dynamics. Tapping was defined as repeated, unilateral lifting of the forepaw without flexing finger

dynamics. Hand-to-mouth movement was defined as repeated, unilateral extensions of the forelimb with flexing finger dynamics directed towards the mouth. Grooming was defined as repeated, bilaterally coordinated lifting of the forelimbs and rhythmic swiping over facial areas. Locomotion was defined as coordinated full-body movement involving the repetitive use of all four limbs to translocate the entire body in a coordinated manner. Head turning was defined as horizontal head rotation that did not involve forelimb movements. No behaviour was used for events during which no discernible movement was elicited upon optogenetic stimulation. For analysis of forelimb trajectories during the various different forelimb behaviours elicited from the distinct subpopulations, the machine learning algorithm DeepLabCut (Mathis et al. 2018, Nath et al. 2019) was used in combination with high-speed videography to characterize behavioural phenotypes (uEyeCP, IDS, 450–668 fps). We trained the network with an initial dataset for each kind of elicited behaviour using at least 200 frames to annotate individual parts of the forelimb. Subsequent unsupervised training involved at least 600,000 iteration rounds, after which no improvement of the pose estimation reliability could be observed. Extracted pixel coordinates were plotted using customized MATLAB or Python scripts. For reaching analysis, trajectory coordinates were relative to the resting position of the paw before stimulation. Time coordinates were normalized using the time from movement onset to maximum extension (along the anterior–posterior axis) of the reach episode and discretized into equal bins. For tapping analysis, dorsoventral coordinates were relative to the resting position of the paw before stimulation. Time coordinates were normalized by the time between motion onset and the maximum dorsoventral position of the tap episode, discretized into equal bins and offset such that $t = 0$ occurs at the tapping peak. For grooming analysis, trajectory coordinates were relative to the resting position of the paws before stimulation. Time coordinates were normalized by the time between motion onset and completion of a grooming bout, and discretized into equal bins. For EMG experiments, only reaching start time points with respect to the laser stimulation were assessed, aligned to the EMG traces and analysed as detailed in 'EMG analysis'.

Electrophysiology Analysis: All spiking time points of single-unit data were imported for further analysis to MATLAB from NeuroExplorer v.5 (Plexon). We determined the distribution of average firing rates for latRM neurons during behaviour and found that most exhibited values below 20 Hz, with only a minority displaying higher values (Fig. 4.2.c). To determine how individual neurons contribute to changes in activity profiles, we aligned the relative mean-subtracted firing rates according to timing of peak changes. Spiking events were aligned with individual behavioural time points in a window of ±8 s and for individual behavioural sessions, average firing frequencies were calculated using 50-ms binning. Baseline firing rates were determined during the time window between −6 to −2 s for each behaviour and are indicated separately in displayed raster plots throughout the presented figures (scale of 0–100 Hz). For analysis defining neuronal tuning to task, we used the reaching start as an alignment point in the pellet and lever task, and the start of locomotion in the open field task for locomotion. To illustrate single example neurons graphically, alignment was sometimes performed to different time points as indicated and the display of single trial raster plots was limited to a subset of ten randomly selected trials. For tuning analysis to pellet or lever tasks, we included neurons for which the average firing rate reached 20 Hz at least once during the task-relevant time window (±2.5 s; task-relevant neurons, n = 84 for pellet task, n = 81 for lever task; n = 48 for locomotion). Task-tuned neurons were selected on the basis of changes in firing rate more than 3 s.d. above baseline firing at least for one bin during the time window of −1.5 s to +0.5 s from onset of the task (n = 49 for pellet task; n = 43 for lever task; n = 4 for open field) (Fig. 4.2.). Average overall firing rates of neurons displayed in Fig. 4.2. were calculated from the ±8-s time period for the lever or pellet task individually. To assess task specificity to forelimb behaviours at the population level, we compared the baseline-subtracted firing rate of task-tuned neurons in the pellet or lever task to the activity of the same neurons during open field locomotion or shuffled data (100×) in 250-ms bins (Fig. 4.1.a) (statistical details are provided in 'Statistics'). Heat map plots (Figs. 4.1.b, 4.7.d, Fig. 4.3.) were generated from mean-subtracted firing rates normalized for every neuron. Fifty-ms bins were assigned a colour in a 64-colour range, over which the mean-subtracted firings rates were scaled. Baseline firing

rates were calculated as average firing rates of individual neurons during the baseline period. The colour scale for the baseline shown in the sidebar was generated by scaling the range of baseline firing rate values over a 64-colour range displaying the 0–100 Hz range. Average firing rates during behaviour were calculated as average firing rates of individual neurons during the behaviour period. Relative behaviour firing rates were calculated as the difference between baseline and average behaviour firing rates (Fig. 4.2.d). To determine behavioural-phase tuning correlations, we selected neurons tuned to the behavioural phase of pellet reaching, lever reaching, handling or swing phase of locomotion. We determined the peak firing rate of individual neurons during the respective behavioural

phases as defined below (each annotated on a trial-by-trial basis), from which the mean baseline firing rate was subtracted (50-ms bins). Only trials with firing rate changes at least three s.d. above baseline firing frequency, in the annotated time windows for the specific behavioural phase, were included in our analysis. We applied a reliability cut-off of 0.4 for neurons to be included into a behaviourally tuned group. Reliability of a neuronal response was calculated from the number of trials for which the firing rate of the analysed neuron crossed the three s.d. threshold, divided by the total number of trials recorded. Additionally, to be included in the behaviourally tuned group, a neuron must have reached an average firing rate of at least 10 Hz during the task time window, and a maximum average firing rate that is greater during the behavioural phase than the baseline. The time window used for analysis of pellet or lever reaching was confined to 1.5 s before reaching onset to the end of the reaching phase. For handling, the time window used for analysis was from the start of handling onset to the end of handling. Determined maximum trial-averaged firing rate values in the defined behavioural phase of the analysed neurons subtracted by the maximum trial-averaged baseline firing rates were plotted against each other and correlated to assess significance (Fig. 4.3.e) (as discussed in 'Statistics'). For visualization purposes, 5 data points above 30 Hz and 2 below −5 Hz contributing to the regression line are not displayed in top left panel of Fig. 4.3.e. For recordings along the dorsoventral axis of latRM, we plotted the average baseline-subtracted peak firing rate of significantly behaviour-tuned neurons in the two dorsal recording

depths (Fig. 4.7.c top; aligned to handling onset) and two ventral recording depths (Fig. 4.7.c bottom; aligned to reaching onset). The activity of the reaching- and handling-tuned neurons in these recordings was compared to the activity of the same neurons shuffled randomly (100×) in 250-ms bins (Fig. 4.10.b) (statistical details are provided in 'Statistics'). The four recorded depths are marked by colour bars next to raster plots of individual neurons, with two shades of magenta indicating dorsal depths and two shades of cyan indicating ventral depths. For directionality analysis, task-tuned neurons in either direction were selected and relative average peak behaviour firing rates (average peak behaviour firing rate – average baseline firing rate) were calculated for both directions separately. The directionality index is the difference in average peak firing rates for the two directions in Hz. For plotting, we sorted the differential firing rates in ascending direction. We included a shadow depicting the standard deviations during the baseline of both directions for the corresponding neuron in the plot (Fig. 4.5.).

EMG Analysis: For analysis of latencies and plotting of the EMG data (Fig. 4.14.) amplified and bandpass-filtered raw signals were used for further analysis. A baseline period of 200 ms before the reaching start (as described in 'Pellet task' in 'Behavioural analysis, scripts and statistics') or the laser onset was used to calculate the average baseline activity and s.d. After mean subtraction, a threshold of three s.d. of the baseline was used to derive latencies for the different muscles when the raw trace crossed this threshold for at least four consecutive frames. We analysed at least ten trials per mouse and condition. For the relative onset of muscle activity, average activation time points were normalized to time between the reaching start and the point of maximum forelimb extension (as described in 'Pellet task' in 'Behavioural analysis, scripts and statistics'). For the average plot, the raw trace was smoothened using a moving average window (29 frames for laser and 99 frames for pellet reaching).

Photometry analysis: Raw fluorescence and background fluorescent data were used to calculate $\Delta F/F$ values based on a 3-s moving-average window. Recording sessions in which the mean value of the 1,000 maximum $\Delta F/F$ single-frame peaks was either 50% higher or lower than on the first day of recording were excluded. Fluorescent traces were then aligned with

individual behavioural events (reaching, handling or locomotion start) and normalized in between the maximum and minimum ΔF/F values observed during all recording sessions. For shuffled data, the same number of random time points as pellet-reaching events was generated from the pellet-reaching experimental session. Average traces were plotted on a time scale from −1 to 5 s around the respective behaviour.

Scripts and plotting: All plots, scripts and analysis were generated or performed in MATLAB v.2017b (The Mathworks), Python3 (www. Python.org) or GraphPadPrism7 (GraphPad) and figures were assembled using CorelDRAW X6 to X9 (Corel). Mouse drawings were provided by E. Tyler and L. Kravitz through the SciDraw repository (www.scidraw.io) and adapted in Corel X6 or X8.

Statistics: Significance levels indicated are as follows: *P < 0.05, **P < 0.01, ***P < 0.001, unless otherwise specified. All data are presented as mean ± s.e.m., except where otherwise indicated. In all statistical comparisons, normality of the data was checked with quantile plots and/or with D'Agostino and Pearson, Shapiro–Wilk and Kolmogorov– Smirnov normality test in Prism. Non-normally distributed data were subsequently compared with non-parametric tests. The following statistical tests were used to assess significance when indicated. Firing specificity of latRM neurons according to task (Fig. 4.1.a) was assessed by comparing the peak firing rates of 250-ms bins in the task window (defined by −1.5 to 0.5 s) between all neuronal data pairwise with the Wilcoxon signed-rank test. The Bonferroni correction was applied to account for multiple comparisons and the significance levels were adjusted as *P < 0.0167, **P < 0.0033, ***P < 0.00033. For shuffled data, the average P value of all shuffles (100×) was used to assess significance (P values: pellet task versus shuffled: <0.0001; pellet task versus locomotion: <0.0001; locomotion versus shuffled: 0.245; lever task versus shuffled: <0.0001; lever task versus locomotion: <0.0001; locomotion versus shuffled: 0.568). Similarly, the activity of neurons along the dorsoventral axis, specifically tuned to the behavioural time window of reaching or handling, was compared to the shuffled data (Fig. 4.10.b: pellet reach versus shuffled: P ≤ 0.0001; handling versus shuffled: P ≤ 0.0001). The same approach was used to probe the activity of the handling-tuned and lever-reach-tuned latRM neurons during

other behaviours, with a Bonferroni correction for 4 comparisons leading to adjusted significance levels of *P < 0.0125, **P < 0.0025, ***P < 0.00025 (Fig. 4.3.a, b; time window was defined from 0 to 2 s only for pellet-reaching aligned activity for the handling-tuned neurons as the onset of activity was delayed with respect to reaching start; P values in Fig. 4.3.a: pellet reaching versus shuffled: P ≤ 0.0001; handling versus shuffled: P ≤ 0.0001; lever reach versus shuffled: P = 0.2281; locomotion versus shuffled: P = 0.9523; in Fig. 4.3.b: pellet reaching versus shuffled: P = 0.002548; handling versus shuffled: P = 0.201408; lever reach versus shuffled: P ≤ 0.0001; locomotion versus shuffled: P = 0.700481). To quantify action cotuning between different behaviours (Fig. 4.2.d) we used a Spearman's rank correlation test to assess significance (Spearman r and P values, upper left r: 0.43539, P: 0.00673; lower left r: −0.39194, P: 0.01495; upper right r: 0.39915, P: 0.02888; lower right r: -0.1315, P: 0.48852). All data shown in Fig. 4.4. and Fig. 4.5. were compared using the two-sided paired t-test unless otherwise specified (P values in Fig. 4.4.b left experimental: <0.0001; Fig. 4.4.b left control: 0.3539; Fig. 4.4.b right, from left to right: <0.0001, 0.0003, <0.0001, <0.0001; all other comparisons within CNO or within the PBS group did not result in significant changes; Fig. 4.4.c: 0.0002; a Wilcoxon signed-rank test was used for Fig. 4.4.f: 0.007 and Fig. 4.4.g: 0.006; Fig. 4.5.b left: 0.5601; Fig. 4.5.b middle: 0.6002; Fig. 4.5.b right: 0.3892; Fig. 4.5.c left: 0.0029; Fig. 4.5.c middle: 0.0073; Fig. 4.5.c right: 0.0034; Fig. 4.5.e left: 0.0162; Fig. 4.5.e middle: 0.0148; Fig. 4.5.e right: 0.0095). Grip test analysis in Fig. 4.6.b is shown as percentage on the PBS day using a Wilcoxon rank-sum test (0.4237). Overlap ratios between distinct latRM or medRM subpopulations in triple injections are displayed as averages of all mice with respective subpopulation as a reference (Fig. 4.9.b; latRM, left: 19.2 ± 5.5% and 17.2 ± 5.1%, middle: 12.3 ± 3.1% and 6.9 ± 1.4%, right: 7.3 ± 0.6% and 4.1 ± 1.3%; Fig. 4.9.c; medRM: 70.9 ± 18.7% and 53.8 ± 13.2%). To compare spatial distributions of latRM sub-populations between the medRM and latRM (Fig. 4.9.c), we used a two-sided paired t-test (P values: spinally projecting: 0.0019; MdV-projecting: 0.0037; contralateral-projecting: 0.0058; MdD-projecting population: 0.0162). Reaching trajectory endpoints (Fig. 4.13.b, right) were compared using the summed distance of individual endpoints to the centroid (grouped by mouse, distance =

718 pixels; all mice grouped together, distance = 1,025 pixels). A two-sided, unpaired t-test was used to compare EMG responses after light stimulation (Fig. 4.14.b; P values: latency biceps versus triceps: 0.0093; relative onset for biceps versus triceps: 0.0383).

4.6. Acknowledgements

4.7. Author Contributions

All authors were involved in the design of experiments. L.R. together with C.P. carried out most experiments, and acquired and analysed data. R.S. was mainly involved in functional and anatomical experiments related to intra-brainstem interactions, fibre photometry experiments and loss-of-function experiments. H.K. was involved in electrophysiology analysis and loss-of-function experiments. S.V.-G. was involved in early experiments related to intra-brainstem interactions and anatomy. S.A. initiated the project, designed experiments, analysed data and wrote the manuscript. All authors discussed the experiments and commented on the manuscript.

4.8. Author Information

The authors declare no competing financial interests. Correspondence and requests for material should be addressed to S.A. (silvia.arber@unibas.ch).

5. Connecting circuits for supraspinal control of locomotion

Manuel J. Ferreira-Pinto[1], Ludwig Ruder[1], Paolo Capelli[1] and Silvia Arber

[1] these authors contributed equally

5.1. Summary

Locomotion is regulated by distributed circuits and it is achieved by the concerted activation of body musculature. While the basic properties of executive circuits in the spinal cord are fairly well understood, the precise mechanisms by which the brain impacts locomotion are much less clear. This review discusses recent work unraveling the cellular identity, connectivity and function of supraspinal circuits. We focus on their involvement in the regulation of the different phases of locomotion and their interaction with spinal circuits. Dedicated neuronal populations in the brainstem carry locomotor instructions including initiation, speed and termination. To align locomotion with behavioral needs, brainstem output structures are recruited by midbrain and forebrain circuits that compute and infer volitional, innate and context-dependent locomotor properties. We conclude that the emerging logic of supraspinal circuit organization helps to understand how locomotor programs from exploration to hunting and escape are regulated by the brain.

5.2. Introduction

Locomotion is the undoubtedly most universal and conserved form of movement of the virtually endless variety of behaviors that animal and human bodies perform. Understanding the mechanisms within the nervous system involved in controlling its planning and execution has been a longstanding scientific quest. Early studies have advanced the field by delineating regions in the nervous system linked to the control of locomotion through performing lesion experiments, pharmacological interventions, electrical stimulations and neuronal recordings. This body of work provided first important insights into how the nervous system controls locomotion, including the identification of key regions distributed throughout the nervous system, which will provide the organizational anchor points for this review.

Recent technological advances have revolutionized neuroscience and in parallel also strongly influenced research on the control of movement. These novel insights have transformed the way we think about the control of locomotion. It is now clear that defined neuronal cell types, characterized by various means including molecular, developmental and/or distinct synaptic input-output organization, are embedded into specifically wired neuronal circuits to implement many different aspects of locomotor function. Such work has been pioneered in the spinal cord and reviewed extensively (Goulding 2009, Grillner and Jessell 2009, Alaynick et al. 2011, Arber 2012, Kiehn 2016), allowing us to here only briefly summarize this work with an emphasis on some of the most recent relevant studies. On the other hand, the elucidation of specific supraspinal circuit architecture and organization using these emerging technologies has only just begun. We will highlight and synthesize predominantly a selection of this most recent literature on supraspinal control of locomotion. Our emphasis will be on circuit- and cell type-level insight and how identified neuronal populations integrate into the complex locomotion-controlling circuitry of the nervous system. We refer readers to previously published review articles for historic coverage of this topic. To set the stage for this review, we will first briefly dissect the behavioral process of locomotion into temporal and regulatory categories. We will

return to these definitions throughout the review with the goal to identify circuit level solutions for controlling and adjusting locomotion according to behavioral needs.

5.3. Main part

Dividing locomotion into temporal and regulatory behavioral categories

Three temporally separate behavioral phases accompany locomotion (Figure 5.1.A). Initiation and termination are the two boundary events defining a locomotor episode. Transition from a stationary period or from another motor behavior to a locomotor episode can entail different circuit-level events to begin this full body action. It can be caused by a sensory stimulus such as a fearful encounter with a predator leading to an escape response, but also often occurs in the absence of obvious external triggers. Such initiations can be linked to internal needs, including hunger and thirst, but can also be caused by planning or cognitive decisions leading to exploration. In analogy, termination of locomotion can occur for a variety of reasons depending on behavioral context, ranging from immediate stopping with a freezing response to more gradual termination due to arrival at a food source or encountering an interesting object.

The time frames flanked by initiation and termination encompass the locomotor episode itself (Figure 5.1.B). Each episode can be described by a set of behavioral attributes, patterns or categories. One important attribute during ongoing locomotion is speed. Locomotor behavior ranges from low-speed exploration to high-speed escape running. Speed can also fluctuate within a given locomotor episode by virtue of acceleration and deceleration. Second, during locomotion, quadrupedal animals move their limbs in coordinated and stereotype patterns called gaits (Halbertsma 1983, Bellardita and Kiehn 2015, Lemieux et al. 2016). Behavioral studies in different species provide evidence that gait selection occurs linked to different speed ranges. Notably, during low-speed exploratory locomotion, many quadrupedal animals alternate paired fore- and hindlimbs respectively and exhibit synchrony in diagonal fore- and hindlimbs. In contrast, high-speed escape running goes hand in hand with bound gait selection.

These observations suggest that a given gait likely represents the optimal biomechanical solution for the chosen speed range. Another behavioral attribute during locomotion is its directionality. Animals only rarely locomote along the shortest straight trajectory and they as well as humans also have the ability to locomote backwards, using the same muscles in different configurations, likely controlled and mediated by different networks (Choi and Bastian 2007, Wang et al. 2011). This review will focus mainly on quadrupedal locomotion, although likely similar principles apply to bipedal locomotion, swimming, and flight.
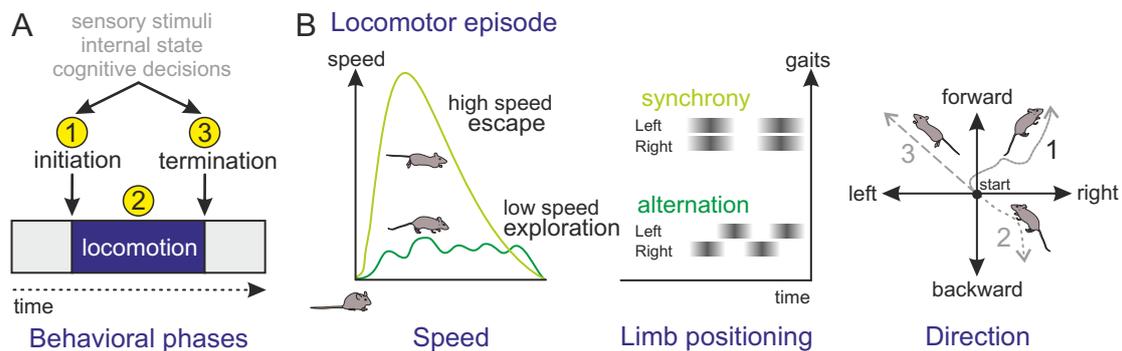
Figure 5.1. Temporal and regulatory categories of locomotion

(A) Division of the locomotor process in three behavioral phases (initiation, locomotion, and termination).

(B) A locomotor episode can range from low-speed exploration to high-speed escaping, during which different locomotor speeds align with alternating or synchronous gait patterns, and can have different directions of the chosen trajectory (illustrated by three example mice; 1: low-speed exploration, 2: backwards walking, 3: high-speed locomotion).

Diversity and specificity in spinal circuits for execution of locomotion

The spinal cord harbors neuronal circuits required for the execution of locomotion. Skeletal muscles receive their commands for contraction from spinal motor neurons that are grouped into topographically arranged motor pools according to the innervated muscles (Romanes 1951). Understanding the behavioral phenomenon of locomotion can therefore essentially be paraphrased into the question of how the temporally stereotypically patterned muscle activation inherent to locomotion is achieved through regulation of synaptic inputs to motor

pools. Although many of these inputs arise from spinal neurons, the locomotor program requires supraspinal or sensory sources located outside the spinal cord for initiation, maintenance and adjustment. In fact, complete spinal transection in mammals leads to permanent paralysis of body parts innervated by segments below injury (Shik and Orlovsky 1976, Dietz 2010). In the absence of supraspinal input, spinal circuits can still be recruited for basic locomotion by either sensory feedback activation or application of neurochemical substances (Miller and van der Meché 1976, Forssberg et al. 1980). These observations were extensively leveraged in reduced *in vitro* preparations, in which neonatal spinal cords are stimulated electrically or pharmacologically to delineate the function of broad spinal interneuron classes defined by genetics. It is now clear that the different spinal subpopulations are organized into specific circuit modules and contribute differentially to locomotion. These spinal networks that are also referred to as central pattern generators (CPGs) can generate locomotor pattern and rhythm upon extrinsic synaptic input, through microcircuits encompassing interneuron subtypes and motor neurons (Goulding 2009, Grillner and Jessell 2009, Alaynick et al. 2011, Arber 2012, Kiehn 2016).

Spinal neurons are derived from different, transcriptionally-defined dorso-ventral progenitor domains during development, with several classes implicated in the regulation of important aspects of locomotion including interlimb coordination, speed and rhythmicity, work reviewed extensively elsewhere (Jessell 2000, Goulding 2009, Arber 2012, Kiehn 2016). While the existence of diversity beyond single progenitor domain origin was already apparent early on (Alaynick et al. 2011), a key open question has been the extent to which neurons diversify in the spinal cord to support generation of locomotor and other movement output of the body. It is also essential to resolve how a given population of spinal neurons defined by developmental and/or transcriptional entry points aligns to the functional attributes observed during *in vivo* locomotion. Recent work reviewed below has begun to shed light on these aspects of spinal neuron diversification, focusing on dorso-ventral and rostro-caudal axis, as well as the

organization and connectivity of spinal neurons into circuits beyond local microcircuits (Figure 5.2.A-D).

In adult zebrafish, motor neurons of the slow, intermediate and fast subtype are recruited progressively with increasing swimming speed (Ampatzis et al. 2013). Intriguingly, separate and speed-dependent modules also exist within the V2a spinal neuron population (Figure 5.2.A). These V2a subpopulations exhibit preferential connectivity to corresponding motor neuron subtypes, and neurons within the same V2a submodule are interconnected but only rarely connect across submodules (Ampatzis et al. 2014). This study thus defines specific V2a neuron ensembles in the spinal cord aligned with locomotor speed to match behavioral need. In mice, execution of quadrupedal locomotion at higher speeds is accompanied by gait changes with limb coordination changing from alternating to synchronous patterns (Bellardita and Kiehn 2015, Lemieux et al. 2016), raising the question of how speed- and gait phenomena are linked and whether they are mediated at least in part by spinal circuits. Developmental ablation of V2a neurons leads to deficits in hindlimb coordination exclusively at higher speeds in adult mice (Crone et al. 2009). These findings suggest that V2a neurons also exhibit speed-dependent roles in mice, but it is currently unclear whether functional subdivisions for V2a neurons similar to zebrafish exist. In addition, V0 spinal neurons subdivide into predominantly excitatory V0v (marked by Evx1) and mostly inhibitory V0d (marked by Pax7) subtypes, and these two classes exhibit distinct roles in maintenance of gait parameters adequately aligned with increasing speed during quadrupedal locomotion (Talpalar et al. 2013) (Figure 5.2.A), phenotypes not discernable by studying V0 neurons as an entity. Locomotor parameters are also shaped by central processing of sensory feedback (Rossignol 2006, Windhorst 2007). Recent work identified an inhibitory spinal interneuron class characterized by the expression of RORβ orphan nuclear receptor (Koch et al. 2017) (Figure 5.2.B). This population might gate proprioceptive information during the swing phase of the step cycle, acting by virtue of presynaptic inhibition of myelinated sensory and likely proprioceptive afferents. In the absence of these neurons, mice exhibit a peculiar duck-gait locomotor phenotype.

Gene expression analysis and computational methods are potent catalyzers to systematically unravel cellular diversity, also in the spinal cord (Bikoff et al. 2016, Hayashi et al. 2018, Sweeney et al. 2018). Focusing on V0-V2 spinal neuron distribution along the rostro-caudal axis, different patterns and gene expression profiles were observed comparing cervical, thoracic and lumbar levels (Francius et al. 2013). A more recent study dissected V2a neuron diversity in mice, demonstrating that the expression of one of its canonical markers *Chx10* shows postnatal rostro-caudal expression differences (Hayashi et al. 2018) (Figure 5.2.C). Notably, V2a type II neurons are characterized by low Chx10 expression, preferential residence at cervical segments and establishment of ascending axons to supraspinal targets. In contrast, the V2a type I cohort maintains Chx10 expression and is present at both lumbar and cervical levels (Figure 5.2.C). What might be the mechanisms by which spinal neurons diversify along the rostro-caudal axis? It is well-established that rostro-caudal identity in motor neurons is driven by differential developmental expression of Hox transcription factors (Philippidou and Dasen 2013). Evidence now supports the idea that this principle extends to other spinal neurons, where V1 spinal neuron diversification along the rostro-caudal axis can be regulated by Hox transcription factors independent of segmental motor neurons (Sweeney et al. 2018).

Most work aimed at understanding neuronal diversity in the spinal cord has focused on local circuit mechanisms. Yet, precise interactions of distributed spinal microcircuits along the length of the spinal cord is essential for locomotion, especially in quadrupedal animals where distant limbs must be coordinated to enable locomotion. While neuronal mechanisms involved in left-right coordination of hindlimbs are mostly driven by segmental spinal neurons and fairly well understood (Kiehn 2016), much less is known about circuit mechanisms for fore- and hindlimb coordination. A recent study demonstrated that long projection neurons interconnecting the cervical and lumbar spinal cord are important in coordinating fore- and hindlimb patterns during high-speed locomotion as well as for maintenance of postural stability (Figure 5.2.C) (Ruder

et al. 2016). The characterized long projection neurons are composed of a major excitatory and a minor inhibitory population derived from distinct developmental origin, each establishing specific projection patterns (Figure 5.2.C). Furthermore, long descending projection neurons receive synaptic inputs from many centers in the brain engaged in the regulation of locomotion, and thus provide a neuronal substrate for integration and broadcasting of supraspinal information throughout the circuitry of spinal cord to coordinate locomotion.

Together, these findings demonstrate that important parameters of subtype identity for spinal neurons during early development arise by transcriptional programs intersecting along the dorso-ventral and rostro-caudal axis. These interactions as well as usage of emergent spinal networks likely dictate the ultimate connectivity of neurons into specific circuit modules as well as their function. Recent work demonstrates that the diversity of spinal neurons is higher than originally anticipated, foreshadowing the likely existence of microcircuits endowed with dedicated functions in the execution of locomotion. One big challenge is to unravel how such spinal microcircuits process input from descending pathways and sensory feedback circuits. Clearly, how long-range supraspinal inputs trigger the engagement of specific spinal microcircuit modules is instrumental for the execution of motor programs driving any form of body movement including locomotion (Figure 5.2.D). We will now focus on supraspinal locomotion-regulatory signals in the brain and how they are conveyed to executive circuits in the spinal cord.
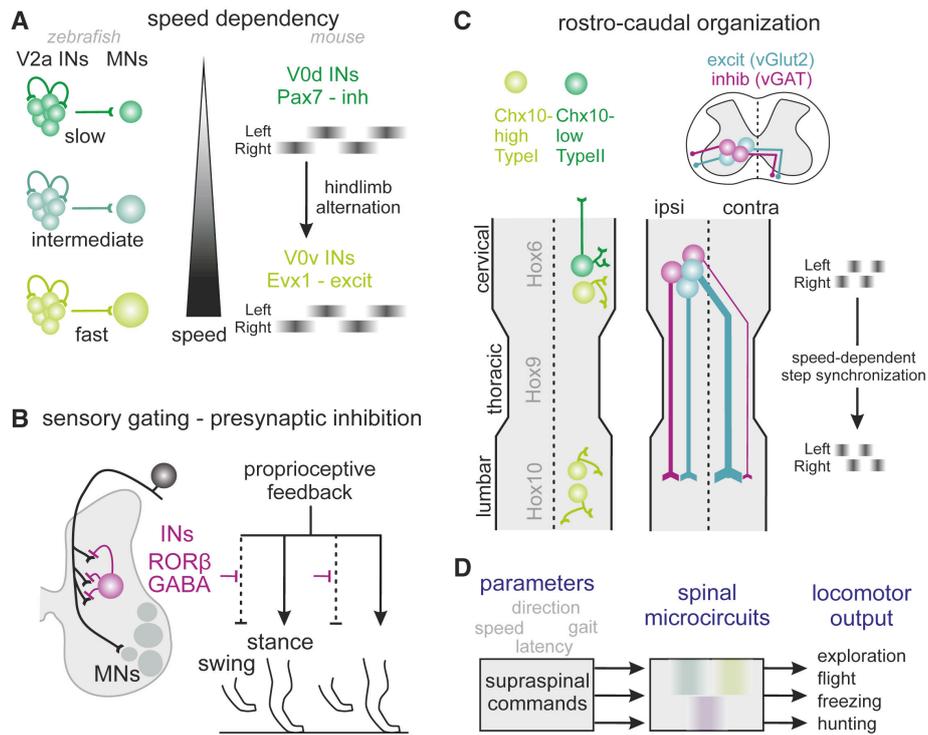
Figure 5.2. Diversity and specificity in spinal circuits for execution of locomotion

(A) Summary diagram of spinal circuits in zebrafish (left) and mice (right) implicated in speed control.

(B) Schematic summary of the role of RORβ-expressing spinal GABAergic neurons in sensory gating through presynaptic inhibition and influence on behavior.

(C) Rostro-caudal organization of spinal circuits based on Chx10-expression levels, Hox transcription factor expression (left), or the organization of descending projections from the cervical to the lumbar spinal cord and their influence on fore- and hindlimb coordination during locomotion (right).

(D) Proposed model of how supraspinal commands may signal locomotor parameters including speed, gait, latency or direction to spinal executive microcircuits that in turn regulate locomotor output.

Dissection of brainstem circuits regulating locomotor execution

Classical work performed in cats has mapped regions in the brain whose electrical stimulation elicits coordinated locomotion (Shik et al. 1966, Shik and Orlovsky 1976, Mori et al. 1989).

Several prominent regions were identified in the diencephalon, midbrain and ventral to the cerebellum. We will focus here on the mesencephalic locomotor region (MLR) in the midbrain due to recent progress in its characterization. Electrical stimulation of the MLR in cats elicits coordinated locomotion at a wide range of speeds and gaits scaling with applied stimulation frequency (Shik and Orlovsky 1976). Still today, this functionally defined site is considered a key region in the supraspinal orchestration of locomotion. According to a unifying model based on many studies, the MLR integrates inputs from numerous brain regions and regulates locomotion in a context-adequate manner (Jordan 1998, Ryczko and Dubuc 2013) (Figure 5.3.A). It accesses executive spinal circuits mostly by recruiting neurons residing in the reticular formation of the caudal brainstem acting as intermediaries to transmit locomotor signals to the spinal cord. Supporting such a model, MLR stimulation in conjunction with cooling the ventral medulla to attenuate synaptic transmission blunts transfer of the locomotor signal and its execution to the spinal cord (Shefchyk et al. 1984). This work suggests the existence of neurons in the reticular formation with a key role in the locomotor process. Homologous regions in the brainstem of several vertebrate species including humans have been identified (Grillner et al. 1997, Le Ray et al. 2011). These findings suggest that the concept of an MLR region and associated downstream structures in the brainstem are evolutionarily conserved throughout the vertebrate lineage, although some connectivity differences likely exist, perhaps also reflecting the adaptation of neuronal circuits to support bipedalism (Alam et al. 2011). We will now briefly summarize historic entry points and debates in the field of how brainstem circuits between the MLR and the reticular formation impact locomotion and describe the most recent studies beginning to resolve the circuit mechanisms underlying these processes.

Historical perspective and open questions on MLR organization and function

Since the first description of the MLR following a functional definition, many studies have sought to pinpoint the exact location of the locomotion-promoting site and its neuronal identity in numerous animal models. Original studies in cats reported that the anatomical substrate of

the MLR corresponds to the cuneiform nucleus (CnF) and its vicinity (Shik and Orlovsky 1976). Interestingly, CnF stimulation in both rats and cats generates a type of locomotion that resembles aversive, escaping behavior with high-speed running at synchronous gaits and explosive jumps (Mori et al. 1989, Depoortere et al. 1990). Given the findings that the CnF also modulates nociception, cardiovascular and respiratory responses (Ryczko and Dubuc 2013), it was proposed that the CnF supports defensive forms of locomotion (Jordan 1998). Electrical mapping of the MLR in rats demonstrated that locomotion could be elicited by stimulation of both the CnF and the pedunculopontine nucleus (PPN) (Skinner and Garcia-Rill 1984), but the region with the shortest latency was mapped to the caudal part of the PPN, coinciding with a distinct cholinergic cell cluster and its vicinity (Garcia-Rill et al. 1987). Given the absence of explosive behaviors elicited by PPN stimulation and the selective connectivity of the basal ganglia (BG) with the PPN (Martinez-Gonzalez et al. 2011), it was proposed that the PPN might mediate exploratory locomotor behaviors driven and actively selected by the BG, while the CnF mediates defensive locomotion for example in the context of an urgent need to escape from dangerous contexts (Jordan 1998). Another layer of complexity emerges from the fact that electrical stimulations along a dorso-ventral axis encompassing the CnF and PPN region can elicit variable responses ranging from opposing changes in muscle tone and posture to locomotion-promotion ones (Figure 5.3.B) (Takakusaki et al. 2016).

Together, these experiments suggest that locomotion and posture controlling functional attributes in the MLR cannot be fully explained by neuronal position alone. While the literature consistently supports a role for the CnF as locomotion-promoting site, the PPN and adjacent regions might be composed of closely-located or even intermingled populations of locomotion-promoting and opposing posture-regulating neurons. In addition, PPN neurons also contact numerous rostral brain regions (Martinez-Gonzalez et al. 2011), making it challenging to dissociate direct effects on locomotion through descending pathways from indirect effects through ascending interactions. Thus, studies using electrical stimulation or pharmacology cannot disentangle the complexity of these circuits. Work described below and mostly carried

out in mice makes use of viral and genetic tools to elucidate the cellular and functional identity within the MLR, with a focus on its descending circuits.

Neuronal and functional diversity in the mouse MLR

To consolidate results of experiments performed in other species in mice, electrical mapping of the mouse MLR revealed that the effective stimulation sites to elicit locomotion span over a rostro-caudally and dorso-ventrally broad region including the PPN, CnF, pre-CnF and the adjacent mesencephalic reticular formation (Roseberry et al. 2016). These regions contain intermingled glutamatergic, GABAergic and, exclusively in the case of the PPN, cholinergic neurons (Martinez-Gonzalez et al. 2011) (Figure 5.3.C). The most advanced insight on control of locomotion emerged from studying glutamatergic MLR neurons marked by the expression of the vesicular glutamate transporter vGlut2 (Lee et al. 2014, Roseberry et al. 2016, Caggiano et al. 2018, Josset et al. 2018), which will be the main focus here. All four studies demonstrate that optogenetic activation of glutamatergic neurons in the broad MLR region in mice recapitulates short latency initiation of locomotion with a stimulus intensity-to-speed correlation analogous to electrical stimulation experiments. Furthermore, optogenetic stimulation triggered during ongoing locomotion increases speed, by shortening the duration of hindlimb extensor muscle activation during stance and anticipating the next swing phase (Roseberry et al. 2016, Josset et al. 2018). Single unit neuronal recording experiments *in vivo* revealed that general vGlut2-MLR neurons correlate with locomotor state with a fraction of neurons also tracking locomotor speed (Roseberry et al. 2016, Caggiano et al. 2018). Optogenetic stimulation experiments were also carried out for other MLR populations. While the experimental outcome for stimulating cholinergic PPN neurons was somewhat contradictory across studies (Dautan et al. 2016, Roseberry et al. 2016, Xiao et al. 2016, Caggiano et al. 2018, Josset et al. 2018), it is nevertheless clear that they likely exhibit a modulatory rather than a driver role in locomotion. This seems to be at least partially mediated by direct regulation of dopaminergic neuronal activity in the SNc and the VTA (Dautan et al. 2016, Xiao et al. 2016), and possibly other ascending and descending targets (Mena-Segovia and Bolam 2017,

127

Moehle et al. 2017). In contrast, GABAergic neurons influence locomotion negatively through both local and distant circuit mechanisms (Roseberry et al. 2016, Caggiano et al. 2018). Taken together, these results demonstrate that glutamatergic MLR neurons constitute the neuroanatomical basis for the functionally-described short latency locomotion-promoting MLR site in the midbrain.

A long-lasting quest concerns the possible functional subdivision of regions residing within the MLR boundaries. While studies in mice consistently find that optogenetic stimulation of CnF-vGlut2 neurons can elicit locomotion, analogous evidence for PPN-vGlut2 neurons is variable (Caggiano et al. 2018, Josset et al. 2018). One study puts forward a model in which the PPN controls low-speed locomotion while the CnF regulates high-speed locomotion (Caggiano et al. 2018) (Figure 5.3.C). In support, optogenetic activation of PPN-vGlut2 neurons induces low-speed, long-latency locomotion with alternating gaits, while CnF-vGlut2 neuron activation generates short-latency locomotion with speed scaling according to stimulation intensity and aligned with the selection of speed-appropriate gait types. Single unit recordings from PPN and CnF neurons during locomotion on a head-fixed treadmill also revealed differences in firing properties aligned with speed. Moreover, glutamatergic PPN neurons integrate inputs from a wide variety of brain structures contributing to action selection and voluntary movements including BG, while CnF neurons receive preferential input from structures implicated in escaping behavior, including the periaqueductal grey (PAG) and the inferior colliculus. The second study demonstrates that stimulation of either PPN or CnF glutamatergic neurons elicits short-latency EMG responses in both ankle flexor and extensor muscles, with the strongest responses in the ankle flexor (Josset et al. 2018). This study further compared the effects of stimulation at rest to during ongoing locomotion. Glutamatergic CnF neuron stimulation at rest increased postural muscle tone before eliciting locomotion, and shortened the extensor bursts to accelerate locomotion with transition to gaits typical for high-speed during ongoing locomotion. In contrast, stimulation of PPN-vGlut2 neurons at rest elicited phasic muscle activity but no locomotion, but surprisingly, either stimulation or silencing of these neurons

during locomotion slowed down locomotor rhythm rather than speeding it up. It is not straightforward to reconcile the results of these two studies on PPN-vGlut2 neurons, but one possibility is that subtle differences in neuronal targeting locations within the PPN area and/or currently unidentified cell type diversity provide explanations.

Overall, recent studies support the existence of at least two midbrain circuits, spatially segregated between the PPN and CnF regions, embedded within specific input-output matrices providing differential control over circuitry regulating the scale from low-speed to high-speed locomotion (Figure 5.3.C). It is likely that these populations are recruited in a context-dependent manner, shaped by emotional valence, internal homeostatic needs and sensory perception, ultimately producing forms of locomotion with speed and gait needed for the respective context. These programs must include the full range of possible locomotor forms from quiet actively selected exploration to urgent, reflexive, escaping behavior from imminent dangers.

MLR-induced locomotion is preserved after precollicular transection, supporting a model in which locomotion-promoting effects are conveyed via caudal projections. Yet, an interesting additional aspect to consider in the equation of MLR function is that glutamatergic MLR neurons also provide input to rostral brain structures (Figure 5.3.D). The PPN establishes connections with most BG nuclei as well as dopaminergic neurons in the ventral tegmental area (VTA) and substantia nigra compacta (SNc), the thalamus and the basal forebrain (Martinez-Gonzalez et al. 2011). These findings implicate the MLR not only in behavioral execution, but also put it in a position to influence rostral computations involved in motor program selection or reinforcement such as cortical processing. The role of rostral projections by glutamatergic MLR neurons remains mostly unexplored, with some notable exceptions. Stimulation of glutamatergic MLR projections to the basal forebrain increases the gain of visual responses and generates gamma oscillations in the primary visual cortex (Lee et al. 2014), reproducing the previously described effects of spontaneous locomotion in cortical processing

(Niell and Stryker 2010). Interestingly, cortical effects were seen even at stimulation strengths below the threshold to induce locomotion by MLR neuron stimulation, demonstrating that the cortical changes and the production of the locomotor behavior are dissociable. Additionally, projections of PPN-vGlut2 neurons to the VTA target dopaminergic neurons and promote behavioral reinforcement (Yoo et al. 2017), presumably by promoting dopamine release in the nucleus accumbens and activating reward processing circuits. By demonstrating that MLR glutamatergic neurons not only convey descending signals for motor execution, but also send ascending projections to multiple brain regions that influence cortical processing and motivation/behavioral reinforcement, these studies suggest that the complexity of the MLR goes far beyond neurotransmitter identity and might also depend on target specificity, models to be explored in the future.

A

contextual information

MLR

caudal brainstem

locomotor output

B MLR site mapping

PAG

CnF & PPN

electrical stimulation

- locomotion
- atonia
- mixed behavior

C MLR-vGlut2 neuron function

PAG

limbic structures

CnF-vGlut2

high-speed limb synchrony escape

PPN-vGlut2

basal ganglia

muscle tone low or reduced speed limb alternation exploration

○ vGAT: inhibitory
● ChAT: modulatory

D MLR ascending targets

reinforcement

basal ganglia

VTA SNc
Dopamine

gain modulation visual cortex

thalamus

basal forebrain

PPN-vGlut2

descending pathways
motor program execution

Figure 5.3. Functional and cellular diversity of the mouse MLR

(A) MLR processes contextual information and its descending pathways signal to caudal brainstem neurons to influence locomotor output.

(B) Summary diagram of historical electrical site mapping experiments in the cat CnF and PPN to define locations influencing locomotion (see (Takakusaki et al. 2016) for review).

(C) Schematic diagram summarizing recent findings on the role of mouse MLR-vGlut2 neurons subdivided by location within CnF (cuneiform nucleus) and PPN (pedunculopontine nucleus). Both CnF and PPN also contain vGAT-neurons, but only PPN contains cholinergic neurons.

(D) Summary diagram of PPN-vGlut2 neuron projections to ascending targets and known implicated functions.

Identification of lower brainstem cell types conveying locomotor speed signals

The functional linkage between brain locomotor centers (most notably MLR) and executive circuits in the spinal cord has long been proposed to involve neurons in the lower brainstem reticular formation (Orlovsky et al. 1999). This model is based on experiments including regional injections of pharmacological substances and/or inactivation approaches using tissue cooling methods in conjunction with electrical microstimulation in several species including cats, rats and lampreys that have been extensively reviewed (Mori 1989, Orlovsky et al. 1999, Ryczko and Dubuc 2013, Takakusaki et al. 2016, Brownstone and Chopek 2018). Despite strong evidence supporting such a model however, the precise identity of neurons in the reticular formation acting as intermediaries between MLR and the spinal cord was long unclear. Unlike in the midbrain, within the caudal brainstem reticular formation, electrical stimulation experiments produced variable results with no clear consensual sites able to elicit full body locomotion (Ross and Sinnamon 1984, Drew and Rossignol 1990, Kinjo et al. 1990), and it had been argued that neuronal cell type diversity might be the underlying reason for this failure of identification (Orlovsky et al. 1999).

Several studies in mice employing genetics and viruses intersectionally have addressed the identity of neurons in the caudal brainstem involved in regulation of locomotor speed (Bouvier et al. 2015, Giber et al. 2015, Capelli et al. 2017). These studies identify brainstem neurons with locomotion-promoting and/or locomotion-attenuating functional properties and jointly demonstrate that criteria other than simply location are often needed to unravel functional cellular identities in the brainstem.

Within the caudal medulla, the two broad regions magnocellular nucleus (Mc) and gigantocellular nucleus (Gi) have been shown to contain neurons with connections to both

cervical and lumbar motor neurons (Esposito et al. 2014). These neurons are thus in a position to influence spinal locomotor circuits throughout their rostro-caudal extent as might be expected for descending neurons targeting locomotor circuits. To map the precise location and neurotransmitter identity of these neurons in the adult, retrograde tracing from the spinal cord demonstrated that all three Mc subdomains (LPGi: lateral paragigantocellular nucleus; GiA: gigantocellular nucleus alpha; and GiV: gigantocellular nucleus ventral) and the more dorsally located Gi contain intermingled excitatory and inhibitory neurons (Capelli et al. 2017) (Figure 5.4.A). Optogenetic activation of neurons confined to any of these four regions indiscriminate of neurotransmitter identity did not lead to changes in locomotor behavior (Figure 5.4.A). Strikingly however, selective stimulation of vGlut2 neurons located in LPGi but not in any of the other three studied subdomains induced short latency locomotion from rest and increased speed of ongoing locomotion (Capelli et al. 2017). Elimination of LPGi-vGlut2 neurons selectively impaired high-speed locomotion but left exploratory low-speed locomotion unperturbed (Figure 5.4.B). Given these functional studies on the role of LPGi-vGlut2 neurons in natural locomotion, and mapping experiments defining the descending synaptic outputs of CnF-vGlut2 neurons (Caggiano et al. 2018), it is likely that high-speed locomotor signals reach these caudal brainstem neurons from CnF-vGlut2 neurons. Indeed, locomotion-promoting signals from the MLR can be significantly attenuated by selective ablation of LPGi-vGlut2 neurons (Figure 5.4.C), and optogenetic stimulation of MLR-vGlut2 axon terminals in the caudal medulla can also elicit locomotion (Capelli et al. 2017). Together, these findings demonstrate that at least in part, descending locomotion-promoting signals from the MLR reach spinal circuits by recruiting LPGi-vGlut2 neurons in the caudal brainstem. Yet, the findings also demonstrate the need to search for additional neuronal populations that transmit signals for low-speed exploratory locomotion to the spinal cord. Such a network might be more distributed over several populations given its importance for survival, and/or perhaps an even finer dissection of cell types will be required to unravel identity of brainstem neurons involved in exploratory locomotion. Of note, some MLR neurons have been described to project directly to the spinal cord (Liang et al. 2012), but possible functional implications have not been tested.

The search for dissecting cell types according to a locomotion-attenuating activity in the lower brainstem has already provided more insight. Using developmental ontogeny as an entry point to stratify neurons, a study dissected the role of brainstem neurons expressing the transcription factor Chx10 in excitatory neurons (Bouvier et al. 2015). Optogenetic activation of Chx10 neurons in specific domains of the rostral medulla and caudal pons, but not the caudal medulla, attenuated ongoing locomotion (Figure 5.4.D). Neuronal silencing by selective expression of a tetanus toxin variant led to behavioral hyperactivity with increased locomotion in an open field assay and a decreased ability to halt locomotion in a reward task. The study also demonstrates that the characterized excitatory Chx10 neurons connect to glycinergic spinal neurons that are likely mediators to execute behavioral arrest (Bouvier et al. 2015) (Figure 5.4.D). There are also inhibitory brainstem neurons that can induce behavioral arrest (Giber et al. 2015, Capelli et al. 2017). Within the caudal medulla, separate optogenetic stimulation of each of 4 studied populations induced short-latency behavioral arrest during ongoing locomotion, ranging from simple stopping behavior to full body collapse reminiscent of atonia (Capelli et al. 2017) (Figure 5.4.A), suggesting that different populations are involved in dissimilar forms of behavioral arrest. Interestingly, glycinergic LPGi neurons connect to motor neurons, whereas intermingled LPGi-vGlut2 neurons needed for high-speed locomotion target mostly spinal neurons in intermediate lamina where rhythm- and pattern generating interneurons of the CPG reside, suggesting that functionally opposing brainstem populations act through different downstream circuits. Lastly, glycinergic neurons in the pontine reticular formation project to the intralaminar thalamic nucleus and optogenetic stimulation of their axon terminals induces behavioral arrest (Giber et al. 2015) (Figure 5.4.E), indicating that also ascending brainstem pathways can indirectly impact locomotion controlling pathways.

The concept of brainstem neurons in the reticular formation acting as intermediaries to coordinate spinal locomotion is evolutionarily conserved. Lamprey serves as a successful model organism to dissect circuitry regulating locomotion that recapitulates many of the

organizational principles seen in mammals (Grillner 2003, Ryczko and Dubuc 2013). A recent calcium imaging study analyzed neurons in the reticular formation during MLR stimulation (Juvin et al. 2016), and identified three types of reticulospinal neurons based on their response properties (Figure 5.4.F). One neuronal population maintained firing activity throughout the duration of MLR stimulation (i.e. maintain cells), a second exhibited a firing burst at the onset of MLR stimulation (i.e. start cells) and a third showed a two-phasic activity profile with a burst at the onset and another one at offset of MLR stimulation coinciding with the stop of swimming (i.e. stop cells). Because stop cells exhibited a spatially slightly segregated location from the other two cell types, the authors carried out local pharmacological gain- and loss-of-function experiments and found that while stop cell region activation terminated ongoing swimming, inactivation prolonged swimming (Juvin et al. 2016). Upstream drivers responsible for the different neuronal activity phases of the identified stop, maintain and start cells are currently unknown. Lower organisms also have highly developed circuits to mediate rapid escape behavior and one well-understood brainstem cell type is the Mauthner cell extensively studied in fish and amphibia (Gahtan and Baier 2004, Hale et al. 2016). The activation of a single Mauthner cell by mostly unilateral sensory information rapidly induces turning behavior away from dangerous stimuli. Thus, also studies in evolutionarily less developed species underscores the fact that functionally diverse cell types tuned to different locomotor parameters exist within the reticular formation and are embedded in specific circuits to process relevant inputs and transmit their output to spinal circuits for execution.
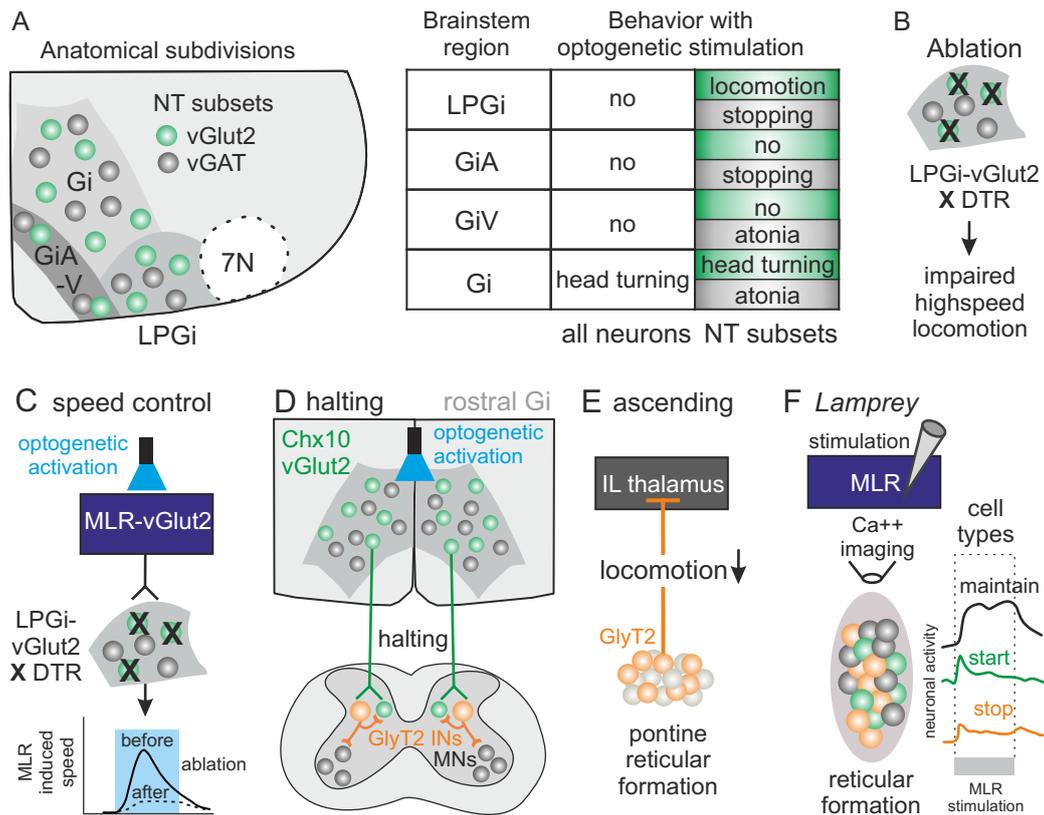
Figure 5.4. Brainstem cell types regulating locomotion

(A) Subdivision of ventral medulla into four regions (LPGi: lateral paragigantocellular nucleus; GiA: gigantocellular nucleus alpha; and GiV: gigantocellular nucleus ventral) all containing intermingled neurotransmitter (NT)-stratified (vGlut2/vGAT) neurons (7N demarcates facial motor nucleus). Table (right) summarizes behavioral findings from optogenetic activation experiments of different neuronal subpopulations.

(B, C) Ablation of LPGi-vGlut2 neurons impairs high-speed locomotion and attenuates speed of locomotion induced by optogenetic stimulation of MLR-vGlut2 neurons.

(D) vGlut2-neurons expressing the transcription factor Chx10 in the rostral gigantocellular region (Gi) implicated in halting by signaling through locomotion inhibiting circuits in the spinal cord.

(E) Glycinergic neurons in the pontine reticular formation project ascendingly to the intralaminar nucleus of the thalamus (IL) to attenuate locomotion.

(F) Summary of firing properties of three populations of neurons in the lamprey reticular formation implicated in locomotor control.

Upstream circuitry supporting locomotor behavior from exploration to escape

One key question is how an animal selects the appropriate locomotor behavior, as well as its vigor, aligned with environmental constraints and needs. As summarized in work above, an important contributor to determine the vigor of a locomotor behavior in its execution phase from low-speed exploration to high-speed escape behavior is the recruitment of specific and distinct circuit elements within the broader MLR area. Conceptual division of locomotion into three categories has been proposed to be computed by different forebrain regions, reflecting the contexts in which locomotion is performed (Sinnamon 1993). The described categories and structures would be exploratory locomotion (i.e. actively selected by volition and through the BG), primary appetitive locomotion (i.e. promoted by the lateral hypothalamus), and primary defensive locomotion (regulated by the medial hypothalamus and the PAG). These rostral regions would signal through selected MLR-reticulo-spinal networks to orchestrate behavioral execution (Jordan 1998). Recent studies have addressed these concepts and dissected cell type identity of the more rostral brain structures involved in context-specific forms of locomotion. We will discuss the organization and function of these upstream structures with the goal to explain how appropriate locomotor vigor along a continuous scale can be implemented to regulate locomotion.

Supraspinal regulation of locomotion through basal ganglia circuits

The BG are interconnected brain structures that are involved in motor program selection (Albin et al. 1989, DeLong 1990, Chakravarthy et al. 2010). The different components of the BG motor loop are connected in an interactive network that integrates and processes information from the cortex and thalamus. In such a model, the combined computations of these BG-thalamo-cortical circuits influence the activity of brainstem motor circuits to select the movement to be executed in a volitional context (Hikosaka et al. 2000). BG activity is also modulated at several levels by dopaminergic neurons residing in the midbrain VTA and SNc

providing crucial signals for motivation and movement initiation and vigor, respectively (Cohen et al. 2012, Howe and Dombeck 2016, da Silva et al. 2018) (Figure 5.5.A).

Despite its complex organization, the BG motor loop has been classically divided into two major pathways, diverging at the level of the striatum, the major BG input structure (Figure 5.5.A). Two classes of GABAergic striatal spiny projection neurons (SPNs) stratify by distinct projection patterns and by differential expression of dopamine receptors D1 and D2 (Albin et al. 1989, Kreitzer and Malenka 2008). D1-SPNs are the origin of the direct pathway and project to the main and inhibitory BG output structures, the internal globus pallidus (GPi, in rodents mostly referred to as entopeduncular nucleus) and the substantia nigra reticulata (SNr). D2-SPNs form the indirect pathway with the external globus pallidus (GPe) and the subthalamic nucleus (STN) as intermediate targets. However, the view of BG circuits being two parallel pathways independently influencing BG output structures is clearly too simplistic and the two pathways are interconnected at different levels (Taverna et al. 2008, Mallet et al. 2012, Cazorla et al. 2014).

Functionally, the classical model regarded the direct and indirect pathways as prokinetic and antikinetic, respectively (Albin et al. 1989, DeLong 1990). This notion was supported by optogenetic experiments showing that D1-SPN activation throughout a broad striatal region enhances movement and D2-SPN activation produces bradykinesia (Kravitz et al. 2010). However, recent evidence monitoring neuronal activity of striatal subpopulations during natural behaviors points to a more complex involvement of BG circuitry in movement regulation. Endogenous neuronal activity of the two striatal subpopulations demonstrated that both D1- and D2-SPNs are active during movement initiation and execution (Cui et al. 2013, Jin et al. 2014, Tecuapetla et al. 2014, Barbera et al. 2016, Klaus et al. 2017, Parker et al. 2018). In addition, the activity of each neuronal population is necessary for the proper execution of an intended movement (Tecuapetla et al. 2014, Tecuapetla et al. 2016) and sufficient to bidirectionally modulate the speed of ongoing movement without affecting action selection

(Yttri and Dudman 2016). It is therefore likely that dedicated neuronal ensemble activity within the striatum, composed of D1- and D2-SPNs, is involved in movement orchestration. Such SPN ensembles could be viewed as the functional units of the striatum contributing to the selection of concrete forms of movement such as locomotion. In agreement with this model, D1 or D2 functional ensembles coherently active during locomotion are spatially closer and more correlated to each other than neurons engaged in other forms of movement (Figure 5.5.B) (Barbera et al. 2016, Klaus et al. 2017, Parker et al. 2018), suggesting that different actions likely recruit mostly distinct subpopulations of SPNs.

When focusing on descending motor pathway function, understanding how BG link to locomotor output circuitry is an important question. Optogenetic stimulation of D1- or D2-SPNs elicits opposing neuronal activity changes in glutamatergic MLR neurons (Figure 5.5.C) (Roseberry et al. 2016). Furthermore, initiation of head-fixed treadmill locomotion upon bilateral stimulation of dorso-medial striatal D1-SPNs correlates with and depends on glutamatergic MLR neuron activity, whereas analogous experiments with D2-SPNs stop ongoing locomotion by decreasing the firing rate of glutamatergic MLR neurons (Roseberry et al. 2016). The involved anatomical link between D1 and D2 striatal neurons and glutamatergic MLR neurons has not been directly addressed but it is thought that the SNr, the most prominent BG output structure in rodents (Hikosaka et al. 2000, Alam et al. 2011), provides tonic inhibitory control to MLR neurons (Noda and Oka 1984, Garcia-Rill et al. 1985, Mori 1987). Indeed, glutamatergic MLR neurons receive inhibitory input from GABAergic SNr neurons (Roseberry et al. 2016) that mostly target the PPN (Caggiano et al. 2018). In addition, individual SNr neurons are modulated by the activity of D1- and D2 SPNs (Figure 5.5.D) (Kravitz et al. 2010, Freeze et al. 2013, Tecuapetla et al. 2016). Interestingly, optogenetic activation of either D1- or D2-SPNs produces heterogeneous responses in the SNr, with some neurons being excited and others inhibited by activation of each pathway. However, only SNr neurons suppressed by D1-SPN activation predict locomotion initiation, while D2-SPN-induced movement arrest was most strongly correlated with the activity of excited SNr neurons (Freeze et al. 2013).

These activity changes in locomotion-related SNr neurons are probably transmitted downstream to glutamatergic MLR neurons, which influence locomotion. Although it is unknown whether locomotion-predictive SNr neurons are preferentially connected to locomotion-promoting neurons in the MLR, this is certainly an interesting possibility.

While these results support the idea that the BG output nucleus SNr constitutes a gate for movement, they also underscore the complexity of intrinsic SNr and BG organization, where likely neuronal subpopulations specialize in the regulation of different aspects of movement. In addition to the SNr, the MLR also receives input from other BG structures such as the GPi, the striatum and the STN (Roseberry et al. 2016, Caggiano et al. 2018), but the functional significance of SNr-bypassing circuits remains unaddressed.

BG circuits are also influenced by neuromodulators, most notably dopamine. The essential role of dopamine is most strikingly revealed in Parkinson's patients, whose dopamine-depleted state is associated with akinesia and bradykinesia (Albin et al. 1989, DeLong 1990, Dauer and Przedborski 2003), and for whom dopamine replacement therapy provides the main intervention to alleviate symptoms. Early work suggested that dopamine might act as a modulator of striatal and cortical firing by activating striatal D1-SPNs and repressing D2-SPNs. However, augmenting or lowering dopamine signaling does not alter striatal and cortical firing rates similarly across the board, but rather influences individual neurons differentially (Costa et al. 2006). Following the same striatal neurons using calcium imaging across different dopaminergic states in a mouse model demonstrated that D1-SPNs and D2-SPNs respond differently to altered dopamine levels (Parker et al. 2018). Interestingly, movement-related activity of D2-SPNs in the dopamine-depleted state became less spatially biased and less correlated to movement on- and offset, whereas D1-SPNs showed analogous response pattern changes in the hyper-dopaminergic state (Parker et al. 2018). To more clearly resolve the temporal and behavioral role of SNc dopamine signaling in the regulation of locomotion and movement in general, several recent studies used high spatial precision at the level of

single neurons or axons (Dodson et al. 2016, Howe and Dombeck 2016, da Silva et al. 2018, Parker et al. 2018). Notably, movement-related dopaminergic SNc neurons do not only signal by slow tonic activity, but also display phasic bursting activity shortly before the onset of locomotion or other self-paced movements (Figure 5.5.E). These observations suggest that locomotion-related dopamine signals can act at fast sub-second timescales, an activity pattern affected in a mouse model of Parkinson's disease (Dodson et al. 2016).

Calcium imaging of individual midbrain dopaminergic axons in the striatum revealed that locomotor- and reward-related signals were largely found in different axons, suggesting spatial and functional segregation (Howe and Dombeck 2016). Supporting a role of dopaminergic SNc neurons in movement initiation but not maintenance, their optogenetic stimulation increases the probability for movement initiation, whereas optogenetic inhibition only affects resting but not moving animals, by decreasing the probability of movement initiation (da Silva et al. 2018). Interestingly, the SNc dopamine signal is not specific for a certain type of movement such as locomotion, but rather represents a more general "go" signal and encodes the vigor of an upcoming movement (Howe and Dombeck 2016, da Silva et al. 2018) (Figure 5.5.E). Therefore, dopamine might provide a general motivational signal that modulates activity throughout the BG network, influencing the initiation of context-adequate movements with desired vigor. Such context-dependent modulation by dopamine could help to explain the heterogeneity of movement-related activity patterns observed in different SPN classes. Furthermore, in the specific case of locomotion, BG-imposed vigor needs to be translated into the desired speed of body translocation mediated by downstream brainstem centers, where speed-encoding neurons reside and receive input from BG output structures (Roseberry et al. 2016, Caggiano et al. 2018). It is also interesting to reflect on the fact that initiation of locomotion requires the simultaneous suppression of competing limb-dependent movements (such as grooming, scratching or reaching) through precise orchestration of activity between BG-thalamo-cortical circuits and brainstem centers. Although important questions remain to be addressed pertaining to how brainstem centers are regulated by dopaminergic signals

influencing action initiation and vigor, these combined recent results call for an updated view on the role of dopaminergic SNc neurons and BG pathways in locomotion and movement in general.

Figure 5.5. Basal Ganglia circuit control of locomotion

(A) Schematic diagram of the main feed-forward connectivity by indirect (D2) and direct (D1) striatal spiny projection neurons (SPNs) within the basal ganglia, as well as their dopaminergic inputs.

(B) D1- and D2-SPNs containing striatal functional ensembles exhibit a proximity-biased spatial distribution, according to different behaviors (e.g. locomotion or rearing). Summary of their neuronal activity patterns is depicted on the right.

(C, D) Recording of MLR-vGlut2 (C) or SNr-inhibitory (D) neurons upon optogenetic stimulation of D1- or D2-SPNs. Note that not all SNr neurons are predictive of locomotor behavior, likely a reflection of further neuronal diversity yet to be identified.

(E) SNc-derived dopamine signaling to the dorsal striatum before movement initiation (e.g. locomotion) determines the vigor of the future executed action.

How circuits for behavioral needs and contexts interface with action programs

While BG are essential for the smooth execution of planned movements including exploratory or goal-directed locomotion, locomotion can also be strongly shaped by emotional valance of a behavioral context as well as internal physiological needs. These internal and external cues can lead to abrupt changes of locomotor states, overriding ongoing plans and the complex information processing they entail. Escaping and hunting are examples of such behaviors classified as primary defensive and appetitive motivational locomotor forms (Sinnamon 1993). We will discuss selected examples of circuits influencing defensive (escaping and freezing) and predatory (hunting) actions to illustrate this point, with a focus on their locomotor components. Brain structures implicated in these behaviors and mentioned here are hypothalamic nuclei, the central amygdala (CeA) and the superior colliculus. A frequent pattern of these upstream structures is the convergence of some of their outputs to the PAG, an intermediary midbrain structure between regions encoding internal and external states and locomotor executive centers in the brainstem (Figure 5.6.A). It is important to note that the nervous system output accompanying innate responses goes well beyond the locomotion aspects discussed here, including other motor outputs (such as capture, biting, tail rattling, stretch posture, and actions related to internal needs including hunger, fear, social and sexual behavior) as well as autonomic responses (Stuber and Wise 2016, Fadok et al. 2018).

Exposure to threatening situations such as predators induces a state of increased anxiety and fear. Two opposing reactive responses affecting locomotor states are flight, a high-speed form of locomotion intended to escape from a threat, and freezing, a sudden arrest of body movement intended to avoid detection. Freezing is produced by activation of glutamatergic lateral and ventrolateral PAG (l/vlPAG) neurons with connections to medullary premotor neurons, while flight is mediated by activation of glutamatergic neurons in the dorso-lateral PAG (dlPAG) (Figure 5.6.B) (Tovote et al. 2016). Also excitatory neurons in a more dorsal region of the PAG (dPAG) can control escape behavior and its vigor, by receiving processed visual information about looming stimuli from superior collicular neurons (Evans et al. 2018).

The target regions that mediate escaping responses of d/dlPAG circuits have not yet been described, but glutamatergic CnF and/or LPGi neurons might be direct or indirect targets, since both receive input from more dorsal regions of the PAG, and control high-speed locomotion (Capelli et al. 2017, Caggiano et al. 2018). Lastly, defensive behavior can be elicited by neurons in the superior colliculus marked by parvalbumin, whose axons bypass PAG circuitry altogether, inducing escape followed by freezing through outputs to the parabigeminal nucleus and immediate freezing via the lateral posterior thalamic nucleus (LPTN) (Figure 5.6.C) (Shang et al. 2018).

The situation is clearly more complex than simple PAG input-output transmission since intra-PAG circuitry is involved in guiding appropriate behavioral responses. Notably, GABAergic l/vlPAG interneurons locally inhibit freeze-neurons and can act as a switch to ensure that the execution of flight and freezing motor programs are mutually exclusive (Tovote et al. 2016). In support, freezing information is transmitted by long-range inhibitory projections from the central amygdala (CeA) that decrease the activity of GABAergic l/vlPAG interneurons with consequent disinhibition of l/vlPAG freeze-neurons. On the other hand, dlPAG flight-neurons contact and likely excite GABAergic l/vlPAG interneurons, thus silencing l/vlPAG freeze-neurons (Tovote et al. 2016). Additionally, glutamatergic lateral hypothalamus (LH) flight-neurons (Li et al. 2018) could also connect to the GABAergic l/vlPAG interneurons and silence the l/vlPAG freeze-neurons, similar to the excitatory dlPAG flight-neurons. Lastly, neurons in the dorsomedial and central parts of the ventromedial hypothalamus (VMHdm/c) tailor their function according to environmental cues, with a population defined by the expression of Steroidogenic factor 1 (SF1) promoting the expression of either freezing or escaping responses depending on the magnitude of their activation and whether or not a shelter is present (Figure 6D) (Wang et al. 2015). Whereas flight responses are transmitted via projections to the AHN, freezing responses pass via descending projections to the dPAG, suggesting that SF1-expressing VMHdm/c neurons might even be further divisible.

The PAG is also a central player in the regulation of predatory hunting, for which prey pursuit requires suppression of glutamatergic l/vlPAG neurons (Figure 5.6.D) (Han et al. 2017, Li et al. 2018). Individual GABAergic CeA neurons encode pursuit, capture and consumption during predatory hunting, and CeA pursuit-phase locomotor signals are conveyed to the l/vlPAG (Han et al. 2017). Predation-encoding GABAergic neurons projecting to l/vlPAG were also identified in the LH (Li et al. 2018). But whereas optogenetic stimulation of l/vlPAG projecting CeA neurons elicited only prey pursuit (Han et al. 2017), the analogous experiment with LH neurons additionally induced prey capture and consumption and even led to conspecific attacks (Li et al. 2018), suggesting only partially overlapping information coding for these two populations. Evidence is still insufficient to conclude whether the glutamatergic l/vlPAG neurons inhibited during predation are the same neurons active during freezing (Tovote et al. 2016, Han et al. 2017, Li et al. 2018), and what are the precise downstream targets receiving their output signals. Although data suggest that the predatory signal is conveyed to the MLR, it will be important to clarify which MLR subpopulations are targeted by these glutamatergic l/vlPAG neurons suppressed during predatory hunting (Figure 5.6.D). Glutamatergic MLR neurons seem unlikely candidates, as they are active during locomotion and receive most of their PAG input from dorsal domains (Roseberry et al. 2016, Caggiano et al. 2018). Instead, GABAergic MLR neurons might be candidates as they receive direct input from the PAG and exert local inhibitory effects on glutamatergic neurons (Roseberry et al. 2016).
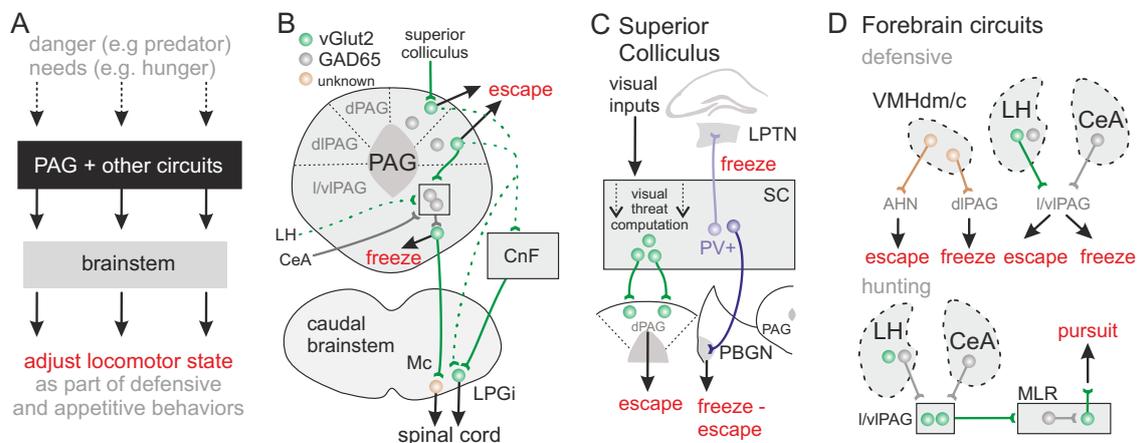
Figure 5.6. Circuits for behavioral need and context influencing locomotion

(A) Periaqueductal gray (PAG) and associated structures are central in processing information about danger and needs, to then signal through brainstem circuits to adjust locomotor state as part of numerous defensive and appetitive behaviors.

(B-D) Summary of functionally known (solid) and inferred (dashed) circuit organization for the PAG (B), superior colliculus (C) and forebrain circuits implicated in defensive and hunting behaviors (D). Neurons shown in boxes implies that there might be multiple neuronal subpopulations processing the shown inputs.

In summary, innate forms of locomotion involve many neuronal subpopulations located in the mid- and forebrain (Figure 6B-D). The LH segregates neurons involved in predatory and escaping locomotion, while the CeA promotes both hunting and freezing. Several appetitive and defensive locomotion motives are also present in the PAG as a key intermediary structure. Revealing the detailed functional links between escape and predation-related PAG neurons and connected output brainstem neurons will contribute to understanding if these functionally distinct channels extend into downstream circuits or if they align with the described speed related populations distributed between PPN for exploration and CnF for fast locomotion.

5.4. Outlook

Supraspinal circuits involved in the control of locomotion are distributed over many brain areas, making their comprehensive understanding a challenging task. Yet it has become clear that for many behavioral choices linked to locomotion, neuronal populations encoding and responsible for the implementation of specific functional attributes of locomotion are embedded in complex circuitry and can be recruited by different encountered contexts. The networks described in this review represent only a fraction of involved circuits, and as circuit dissection proceeds, connectivity matrices and functions will be understood better. Also other brain structures including the cerebellum and the cortex not described here contribute to shaping appropriate locomotor responses. Finally, another important question to consider will be how behavioral choice occurs at a more general level to select locomotion over the many other

behaviors an animal can execute, for which supraspinal circuits are also responsible. Answers

to all of these questions lie buried deep in the intricate circuitry of the brain.

5.5. Acknowledgements

6. Brainstem circuits controlling action diversification

Ludwig Ruder and Silvia Arber

6.1. Abstract

Neuronal circuits regulating movement are distributed throughout the nervous system. The brainstem is an important interface between upper motor centers involved in action planning and circuits in the spinal cord ultimately leading to execution of body movements. Here we focus on recent work using genetic and viral entry points to reveal the identity of functionally dedicated and frequently spatially intermingled brainstem populations essential for action diversification, a general principle conserved throughout evolution. Brainstem circuits with distinct organization and function control skilled forelimb behavior, orofacial movements and locomotion. They convey regulatory parameters to motor output structures and collaborate in the construction of complex natural motor behaviors. Functionally-tuned brainstem neurons for different actions serve as important integrators of synaptic inputs from upstream centers including basal ganglia and cortex to regulate and modulate behavioral function in different contexts.

6.2. Introduction

The brainstem is a key structure rostral to the spinal cord involved in the regulation of many forms of movement and other physiological functions. Brainstem neurons were inherently difficult to study in the past due to their functional diversity, neuronal intermingling and complex integration into local, ascending and descending circuits (Valverde 1961, Kuypers 1981, Newman 1985, Newman 1985, Jones 1995, Orlovsky et al. 1999). As a consequence, brainstem neurons have frequently simply been referred to as relay neurons linking upstream and downstream neurons without clear functional assignments. Nevertheless, a series of lesion experiments in different species demonstrated the necessity of the brainstem in the control of movement. In frogs, transection of the neuraxis at progressively more caudal levels allowed to determine remaining motor abilities after lesion (Roh et al. 2011). Frogs with intact brainstem but without forebrain performed most behaviors displayed by intact frogs, including jumping, stepping and swimming. Frogs with transections at the rostral medulla showed partially remaining abilities, whereas all but reflexive behaviors were lost upon transection at the brainstem-spinal cord junction (Roh et al. 2011). While analogous experiments are more challenging in mammals also for ethical reasons, decorticated cats still perform many movements (Bjursten et al. 1976), and cats still locomote after premammillary lesions introduced rostral to the superior colliculus (Hinsey et al. 1930, Whelan 1996). These combined studies demonstrate that the brainstem harbors essential neuronal substrates to generate diverse forms of movement.

One important question in the field is precisely how the brainstem contributes to movement generation and coordination. Natural behaviors combine different forms of movements that either occur jointly or in succession, each ultimately implemented by motor neurons located in the brainstem and/or the spinal cord regulating peripheral muscle contractions (Figure 6.1.). During environmental exploration for example, locomotion and orofacial behaviors are frequently combined, and when animals arrive at a food source, they transport food to their mouth with their forelimb and begin chewing. Identification of neuronal cell types stratified by

different functions has awaited the recent implementation of genetic and viral tools, combined with cell-type specific perturbation experiments and refined behavioral analysis.
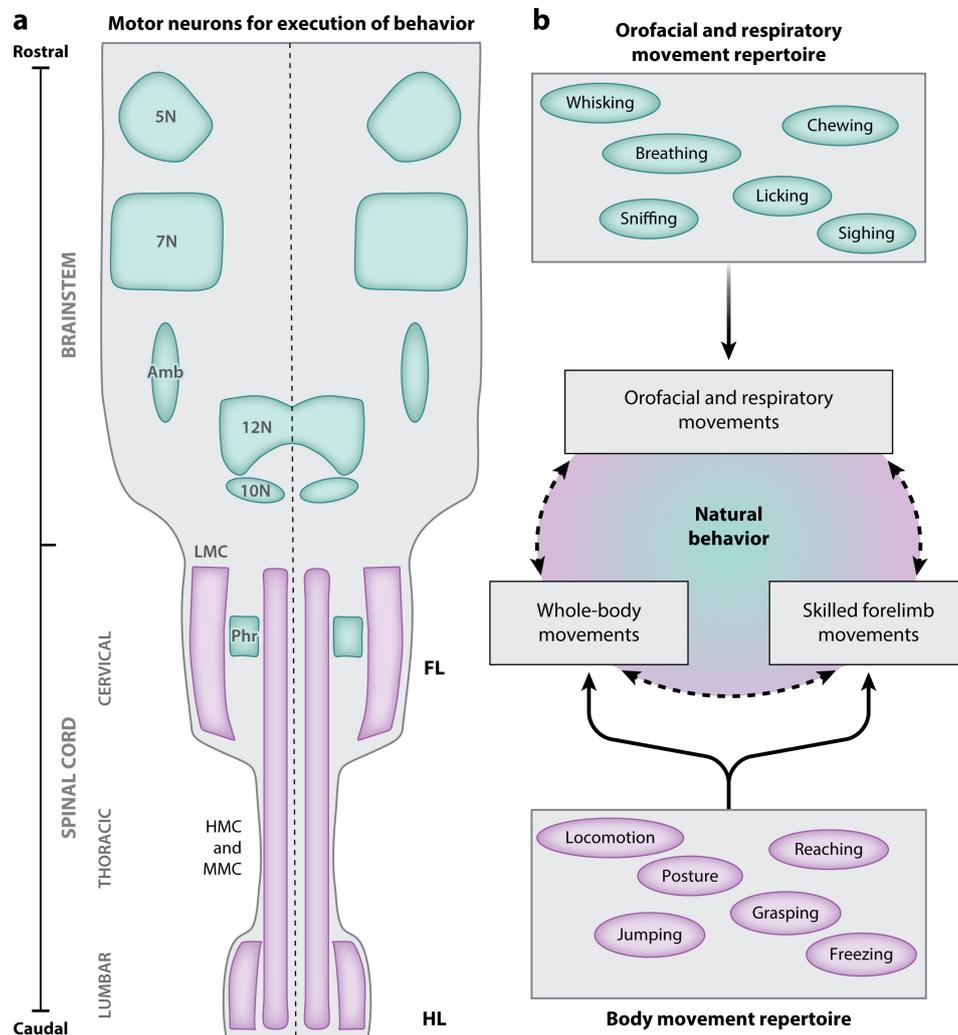
Figure 6.1. Movement programs regulated by brainstem circuits

Scheme illustrating the distribution of motor neurons in the brainstem and the spinal cord responsible for the regulation of skilled forelimb behaviors, orofacial and respiratory movements, and whole body movements. Left side shows schematic, not drawn to scale, top-down view of the brainstem (rostral; containing cranial motor nuclei; 5N: trigeminal; 7N: facial; Amb: ambiguous; 12N: hypoglossal; 10N: vagus) and the spinal cord (caudal; containing cervical, thoracic and lumbar segments; LMC: lateral motor column, innervating limb muscles; MMC: medial motor column, innervating axial muscles; HMC: innervating hypaxial muscles). Cervical motor neurons innervate forelimb (FL) muscles and lumbar motor neurons innervate hindlimb (HL) muscles. Right side illustrates examples of different behavioral elements of the

three different categories covered in this review, and how they can be combined during natural behaviors.

Here we will review work on three large behavioral categories with important brainstem contributions on which there has been significant recent progress in understanding function and connectivity of involved neuronal cell types – skilled forelimb movement, forms of orofacial and breathing behavior as well as whole-body locomotion (Figure 6.1.). Recent studies identified specific neuronal populations in the brainstem playing roles in these behaviors, allowing us to ask how these circuit elements and their combined usage regulate and coordinate action diversification. How brainstem circuits regulate functions associated with other behaviors (e.g. eye or head movement) or not related to movement (e.g. sleep) will not be discussed here.

6.3. Main Part

Brainstem and spinal circuits for the control of skilled forelimb behaviors

Skilled forelimb behaviors rely on the activation of forelimb muscles in diverse sequences to produce an almost infinite number of movement patterns we and other mammals can perform. Proximal and distal limb muscles represent a constrained spatial continuum along extremities. The act of moving the arm transports the hand to particular locations (e.g. through the process of reaching), and within these constraints, the hand can carry out myriads of movements (e.g. grasping, scratching, object manipulation) (Figure 6.2.). The generation of these complex behaviors as well as the monitoring of its execution requires modular, adaptable and highly organized neuronal circuits. They are needed to carry out these behaviors with high temporal precision and allow for adjustments during ongoing movements. The reach-to-grasp task is a frequently used behavioral paradigm to dissect circuits involved in skilled forelimb movement that rodents execute using strategies and behavioral phases similar to humans (Whishaw and Pellis 1990, Lemon 2008, Sacrey et al. 2009). Therefore, while comprehension of neuronal circuits controlling skilled forelimb behaviors is a challenging task, it opens the possibility to

define and study the function of core circuit elements both in the genetically accessible rodent model and in higher order species.

A large body of work in the past has focused on cortico-spinal connectivity and the role of these pathways in complex forelimb movements, with particular emphasis on direct connections from the cortex to spinal premotor and motor neurons (Dum and Strick 1991, Lemon 2008, Levine et al. 2012, Wang et al. 2017, Ueno et al. 2018). The reason for a high interest in this question was the observation that cortico-motoneuronal synapses increase in abundance with advancing evolution from rodents to monkeys to humans (Kuypers 1964, Lemon 2008). This process is paralleled by increasing levels of sophistication in dexterous movements, culminating in the ability to control single digits (Kuypers 1964, Lemon 2008). Already early on, it has however been clear that also circuits in the brainstem are involved in controlling skilled forelimb movements as evidenced by lesion studies and electrophysiological recordings in cats and monkeys (Kuypers and Lawrence 1967, Buford and Davidson 2004, Schepens and Drew 2004, Soteropoulos et al. 2012). Moreover, work with cortical or spinal cord injury models suggests that brainstem circuits in the reticular formation and red nucleus gain functional importance under these compromised experimental conditions. Proposed mechanisms contributing to recovery of hand function after injury include axonal sprouting by cortical axons at the brainstem level and/or by reticulo-spinal axons in the spinal cord, thus compensating for the reduction or lack of cortical access to the spinal cord (Baker 2011, Baker et al. 2015, Fregosi et al. 2018, Mosberger et al. 2018). Here, we will review progress on the identification, anatomical organization and function of neuronal circuits connecting brainstem and spinal cord bidirectionally, thereby contributing to shaping skilled forelimb behaviors in the uninjured nervous system.

A key requirement for the generation of skilled forelimb movements is the ability of spinal circuitry to integrate supraspinal motor instructions, process this information and send commands to cervical motor neurons innervating forelimb muscles. Classical studies noted a

medio-lateral division in the lower brainstem, with lateral regions more prominently accessing intermediate and dorso-lateral spinal domains proposed to be involved in distal forelimb control (Kuypers 1964, Lemon 2008). Recent work demonstrates that some brainstem populations preferentially communicate with cervical spinal neurons in mice (Esposito et al. 2014) (Figure 6.2.). Of the identified brainstem regions, glutamatergic (vGlut2) neurons in a caudal brainstem area named medullary reticular formation ventral part (MdV) connect to interneurons and specific cervical motor neuron pools encompassing extensor and flexor subtypes (Esposito et al. 2014). Functional work further demonstrated that MdV-vGlut2 neurons are required for the execution of skilled forelimb movements. Most notably, in a single food pellet retrieval task, during which mice carry out the modular sequence of reaching, grasping and retrieval of a food pellet, MdV-vGlut2 neurons are needed for efficient execution of specifically the grasping phase (Figure 6.2.). The work identified additional brainstem regions with distinct connectivity profiles to the cervical spinal cord but their behavioral role remains to be studied. In addition, the red nucleus located in the midbrain projects to the spinal cord in a dorso-lateral tract and has also been implicated in the control of skilled forelimb movement (Kuypers and Lawrence 1967, Whishaw et al. 1998, Jarratt and Hyland 1999) (Figure 6.2.). Specifically, tract lesions in rats leads to defects in the arpeggio phase of the reach-grasp behavior (Morris et al. 2011). Jointly, these observations suggest that distinct brainstem populations control specific aspects or phases of skilled forelimb behaviors by accessing specialized spinal circuits.

How do descending pathways implicated in skilled forelimb behaviors interact with spinal neurons? Experiments performed in cats identified cervical spinal neurons that receive direct input from cortical, reticular and rubro-spinal neurons, and connect intraspinally mostly to neurons within the cervical spinal cord including motor neurons (Illert et al. 1978, Alstermark and Kummel 1986, Alstermark et al. 2007). Since such neurons were preferentially found at cervical levels C3 and C4, they were named C3-C4 propriospinal neurons. Early experiments in cats using spinal tract lesions of C3-C4 projections suggested an involvement of these neurons in forelimb-specific behaviors such as reaching (Alstermark et al. 1981). A more

recent study performed in monkeys and using a mix of retrograde and anterograde viral tools showed that silencing of neurons located at C3-C5 and projecting to C6-T1 induces impairments in forelimb reaching and grasping behaviors (Kinoshita et al. 2012). These deficits reversed after a few days, suggesting that compensatory mechanisms developed via other, unaffected descending pathways such as cortico-, reticulo- or rubro-spinal projections or other intraspinal relays (Kinoshita et al. 2012). Interestingly, in addition to their direct connections to motor neurons and other spinal interneurons, a fraction of C3-C4 propriospinal neurons also sends ascending projections to the precerebellar lateral reticular nucleus (LRN) in the brainstem, neurons that in turn give rise to cerebellar mossy fibers (Alstermark et al. 1981, Alstermark and Ekerot 2013). Bifurcating spinal neurons therefore serve both for descending motor command integration and production of ascending efference copy pathways to update and potentially adapt ongoing behavior through cerebellar circuitry.

Recent studies have addressed the identity and functional organization of cervical neurons with supraspinal ascending projections (Azim et al. 2014, Pivetta et al. 2014, Hayashi et al. 2018) (Figure 6.2.). A common entry point for these studies was the finding that during development, spinal populations with involvement in functionally specific aspects of motor behavior are often derived from distinct progenitor domains (Goulding 2009, Alaynick et al. 2011, Arber 2012, Kiehn 2016). Different spinal populations are characterized by expression of selective transcription factors, allowing for their genetic targeting. Anatomically mapping bifurcating cervical projection neurons in mice revealed that they distribute much more broadly than just to C3-C4 segments, although they are nevertheless confined to cervical levels (Pivetta et al. 2014). LRN-projecting cervical neurons also fractionate into several genetically distinct populations encompassing excitatory and inhibitory subsets, as demonstrated by intersectional genetic and viral tracing methods that permanently label neurons derived from distinct progenitor domains or neurotransmitter identity (Figure 6.2.). Interestingly, identified populations establish anatomically divergent terminal arborizations within the LRN (Pivetta et al. 2014). The excitatory V2a population contains a fraction of these ascending projection

neurons and targeted ablation of the overall V2a population at cervical levels in mice elicits defects in reaching but not grasping in a goal-directed pellet retrieval task (Azim et al. 2014, Ueno et al. 2018). Furthermore, optogenetic activation of ascending branches of cervical V2a neurons in the LRN severely perturbs the forelimb reaching trajectory (Figure 6.2.), providing evidence that the ascending V2a branch can affect forelimb behavior (Azim et al. 2014).
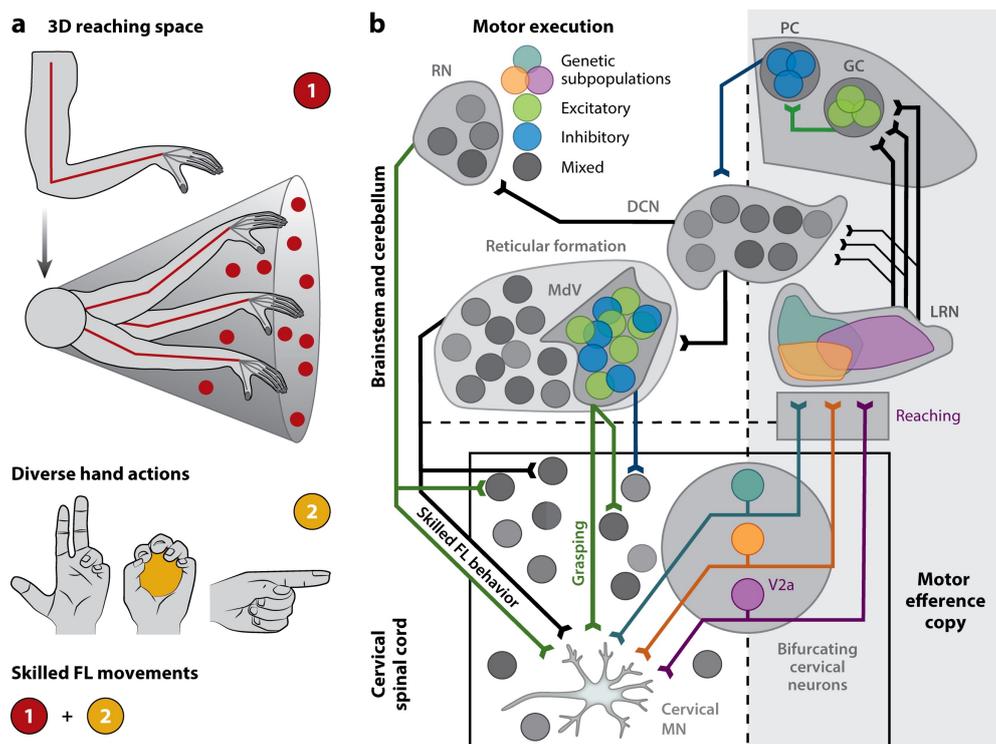
Figure 6.2. Brainstem-centric view on skilled forelimb behaviors

(Left) Schematic illustration on the usage of forelimbs in skilled behaviors. Briefly, the arm makes use of the 3D reaching space to bring the hand to a desired location (indicated by the cone and the red spots) in a first phase of the behavior, and the hand then carries out one of many diverse actions in a second phase. (Right) Incomplete scheme of brainstem/cerebellum (top) and spinal (bottom) circuitry described in this review implicated in skilled forelimb behavior. Left side of the scheme focuses on descending circuit organization for motor execution, and right side depicts circuits for computation of motor efference information. Note that bifurcating cervical neurons reside at the boundary between these two categories connecting to cervical motor neurons and neurons in the lateral reticular nucleus (LRN) in the brainstem. LRN neurons in turn connect to cerebellar circuits (GC: granule cells; PC: Purkinje cells) and deep cerebellar nuclei (DCN). Reticular formation including medullary reticular

formation ventral part (MdV) and the red nucleus (RN) are regions implicated in different aspects of skilled forelimb behavior.

The overall V2a population is still a diverse population. Besides its involvement in forelimb reaching, it was functionally linked to left-right alternation in a speed-dependent manner (Crone et al. 2008, Crone et al. 2009). This functional heterogeneity suggests the existence of more distinct subpopulations within the V2a population, and indeed two different types (V2a type I: low Chx10 expression, present throughout the spinal cord; and V2a type II: high Chx10 expression, preferentially located at cervical levels and with ascending projections to the brainstem) were recently described (Hayashi et al. 2018). Furthermore, single-cell RNA sequencing of V2a neurons revealed 11 clusters with different fractions of type I and type II V2a neurons leading to the speculation that specific clusters of type I V2a neurons might be involved in whole body locomotion, whereas other type II, cervical-enriched V2a neuron clusters might be involved in skilled forelimb movements (Hayashi et al. 2018).

Together, functionally diverse subsets of cervical spinal neurons integrate descending motor commands and establish ascending axons to precerebellar neurons in the LRN (Figure 6.2.). This raises the question of whether and how information passing through the cerebellum to deep cerebellar nuclei (DCNs) influences skilled (forelimb) behavior to close the loop. Such a looped circuit structure would allow for comparison of executed to intended movement to adjust movement if needed. Integration already seems to occur at the level of granule cells for a variety of behavioral paradigms even incorporating learning-related information including reward and punishment, as well as anticipatory movement-related signals (Huang et al. 2013, Giovannucci et al. 2017, Wagner et al. 2017). Purkinje cells (PCs) represent the output channels of the cerebellar cortex, signaling by inhibition to DCN neurons that as a population target both ascending and descending structures. It is well established that cerebellar circuitry and the PC-to-DCN pathway is involved in associative forms of learning (Medina 2011). To understand whether changing PC firing rate influences behavior instantaneously, optogenetic

manipulation studies were informative (Heiney et al. 2014, Lee et al. 2015). PCs fire at high rates spontaneously (50-100Hz) and reducing or pausing their firing is predicted to disinhibit downstream DCN neurons and influence movement. Indeed, transient silencing of PCs by either activation of inhibitory molecular layer interneurons or direct optogenetic inhibition of PCs elicits discrete behaviors, according to the inhibited region either eyelid or forelimb movement (Heiney et al. 2014, Lee et al. 2015). Distinct DCN neurons are also accessible genetically. Optogenetic activation and ablation demonstrates that a molecularly-defined population in the DCN IntA (Ucn3+) influences both fore- and hindlimb positioning (Low et al. 2018).

These combined data show that a looped and bidirectionally communicating network between the brainstem and spinal cord plays important roles in the control of skilled forelimb movements. Future work will reveal identity and connectivity of circuit components responsible for parsing together the distinct behavioral elements of skilled forelimb movement and how these behaviors can be adjusted. This will embrace understanding their synaptic and functional interactions with higher motor centers including cortical, thalamic and basal ganglia components, but also includes intra-brainstem connectivity between functionally distinct areas.

Coordination of orofacial and respiratory movements by brainstem circuits

Another complex set of behaviors coordinated by circuits in the brainstem are breathing and orofacial movements, including whisking, sniffing, licking, swallowing and chewing (Figure 6.3.). These behaviors are often temporally tightly coordinated with each other to elicit the desired movement sequence, e.g. to couple jaw and tongue muscles during eating or drinking (Welzl and Bures 1977, Naganuma et al. 2001, Kurnikova et al. 2017, McElvain et al. 2018). They also frequently maintain a strong oscillatory component with rhythmic repetition of the same movement at a frequency (Kurnikova et al. 2017, McElvain et al. 2018).

Work on a number of neuronal networks producing rhythmic outputs have suggested important contributions for neurons with intrinsic oscillatory capacity implemented through their physiological properties, even within very simple networks (Marder and Bucher 2001). For breathing, several brainstem regions with oscillatory properties linked to behavior were identified, most notably the rhythmic oscillators within the pre-Bötzinger complex, the Bötzinger complex and the parafacial respiratory groups regulating inspiration and expiration during breathing (Moore et al. 2014, Del Negro et al. 2018) (Figure 6.3.). Several recent studies addressed the cellular organization, subpopulation identity and potential interactions between these and circuits involved in the regulation of orofacial movements and breathing.

Motor neurons innervating oral and facial muscles used to produce orofacial movements are clustered into specific brainstem motor nuclei and project to their target muscles through cranial motor nerves (Guthrie 2007). One recent entry point to uncover the organizational principles of networks underlying orofacial behaviors has been to study the organization of premotor neurons to brainstem motor neurons responsible for driving respective behaviors. Technology to map overall direct synaptic inputs to specific neurons through monosynaptic rabies viruses (Wickersham et al. 2007) was applied to reveal organizational differences of premotor neurons to motor neuron pools innervating functionally distinct limb muscles (Stepien et al. 2010, Tripodi et al. 2011). Studies analyzing the last-order premotor neuron distribution for different oral, facial and phrenic motor neuron pools revealed interesting organizational differences (Takatoh et al. 2013, Stanek et al. 2014, Sreenivasan et al. 2015, Deschenes et al. 2016, Wu et al. 2017).

The pre-Bötzinger complex (preBötC), the site of oscillatory rhythmic activity coupled with the inspiratory respiration cycle, has almost no direct connections to diaphragm-innervating phrenic motor neurons (Smith et al. 1991, Del Negro et al. 2018). Instead, the preBötC signals through the rostral, ventral respiratory group to access phrenic motor neurons (rVRG) (Feldman et al. 2013, Del Negro et al. 2018). A recent study showed that both structures share

the developmental expression of the transcription factor Dbx1 (Wu et al. 2017), demonstrating that the V0 progenitor domain does not only generate preBötC neurons (Cui et al. 2016) within the breathing network. Moreover, Dbx1+ rVRG neurons connect to phrenic motor neurons on both sides (Wu et al. 2017), ensuring tight inspirational control through regulation of the diaphragm muscle across the midline. Neurons in preBötC can also be influenced to produce different breathing behaviors according to motivational and physiological need. To induce a sigh, preBötC neurons are regulated by a population of only 200 upstream neurons in the retrotrapezoid nucleus/parafacial respiratory group, marked by the expression of bombesin-like neuropeptides (Li et al. 2016).

Recent work revealed that premotor neurons connected to different brainstem motor neurons can be in close proximity to each other or even intermingled. For example, neurons premotor to facial motor neurons (7N) controlling whisking movements are close to and within the preBötC (Takatoh et al. 2013, Sreenivasan et al. 2015). These premotor neurons show mixed neurotransmitter phenotypes constituting potentially different premotor populations responsible for the protraction and retraction phases of whisking, reinforcing the concept of distinct subpopulations controlling specific motor behaviors (Takatoh et al. 2013). The spatial proximity of vibrissa premotor neurons to the preBötC as well as the rhythmic nature of whisking itself raises the question of whether a potential oscillatory center for rhythmic whisking interacts with circuits controlling breathing.

Breathing and whisking are functionally tightly coupled but each can occur in the absence of the other (Moore et al. 2013). This suggests linked, but distinct neuronal circuitry responsible for respective oscillatory control mechanisms. Additionally, since the breathing rhythm can reset the whisking rhythm but not vice versa, the preBötC seems to act as a master regulator of these behaviors (Moore et al. 2013, Kleinfeld et al. 2014) (Figure 6.3.). Functionally, a subregion of the brainstem intermediate reticular nucleus (IRt, sometimes also referred to as the intermediate band of the reticular formation), in close proximity to the preBötC and site of

whisker premotor neurons, harbors neurons whose activity is tightly locked with rhythmic whisking movements (Moore et al. 2013, Takatoh et al. 2013, Deschenes et al. 2016) (Figure 6.3.). A combination of activation and lesion experiments provide evidence for sufficiency and necessity of this region for whisking, demonstrating its role as an oscillatory center under potential master regulation of the preBötC (Moore et al. 2013, Deschenes et al. 2016). As a further extension of these findings on closely spaced and interacting brainstem networks, oscillatory activity coupled to licking movements as well as the necessity for licking have also been attributed to the IRt (Travers et al. 2000) (Figure 6.3.). Circuits controlling chewing, a behavior that is not phase-locked with breathing (McFarland and Lund 1993), also appear to reside within the rather lateral brainstem, but rostrally to the breathing and whisking oscillators (Dellow and Lund 1971, Kolta et al. 2007, Morquette and Kolta 2014).

What is the circuit architecture controlling these interrelated behaviors? A common denominator using anterograde, retrograde and trans-synaptic tracers is that most premotor neurons innervating orofacial and breathing motor neurons reside in intermediate to lateral brainstem areas occupying partly intermingling or distinct regional hotspots, prominently within the IRt, PCRt and preBötC regions (Takatoh et al. 2013, Stanek et al. 2014, Sreenivasan et al. 2015, Deschenes et al. 2016, Wu et al. 2017). Premotor neurons are also molecularly diverse, but common principles are beginning to emerge for some behaviors (Wu et al. 2017). It is currently unclear whether circuits responsible for different behaviors engage shared neuronal populations. Behavioral and electrophysiological experiments suggest that individual oscillatory centers control distinct movements including swallowing, licking and whisking, and that the breathing oscillator can act as master regulator (Moore et al. 2014) (Figure 6.3.). Taken together, brainstem circuits controlling orofacial and breathing behaviors are made up of specific neuronal subpopulations responsible for individual motor attributes that are tightly coupled to enable complex behaviors present during exploration or feeding.
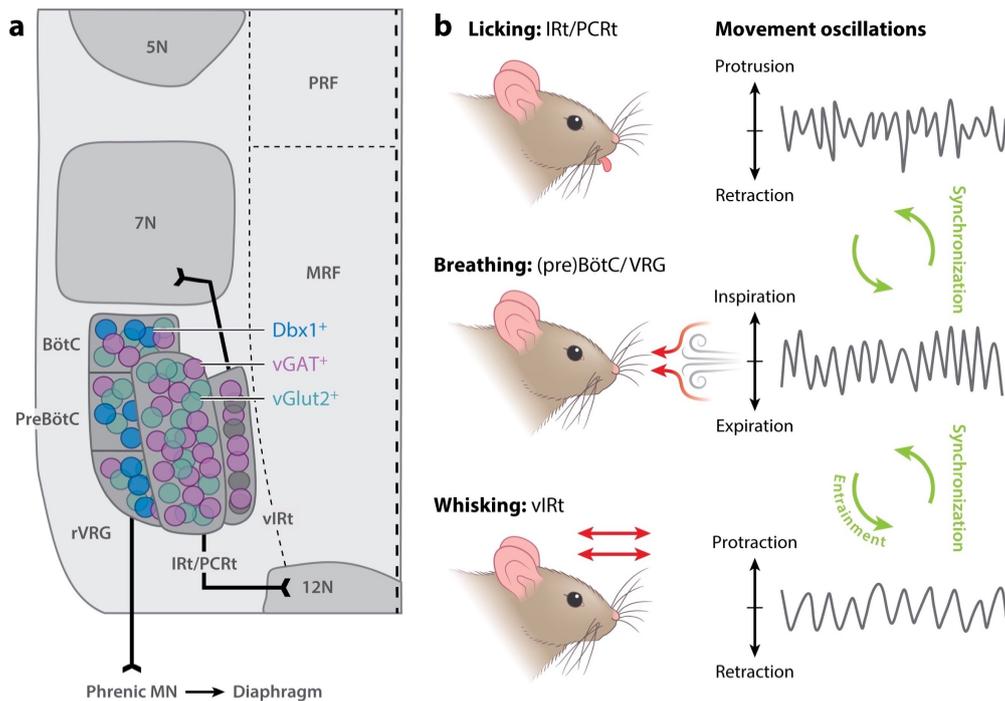
Figure 6.3. Generation of orofacial and respiratory behaviors by brainstem circuits

Schematic diagram illustrating the close spatial proximity of brainstem neurons implicated in the regulated orofacial and respiratory behaviors. (Left) Top-down anatomical depiction of Bötzinger complex (BötC), pre-Bötzinger complex (preBötC), rostral ventral respiratory group (rVRG) accessing phrenic motor neurons that in turn innervate the diaphragm muscle, the intermediate reticular nucleus (IRt), and the parvicellular reticular nucleus (PCRt). Excitatory (vGlut2) and inhibitory (vGAT), as well as developmentally Dbx1-originating neurons are shown in different colors. Rostro-caudal boundary between medullary (MRF) and pontine (PRF) reticular formation is indicated and relevant cranial motor nuclei are shown in grey. (Right) Depiction of three described behaviors, implicated brainstem structures, and how rhythms between these behaviors can be synchronized. The breathing rhythm has been demonstrated to be able to entrain the whisking rhythm, indicating close collaboration between relevant circuit elements.

An interesting aspect that has not been addressed yet is the potential interactions between orofacial and breathing circuits with networks involved in skilled forelimb movements or locomotion. Orofacial behaviors are coordinated with body actions occurring during natural

complex movements (Figure 6.1.). These include reaching for and consuming food, during which the mouth opens to take up food that is subsequently chewed and swallowed. To find food, animals explore the environment, hunt at high speed requiring an increase in the respiratory rate, and fight with and kill their prey, again requiring tight coordination between body and orofacial muscles. Now that specific brainstem subpopulations responsible for both orofacial, breathing and body behaviors are beginning to be identified, studies on the interactions between different neuronal populations to understand how complex behaviors are coordinated through brainstem motor circuitry at a more global level will be possible.

Brainstem circuits controlling full body movement

Locomotion is a universal behavior in the animal kingdom. This form of full-body movement manifests itself differentially according to species as walking to running, swimming, crawling or flying to mention the most prominent forms (Orlovsky et al. 1999). One common denominator in all species is the need for behavioral coordination throughout the body to move it forward, and the ability to optimize speed for controlled interactions with the environment. The brainstem plays important roles in the regulation of locomotion, and recent work reviewed here begins to delineate the identity of circuits between the midbrain and more caudally located brainstem regions as instrumental for the control of specific locomotor parameters (Figure 6.4.).

The mesencephalic locomotor region (MLR) in the midbrain is a historically identified area, the stimulation of which elicits coordinated full-body locomotion in a variety of species including cat, rat and lamprey (Shik and Orlovsky 1976, Skinner and Garcia-Rill 1984, Mori et al. 1989, Ryczko and Dubuc 2013). Recent studies provide evidence that despite spatial intermingling of glutamatergic, inhibitory and cholinergic cell types within the MLR, specifically vGlut2-expressing neurons are central for the locomotion-promoting properties of the MLR (Niell and Stryker 2010, Roseberry et al. 2016, Caggiano et al. 2018, Josset et al. 2018). It is also clear that there is further functional diversity within the MLR. Stimulation of vGlut2-expressing

neurons within and close to the pedunculopontine nucleus (PPN) in the ventro-laterally located MLR only influences limb muscle activity or elicits low-speed locomotion, while stimulation of vGlut2 neurons in the dorso-medial cuneiform nucleus (CnF) of the MLR induces high-speed locomotion (Caggiano et al. 2018, Josset et al. 2018) (Figure 6.4.). This work is in agreement with a proposed model in which the CnF is involved in defensive and the PPN in exploratory forms of locomotion (Jordan 1998). In addition to locomotion-promoting properties, the MLR also seems to house circuits for attenuation of locomotor behaviors. This was suggested from both electrical (Takakusaki et al. 2016) and neurotransmitter-stratified optogenetic (Roseberry et al. 2016, Josset et al. 2018) stimulation experiments. Yet how these neurons relate to and/or interact with the locomotion-promoting counterparts remains to be defined.

Locomotion-promoting signals of the MLR have been proposed to reach the spinal cord mostly through di-synaptic pathways through intermediary neurons in the caudal brainstem, since cooling experiments in the ventral medulla severely reduces the effects of MLR-stimulation on locomotion (Shefchyk et al. 1984). Electrophysiological recordings in the medullary reticular formation in cats and mice revealed patterns of neuronal activity that correlate with locomotor parameters (Drew et al. 1986, Weber et al. 2015). Paired EMG and neuronal recordings showed highly diverse neuronal discharge patterns linked to the activity of individual or groups of muscles in cats (Drew et al. 1986). Despite these locomotion-correlated activity patterns, electrical stimulation experiments in the caudal brainstem failed to show consistent induction of full-body locomotion, leading to the idea that neuronal diversity might mask the regional properties to bring about such effects (Orlovsky et al. 1999). Indeed, a recent study demonstrated that also optogenetic stimulation at different sites within the caudal medulla in mice cannot induce full-body locomotion (Capelli et al. 2017). However, specific optogenetic activation of excitatory neurons in the lateral paragigantocellular nucleus (LPGi) elicited reliable and short-latency locomotion (Figure 6.4.). Functional studies further demonstrated that these vGlut2-LPGi neurons were essential for high-speed locomotion, and that the MLR locomotion-promoting signal is reduced in the absence of these neurons (Capelli et al. 2017).

Conversely, restricting optogenetic stimulation to intermingled inhibitory neurons within LPGi and neighboring medullary subregions attenuated locomotor behaviors ranging from simple behavioral stopping to body collapse akin to atonia (Capelli et al. 2017). In addition, another study demonstrated that a more rostrally located excitatory brainstem population marked by the V2a-population specific transcription factor Chx10 also influences halting of ongoing locomotion, likely through accessing locomotion-inhibiting spinal circuits (Bouvier et al. 2015), and glycinergic neurons in the pontine reticular formation influence locomotor speed negatively too through ascending projections to the thalamus (Giber et al. 2015) (Figure 6.4.). Surprisingly, V2a neurons in the zebrafish brainstem have opposite behavioral roles, in that they promote swimming and upon silencing lead to stopping of this behavior (Kimura et al. 2013). These findings might point to some changes during evolution in how neurons of similar genetic identity in analogous regions of the nervous system are engaged. Nevertheless, the existence of specific neuronal populations encoding distinct locomotor attributes is conserved across species (Kimura et al. 2013, Juvin et al. 2016).

Together, these findings demonstrate the existence of specific neuronal populations within the brainstem network between the midbrain and more caudal brainstem regions, regulating different attributes of locomotor behavior (Figure 6.4.). The execution of locomotor commands from the brainstem likely occurs through interactions with distinct circuits at the level of the spinal cord. Indeed, it has already become apparent that descending pathways originating from identified neuronal populations access spinal circuits differentially (Bouvier et al. 2015, Capelli et al. 2017).
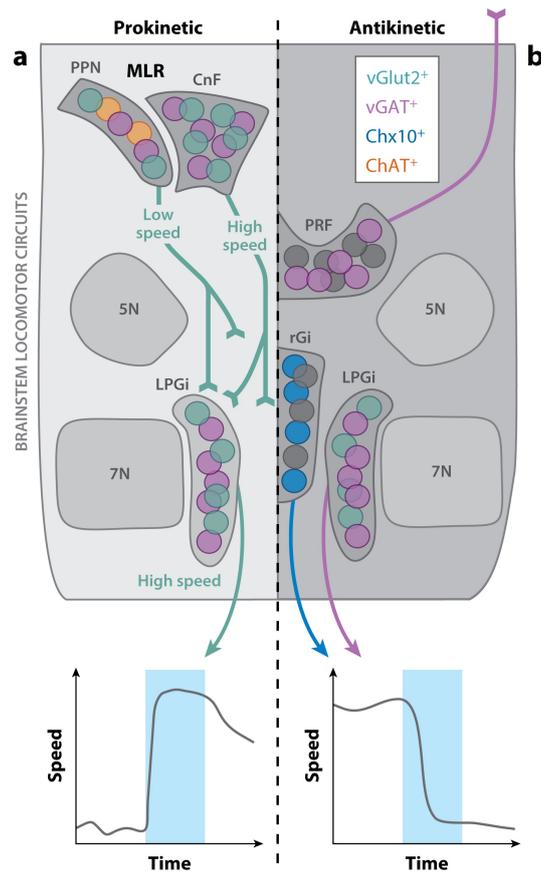
Figure 6.4. Brainstem circuits for regulation of locomotion

Schematic diagram depicting some of the brainstem circuit elements described in this review implicated in supraspinal control of locomotion. The left side of the scheme focuses on prokinetic, locomotion-promoting circuit organization. Briefly, the mesencephalic locomotor region (MLR) in the midbrain contains the pedunculopontine nucleus (PPN) and the cuneiform nucleus (CnF) implicated in low- and high-speed locomotion respectively. Excitatory neurons in the lateral paragigantocellular nucleus (LPGi) are implicated in high-speed locomotion. The right side of the scheme depicts antikinetic, behavioral-arrest-promoting circuits. Different forms of behavioral arrest are induced by optogenetic stimulation of inhibitory LPGi neurons, rostral Gi (rGi) Chx10-expressing neurons, or rostrally projecting inhibitory neurons in the pontine reticular formation (PRF). Speed vs time plot illustrates that optogenetic stimulation of respective neuronal populations (blue box) leads to either induction of locomotion with increased speed (left) or decrease of speed with behavioral arrest (right) in mice.

167

Modulatory and instructive inputs to brainstem circuits

The brainstem is critically involved in many movements including whole-body actions, skilled forelimb behaviors and orofacial coordination. Mammalian nervous system lesions eliminating cortex, basal ganglia and thalamus result in movements with highly reduced complexity (Whelan 1996). Several recent studies have assessed the functional role of interacting upstream structures with specific brainstem or midbrain circuits to instruct or modulate specific motor actions.

In the cortex, a fraction of layer 5 neurons also often referred to as pyramidal tract (PT) neurons projects to subcortical areas including colliculi, brainstem and spinal cord (Shepherd 2013), raising the question of the nature of their influence on behavior. PT neurons located in the anterior lateral motor cortex (ALM) and projecting to the brainstem often showed contralaterally-biased task-related activity before movement onset during a sensorimotor delayed discrimination task involving directional licking (Li et al. 2015) (Figure 6.5.). Interestingly, bilateral ALM silencing during the motor planning phase randomizes licking direction but does not abolish licking in general (Li et al. 2016), indicating a modulatory role for these neurons possibly by acting on brainstem targets to orchestrate specifically the licking direction. In a more complex motor task involving the learning of a skilled forelimb movement, learning-related changes in PT neuron activity in the motor cortex provide a possible cellular mechanism for how movement refinement occurs during learning (Peters et al. 2017), but whether this is implemented through interaction with brainstem circuits is currently unclear. Together, these studies suggest a role for cortical neurons projecting to the brainstem and spinal cord in modulating the activity of specific circuits in response to behavioral requirements involving fine aspects of motor performance and learning.

It is also interesting to understand interactions between different types of subcortical neurons and the brainstem. These interactions can also be dissected according to their specific projections and neuronal functions. The central Amygdala (CeA) sends long-range inhibitory

projections to distinct centers in the midbrain and brainstem (Tovote et al. 2015). Specifically manipulating CeA projections to the periaqueductal gray (PAG) or the parvicellular reticular nucleus (PCRt) revealed their differential contribution to hunting and killing behaviors respectively (Han et al. 2017) (Figure 6.5.). Coincident optogenetic stimulation of axonal terminals in both target areas was sufficient to elicit a complete predatory hunting sequence. Interestingly however, some effects were only observed in the presence of natural or artificial preys, suggesting a context-dependent component in the ability to elicit the behavior (Han et al. 2017). The PAG also receives different inputs from the hypothalamus and superior colliculus involved in regulating distinct locomotor modes ranging from freezing to escaping (Evans et al. 2018, Li et al. 2018).
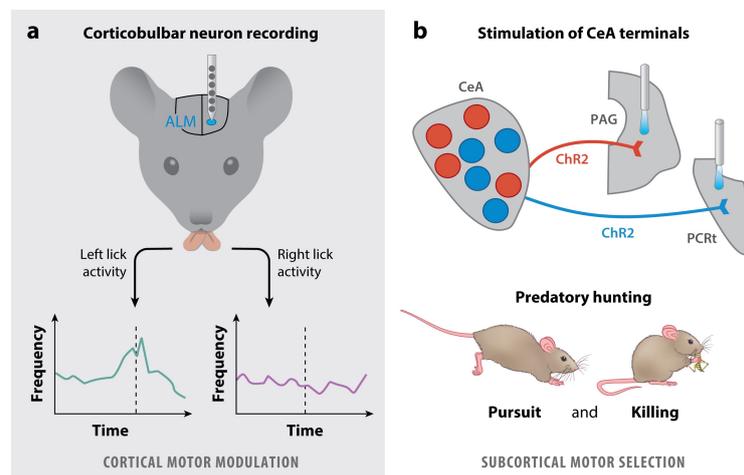
Figure 6.5. Modulatory and regulatory circuits impacting on the brainstem

Two examples of how upper motor centers interact with brainstem circuits. (Left) Neurons in the anterior lateral motor cortex (ALM) influence the directional bias of licking in a delayed discrimination task. Preparatory cortical activity ramping up during the delay period in right-sided ALM layer 5 pyramidal tract (PT) neurons with brainstem projections, preceding left-directional licking activity before action is initiated. Note that during right-directional licks, similar neuronal activity cannot be observed. (Right) Predatory hunting behavior composed of pursuit and killing phases is regulated by inhibitory neurons in the central amygdala (CeA) projecting to the periaqueductal gray (PAG) or the parvicellular reticular nucleus (PCRt)

respectively. Only joint axonal stimulation (blue light) in both target regions elicits full behavior, but in a behavioral context-dependent manner.

Some basal ganglia regions including the output structure substantia nigra pars reticulata (SNr) also project to motor related areas in the brainstem (Mena-Segovia and Bolam 2017, Arber and Costa 2018). Although functional studies linking basal ganglia projections to the brainstem are rare, the revealed neuronal coding within these circuits allows for an interesting hypothesis. Neurons in the striatum, the major basal ganglia input structure, encode various behavior-related parameters, with specific populations preferentially active during different behaviors such as grooming, locomotion, turning or rearing (Barbera et al. 2016, Klaus et al. 2017, Parker et al. 2018). Such specific activity patterns are likely transferred and processed between functionally-related cell populations within connected basal ganglia circuitry. Indeed, the SNr also harbors action-specific neuronal coding and this information might be differentially fed towards brainstem circuits (Arber 2012, Jin et al. 2014, Jin and Costa 2015, Rossi et al. 2016, Tecuapetla et al. 2016, Mena-Segovia and Bolam 2017).

These results lead to the hypothesis that subcortical regions contain channels to specific brainstem centers to aid the selection and execution of certain motor behaviors, depending on context. In contrast, direct cortical inputs to the brainstem might rather act as behavioral modulators allowing adaptation according to behavioral need, challenges and motivation.

Outlook and evolutionary conservation of brainstem organizational logic

The work reviewed here demonstrates that the brainstem harbors a distributed assembly of neuronal populations important for the regulation of diverse motor behaviors. A general principle that emerges is that neurons with different functions are frequently spatially intermingled but connected into precise circuitry ensuring different behavioral roles. Thus, it is critical to isolate neuronal populations based on their neurotransmitter and genetic identity to understand their function. Neuronal populations include dedicated communication channels to

the spinal cord involved in diverse aspects of controlling body movement as well as to networks regulating behaviors steered by motor neurons embedded within the brainstem proper. Although the overall organization of brainstem structures differs between species, the concept of descending pathways communicating specific information for action program execution is evolutionarily conserved.

To illustrate this point, we will briefly summarize progress in understanding the organization and function of descending neurons in insects that with only a few hundred neurons (Gronenberg and Strausfeld 1990, Hsu and Bhandawat 2016) represent simpler models than mammals. Genetic approaches in *Drosophila melanogaster* were used to systematically assess the organization and function of individual neurons, covering about half the known neurons with projections to the ventral nerve cord (Namiki et al. 2018), the structure analogous to the vertebrate spinal cord. Two groups of descending neurons target non-overlapping neuropil territories responsible for the control of flight and walking respectively. A third group projects to the intermediate neuropil and might drive more complex integrative motor behaviors requiring both types of behaviors such as e.g. grooming or take-off for flying (Namiki et al. 2018). Optogenetic activation in these genetically stratified backgrounds assessed the functional impact of identified descending neurons (Cande et al. 2018). Notably, activation of specific descending neurons frequently elicited stereotyped behaviors. Interestingly however, some induced behaviors depended on the fly's behavioral state before manipulation. These results suggest that information conveyed by upper centers or feedback mechanisms can be reconfigured in a state-dependent manner and can differentially impact movement regulation. This concept will also be interesting to study in evolutionarily higher species where state-dependency might play more prominent roles in behavioral regulation.

Important questions on understanding how brainstem circuits orchestrate the execution and learning of actions remain to be addressed. While control elements for specific behaviors in the brainstem are beginning to be unraveled, future work will determine how combination of

individual elements for one behavior or the generation of action sequences are achieved. We also need to understand how movement elements occurring in parallel are aligned and coordinated to achieve the overall animal behavior. Moreover, certain action programs that should not occur concurrently most likely rely on inhibitory mechanisms that prevent the unwanted behavior on the one hand and enhance the chosen motor program on the other hand. Some of these regulatory and interactive mechanisms likely depend on upstream circuits including basal ganglia, cortex and thalamus, as well as the integration of feedback circuits from the periphery. Ultimately however, integrated information passes through neuronal populations in the brainstem who themselves likely also contribute to all of these processes.

6.4. Acknowledgements

7. Conclusions

The central control over movements is coordinated by circuits distributed all over the nervous system. In this dissertation, networks within the spinal cord controlling long-distance interlimb coordination and brainstem circuits important for diversification of complex forelimb movements are described. We identified distinct circuit elements stratified by neurotransmitter identity, developmental origin or projection pattern and relate them to specific contributions in motor actions uncovering important principles of how the caudal circuits in the nervous system control behavioral output. Here we will discuss these findings in the light of integration into the broader network of locomotor and forelimb control and hypothesize on motor circuits for natural, holistic behavior.

7.1. Beyond the spinal cord – Connecting long projection neurons with supraspinal locomotor commands

We and others showed that long projecting neurons in the spinal cord are located most densely in Rexed's laminae VII and VIII in the ventromedial parts of the spinal cord (Matsushita et al. 1979, Alstermark et al. 1987). Interestingly this is also the site where commissural spinal interneurons projecting across the midline reside (Alaynick et al. 2011). We demonstrated that these long projection neurons are important for the coordination of fore- and hindlimbs during locomotion, a whole-body behavior. Additionally, besides their long projections connecting the cervical and lumbar spinal cord, they synapse throughout their projections in the spinal cord also at thoracic levels. The functional role and anatomical organization therefore make long spinal projection neurons an ideal circuit to integrate and broadly distribute whole-body related supraspinal motor commands throughout both halves of spinal circuitry. Intriguingly, many brain structures with spinal projections thought or shown to be involved with the motor aspects of whole-body behaviors are preferentially projecting to ventromedially located spinal laminae where long spinal projection neurons reside. This includes projections from the vestibular nuclei, medial reticular nuclei, pontine reticular nuclei and midbrain areas (Matsuyama et al.

1997, Basaldella et al. 2015, Bouvier et al. 2015, Capelli et al. 2017). In one example, excitatory neurons in a specific nucleus of the medial reticular formation shown to be important for high-speed locomotion have their strongest spinal termination zone in the ventromedial spinal cord where long projection neurons reside (Capelli et al. 2017), while we have further shown that a direct synaptic interaction between these two neuronal populations exist by using transsynaptic tools. Interestingly, using a fictive locomotion *in vitro* preparation in which a bath of neurotransmitters and neuromodulators is used to elicit rhythmic ventral root activity, transmission of brainstem signals throughout brainstem circuits depends on spinal projection neuron activity (Zaporozhets et al. 2006, Cowley et al. 2008, Cowley et al. 2010). This circuit organization positions long spinal projection neurons at the interface between diverse, whole-body behaviors and wide-spread signal distribution in the spinal cord. Future experiments will show how distinct aspects of whole-body behaviors are differentially integrated in long spinal projection neurons and how it affects ongoing spinal activity.

Another interesting angle to further pursue is the role of projection neurons in the recovery from spinal cord injury (Bareyre et al. 2004, Courtine et al. 2008, Filli et al. 2014, Takeoka et al. 2014, Isa 2019). Besides their architecture to broadcast supraspinal information throughout ongoing spinal circuitry, the long projection neuron network setup could be alternatively used to relay information originally transmitted through supraspinal projections via long projection neurons in the case of incomplete spinal cord injury. Indeed, long projection neurons were demonstrated to respond with additional axonal sprouting in response to a dorsal hemisection of the spinal cord and bypass cortical input, severed by the injury, to levels below the injury. A process that is paralleled with functional recovery (Bareyre et al. 2004). The principle of increased axonal arborization applies not only to supraspinal input, but also to sensory feedback, a critical component for recovery after incomplete spinal cord injury. Axon midline crossing of long projection neurons below the injury was strongly decreased in the absence of muscle spindle feedback during which recovery after incomplete spinal cord injury is very minimal (Takeoka et al. 2014). Together, incomplete spinal cord injury experiments point

towards a network of long projection neurons that can take over to relay supraspinal information and increase excitability in input-deprived circuits below the injury.

7.2. The integration of brainstem circuits involved in forelimb behavior within broader motor networks and their role in naturalistic behavior

The here described circuits in the lateral rostral medulla establish spatially intermingled, but segregated networks of neurons differentially involved in forelimb movements ranging from simple to complex. While direct spinal cord projections trigger a clean reaching movement, much more sophisticated and diverse forelimb behaviors are elicited when involving projections through the caudal medulla provoking the question of how upstream inputs are interacting with these circuits to recruit and choose appropriate networks involved in the intended behaviors. Interestingly, regions in the latRM receive diverse, functionally relevant inputs from motor related upstream areas (Li et al. 2015, Han et al. 2017, Mercer Lindsay et al. 2019). The central amygdala (CeA), as the output nucleus from amygdala circuitry, sends strong projections to the latRM centered in the PCRt, while other populations in the CeA send segregated output to other structures. Optogenetic activation of the latRM specific output from the CeA elicits forelimb capturing and biting movements targeted towards natural as well as artificial prey implicating the latRM in the output stream of context specific motor actions depending on behavioral state (Han et al. 2017). Cortical projections from the motor cortex to the IRt, a region more medially located in the latRM, are involved with signaling motor plans and intentions. Pyramidal neurons projecting to the IRt develop a licking direction signal predicting the directionality of subsequent licking movements. Importantly, many of these directionality signals ramp up activity in preparation to the onset of the movement (Li et al. 2015). While these observed signals are in the context of licking movements, the existence of direction-selective coding for reaching movements has been shown for other cortical structures in monkeys and mice (Tanji and Evarts 1976, Galinanes et al. 2018) making it persuasive to hypothesize about the nature and meaning of preparatory activity as well as directionality signals we observe in the latRM. In one possible scenario, the observed cortical patterns could

be used as an output to the brainstem "priming" forelimb related circuits in the latRM for upcoming reaching movements and thus influence reaching movements and directionality. Other experiments further investigated the direct link between the cortex and the latRM in the context of orofacial and forelimb behaviors and found that projections from layer 5 of the cortex to the latRM are able to influence behavior directly by changing the activity of orofacial and forelimb muscles (Mercer Lindsay et al. 2019). Finally, besides the projections from the cortex and the CeA, the latRM receives also strong basal ganglia output projections from the substantia nigra pars reticulata (SNr) that also arises not from all SNr output neurons, but from a specific spatially localized population (Chronister et al. 1988). All together there are two important takeaways regarding the broader motor circuitry of forelimb behaviors in the brainstem. First, the latRM receives input from many higher centers in the cortex and basal ganglia output structures suggesting a convergence of multiple motor signals rendering the latRM as an integrator that engages specific, intermingled networks to act as a commanding center instructing spinal circuits crucial for the execution of a desired movement. Second, these inputs are derived from highly specific neuronal populations within the originating structure and not from a general, regional output. Interestingly, within the striatum, the input stage of the basal ganglia, different motor behaviors are encoded by distinct neuronal ensembles, a feature that is probably carried all throughout the widely distributed motor circuitry(Barbera et al. 2016, Klaus et al. 2017, Parker et al. 2018). It remains to be seen how behavioral related neuronal populations in distinct areas are connected with each other and what differences exist in the nature of their encoding.

While in the present experimental work we focused on forelimb movements, most natural behaviors are a mix of whole body, forelimb and orofacial movements (see chapter 6). Just imagine a mouse foraging for, retrieving and consuming water and food during which the animal is locomoting to explore the environment, engages its forelimb to retrieve or explore different objects and uses multiple orofacial muscles all throughout to probe the environment and consume food and drink. In the future, it will be key to establish and develop methods that allow for reliable tracking, categorization and quantification of this constant natural interplay of

different behaviors (Klaus et al. 2017). Translating such fine-grained readout to a neuronal network level for brainstem circuitry to study potential circuit interactions during simultaneously occurring behaviors such as forelimb and orofacial motor actions during food handling will lead to a more holistic understanding how brainstem circuits for movement are constructed.

8. Acknowledgements

This work would not exist without the help and support from many people involved and this is the right place to thank them.

First and foremost, I want to thank my supervisor Silvia Arber. Her enthusiasm, drive, deep scientific thinking and dedication thoroughly shaped me in my own approach to scientific problems. She has supported me in many, many aspects throughout my years in her lab way beyond my expectations and for this I am deeply grateful.

Further I am very thankful to Aya Takeoka who introduced and supervised me upon joining the lab, supported me in my own first scientific endeavors and provided a critical contribution to the first experimental part of this thesis in the spinal cord.

Chiara Pivetta, Riccardo Schina and Harsh Kanodia shared the forelimb project in the lateral medulla with me. I thank them very much for their invaluable support, commitment and expertise without which this work would surely not have been possible.

I want to also thank Paolo Capelli. I will always remember our thorough and engaged scientific discussions be it in the lab or somewhere in the Norwegian wilderness.

Also, to the whole rest of the Arber lab, thank you! It was exciting and inspiring to do and discuss science in such a stimulating environment.

Pico Caroni and Botond Roska were the two other members of my PhD committee and our meetings always greatly moved the project forward. I want to thank them for their investment, expertise and inspiration to this work.

The Biozentrum of the University of Basel and the Friedrich Miescher Institute for Biomedial Research have provided me with an incredible scientific environment from technical facilities providing expert help all the way to the stimulating scientific interactions with other research groups.

My parents who guided and educated me in so many ways in science and beyond, where I can only ascertain that I would not be here without them. Thank you!

Thanks also to my siblings and friends who were there for me throughout these years for all the moments that directly or indirectly shaped aspects of this work. A special thank you goes out to my sister Josefine who gave feedback on some parts of this thesis as well as to Dario, a friend whose support has carried me for a very long way already.

Lastly, I want to thank Christina. My own words cannot describe my gratefulness; therefore, I shall remain with the following:

"To get the full value of joy you must have someone to divide it with."

- Mark Twain

9. References

Alam, M., K. Schwabe and J. K. Krauss (2011). The pedunculopontine nucleus area: critical evaluation of interspecies differences relevant for its use as a target for deep brain stimulation. Brain *134*(Pt 1): 11-23.

Alaynick, W. A., T. M. Jessell and S. L. Pfaff (2011). SnapShot: spinal cord development. Cell *146*(1): 178-178.e171.

Albin, R. L., A. B. Young and J. B. Penney (1989). The functional anatomy of basal ganglia disorders. Trends Neurosci *12*(10): 366-375.

Alstermark, B. and C. F. Ekerot (2013). The lateral reticular nucleus: a precerebellar centre providing the cerebellum with overview and integration of motor functions at systems level. A new hypothesis. J Physiol *591*(22): 5453-5458.

Alstermark, B. and T. Isa (2012). Circuits for skilled reaching and grasping. Annu Rev Neurosci *35*: 559-578.

Alstermark, B., T. Isa, L. G. Pettersson and S. Sasaki (2007). The C3-C4 propriospinal system in the cat and monkey: a spinal pre-motoneuronal centre for voluntary motor control. Acta Physiol (Oxf) *189*(2): 123-140.

Alstermark, B. and H. Kummel (1986). Transneuronal labelling of neurones projecting to forelimb motoneurones in cats performing different movements. Brain Res *376*(2): 387-391.

Alstermark, B., S. Lindstrom, A. Lundberg and E. Sybirska (1981). Integration in descending motor pathways controlling the forelimb in the cat. 8. Ascending projection to the lateral reticular nucleus from C3-C4 propriospinal also projecting to forelimb motoneurones. Exp Brain Res *42*(3-4): 282-298.

Alstermark, B., A. Lundberg, U. Norrsell and E. Sybirska (1981). Integration in descending motor pathways controlling the forelimb in the cat. 9. Differential behavioural defects after spinal cord lesions interrupting defined pathways from higher centres to motoneurones. Exp Brain Res *42*(3-4): 299-318.

Alstermark, B., A. Lundberg, M. Pinter and S. Sasaki (1987). Long C3-C5 propriospinal neurones in the cat. Brain Res *404*(1-2): 382-388.

Alstermark, B., A. Lundberg, M. Pinter and S. Sasaki (1987). Subpopulations and functions of long C3-C5 propriospinal neurones. Brain Res *404*(1-2): 395-400.

Ampatzis, K., J. Song, J. Ausborn and A. El Manira (2013). Pattern of innervation and recruitment of different classes of motoneurons in adult zebrafish. J Neurosci *33*(26): 10875-10886.

Ampatzis, K., J. Song, J. Ausborn and A. El Manira (2014). Separate microcircuit modules of distinct v2a interneurons and motoneurons control the speed of locomotion. Neuron *83*(4): 934-943.

Appler, J. M. and L. V. Goodrich (2011). Connecting the ear to the brain: Molecular mechanisms of auditory circuit assembly. Prog Neurobiol *93*(4): 488-508.

Arber, S. (2012). Motor circuits in action: specification, connectivity, and function. Neuron *74*(6): 975-989.

Arber, S. and R. M. Costa (2018). Connecting neuronal circuits for movement. Science *360*(6396): 1403-1404.

Armbruster, B. N., X. Li, M. H. Pausch, S. Herlitze and B. L. Roth (2007). Evolving the lock to fit the key to create a family of G protein-coupled receptors potently activated by an inert ligand. Proc Natl Acad Sci U S A *104*(12): 5163-5168.

Azim, E., J. Jiang, B. Alstermark and T. M. Jessell (2014). Skilled reaching relies on a V2a propriospinal internal copy circuit. Nature *508*(7496): 357-363.

Baker, S. N. (2011). The primate reticulospinal tract, hand function and functional recovery. J Physiol *589*(Pt 23): 5603-5612.

Baker, S. N., B. Zaaimi, K. M. Fisher, S. A. Edgley and D. S. Soteropoulos (2015). Pathways mediating functional recovery. Prog Brain Res *218*: 389-412.

Barbera, G., B. Liang, L. Zhang, C. R. Gerfen, E. Culurciello, R. Chen, Y. Li and D.-T. Lin (2016). Spatially Compact Neural Clusters in the Dorsal Striatum Encode Locomotion Relevant Information. Neuron *92*(1): 202-213.

Bareyre, F. M., M. Kerschensteiner, O. Raineteau, T. C. Mettenleiter, O. Weinmann and M. E. Schwab (2004). The injured spinal cord spontaneously forms a new intraspinal circuit in adult rats. Nat Neurosci *7*(3): 269-277.

Basaldella, E., A. Takeoka, M. Sigrist and S. Arber (2015). Multisensory Signaling Shapes Vestibulo-Motor Circuit Specificity. Cell *163*(2): 301-312.

Bellardita, C. and O. Kiehn (2015). Phenotypic characterization of speed-associated gait changes in mice reveals modular organization of locomotor networks. Curr Biol *25*(11): 1426-1436.

Bernard, J. F., R. Dallel, P. Raboisson, L. Villanueva and D. Le Bars (1995). Organization of the efferent projections from the spinal cervical enlargement to the parabrachial area and periaqueductal gray: a PHA-L study in the rat. J Comp Neurol *353*(4): 480-505.

Bikoff, J. B., M. I. Gabitto, A. F. Rivard, E. Drobac, T. A. Machado, A. Miri, S. Brenner-Morton, E. Famojure, C. Diaz, F. J. Alvarez, G. Z. Mentis and T. M. Jessell (2016). Spinal Inhibitory Interneuron Diversity Delineates Variant Motor Microcircuits. Cell *165*(1): 207-219.

Bjursten, L. M., K. Norrsell and U. Norrsell (1976). Behavioural repertory of cats without cerebral cortex from infancy. Exp Brain Res *25*(2): 115-130.

Bonanomi, D. and S. L. Pfaff (2010). Motor axon pathfinding. Cold Spring Harb Perspect Biol *2*(3): a001735.

Botev Z.I., Grotowski J.F. and Kroese D.B. (2010). Kernel density estimation via diffusion. Ann. Stat. *38*, 2916–2957

Bouvier, J., V. Caggiano, R. Leiras, V. Caldeira, C. Bellardita, K. Balueva, A. Fuchs and O. Kiehn (2015). Descending Command Neurons in the Brainstem that Halt Locomotion. Cell *163*(5): 1191-1203.

Britz, O., J. Zhang, K. S. Grossmann, J. Dyck, J. C. Kim, S. Dymecki, S. Gosgnach and M. Goulding (2015). A genetically defined asymmetry underlies the inhibitory control of flexor-extensor locomotor movements. Elife *4*.

Brown, T. G. (1911). The intrinsic factor in the act of progression in the mammal. Proc Roy Soc, London *84*: 308-319.

Brownstone, R. M. and J. W. Chopek (2018). Reticulospinal Systems for Tuning Motor Commands. Front Neural Circuits *12*: 30.

Buford, J. A. and A. G. Davidson (2004). Movement-related and preparatory activity in the reticulospinal system of the monkey. Exp Brain Res *159*(3): 284-300.

Bui, T. V., T. Akay, O. Loubani, T. S. Hnasko, T. M. Jessell and R. M. Brownstone (2013). Circuits for grasping: spinal dI3 interneurons mediate cutaneous control of motor behavior. Neuron *78*(1): 191-204.

Caggiano, V., R. Leiras, H. Goñi-Erro, D. Masini, C. Bellardita, J. Bouvier, V. Caldeira, G. Fisone and O. Kiehn (2018). Midbrain circuits that set locomotor speed and gait selection. Nature *553*(7689): 455-460.

Callahan, R. A., R. Roberts, M. Sengupta, Y. Kimura, S. I. Higashijima and M. W. Bagnall (2019). Spinal V2b neurons reveal a role for ipsilateral inhibition in speed control. Elife *8*.

Cameron, D., E. Polgar, M. Gutierrez-Mecinas, M. Gomez-Lima, M. Watanabe and A. J. Todd (2015). The organisation of spinoparabrachial neurons in the mouse. Pain *156*(10): 2061-2071.

Cande, J., S. Namiki, J. Qiu, W. Korff, G. M. Card, J. W. Shaevitz, D. L. Stern and G. J. Berman (2018). Optogenetic dissection of descending behavioral control in Drosophila. Elife *7*.

Capelli, P., C. Pivetta, M. Soledad Esposito and S. Arber (2017). Locomotor speed control circuits in the caudal brainstem. Nature *551*(7680): 373-377.

Cazorla, M., F. D. de Carvalho, M. O. Chohan, M. Shegda, N. Chuhma, S. Rayport, S. E. Ahmari, H. Moore and C. Kellendonk (2014). Dopamine D2 receptors regulate the anatomical and functional balance of basal ganglia circuitry. Neuron *81*(1): 153-164.

Ceccato, J. C., M. de Seze, C. Azevedo and J. R. Cazalets (2009). Comparison of trunk activity during gait initiation and walking in humans. PLoS One *4*(12): e8193.

Chakravarthy, V. S., D. Joseph and R. S. Bapi (2010). What do the basal ganglia do? A modeling perspective. Biol Cybern *103*(3): 237-253.

Chen, H. H., S. Hippenmeyer, S. Arber and E. Frank (2003). Development of the monosynaptic stretch reflex circuit. Curr Opin Neurobiol *13*(1): 96-102.

Choi, J. T. and A. J. Bastian (2007). Adaptation reveals independent control networks for human walking. Nat Neurosci *10*(8): 1055-1062.

Chronister, R. B., J. S. Walding, L. D. Aldes and L. A. Marco (1988). Interconnections between substantia nigra reticulata and medullary reticular formation. Brain Res Bull *21*(2): 313-317.

Cohen, J. Y., S. Haesler, L. Vong, B. B. Lowell and N. Uchida (2012). Neuron-type-specific signals for reward and punishment in the ventral tegmental area. Nature *482*(7383): 85-88.

Costa, R. M., S.-C. Lin, T. D. Sotnikova, M. Cyr, R. R. Gainetdinov, M. G. Caron and M. A. L. Nicolelis (2006). Rapid Alterations in Corticostriatal Ensemble Coordination during Acute Dopamine-Dependent Motor Dysfunction. Neuron *52*(2): 359-369.

Courtine, G., B. Song, R. R. Roy, H. Zhong, J. E. Herrmann, Y. Ao, J. Qi, V. R. Edgerton and M. V. Sofroniew (2008). Recovery of supraspinal control of stepping via indirect propriospinal relay connections after spinal cord injury. Nat Med *14*(1): 69-74.

Cowley, K. C., E. Zaporozhets and B. J. Schmidt (2008). Propriospinal neurons are sufficient for bulbospinal transmission of the locomotor command signal in the neonatal rat spinal cord. J Physiol *586*(6): 1623-1635.

Cowley, K. C., E. Zaporozhets and B. J. Schmidt (2010). Propriospinal transmission of the locomotor command signal in the neonatal rat. Ann N Y Acad Sci *1198*: 42-53.

Crone, S. A., K. A. Quinlan, L. Zagoraiou, S. Droho, C. E. Restrepo, L. Lundfald, T. Endo, J. Setlak, T. M. Jessell, O. Kiehn and K. Sharma (2008). Genetic ablation of V2a ipsilateral interneurons disrupts left-right locomotor coordination in mammalian spinal cord. Neuron *60*(1): 70-83.

Crone, S. A., G. Zhong, R. Harris-Warrick and K. Sharma (2009). In mice lacking V2a interneurons, gait depends on speed of locomotion. J Neurosci *29*(21): 7098-7109.

Cui, G., S. B. Jun, X. Jin, M. D. Pham, S. S. Vogel, D. M. Lovinger and R. M. Costa (2013). Concurrent activation of striatal direct and indirect pathways during action initiation. Nature *494*(7436): 238-242.

Cui, Y., K. Kam, D. Sherman, W. A. Janczewski, Y. Zheng and J. L. Feldman (2016). Defining preBotzinger Complex Rhythm- and Pattern-Generating Neural Microcircuits In Vivo. Neuron *91*(3): 602-614.

da Silva, J. A., F. Tecuapetla, V. Paixao and R. M. Costa (2018). Dopamine neuron activity before action initiation gates and invigorates future movements. Nature *554*(7691): 244-248.

Dasen, J. S. and T. M. Jessell (2009). Hox networks and the origins of motor neuron diversity. Current topics in developmental biology *88*: 169-200.

Dana H., Sun Y., Mohar B., Hulse B.K., Kerlin A.M., Hasseman J.P., Tsegaye G., Tsang A., Wong A., Patel R., Macklin J.J., Chen Y., Konnerth A., Jayaraman V., Looger L.L., Schreiter E.R., Svoboda K. and Kim D.S. (2019). High-performance calcium sensors for imaging activity in neuronal populations and microcompartments Nature Methods *16:* 649–657.

Dauer, W. and S. Przedborski (2003). Parkinson's disease: mechanisms and models. Neuron *39*(6): 889-909.

Dautan, D., A. S. Souza, I. Huerta-Ocampo, M. Valencia, M. Assous, I. B. Witten, K. Deisseroth, J. M. Tepper, J. P. Bolam, T. V. Gerdjikov and J. Mena-Segovia (2016). Segregated cholinergic transmission modulates dopamine neurons integrated in distinct functional circuits. Nat Neurosci *19*(8): 1025-1033.

Del Negro, C. A., G. D. Funk and J. L. Feldman (2018). Breathing matters. Nat Rev Neurosci *19*(6): 351-367.

Dellow, P. G. and J. P. Lund (1971). Evidence for central timing of rhythmical mastication. J Physiol *215*(1): 1-13.

DeLong, M. R. (1990). Primate models of movement disorders of basal ganglia origin. Trends Neurosci *13*(7): 281-285.

Depoortere, R., G. Sandner and G. Di Scala (1990). Aversion induced by electrical stimulation of the mesencephalic locomotor region in the intact and freely moving rat. Physiol Behav *47*(3): 561-567.

Deschenes, M., J. Takatoh, A. Kurnikova, J. D. Moore, M. Demers, M. Elbaz, T. Furuta, F. Wang and D. Kleinfeld (2016). Inhibition, Not Excitation, Drives Rhythmic Whisking. Neuron *90*(2): 374-387.

Dietz, V. (2002). Do human bipeds use quadrupedal coordination? Trends Neurosci *25*(9): 462-467.

Dietz, V. (2010). Behavior of spinal neurons deprived of supraspinal input. Nature Rev Neurol *6*(3): 167-174.

Dodson, P. D., J. K. Dreyer, K. A. Jennings, E. C. J. Syed, R. Wade-Martins, S. J. Cragg, J. P. Bolam and P. J. Magill (2016). Representation of spontaneous movement by dopaminergic neurons is cell-type selective and disrupted in parkinsonism. PNAS *113*(15): E2180-E2188.

Dominici, N., Y. P. Ivanenko, G. Cappellini, A. d'Avella, V. Mondi, M. Cicchese, A. Fabiano, T. Silei, A. Di Paolo, C. Giannini, R. E. Poppele and F. Lacquaniti (2011). Locomotor primitives in newborn babies and their development. Science *334*(6058): 997-999.

Dougherty, K. J., L. Zagoraiou, D. Satoh, I. Rozani, S. Doobar, S. Arber, T. M. Jessell and O. Kiehn (2013). Locomotor rhythm generation linked to the output of spinal shox2 excitatory interneurons. Neuron *80*(4): 920-933.

Drew, T., R. Dubuc and S. Rossignol (1986). Discharge patterns of reticulospinal and other reticular neurons in chronic, unrestrained cats walking on a treadmill. J Neurophysiol *55*(2): 375-401.

Drew, T. and S. Rossignol (1990). Functional organization within the medullary reticular formation of intact unanesthetized cat. I. Movements evoked by microstimulation. J Neurophysiol *64*(3): 767-781.

Dum, R. P. and P. L. Strick (1991). The origin of corticospinal projections from the premotor areas in the frontal lobe. J Neurosci *11*(3): 667-689.

Dutton, R. C., M. I. Carstens, J. F. Antognini and E. Carstens (2006). Long ascending propriospinal projections from lumbosacral to upper cervical spinal cord in the rat. Brain Res *1119*(1): 76-85.

Eidelberg, E., J. L. Story, B. L. Meyer and J. Nystel (1980). Stepping by chronic spinal cats. Exp Brain Res *40*(3): 241-246.

English, A. W. and P. R. Lennard (1982). Interlimb coordination during stepping in the cat: in-phase stepping and gait transitions. Brain Res *245*(2): 353-364.

Esposito, M. S., P. Capelli and S. Arber (2014). Brainstem nucleus MdV mediates skilled forelimb motor tasks. Nature *508*(7496): 351-356.

Evans, D. A., A. V. Stempel, R. Vale, S. Ruehle, Y. Lefler and T. Branco (2018). A synaptic threshold mechanism for computing escape decisions. Nature *558*(7711): 590-594.

Fadok, J. P., M. Markovic, P. Tovote and A. Luthi (2018). New perspectives on central amygdala function. Curr Opin Neurobiol *49*: 141-147.

Feldman, J. L., C. A. Del Negro and P. A. Gray (2013). Understanding the rhythm of breathing: so near, yet so far. Annu Rev Physiol *75*: 423-452.

Fenno, L. E., J. Mattis, C. Ramakrishnan, M. Hyun, S. Y. Lee, M. He, J. Tucciarone, A. Selimbeyoglu, A. Berndt, L. Grosenick, K. A. Zalocusky, H. Bernstein, H. Swanson, C. Perry, I. Diester, F. M. Boyce, C. E. Bass, R. Neve, Z. J. Huang and K. Deisseroth (2014). Targeting cells with single vectors using multiple-feature Boolean logic. Nat Methods *11*(7): 763-772.

Ferreira-Pinto, M. J., L. Ruder, P. Capelli and S. Arber (2018). Connecting Circuits for Supraspinal Control of Locomotion. Neuron *100*(2): 361-374.

Filli, L., A. K. Engmann, B. Zorner, O. Weinmann, T. Moraitis, M. Gullo, H. Kasper, R. Schneider and M. E. Schwab (2014). Bridging the gap: a reticulo-propriospinal detour bypassing an incomplete spinal cord injury. J Neurosci *34*(40): 13399-13410.

Forssberg, H., S. Grillner and J. Halbertsma (1980). The locomotion of the low spinal cat. I. Coordination within a hindlimb. Acta Physiol Scand *108*(3): 269-281.

Forssberg, H., S. Grillner, J. Halbertsma and S. Rossignol (1980). The locomotion of the low spinal cat. II. Interlimb coordination. Acta Physiol Scand *108*(3): 283-295.

Francius, C., A. Harris, V. Rucchin, T. J. Hendricks, F. J. Stam, M. Barber, D. Kurek, F. G. Grosveld, A. Pierani, M. Goulding and F. Clotman (2013). Identification of multiple subsets of ventral interneurons and differential distribution along the rostrocaudal axis of the developing spinal cord. PloS one *8*(8): e70325.

Franklin, K. B. and G. Paxinos (2007). The Mouse Brain in Stereotaxic Coordinates. San Diego, Elsevier.

Freeze, B. S., A. V. Kravitz, N. Hammack, J. D. Berke and A. C. Kreitzer (2013). Control of basal ganglia output by direct and indirect pathway projection neurons. J Neurosci *33*(47): 18531-18539.

Fregosi, M., A. Contestabile, S. Badoud, S. Borgognon, J. Cottet, J. F. Brunet, J. Bloch, M. E. Schwab and E. M. Rouiller (2018). Changes of motor corticobulbar projections following different lesion types affecting the central nervous system in adult macaque monkeys. Eur J Neurosci.

Gabitto, M. I., A. Pakman, J. B. Bikoff, L. F. Abbott, T. M. Jessell and L. Paninski (2016). Bayesian Sparse Regression Analysis Documents the Diversity of Spinal Inhibitory Interneurons. Cell *165*(1): 220-233.

Gahtan, E. and H. Baier (2004). Of lasers, mutants, and see-through brains: functional neuroanatomy in zebrafish. J Neurobiol *59*(1): 147-161.

Galinanes, G. L., C. Bonardi and D. Huber (2018). Directional Reaching for Water as a Cortex-Dependent Behavioral Framework for Mice. Cell Rep *22*(10): 2767-2783.

Garcia-Rill, E., C. R. Houser, R. D. Skinner, W. Smith and D. J. Woodward (1987). Locomotion-inducing sites in the vicinity of the pedunculopontine nucleus. Brain Res Bull *18*(6): 731-738.

Garcia-Rill, E., R. D. Skinner and J. A. Fitzgerald (1985). Chemical activation of the mesencephalic locomotor region. Brain Res *330*(1): 43-54.

Georgopoulos, A. P., J. F. Kalaska, R. Caminiti and J. T. Massey (1982). On the relations between the direction of two-dimensional arm movements and cell discharge in primate motor cortex. J Neurosci *2*(11): 1527-1537.

Ghali, M. G. Z. (2017). The brainstem network controlling blood pressure: an important role for pressor sites in the caudal medulla and cervical spinal cord. J Hypertens *35*(10): 1938-1947.

Giber, K., M. A. Diana, V. Plattner, G. P. Dugue, H. Bokor, C. V. Rousseau, Z. Magloczky, L. Havas, B. Hangya, H. Wildner, H. U. Zeilhofer, S. Dieudonne and L. Acsady (2015). A subcortical inhibitory signal for behavioral arrest in the thalamus. Nat Neurosci *18*(4): 562-568.

Giovannucci, A., A. Badura, B. Deverett, F. Najafi, T. D. Pereira, Z. Gao, I. Ozden, A. D. Kloth, E. Pnevmatikakis, L. Paninski, C. I. De Zeeuw, J. F. Medina and S. S. Wang (2017). Cerebellar granule cells acquire a widespread predictive feedback signal during motor learning. Nat Neurosci *20*(5): 727-734.

Gosgnach, S., G. M. Lanuza, S. J. Butt, H. Saueressig, Y. Zhang, T. Velasquez, D. Riethmacher, E. M. Callaway, O. Kiehn and M. Goulding (2006). V1 spinal neurons regulate the speed of vertebrate locomotor outputs. Nature *440*(7081): 215-219.

Goulding, M. (2009). Circuits controlling vertebrate locomotion: moving in a new direction. Nat Rev Neurosci *10*(7): 507-518.

Gramsbergen, A. (1998). Posture and locomotion in the rat: independent or interdependent development? Neurosci Biobehav Rev *22*(4): 547-553.

Grillner, S. (2003). The motor infrastructure: from ion channels to neuronal networks. Nat Rev Neurosci *4*(7): 573-586.

Grillner, S. (2006). Biological pattern generation: the cellular and computational logic of networks in motion. Neuron *52*(5): 751-766.

Grillner, S., A. P. Georgopoulos and L. M. Jordan (1997). Selection and initiation of motor behavior. Neurons, networks, and motor behavior. P. S. G. Stein, S. Grillner, A. I. Selverston and D. G. Stuart. Cambridge, The MIT Press**:** 3-19.

Grillner, S. and T. M. Jessell (2009). Measured motion: searching for simplicity in spinal locomotor networks. Curr Opin Neurobiol *19*(6): 572-586.

Gronenberg, W. and N. J. Strausfeld (1990). Descending neurons supplying the neck and flight motor of Diptera: physiological and anatomical characteristics. J Comp Neurol *302*(4): 973-991.

Guthrie, S. (2004). Neuronal development: putting motor neurons in their place. Curr Biol *14*(4): R166-168.

Guthrie, S. (2007). Patterning and axon guidance of cranial motor neurons. Nat Rev Neurosci *8*(11): 859-871.

Halbertsma, J. M. (1983). The stride cycle of the cat: the modelling of locomotion by computerized analysis of automatic recordings. Acta physiologica Scandinavica *521*: 1-75.

Hale, M. E., H. R. Katz, M. Y. Peek and R. T. Fremont (2016). Neural circuits that drive startle behavior, with a focus on the Mauthner cells and spiral fiber neurons of fishes. J Neurogenet *30*(2): 89-100.

Han, W., L. A. Tellez, M. J. Rangel, Jr., S. C. Motta, X. Zhang, I. O. Perez, N. S. Canteras, S. J. Shammah-Lagnado, A. N. van den Pol and I. E. de Araujo (2017). Integrated Control of Predatory Hunting by the Central Nucleus of the Amygdala. Cell *168*(1-2): 311-324 e318.

Hayashi, M., C. A. Hinckley, S. P. Driscoll, N. J. Moore, A. J. Levine, K. L. Hilde, K. Sharma and S. L. Pfaff (2018). Graded Arrays of Spinal and Supraspinal V2a Interneuron Subtypes Underlie Forelimb and Hindlimb Motor Control. Neuron *97*(4): 869-884 e865.

Heiney, S. A., J. Kim, G. J. Augustine and J. F. Medina (2014). Precise control of movement kinematics by optogenetic inhibition of Purkinje cell activity. J Neurosci *34*(6): 2321-2330.

Hikosaka, O., Y. Takikawa and R. Kawagoe (2000). Role of the basal ganglia in the control of purposive saccadic eye movements. Physiol Rev *80*(3): 953-978.

Hinsey, J. C., S. W. Ranson and M. D. McNattin (1930). The role of the hypothalamus and mesencephalon in locomotion. Arch Neur Psych *23*(1): 1-43.

Hirata, T., P. Li, G. M. Lanuza, L. A. Cocas, M. M. Huntsman and J. G. Corbin (2009). Identification of distinct telencephalic progenitor pools for neuronal diversity in the amygdala. Nat Neurosci *12*(2): 141-149.

Howe, M. W. and D. A. Dombeck (2016). Rapid signalling in distinct dopaminergic axons during locomotion and reward. Nature *535*(7613): 505-510.

Hsu, C. T. and V. Bhandawat (2016). Organization of descending neurons in Drosophila melanogaster. Sci Rep *6*: 20259.

Huang, C. C., K. Sugino, Y. Shima, C. Guo, S. Bai, B. D. Mensh, S. B. Nelson and A. W. Hantman (2013). Convergence of pontine and proprioceptive streams onto multimodal cerebellar granule cells. Elife *2*: e00400.

Illert, M., A. Lundberg, Y. Padel and R. Tanaka (1978). Integration in descending motor pathways controlling the forelimb in the cat. 5. Properties of and monosynaptic excitatory convergence on C3--C4 propriospinal neurones. Exp Brain Res *33*(1): 101-130.

Isa, T. (2019). Dexterous Hand Movements and Their Recovery After Central Nervous System Injury. Annu Rev Neurosci *42*: 315-335.

Ivanenko, Y. P., R. E. Poppele and F. Lacquaniti (2004). Five basic muscle activation patterns account for muscle activity during human locomotion. J Physiol *556*(Pt 1): 267-282.

Iwaniuk, A. N. and I. Q. Whishaw (2000). On the origin of skilled forelimb movements. Trends Neurosci *23*(8): 372-376.

Jarratt, H. and B. Hyland (1999). Neuronal activity in rat red nucleus during forelimb reach-to-grasp movements. Neuroscience *88*(2): 629-642.

Jessell, T. M. (2000). Neuronal specification in the spinal cord: inductive signals and transcriptional codes. Nature Rev Genetics *1*(1): 20-29.

Jin, X. and R. M. Costa (2010). Start/stop signals emerge in nigrostriatal circuits during sequence learning. Nature *466*(7305): 457-462.

Jin, X. and R. M. Costa (2015). Shaping action sequences in basal ganglia circuits. Curr Opin Neurobiol *33*: 188-196.

Jin, X., F. Tecuapetla and R. M. Costa (2014). Basal ganglia subcircuits distinctively encode the parsing and concatenation of action sequences. Nat Neurosci *17*(3): 423-430.

Jones, B. E. (1995). Reticular formation: cytoarchitecture, transmitters and projections. The rat nervous system. G. Paxinos. San Diego, Academic Press. **2:** 155-171.

Jordan, L. M. (1998). Initiation of locomotion in mammals. Ann N Y Acad Sci *860*: 83-93.

Josset, N., M. Roussel, M. Lemieux, D. Lafrance-Zoubga, A. Rastqar and F. Bretzner (2018). Distinct Contributions of Mesencephalic Locomotor Region Nuclei to Locomotor Control in the Freely Behaving Mouse. Curr Biol *28*(6): 884-901 e883.

Juvin, L., S. Gratsch, E. Trillaud-Doppia, J. F. Gariepy, A. Buschges and R. Dubuc (2016). A Specific Population of Reticulospinal Neurons Controls the Termination of Locomotion. Cell Rep *15*(11): 2377-2386.

Juvin, L., J. P. Le Gal, J. Simmers and D. Morin (2012). Cervicolumbar coordination in mammalian quadrupedal locomotion: role of spinal thoracic circuitry and limb sensory inputs. J Neurosci *32*(3): 953-965.

Juvin, L., J. Simmers and D. Morin (2005). Propriospinal circuitry underlying interlimb coordination in mammalian quadrupedal locomotion. J Neurosci *25*(25): 6025-6035.

Kawai, R., T. Markman, R. Poddar, R. Ko, A. L. Fantana, A. K. Dhawale, A. R. Kampff and B. P. Olveczky (2015). Motor cortex is required for learning but not for executing a motor skill. Neuron *86*(3): 800-812.

Kiehn, O. (2006). Locomotor circuits in the mammalian spinal cord. Annu Rev Neurosci *29*: 279-306.

Kiehn, O. (2011). Development and functional organization of spinal locomotor circuits. Curr Opin Neurobiol *21*(1): 100-109.

Kiehn, O. (2016). Decoding the organization of spinal circuits that control locomotion. Nature reviews. Neuroscience *17*(4): 224-238.

Kiehn, O. and S. J. Butt (2003). Physiological, anatomical and genetic identification of CPG neurons in the developing mammalian spinal cord. Prog Neurobiol *70*(4): 347-361.

Kim, L. H., S. Sharma, S. A. Sharples, K. A. Mayr, C. H. T. Kwok and P. J. Whelan (2017). Integration of Descending Command Systems for the Generation of Context-Specific Locomotor Behaviors. Front Neurosci *11*: 581.

Kimura, Y., C. Satou, S. Fujioka, W. Shoji, K. Umeda, T. Ishizuka, H. Yawo and S. Higashijima (2013). Hindbrain V2a neurons in the excitation of spinal locomotor circuits during zebrafish swimming. Curr Biol *23*(10): 843-849.

Kinjo, N., Y. Atsuta, M. Webber, R. Kyle, R. D. Skinner and E. Garcia-Rill (1990). Medioventral medulla-induced locomotion. Brain Res Bull *24*(3): 509-516.

Kinoshita, M., R. Matsui, S. Kato, T. Hasegawa, H. Kasahara, K. Isa, A. Watakabe, T. Yamamori, Y. Nishimura, B. Alstermark, D. Watanabe, K. Kobayashi and T. Isa (2012). Genetic dissection of the circuit for hand dexterity in primates. Nature *487*(7406): 235-238.

Kitazawa, T. and F. M. Rijli (2018). Barrelette map formation in the prenatal mouse brainstem. Curr Opin Neurobiol *53*: 210-219.

Klaus, A., J. Alves da Silva and R. M. Costa (2019). What, If, and When to Move: Basal Ganglia Circuits and Self-Paced Action Initiation. Annu Rev Neurosci *42*: 459-483.

Klaus, A., G. J. Martins, V. B. Paixao, P. Zhou, L. Paninski and R. M. Costa (2017). The Spatiotemporal Organization of the Striatum Encodes Action Space. Neuron *96*(4): 949.

Kleinfeld, D., M. Deschenes, F. Wang and J. D. Moore (2014). More than a rhythm of life: breathing as a binder of orofacial sensation. Nat Neurosci *17*(5): 647-651.

Koch, S. C., D. Acton and M. Goulding (2018). Spinal Circuits for Touch, Pain, and Itch. Annu Rev Physiol *80*: 189-217.

Koch, S. C., M. G. Del Barrio, A. Dalet, G. Gatto, T. Günther, J. Zhang, B. Seidler, D. Saur, R. Schüle and M. Goulding (2017). RORβ Spinal Interneurons Gate Sensory Transmission during Locomotion to Secure a Fluid Walking Gait. Neuron *96*(6): 1419-1431.e1415.

Kolta, A., F. Brocard, D. Verdier and J. P. Lund (2007). A review of burst generation by trigeminal main sensory neurons. Arch Oral Biol *52*(4): 325-328.

Kravitz, A. V., B. S. Freeze, P. R. Parker, K. Kay, M. T. Thwin, K. Deisseroth and A. C. Kreitzer (2010). Regulation of parkinsonian motor behaviours by optogenetic control of basal ganglia circuitry. Nature *466*(7306): 622-626.

Kreitzer, A. C. and R. C. Malenka (2008). Striatal plasticity and basal ganglia circuit function. Neuron *60*(4): 543-554.

Kremer, E. J., S. Boutin, M. Chillon and O. Danos (2000). Canine adenovirus vectors: an alternative for adenovirus-mediated gene transfer. J Virol *74*(1): 505-512.

Krouchev, N., J. F. Kalaska and T. Drew (2006). Sequential activation of muscle synergies during locomotion in the intact cat as revealed by cluster analysis and direct decomposition. J Neurophysiol *96*(4): 1991-2010.

Kurnikova, A., J. D. Moore, S. M. Liao, M. Deschenes and D. Kleinfeld (2017). Coordination of Orofacial Motor Actions into Exploratory Behavior by Rat. Curr Biol *27*(5): 688-696.

Kuypers, H. G. (1964). The Descending Pathways to the Spinal Cord, Their Anatomy and Function. Prog Brain Res *11*: 178-202.

Kuypers, H. G. (1981). Anatomy of the descending pathways. Comprehensive Physiology *2*(2): 597-666.

Kuypers, H. G. and D. G. Lawrence (1967). Cortical projections to the red nucleus and the brain stem in the Rhesus monkey. Brain Res *4*(2): 151-188.

Lai, H. C., R. P. Seal and J. E. Johnson (2016). Making sense out of spinal cord somatosensory development. Development *143*(19): 3434-3448.

Lanuza, G. M., S. Gosgnach, A. Pierani, T. M. Jessell and M. Goulding (2004). Genetic identification of spinal interneurons that coordinate left-right locomotor activity necessary for walking movements. Neuron *42*(3): 375-386.

Lawrence, D. G. and H. G. Kuypers (1968). The functional organization of the motor system in the monkey. I. The effects of bilateral pyramidal lesions. Brain *91*(1): 1-14.

Lawrence, D. G. and H. G. Kuypers (1968). The functional organization of the motor system in the monkey. II. The effects of lesions of the descending brain-stem pathways. Brain *91*(1): 15-36.

Le Ray, D., L. Juvin, D. Ryczko and R. Dubuc (2011). Chapter 4--supraspinal control of locomotion: the mesencephalic locomotor region. Prog Brain Res *188*: 51-70.

Lee, A. M., J. L. Hoy, A. Bonci, L. Wilbrecht, M. P. Stryker and C. M. Niell (2014). Identification of a brainstem circuit regulating visual cortical state in parallel with locomotion. Neuron *83*(2): 455-466.

Lee, K. H., P. J. Mathews, A. M. Reeves, K. Y. Choe, S. A. Jami, R. E. Serrano and T. S. Otis (2015). Circuit mechanisms underlying motor memory formation in the cerebellum. Neuron *86*(2): 529-540.

Lemieux, M., N. Josset, M. Roussel, S. Couraud and F. Bretzner (2016). Speed-Dependent Modulation of the Locomotor Behavior in Adult Mice Reveals Attractor and Transitional Gaits. Front Neurosci *10*: 42.

Lemon, R. N. (2008). Descending pathways in motor control. Annu Rev Neurosci *31*: 195-218.

Lemon, R. N., P. A. Kirkwood, M. A. Maier, K. Nakajima and P. Nathan (2004). Direct and indirect pathways for corticospinal control of upper limb motoneurons in the primate. Prog Brain Res *143*: 263-279.

Lemon, R. N., W. Landau, D. Tutssel and D. G. Lawrence (2012). Lawrence and Kuypers (1968a, b) revisited: copies of the original filmed material from their classic papers in Brain. Brain *135*(Pt 7): 2290-2295.

Levine, A. J., K. A. Lewallen and S. L. Pfaff (2012). Spatial organization of cortical and spinal neurons controlling motor behavior. Curr Opin Neurobiol *22*(5): 812-821.

Li, N., T. W. Chen, Z. V. Guo, C. R. Gerfen and K. Svoboda (2015). A motor cortex circuit for motor planning and movement. Nature *519*(7541): 51-56.

Li, N., K. Daie, K. Svoboda and S. Druckmann (2016). Robust neuronal dynamics in premotor cortex during motor planning. Nature *532*(7600): 459-464.

Li, P., W. A. Janczewski, K. Yackle, K. Kam, S. Pagliardini, M. A. Krasnow and J. L. Feldman (2016). The peptidergic control circuit for sighing. Nature *530*(7590): 293-297.

Li, Y., J. Zeng, J. Zhang, C. Yue, W. Zhong, Z. Liu, Q. Feng and M. Luo (2018). Hypothalamic Circuits for Predation and Evasion. Neuron *97*(4): 911-924 e915.

Liang, H., G. Paxinos and C. Watson (2012). Spinal projections from the presumptive midbrain locomotor region in the mouse. Brain Struct Funct *217*(2): 211-219.

Low, A. Y. T., A. R. Thanawalla, A. K. K. Yip, J. Kim, K. L. L. Wong, M. Tantra, G. J. Augustine and A. I. Chen (2018). Precision of Discrete and Rhythmic Forelimb Movements Requires a Distinct Neuronal Subpopulation in the Interposed Anterior Nucleus. Cell Rep *22*(9): 2322-2333.

Madisen, L., T. A. Zwingman, S. M. Sunkin, S. W. Oh, H. A. Zariwala, H. Gu, L. L. Ng, R. D. Palmiter, M. J. Hawrylycz, A. R. Jones, E. S. Lein and H. Zeng (2010). A robust and high-throughput Cre reporting and characterization system for the whole mouse brain. Nat Neurosci *13*(1): 133-140.

Mallet, N., B. R. Micklem, P. Henny, M. T. Brown, C. Williams, J. P. Bolam, K. C. Nakamura and P. J. Magill (2012). Dichotomous organization of the external globus pallidus. Neuron *74*(6): 1075-1086.

Marder, E. and D. Bucher (2001). Central pattern generators and the control of rhythmic movements. Curr Biol *11*(23): R986-996.

Martinez-Gonzalez, C., J. P. Bolam and J. Mena-Segovia (2011). Topographical organization of the pedunculopontine nucleus. Front Neuroanat *5*: 22.

Mathis, A., P. Mamidanna, K. M. Cury, T. Abe, V. N. Murthy, M. W. Mathis and M. Bethge (2018). DeepLabCut: markerless pose estimation of user-defined body parts with deep learning. Nat Neurosci *21*(9): 1281-1289.

Matsushita, M., M. Ikeda and Y. Hosoya (1979). The location of spinal neurons with long descending axons (long descending propriospinal tract neurons) in the cat: a study with the horseradish peroxidase technique. J Comp Neurol *184*(1): 63-80.

Matsuyama, K., K. Takakusaki, K. Nakajima and S. Mori (1997). Multi-segmental innervation of single pontine reticulospinal axons in the cervico-thoracic region of the cat: anterograde PHA-L tracing study. J Comp Neurol *377*(2): 234-250.

McElvain, L. E., B. Friedman, H. J. Karten, K. Svoboda, F. Wang, M. Deschenes and D. Kleinfeld (2018). Circuits in the rodent brainstem that control whisking in concert with other orofacial motor actions. Neuroscience *368*: 152-170.

McFarland, D. H. and J. P. Lund (1993). An investigation of the coupling between respiration, mastication, and swallowing in the awake rabbit. J Neurophysiol *69*(1): 95-108.

Medina, J. F. (2011). The multiple roles of Purkinje cells in sensori-motor calibration: to predict, teach and command. Curr Opin Neurobiol *21*(4): 616-622.

Melzer, S., M. Michael, A. Caputi, M. Eliava, E. C. Fuchs, M. A. Whittington and H. Monyer (2012). Long-range-projecting GABAergic neurons modulate inhibition in hippocampus and entorhinal cortex. Science *335*(6075): 1506-1510.

Mena-Segovia, J. and J. P. Bolam (2017). Rethinking the Pedunculopontine Nucleus: From Cellular Organization to Function. Neuron *94*(1): 7-18.

Menetrey, D., J. de Pommery and F. Roudier (1985). Propriospinal fibers reaching the lumbar enlargement in the rat. Neurosci Lett *58*(2): 257-261.

Mercer Lindsay, N., P. M. Knutsen, A. F. Lozada, D. Gibbs, H. J. Karten and D. Kleinfeld (2019). Orofacial Movements Involve Parallel Corticobulbar Projections from Motor Cortex to Trigeminal Premotor Nuclei. Neuron.

Miller, S., J. Van Der Burg and F. Van Der Meche (1975). Coordination of movements of the kindlimbs and forelimbs in different forms of locomotion in normal and decerebrate cats. Brain Res *91*(2): 217-237.

Miller, S., J. Van Der Burg and F. Van Der Meche (1975). Locomotion in the cat: basic programmes of movement. Brain Res *91*(2): 239-253.

Miller, S. and F. G. A. van der Meché (1976). Coordinated stepping of all four limbs in the high spinal cat. Brain research *109*(2): 395-398.

Miri, A., C. L. Warriner, J. S. Seely, G. F. Elsayed, J. P. Cunningham, M. M. Churchland and T. M. Jessell (2017). Behaviorally Selective Engagement of Short-Latency Effector Pathways by Motor Cortex. Neuron *95*(3): 683-696.e611.

Mitchell, E. J., S. McCallum, D. Dewar and D. J. Maxwell (2016). Corticospinal and Reticulospinal Contacts on Cervical Commissural and Long Descending Propriospinal Neurons in the Adult Rat Spinal Cord; Evidence for Powerful Reticulospinal Connections. PLoS One *11*(3): e0152094.

Moehle, M. S., T. Pancani, N. Byun, S. E. Yohn, G. H. Wilson, 3rd, J. W. Dickerson, D. H. Remke, Z. Xiang, C. M. Niswender, J. Wess, C. K. Jones, C. W. Lindsley, J. M. Rook and P. J. Conn (2017). Cholinergic Projections to the Substantia Nigra Pars Reticulata Inhibit Dopamine Modulation of Basal Ganglia through the M4 Muscarinic Receptor. Neuron *96*(6): 1358-1372 e1354.

Moore, J. D., M. Deschenes, T. Furuta, D. Huber, M. C. Smear, M. Demers and D. Kleinfeld (2013). Hierarchy of orofacial rhythms revealed through whisking and breathing. Nature *497*(7448): 205-210.

Moore, J. D., D. Kleinfeld and F. Wang (2014). How the brainstem controls orofacial behaviors comprised of rhythmic actions. Trends Neurosci *37*(7): 370-380.

Mori, S. (1987). Integration of posture and locomotion in acute decerebrate cats and in awake, freely moving cats. Prog Neurobiol *28*(2): 161-195.

Mori, S. (1989). Contribution of postural muscle tone to full expression of posture and locomotor movements: multi-faceted analyses of its setting brainstem-spinal cord mechanisms in the cat. Jpn J Physiol *39*(6): 785-809.

Mori, S., T. Sakamoto, Y. Ohta, K. Takakusaki and K. Matsuyama (1989). Site-specific postural and locomotor changes evoked in awake, freely moving intact cats by stimulating the brainstem. Brain Res *505*(1): 66-74.

Morquette, P. and A. Kolta (2014). How do we walk and chew gum at the same time? Elife *3*: e03235.

Morris, R., A. P. Tosolini, J. D. Goldstein and I. Q. Whishaw (2011). Impaired arpeggio movement in skilled reaching by rubrospinal tract lesions in the rat: a behavioral/anatomical fractionation. J Neurotrauma *28*(12): 2439-2451.

Mosberger, A. C., J. C. Miehlbradt, N. Bjelopoljak, M. P. Schneider, A. S. Wahl, B. V. Ineichen, M. Gullo and M. E. Schwab (2018). Axotomized Corticospinal Neurons Increase Supra-Lesional Innervation and Remain Crucial for Skilled Reaching after Bilateral Pyramidotomy. Cereb Cortex *28*(2): 625-643.

Naganuma, K., M. Inoue, K. Yamamura, K. Hanada and Y. Yamada (2001). Tongue and jaw muscle activities during chewing and swallowing in freely behaving rabbits. Brain Res *915*(2): 185-194.

Namiki, S., M. H. Dickinson, A. M. Wong, W. Korff and G. M. Card (2018). The functional organization of descending sensory-motor pathways in Drosophila. Elife *7*.

Nath, T., A. Mathis, A. C. Chen, A. Patel, M. Bethge and M. W. Mathis (2019). Using DeepLabCut for 3D markerless pose estimation across species and behaviors. Nat Protoc *14*(7): 2152-2176.

Nathan, P. W., M. Smith and P. Deacon (1996). Vestibulospinal, reticulospinal and descending propriospinal nerve fibres in man. Brain *119 (Pt 6)*: 1809-1833.

Newman, D. B. (1985). Distinguishing rat brainstem reticulospinal nuclei by their neuronal morphology. I. Medullary nuclei. J Hirnforsch *26*(2): 187-226.

Newman, D. B. (1985). Distinguishing rat brainstem reticulospinal nuclei by their neuronal morphology. II. Pontine and mesencephalic nuclei. J Hirnforsch *26*(4): 385-418.

Ni, Y., H. Nawabi, X. Liu, L. Yang, K. Miyamichi, A. Tedeschi, B. Xu, N. R. Wall, E. M. Callaway and Z. He (2014). Characterization of long descending premotor propriospinal neurons in the spinal cord. J Neurosci *34*(28): 9404-9417.

Niell, C. M. and M. P. Stryker (2010). Modulation of visual responses by behavioral state in mouse visual cortex. Neuron *65*(4): 472-479.

Noda, T. and H. Oka (1984). Nigral inputs to the pedunculopontine region: intracellular analysis. Brain Res *322*(2): 332-336.

Orlovsky, G. N., T. G. Deliagina and S. Grillner (1999). Neuronal control of locomotion: From mollusc to man. Oxford, Oxford University Press.

Osakada, F. and E. M. Callaway (2013). Design and generation of recombinant rabies virus vectors. Nat Protoc *8*(8): 1583-1601.

Otchy, T. M., S. B. Wolff, J. Y. Rhee, C. Pehlevan, R. Kawai, A. Kempf, S. M. Gobes and B. P. Olveczky (2015). Acute off-target effects of neural circuit manipulations. Nature *528*(7582): 358-363.

Palmiter, R. D. (2018). The Parabrachial Nucleus: CGRP Neurons Function as a General Alarm. Trends Neurosci *41*(5): 280-293.

Parker, J. G., J. D. Marshall, B. Ahanonu, Y. W. Wu, T. H. Kim, B. F. Grewe, Y. Zhang, J. Z. Li, J. B. Ding, M. D. Ehlers and M. J. Schnitzer (2018). Diametric neural ensemble dynamics in parkinsonian and dyskinetic states. Nature *557*(7704): 177-182.

Peters, A. J., J. Lee, N. G. Hedrick, K. O'Neil and T. Komiyama (2017). Reorganization of corticospinal output during motor learning. Nat Neurosci *20*(8): 1133-1141.

Peters, A. J., H. Liu and T. Komiyama (2017). Learning in the Rodent Motor Cortex. Annu Rev Neurosci *40*: 77-97.

Petersen, C. C. H. (2019). Sensorimotor processing in the rodent barrel cortex. Nat Rev Neurosci *20*(9): 533-546.

Philippidou, P. and J. S. Dasen (2013). Hox genes: choreographers in neural development, architects of circuit organization. Neuron *80*(1): 12-34.

Pivetta, C., M. S. Esposito, M. Sigrist and S. Arber (2014). Motor-circuit communication matrix from spinal cord to brainstem neurons revealed by developmental origin. Cell *156*(3): 537-548.

Roh, J., V. C. Cheung and E. Bizzi (2011). Modules in the brain stem and spinal cord underlying motor behaviors. J Neurophysiol *106*(3): 1363-1378.

Romanes, G. J. (1951). The motor cell columns of the lumbo-sacral spinal cord of the cat. J Comp Neurol *94*(2): 313-363.

Roseberry, T. K., A. M. Lee, A. L. Lalive, L. Wilbrecht, A. Bonci and A. C. Kreitzer (2016). Cell-Type-Specific Control of Brainstem Locomotor Circuits by Basal Ganglia. Cell *164*(3): 526-537.

Ross, G. S. and H. M. Sinnamon (1984). Forelimb and hindlimb stepping by the anesthetized rat elicited by electrical stimulation of the pons and medulla. Physiol Behav *33*(2): 201-208.

Rossi, M. A., H. E. Li, D. Lu, I. H. Kim, R. A. Bartholomew, E. Gaidis, J. W. Barter, N. Kim, M. T. Cai, S. H. Soderling and H. H. Yin (2016). A GABAergic nigrotectal pathway for coordination of drinking behavior. Nat Neurosci *19*(5): 742-748.

Rossignol, S. (2006). Dynamic Sensorimotor Interactions in Locomotion. Physiological reviews *86*(1): 89-154.

Roth, B. L. (2016). DREADDs for Neuroscientists. Neuron *89*(4): 683-694.

Ruder, L. and S. Arber (2019). Brainstem Circuits Controlling Action Diversification. Annu Rev Neurosci *42*: 485-504.

Ruder, L., A. Takeoka and S. Arber (2016). Long-Distance Descending Spinal Neurons Ensure Quadrupedal Locomotor Stability. Neuron *92*(5): 1063-1078.

Ryczko, D. and R. Dubuc (2013). The multifunctional mesencephalic locomotor region. Curr Pharm Des *19*(24): 4448-4470.

Sacrey, L. A., M. Alaverdashvili and I. Q. Whishaw (2009). Similar hand shaping in reaching-for-food (skilled reaching) in rats and humans provides evidence of homology in release, collection, and manipulation movements. Behav Brain Res *204*(1): 153-161.

Sapir, T., E. J. Geiman, Z. Wang, T. Velasquez, S. Mitsui, Y. Yoshihara, E. Frank, F. J. Alvarez and M. Goulding (2004). Pax6 and engrailed 1 regulate two distinct aspects of renshaw cell development. J Neurosci *24*(5): 1255-1264.

Satoh, D., C. Pudenz and S. Arber (2016). Context-Dependent Gait Choice Elicited by EphA4 Mutation in Lbx1 Spinal Interneurons. Neuron *89*(5): 1046-1058.

Schepens, B. and T. Drew (2004). Independent and convergent signals from the pontomedullary reticular formation contribute to the control of posture and movement during reaching in the cat. J Neurophysiol *92*(4): 2217-2238.

Shang, C., Z. Chen, A. Liu, Y. Li, J. Zhang, B. Qu, F. Yan, Y. Zhang, W. Liu, Z. Liu, X. Guo, D. Li, Y. Wang and P. Cao (2018). Divergent midbrain circuits orchestrate escape and freezing responses to looming stimuli in mice. Nat Commun *9*(1): 1232.

Shefchyk, S. J., R. M. Jell and L. M. Jordan (1984). Reversible cooling of the brainstem reveals areas required for mesencephalic locomotor region evoked treadmill locomotion. Exp Brain Res *56*(2): 257-262.

Shepherd, G. M. (2013). Corticostriatal connectivity and its role in disease. Nat Rev Neurosci *14*(4): 278-291.

Shik, M. L. and G. N. Orlovsky (1976). Neurophysiology of locomotor automatism. Physiological reviews *56*(3): 465-501.

Shik, M. L., F. V. Severin and G. N. Orlovskii (1966). [Control of walking and running by means of electric stimulation of the midbrain]. Biofizika *11*(4): 659-666.

Sinnamon, H. M. (1993). Preoptic and hypothalamic neurons and the initiation of locomotion in the anesthetized rat. Prog Neurobiol *41*(3): 323-344.

Skinner, R. D., R. J. Adams and R. S. Remmel (1980). Responses of long descending propriospinal neurons to natural and electrical types of stimuli in cat. Brain Res *196*(2): 387-403.

Skinner, R. D., J. D. Coulter, R. J. Adams and R. S. Remmel (1979). Cells of origin of long descending propriospinal fibers connecting the spinal enlargements in cat and monkey determined by horseradish peroxidase and electrophysiological techniques. J Comp Neurol *188*(3): 443-454.

Skinner, R. D. and E. Garcia-Rill (1984). The mesencephalic locomotor region (MLR) in the rat. Brain Res *323*(2): 385-389.

Smith, J. C., H. H. Ellenberger, K. Ballanyi, D. W. Richter and J. L. Feldman (1991). Pre-Botzinger complex: a brainstem region that may generate respiratory rhythm in mammals. Science *254*(5032): 726-729.

Soteropoulos, D. S., E. R. Williams and S. N. Baker (2012). Cells in the monkey ponto-medullary reticular formation modulate their activity with slow finger movements. J Physiol *590*(16): 4011-4027.

Sreenivasan, V., K. Karmakar, F. M. Rijli and C. C. Petersen (2015). Parallel pathways from motor and somatosensory cortex for controlling whisker movements in mice. Eur J Neurosci *41*(3): 354-367.

Srinivas, S., T. Watanabe, C. S. Lin, C. M. William, Y. Tanabe, T. M. Jessell and F. Costantini (2001). Cre reporter strains produced by targeted insertion of EYFP and ECFP into the ROSA26 locus. BMC Dev Biol *1*: 4.

Stanek, E. t., S. Cheng, J. Takatoh, B. X. Han and F. Wang (2014). Monosynaptic premotor circuit tracing reveals neural substrates for oro-motor coordination. Elife *3*: e02511.

Stepien, A. E., M. Tripodi and S. Arber (2010). Monosynaptic rabies virus reveals premotor network organization and synaptic specificity of cholinergic partition cells. Neuron *68*(3): 456-472.

Stuber, G. D. and R. A. Wise (2016). Lateral hypothalamic circuits for feeding and reward. Nat Neurosci *19*(2): 198-205.

Svoboda, K. and N. Li (2018). Neural mechanisms of movement planning: motor cortex and beyond. Curr Opin Neurobiol *49*: 33-41.

Sweeney, L. B., J. B. Bikoff, M. I. Gabitto, S. Brenner-Morton, M. Baek, J. H. Yang, E. G. Tabak, J. S. Dasen, C. R. Kintner and T. M. Jessell (2018). Origin and Segmental Diversity of Spinal Inhibitory Interneurons. Neuron *97*(2): 341-355.e343.

Takakusaki, K., R. Chiba, T. Nozu and T. Okumura (2016). Brainstem control of locomotion and muscle tone with special reference to the role of the mesopontine tegmentum and medullary reticulospinal systems. J Neural Transm (Vienna) *123*(7): 695-729.

Takatoh, J., A. Nelson, X. Zhou, M. M. Bolton, M. D. Ehlers, B. R. Arenkiel, R. Mooney and F. Wang (2013). New modules are added to vibrissal premotor circuitry with the emergence of exploratory whisking. Neuron *77*(2): 346-360.

Takeoka, A., I. Vollenweider, G. Courtine and S. Arber (2014). Muscle spindle feedback directs locomotor recovery and circuit reorganization after spinal cord injury. Cell *159*(7): 1626-1639.

Talpalar, A. E., J. Bouvier, L. Borgius, G. Fortin, A. Pierani and O. Kiehn (2013). Dual-mode operation of neuronal networks involved in left-right alternation. Nature *500*(7460): 85-88.

Tanji, J. and E. V. Evarts (1976). Anticipatory activity of motor cortex neurons in relation to direction of an intended movement. J Neurophysiol *39*(5): 1062-1068.

Taverna, S., E. Ilijic and D. J. Surmeier (2008). Recurrent collateral connections of striatal medium spiny neurons are disrupted in models of Parkinson's disease. J Neurosci *28*(21): 5504-5512.

Tecuapetla, F., X. Jin, S. Q. Lima and R. M. Costa (2016). Complementary Contributions of Striatal Projection Pathways to Action Initiation and Execution. Cell *166*(3): 703-715.

Tecuapetla, F., S. Matias, G. P. Dugue, Z. F. Mainen and R. M. Costa (2014). Balanced activity in basal ganglia projection pathways is critical for contraversive movements. Nat Commun *5*: 4315.

Tennant, K. A., A. L. Asay, R. P. Allred, A. R. Ozburn, J. A. Kleim and T. A. Jones (2010). The vermicelli and capellini handling tests: simple quantitative measures of dexterous forepaw function in rats and mice. J Vis Exp(41).

Tervo, D. G., B. Y. Hwang, S. Viswanathan, T. Gaj, M. Lavzin, K. D. Ritola, S. Lindo, S. Michael, E. Kuleshova, D. Ojala, C. C. Huang, C. R. Gerfen, J. Schiller, J. T. Dudman, A. W. Hantman, L. L. Looger, D. V. Schaffer and A. Y. Karpova (2016). A Designer AAV Variant Permits Efficient Retrograde Access to Projection Neurons. Neuron *92*(2): 372-382.

Tovote, P., M. S. Esposito, P. Botta, F. Chaudun, J. P. Fadok, M. Markovic, S. B. Wolff, C. Ramakrishnan, L. Fenno, K. Deisseroth, C. Herry, S. Arber and A. Luthi (2016). Midbrain circuits for defensive behaviour. Nature *534*(7606): 206-212.

Tovote, P., J. P. Fadok and A. Luthi (2015). Neuronal circuits for fear and anxiety. Nat Rev Neurosci *16*(6): 317-331.

Travers, J. B., L. A. DiNardo and H. Karimnamazi (2000). Medullary reticular formation activity during ingestion and rejection in the awake rat. Exp Brain Res *130*(1): 78-92.

Tripodi, M., A. E. Stepien and S. Arber (2011). Motor antagonism exposed by spatial segregation and timing of neurogenesis. Nature *479*(7371): 61-66.

Ueno, M., Y. Nakamura, J. Li, Z. Gu, J. Niehaus, M. Maezawa, S. A. Crone, M. Goulding, M. L. Baccei and Y. Yoshida (2018). Corticospinal Circuits from the Sensory and Motor Cortices Differentially Regulate Skilled Movements through Distinct Spinal Interneurons. Cell Rep *23*(5): 1286-1300 e1287.

Ulrich-Lai, Y. M. and J. P. Herman (2009). Neural regulation of endocrine and autonomic stress responses. Nat Rev Neurosci *10*(6): 397-409.

Valverde, F. (1961). Reticular formation of the pons and medulla oblongata. A Golgi study. J Comp Neurol *116*: 71-99.

Vong, L., C. Ye, Z. Yang, B. Choi, S. Chua, Jr. and B. B. Lowell (2011). Leptin action on GABAergic neurons prevents obesity and reduces inhibitory tone to POMC neurons. Neuron *71*(1): 142-154.

Vrieseling, E. and S. Arber (2006). Target-induced transcriptional control of dendritic patterning and connectivity in motor neurons by the ETS gene Pea3. Cell *127*(7): 1439-1452.

Wagner, M. J., T. H. Kim, J. Savall, M. J. Schnitzer and L. Luo (2017). Cerebellar granule cells encode the expectation of reward. Nature *544*(7648): 96-100.

Wang, F., J. Zhu, H. Zhu, Q. Zhang, Z. Lin and H. Hu (2011). Bidirectional control of social hierarchy by synaptic efficacy in medial prefrontal cortex. Science *334*(6056): 693-697.

Wang, L., I. Z. Chen and D. Lin (2015). Collateral pathways from the ventromedial hypothalamus mediate defensive behaviors. Neuron *85*(6): 1344-1358.

Wang, X., Y. Liu, X. Li, Z. Zhang, H. Yang, Y. Zhang, P. R. Williams, N. S. A. Alwahab, K. Kapur, B. Yu, Y. Zhang, M. Chen, H. Ding, C. R. Gerfen, K. H. Wang and Z. He (2017). Deconstruction of Corticospinal Circuits for Goal-Directed Motor Skills. Cell *171*(2): 440-455 e414.

Wannier, T., C. Bastiaanse, G. Colombo and V. Dietz (2001). Arm to leg coordination in humans during walking, creeping and swimming activities. Exp Brain Res *141*(3): 375-379.

Weber, F., S. Chung, K. T. Beier, M. Xu, L. Luo and Y. Dan (2015). Control of REM sleep by ventral medulla GABAergic neurons. Nature *526*(7573): 435-438.

Weber, F. and Y. Dan (2016). Circuit-based interrogation of sleep control. Nature *538*(7623): 51-59.

Welzl, H. and J. Bures (1977). Lick-synchronized breathing in rats. Physiol Behav *18*(4): 751-753.

Whelan, P. J. (1996). Control of locomotion in the decerebrate cat. Prog Neurobiol *49*(5): 481-515.

Whishaw, I. Q., B. Gorny and J. Sarna (1998). Paw and limb use in skilled and spontaneous reaching after pyramidal tract, red nucleus and combined lesions in the rat: behavioral and anatomical dissociations. Behav Brain Res *93*(1-2): 167-183.

Whishaw, I. Q. and S. M. Pellis (1990). The structure of skilled forelimb reaching in the rat: a proximally driven movement with a single distal rotatory component. Behav Brain Res *41*(1): 49-59.

Whishaw, I. Q., S. M. Pellis and B. P. Gorny (1992). Skilled reaching in rats and humans: evidence for parallel development or homology. Behav Brain Res *47*(1): 59-70.

Wickersham, I. R., S. Finke, K. K. Conzelmann and E. M. Callaway (2007). Retrograde neuronal tracing with a deletion-mutant rabies virus. Nat Methods *4*(1): 47-49.

Wickersham, I. R., D. C. Lyon, R. J. Barnard, T. Mori, S. Finke, K. K. Conzelmann, J. A. Young and E. M. Callaway (2007). Monosynaptic restriction of transsynaptic tracing from single, genetically targeted neurons. Neuron *53*(5): 639-647.

Windhorst, U. (2007). Muscle proprioceptive feedback and spinal networks. Brain research bulletin *73*(4-6): 155-202.

Wu, J., P. Capelli, J. Bouvier, M. Goulding, S. Arber and G. Fortin (2017). A V0 core neuronal circuit for inspiration. Nat Commun *8*(1): 544.

Xiao, C., J. R. Cho, C. Zhou, J. B. Treweek, K. Chan, S. L. McKinney, B. Yang and V. Gradinaru (2016). Cholinergic Mesopontine Signals Govern Locomotion and Reward through Dissociable Midbrain Pathways. Neuron *90*(2): 333-347.

Xu, T., X. Yu, A. J. Perlik, W. F. Tobin, J. A. Zweig, K. Tennant, T. Jones and Y. Zuo (2009). Rapid formation and selective stabilization of synapses for enduring motor memories. Nature *462*(7275): 915-919.

Yamada, J. and T. Kitamura (1992). Spinal cord cells innervating the bilateral parabrachial nuclei in the rat. A retrograde fluorescent double-labeling study. Neurosci Res *15*(4): 273-280.

Yoo, J. H., V. Zell, J. Wu, C. Punta, N. Ramajayam, X. Shen, L. Faget, V. Lilascharoen, B. K. Lim and T. S. Hnasko (2017). Activation of Pedunculopontine Glutamate Neurons Is Reinforcing. J Neurosci *37*(1): 38-46.

Yttri, E. A. and J. T. Dudman (2016). Opponent and bidirectional control of movement velocity in the basal ganglia. Nature *533*(7603): 402-406.

Zaporozhets, E., K. C. Cowley and B. J. Schmidt (2006). Propriospinal neurons contribute to bulbospinal transmission of the locomotor command signal in the neonatal rat spinal cord. J Physiol *572*(Pt 2): 443-458.

Zeilhofer, H. U., B. Studler, D. Arabadzisz, C. Schweizer, S. Ahmadi, B. Layh, M. R. Bosl and J. M. Fritschy (2005). Glycinergic neurons expressing enhanced green fluorescent protein in bacterial artificial chromosome transgenic mice. J Comp Neurol *482*(2): 123-141.

Zhang, J., G. M. Lanuza, O. Britz, Z. Wang, V. C. Siembab, Y. Zhang, T. Velasquez, F. J. Alvarez, E. Frank and M. Goulding (2014). V1 and v2b interneurons secure the alternating flexor-extensor motor activity mice require for limbed locomotion. Neuron *82*(1): 138-150.

Zhang, Y., S. Narayan, E. Geiman, G. M. Lanuza, T. Velasquez, B. Shanks, T. Akay, J. Dyck, K. Pearson, S. Gosgnach, C. M. Fan and M. Goulding (2008). V3 spinal neurons establish a robust and balanced locomotor rhythm during walking. Neuron *60*(1): 84-96.

Curriculum Vitae – Ludwig Ruder

Address: Oberwilerstrasse 9, 4054 Basel

Contact: ludwig.ruder@unibas.ch, ludwig.ruder@gmail.com

- Born 19th March 1991, Basel, Switzerland (Nationality Swiss and German)

- 1997 – 2009: School education and Matura Certificate at Gymnasium Leonhard, Basel

- 2009 – 2012: University of Basel, Bachelor Studies in Molecular Biology

- 2010 – 2012: University of Basel, Practical Work Experience Student at the Zoological Institute in the laboratory of Prof. Dr. Dieter Ebert

- August 2012 – December 2013: Biozentrum, University of Basel and Friedrich Miescher Institute for Biomedical Research, Basel: Master Studies in Molecular Biology, Major in Neuroscience, Master Thesis in the laboratory of Prof. Dr. Silvia Arber under supervision of Dr. Aya Takeoka: "Characterization of propriospinal circuits and their reorganization after spinal cord injury"

- January 2014 – December 2019: Biozentrum, University of Basel and Friedrich Miescher Institute for Biomedical Research, Basel, Switzerland, Graduate studies in the laboratory of Prof. Dr. Silvia Arber. "Neuronal circuits in the brainstem and spinal cord involved in forelimb behaviors and locomotion"

Fellowships & Prices

- July 2011 – December 2013: Konrad-Adenauer-Foundation Fellowship (KAS)

- January 2017: J.C.W. Shepherd PhD Student Prize

- January 2014 – March 2017: Fellowship for Excellence (Werner-Siemens-Foundation), Biozentrum, University of Basel

International Meetings & Practical experience

- Fall 2015: Karolinska Institutet, Stockholm, practical mouse motor behavior experience in the laboratory of Prof. Dr. Ole Kiehn

- Spring 2016: University of Trondheim, practical electrophysiology experience in the laboratory of Prof. Dr. Edvard Moser

- Spring 2016: HHMI Janelia Conference on "Motor Control Circuits: Structure, Function and Behavior", Poster presentation, Janelia Research Campus, USA

- Fall 2017: Gatsby Conference on "The assembly and function of neuronal circuits", Poster Presentation, Ascona, Switzerland

- Spring 2018: HHMI Janelia Conference on "Mechanisms of dexterity", Selected speaker, Janelia Research Campus, USA

- Fall 2019: Gatsby Conference on "The assembly and function of neuronal circuits", selected Talk and Poster Presentation, Ascona, Switzerland

Research Experience

- Mice: breeding and genotyping (LTK1 certificate)

- Mouse behavior: various motor behavior paradigms in mice such as runway, treadmill, open field, horizontal ladder and lever pressing

- Viral Tools: design, production, and purification of different variants of adeno-associated and rabies viruses for tracing and manipulating neuronal circuits

- Electrophysiology: extracellular *in-vivo* recordings in freely behaving animals

- Surgical: spinal cord and brain injections using stereotaxic and ultrasonic guidance, brain implantation of optical fibers and electrodes

- Molecular Biology and Biochemistry: Multiple standard techniques involving cell fractionation, DNA, RNA and Protein amplification, purification and detection techniques

- Computational: coding and data analysis using MatLab, R, ImageJ and MedPC, Image Processing using Imaris and ImageJ

Publications

Duneau, D, Luijckx, P, Ruder, LF, Ebert, D. Sex-specific effects of a parasite evolving in a female-biased host population. *BMC biology.* 2012, *10*(104)

Ruder L, Takeoka A, Arber S. Long-distance descending spinal neurons ensure quadrupedal locomotor stability. *Neuron.* 2016; 92(5), 1063-1078

Ferreira-Pinto, M. J.*, Ruder, L.*, Capelli, P.*, & Arber, S. Connecting Circuits for Supraspinal Control of Locomotion. *Neuron,* 2018; 100(2), 361–374

Ruder L. & Arber S. Brainstem Circuits Controlling Action Diversification. *Annual Review of Neuroscience*, 2019, 42(1), 485-504

Ruder, L., Schina, R., Kanodia, H., Valencia-Garcia, S., Pivetta, C., & Arber, S. A functional map for diverse forelimb actions within brainstem circuitry. *Nature*, 2021; 590, 445-450

*These authors contributed equally